


*Russian Original Vol. 36, No. 1, January, 1974*

---

July, 1974



SATEAZ 36(1) 1-112 (1974)

# SOVIET ATOMIC ENERGY

АТОМНАЯ ЭНЕРГИЯ  
(ATOMNAYA ÉNERGIYA)

TRANSLATED FROM RUSSIAN



CONSULTANTS BUREAU, NEW YORK

# SOVIET ATOMIC ENERGY

*Soviet Atomic Energy* is a cover-to-cover translation of *Atomnaya Energiya*, a publication of the Academy of Sciences of the USSR.

An agreement with the Copyright Agency of the USSR (VAAP) makes available both advance copies of the Russian journal and original glossy photographs and artwork. This serves to decrease the necessary time lag between publication of the original and publication of the translation and helps to improve the quality of the latter. The translation began with the first issue of the Russian journal.

## Editorial Board of *Atomnaya Energiya*:

**Editor:** M. D. Millionshchikov

Deputy Director  
I. V. Kurchatov Institute of Atomic Energy  
Academy of Sciences of the USSR  
Moscow, USSR

**Associate Editor:** N. A. Vlasov

A. A. Bochvar

N. A. Dollezhal'

V. S. Fursov

I. N. Golovin

V. F. Kalinin

A. K. Krasin

A. I. Leipunskii

V. V. Matveev

M. G. Meshcheryakov

P. N. Palei

V. B. Shevchenko

V. I. Smirnov

A. P. Vinogradov

A. P. Zefirov

Copyright © 1974 Plenum Publishing Corporation, 227 West 17th Street, New York, N.Y. 10011. All rights reserved. No article contained herein may be reproduced, stored in a retrieval system, or transmitted, in any form or by any means, electronic, mechanical, photocopying, microfilming, recording or otherwise, without written permission of the publisher.

Consultants Bureau journals appear about six months after the publication of the original Russian issue. For bibliographic accuracy, the English issue published by Consultants Bureau carries the same number and date as the original Russian from which it was translated. For example, a Russian issue published in December will appear in a Consultants Bureau English translation about the following June, but the translation issue will carry the December date. When ordering any volume or particular issue of a Consultants Bureau journal, please specify the date and, where applicable, the volume and issue numbers of the original Russian. The material you will receive will be a translation of that Russian volume or issue.

**Subscription**  
\$87.50 per volume (6 Issues)

Single Issue: \$50  
Single Article: \$15

Prices somewhat higher outside the United States.

## CONSULTANTS BUREAU, NEW YORK AND LONDON



227 West 17th Street  
New York, New York 10011

4a Lower John Street  
London W1R 3PD  
England

Published monthly. Second-class postage paid at Jamaica, New York 11431.

*Soviet Atomic Energy* is abstracted or indexed in *Applied Mechanics Reviews*, *Chemical Abstracts*, *Engineering Index*, *INSPEC-Physics Abstracts* and *Electrical and Electronics Abstracts*, *Current Contents*, and *Nuclear Science Abstracts*.

# SOVIET ATOMIC ENERGY

A translation of *Atomnaya Énergiya*

July, 1974

Volume 36, Number 1

January, 1974

## CONTENTS

Engl./Russ.

### ARTICLES

The BFS-1 Complex: A Microtron for Studying Fast-Reactor Neutron Spectra — A. I. Leipunskii, V. V. Orlov, Yu. A. Kazanskii, V. P. Zinov'ev, F. I. Ukraintsev, N. A. Klintsov, A. V. Shapar', G. N. Ankin, V. T. Vasin, V. F. Efimenko, P. S. Klemyshev, V. L. Parashchuk, V. A. Romanovskii, V. E. Rydkii, G. V. Sazonenkov, V. I. Sokolov, V. F. Filyaev, and Yu. M. Choropov.....	1	3
Luminescence of Secondary Uranium Minerals at Low Temperatures — B. S. Goborets and G. A. Sidorenko.....	5	6
Ion Field-Emission Microscopy of Uranium. Preliminary Results — A. L. Suvorov, G. M. Kukavadze, T. L. Razinkova, B. V. Sharov, V. A. Fedorchenko, A. F. Bobkov, and B. Ya. Kuznetsov.....	13	14
The Flexural Strengths of Disperse Materials Based on Uranium and Molybdenum Dioxides between 293 and 1870°K — L. E. Kakushadze and R. B. Kotel'nikov....	19	19
Radiation-Induced Swelling of 0Kh16N15M3B Steel — V. N. Bykov, A. G. Vakhtin, V. D. Dmitriev, L. G. Kostromin, A. Ya. Ladygin, and V. I. Shcherbak.....	24	24
Utilization of Pulsed Sorption Columns for the Decontamination of Liquid Radioactive Wastes — F. V. Rauzen, E. I. Zakharov, B. E. Ryabchikov, V. D. Konorchenko, and E. G. Odintsova.....	28	27
Calculation and Prediction of Radioactive Contamination of the Lower Atmosphere by Atomic Power Station Stack Discharges — N. E. Artemova.....	33	32

### REVIEWS

Mixed-Radiation Dosimetry — B. A. Briskman and R. B. Novgorodtsev.....	39	39
--	----	----

### ABSTRACTS

Application of the Bubnov-Galerkin Method to a Multigroup Calculation of a Two-Dimensional Reactor — I. P. Kukharenek.....	51	51
Measurement of the Absolute Intensity of the 278 keV Line of Np <sup>239</sup> — L. N. Yurova, A. V. Bushuev, V. I. Petrov, A. G. Inikhov, V. N. Ozerkov, and V. V. Chachin.....	52	51
Parameters of the Radiation Field near an Apparatus Used for Agricultural Irradiation — V. P. Bulatov and E. I. Tsygankov.....	53	51

### LETTERS TO THE EDITOR

Calculation of Integrated Cross Sections of Compton Interaction, Scattering and Absorption of $\gamma$ Quanta for Statistical Modeling of Transport Processes — O. S. Marenkov and V. N. Mitov.....	54	53
Calorimetric Dosimetry and a Procedure for Irradiating Samples, in Electron Accelerator Investigations of the Radiation Stability of Petroleum Oils — A. D. Stukin and G. I. Shor.....	56	54

**CONTENTS**

(continued)

Engl./Russ.

Stages of Formation of Uranium and Rare Metal Mineralization in Sedimentary Rocks — V. I. Danchev.....	58	55
Geochemical Isotopic Anomalies and the Hypothesis of Natural Nuclear Reactors — R. S. Prasolov.....	61	57
The Thermal Conductivity of Uranium Dioxide — V. I. Kolyadin, É. P. Il'in, A. G. Kharlamov, and V. V. Yakovlev.....	64	59
High-Altitude Measurements of the Natural Radioactivity of the Air — A. E. Shem'i-zade and R. U. Mambetov.....	67	61
Condensation Type Cryostat Channel for Low-Temperature Exposures — V. D. Parkhomenko, B. N. Goshchitskii, S. F. Dubinin, P. M. Korotovskikh, S. K. Sidorov, V. G. Chudinov, and Yu. G. Chukalkin.....	69	62
Dispersity of Aerosols Formed during Combustion of the Coolant and Materials of the Core of a Fast Reactor — B. N. Rakhmanov, S. V. Malyutin, O. M. Zараev, and I. E. Konstantinov.....	73	64
Determination of the Yields of Certain Fragments in the Fission of <sup>238</sup> U by Reactor Spectrum Neutrons — L. N. Yurova, A. V. Bushuev, and A. F. Kozhin.....	75	66
Uranium and Plutonium Losses with Steel in Thermal Decladding of Fuel Elements — G. P. Novoselov, Yu. D. Dogaev, and S. A. Perevozchikov.....	79	69
Thermal Decladding of Oxide Fuel Elements with Steel Separated from Nuclear Fuel by Filtration — G. P. Novoselov, A. T. Ageenkov, V. F. Savel'ev, and S. E. Bibikov	81	70
Temperature Measurement in High-Flux Reactors Using Thermocouples — N. V. Markina and V. A. Tsykanov.....	84	72
The Calculation of the Space-Energy Distribution of Secondary Annihilation Radiation — Sh. S. Nikolaiashvili and G. N. Dzhashiashvili.....	87	74
Test Facility for Studying Kinetics of Release of Gaseous Radioactive Fission Products from Irradiated Materials — D. M. Skorov, A. I. Dashkovskii, A. G. Zaluzhnyi, and O. M. Storozhuk.....	89	76
Interaction of Thermal Neutrons with <sup>152m</sup> Eu Nuclei — I. A. Kondurov, A. M. Berestovoi, A. I. Egorov, E. M. Korotkikh, and Yu. V. Petrov.....	92	77
Limitations of Effective Accelerating Fields in Ring Accelerators — V. G. Makhan'kov and M. G. Meshcheryakov.....	94	78
<b>COMECON NEWS</b>		
Vth International Conference on Mössbauer Spectroscopy (Bratislava, September, 1973) — A. G. Beda and E. P. Stepanov.....	97	80
Collaboration Daybook.....	100	81
<b>INFORMATION</b>		
The International Symposium on Mathematical Models of Power-Industry Economics — Yu. I. Koryakin.....	101	82
The Tenth International Mineral Processing Congress — M. L. Skrinichenko.....	105	84
All-Union Symposium on Radiobiology and Radioecology, Syktyvkar, September, 1973 — R. M. Aleksakhin.....	108	86
Meeting of the International Commission on Radiological Protection — Yu. I. Moskalev ..	110	87

The Russian press date (podpisano k pechati) of this issue was 12/25/1973. Publication therefore did not occur prior to this date, but must be assumed to have taken place reasonably soon thereafter.

## ARTICLES

THE BFS-1 COMPLEX: A MICROTRON FOR STUDYING  
FAST-REACTOR NEUTRON SPECTRA

UDC 621.039.526

A. I. Leipunskii,\* V. V. Orlov,  
 Yu. A. Kazanskii, V. P. Zinov'ev,  
 F. I. Ukraintsev, N. A. Klintsov,  
 A. V. Shapar', G. N. Ankin,  
 V. T. Vasin, V. F. Efimenko,  
 P. S. Klemyshev, V. L. Parashchuk,  
 V. A. Romanovskii, V. E. Rydkii,  
 G. V. Sazonenkov, V. I. Sokolov,  
 V. F. Filyaev, and Yu. M. Choropov

Highly accurate knowledge of the basic characteristics of reactors is required in the design of industrial fast power reactors. That is the reason why comprehensive investigations are carried out on fast zero-power critical assemblies, with the purpose of improving the accuracy of power reactor characteristics calculations. An important place is reserved for the study of neutron spectra in this research. Here the reason is that the number of reactions taking place in a reactor (fission, absorption, scattering) is determined by the interaction between neutrons and nuclei over a broad range of energies (from 100 eV up to 10 MeV), where the interaction cross sections undergo significant changes. Consequently, exact determinations of the number of processes taking place in a reactor are required in order to obtain precise information on neutron spectra. An experimental study of neutron spectra is also needed in order to verify and correct many-group systems of constants, and in order to effect improvements in computational procedures. Various topics associated with the study of neutron spectra in fast reactors were taken up in discussions at the International Conference on Fast Reactor Spectrometry held at the USA Argonne National Laboratory [1]. The time-of-flight method offers the greatest range, of all the methods available for measuring neutron spectra in fast critical assemblies. The lower energy limit in the time-of-flight method is determined by the ratio of the number of neutrons in the spectrum at that energy to the background of delayed neutrons, and falls within a range from 10 to 100 eV, depending on the hardness of the spectrum. The upper limit is set by the path length, and accordingly by the power of the pulsed neutron source.

The time-of-flight method makes it possible to measure the spectra of leakage neutrons from a subcritical reactor (usually at  $k_{\text{eff}} = 0.9$  to  $0.97$ ). The neutron spectra within a critical reactor can be obtained from the measured spectra, if corrections owing to the absence of spectra of scalar and vector neutron flux, perturbation of the spectrum by the exit channel, and the difference in the neutron spectra in a critical reactor and in a subcritical reactor, are introduced. These corrections have been studied by several authors [2-4], and they have been established as small ones. For example, according to data reported in [1, 3, 4], the difference in the spectra at the center of the core in a critical reactor and in a subcritical reactor ( $k_{\text{eff}} = 0.85$  to  $0.87$ ) does not exceed 10% over the energy range from 100 eV to 10 MeV. Perturbation of the spectrum by a 90 mm diameter exit channel amounts to no more than 3%, according to data reported in [2]. At energies below 1 MeV, the difference in the spectra of the scalar neutron flux and vector neutron flux at the center of the reactor, where the neutron flux gradient is small, amounts to several percent [2]. Consequently, computational corrections, amounting to about 15%, have to be introduced into the measured spectra of neutron leakage from the center of the reactor core.

\*Deceased.

Translated from *Atomnaya Energiya*, Vol. 36, No. 1, pp. 3-5, January, 1974. Original article submitted February 1, 1973.

© 1974 Consultants Bureau, a division of Plenum Publishing Corporation, 227 West 17th Street, New York, N. Y. 10011. No part of this publication may be reproduced, stored in a retrieval system, or transmitted, in any form or by any means, electronic, mechanical, photocopying, microfilming, recording or otherwise, without written permission of the publisher. A copy of this article is available from the publisher for \$15.00.

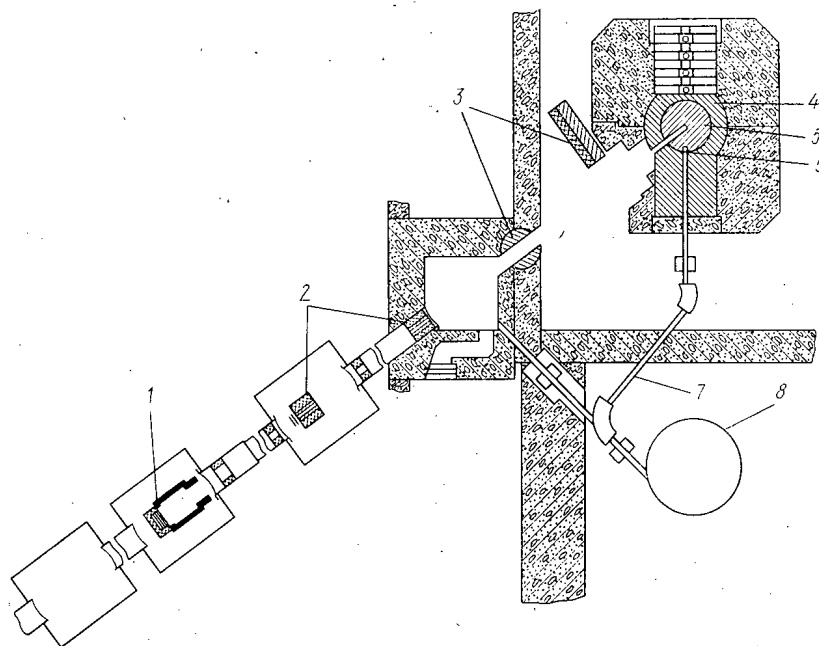


Fig. 1. Layout of the BFS-1 microtron facility. 1) detector in shielding; 2) collimators; 3) gates; 4) BFS-1; 5) core; 6) target; 7) electron guide; 8) microtron.

At the Power Physics Institute (FEI) measurements of neutron spectra in fast assemblies by the time-of-flight method are carried out on the BFS-1 microtron facility.

The BFS-1 testing facility makes it possible to simulate fast assemblies with core dimensions to 1.6 m. The design features a 2 m diameter steel tank standing 2 m high, and surrounded by shielding. Matrix tubes 50 mm in diameter, 1 mm wall thickness, into which reactor materials are loaded in the form of discs 46.7 mm in diameter and either 10 mm or 5 mm thick, are set upright in the steel tank, on a support plate with a 51 mm pitch hexagonal grid. Details on the design of the test facility are given elsewhere [5].

The pulsed mode of reactor operation is brought about by inserting a subcritical assembly ( $k_{\text{eff}} = 0.9$  to 0.97) of a pulsed neutron source into the core. A uranium target or lead target of the type used in the electron accelerator of a microtron facility is used as such a pulsed neutron source, and is placed at the boundary separating the core and the reflector. The target is a cylinder 40 mm in diameter and 60 mm high; it is positioned in one of the reactor channels and is cooled by compressed air.

The microtron employed is described elsewhere [6]. The microtron is operated in the following mode when the reactor spectra are measured by the time-of-flight method: the energy of the accelerated electrons is 29 MeV; pulse width is 2  $\mu\text{sec}$ ; current pulse is 10 mA; frequency 50 Hz; mean neutron yield from target  $10^{11}$  neutrons/sec.

The neutron flux is extracted from the center of the assembly through an exit channel of cross section  $100 \times 100$  mm. The extracted neutrons are directed to an evacuated neutron guide set in the earth; this guide is a 500 mm diameter steel tube. The guide diameter is increased to 800 mm at a distance of 170 m, and to 1000 mm at a distance of 550 m. The total length of the neutron guide extends 750 m; measuring chambers are placed along the length of the guide at distances of 53 m, 230 m, and 760 m from the center of the reactor.

The neutron beam extracted from the reactor is shaped by two collimators. The first collimator is located within the neutron guide at a distance of 10 m from the reactor center, the second in the first measuring chamber at a distance of 53 m from the reactor.

The dimensions of the collimating holes are selected such that neutrons cannot gain access to the detector from the walls of the exit channel, and the same applies to neutrons scattered singly on the walls of the neutron guide. When measurements are taken on a 230 m path length, the diameters of the holes are selected at 64 mm and 86 mm, respectively for the first and second collimators. There are also several

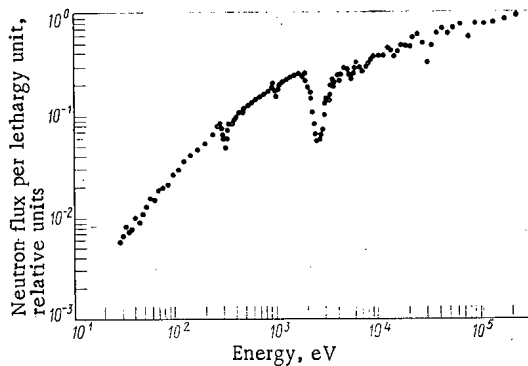


Fig. 2. Spectrum of leakage neutrons from center of BFS-27 critical assembly.

minacy is 2-3  $\mu$ sec; the area of exposed surface is 2500 cm<sup>2</sup>; background proper is 1 cps. The detector is virtually insensitive to  $\gamma$ -radiation. Time analysis is carried out in the course of the measurements using the equipment of the FÉI reactor measurements data center, and the experimental data are processed on the Nairi-2 computer.

At the present time, measurements of neutron spectra are being taken for neutrons from BFS assemblies over the energy range from 30 eV to 200 keV, on a path length extending 230 m. The soft part of the spectrum of leakage neutrons from the BFS-27 assembly is shown in Fig. 2 as an illustrative example. The measurements were taken at reactor breeding ratio  $k = 0.9$ . The energy resolution  $\Delta E/E$  amounted to 60% for neutrons of 100 keV energy and 6% for 1 keV neutrons. The count rate for the 5  $\mu$ sec channel, at microtron current 7 mA, was  $6 \cdot 10^3$  cph at the peak of the spectrum and  $1.5 \cdot 10^2$  cph at energy 1 keV. The constant background due to delayed neutrons and to the intrinsic background of the detector was 4 cph for the 5  $\mu$ sec channel. Background was measured immediately prior to the next burst from the reactor on a time window 1280  $\mu$ sec in width. The variable (correlated) component of background was measured by the resonance-filter method. The resonances used were those of cobalt (132 eV and 5.015 keV), manganese (337 eV and 2.375 keV), and sodium (2.85 keV). The relative background levels are listed below:

Neutron energy, eV	132	337	2850	5015
Total background, %	35	13	20	7
Variable component of background, %	1	1.5	15	5

Corrections were introduced when the results of the measurements were processed, the most essential corrections being for resolution and for attenuation of the beam of neutrons in dead pockets of the neutron guide and in air. For the example cited (see Fig. 2), the first correction was 30% at neutron energy 170 keV and less than 5% at neutron energies below 1 keV. This correction was greatly affected by the duration of the reactor pulse, and decreased as the pulse width was narrowed. The size of the second correction is due to the presence of a relatively large amount of air (15 m) and aluminum (8 mm) on the path traversed by the neutron beam. The error in the measured spectrum of leakage from the subcritical reactor is 15% over the energy range from 500 eV to 10 keV, 20% below 500 eV, and 30% at energies above 50 keV.

Note that the time-of-flight method does not enable us to obtain all of the necessary information on the neutron spectrum of a fast reactor. A hydrogen proportional counter is being used at the BFS-1 test stand in studies of the neutron spectrum over the energy range from 10 keV to 2 MeV, and a scintillation spectrometer with a stilbene crystal is being used for studies in the range of energies upwards of 0.8 MeV.

In conclusion, the authors avail themselves of this opportunity to express their heartfelt thanks to I. G. Morozov for his kind and persistent attention to the progress of the work, to Yu. Ya. Stavisskii and A. I. Abramov for their helpful discussions when the facility was in its design stage, and also to all the staff members of FÉI who took part in building the facility.

\*In the energy range from 30 eV to 50 keV, the relative variation in effectiveness, measured experimentally, is known to within 10%.

LITERATURE CITED

1. Fast Reactor Spectrum Measurements and Their Interpretation, IAEA, Vienna (1971), p. 138.
2. J. Sanders, in: Fast Reactor Spectrum Measurements and Their Interpretation, IAEA, Vienna (1971), p. 36.
3. T. Oei, RCN-122 (1970).
4. M. Coates, et al., J. Nucl. Energy, 22, 547 (1968).
5. V. V. Bondarenko, et al., At. Énerg., 24, 82 (1968).
6. A. I. Abramov, et al., The 30 MeV Microtron at FÉI [in Russian], Preprint FÉI-211 (1970).



## LUMINESCENCE OF SECONDARY URANIUM MINERALS AT LOW TEMPERATURES

B. S. Gorobets and G. A. Sidorenko

UDC 535.372:549.755.35

Numerous secondary uranium minerals, in which uranium is present in the form of uranyl  $UO_2^{2+}$ , must be isolated and recognized in the search for uranium ore. All uranyl minerals are very important indicators of uranium mineralization; some of the uranyl minerals, such as vanadates, uranite, hydroxides, and schroekingerite, are of interest as independent raw material sources, when these minerals are present in considerable quantities.

Mineralogists have for a long time used uranyl minerals' ability to emit ultraviolet luminescence radiation [1-3]. But contrary to the synthetic uranyl compounds [4], the photoluminescence spectra of the uranyl minerals were determined only for a few objects with a bright radiation at room temperature [2, 5]. The majority of secondary uranium minerals exhibit a bright luminescence radiation only at sufficiently low temperatures [6]. The goal of the present work was the determination of the luminescence spectra of the rather complete group of uranyl minerals at 77°K and 298°K and the interpretation of the spectra in terms of physics; detailed investigations of the compositions of the minerals on the basis of the resulting data; and the development of the luminescence technique as a reliable and rapid method for recognizing uranyl minerals present in traces.

The luminescence spectra were recorded with an ISP-51 spectrograph which was equipped with a photoelectric FÉP-1 attachment, an FÉU-38 photomultiplier, and an ÉPP-09mZ recording potentiometer. A test tube, which was made of quartz glass and contained a mineral sample of 5 mg or more, was placed into a transparent Dewar vessel containing liquid nitrogen. Luminescence of the mineral was excited with the light of an SVD-120A mercury-filled quartz lamp. A UFS-2 filter and a layer of 10%  $CuSO_4$  solution were used to single out the excitation interval ranging from 40,000  $cm^{-1}$  to 25,000  $cm^{-1}$ . The accuracy of the frequency measurements and the luminescence spectrum amounted to 10-20  $cm^{-1}$  in the interval 20,000-16,000  $cm^{-1}$ . This accuracy suffices in work on minerals, because various samples of a particular mineral are characterized by a shift of identical lines in the spectrum, with the shift frequently exceeding the above-indicated accuracy limits. The shift results from impurities, various degrees of order of the structure, and deviations from stoichiometry in the samples considered. Table 1 lists the frequencies of the spectral lines; the frequencies were averaged over all samples of a particular mineral. The objects of our investigations were initially identified on the basis of the Debye diagrams.

### Phosphates and Arsenates

The minerals examined were separated into two isostructural groups with basically different luminescence spectra. The first group comprises the uranites: autunite (15),\* torbernite, and mixed copper-calcium uranites (4), natroautunite (1), uranospinite (2), novačekite (2), uranocircite (4), and the following minerals which had been synthesized by I. G. Zhil'tsova from aqueous solutions: Ca-autunite; H-autunite; (Ca, Ba, H)-autunites. The second group comprises phosphuranylite (6), Sr-phosphuranylite (1), and reardite (2).

\*The number of samples is indicated in parentheses. All minerals of the first group contained 6-8 molecules  $H_2O$  (meta-form), but, for the sake of simplicity, we use their names without the prefix "meta."

Translated from *Atomnaya Énergiya*, Vol. 36, No. 1, pp. 6-13, January, 1974. Original article submitted April 19, 1973.

© 1974 Consultants Bureau, a division of Plenum Publishing Corporation, 227 West 17th Street, New York, N.Y. 10011. No part of this publication may be reproduced, stored in a retrieval system, or transmitted, in any form or by any means, electronic, mechanical, photocopying, microfilming, recording or otherwise, without written permission of the publisher. A copy of this article is available from the publisher for \$15.00.

TABLE 1. Spectroscopical Characteristics of the Luminescence of Secondary Uranium Minerals at 77°K

Minerals	Oscillation frequencies ( $\text{cm}^{-1}$ ) of electrons						
	$k_0$	$k_1$	$k_2$	$k_3$	$k_4$	$k_5$	$\Delta k_s$ [ $\Delta k_a$ ]
Phosphates and arsenates:							
a) uranites							
Me[(UO <sub>2</sub> )(XO <sub>4</sub> ) <sub>2</sub> ·(6-8)H <sub>2</sub> O,	I. 19 950±30	19 430	18 310	17 480	16 660		825±5
where Me—Ca, Ba*, Mg, Cu;		[19 060]	[18 230]	[17 400]			[900±10]
X = P, As*	II. 19 500±50	18 730	17 970	17 200	16 420		760±15
natroautunite	III. 19 600±100	18 090	17 320	(16 550)			760±20
Na <sub>2</sub> [(UO <sub>2</sub> )(PO <sub>4</sub> ) <sub>2</sub> ·(6-8)H <sub>2</sub> O	I. 19 980±20	19 180	18 390	17 580	16 820		795±5
		[19 090]	[18 290]	[17 520]	[16 750]		[880±10]
b) phosphuranylite-renardite	II. 19 570±50	18 800	18 050	17 290			760±10
(Ca, Sr, Pb)(UO <sub>2</sub> ) <sub>3</sub> (PO <sub>4</sub> ) <sub>2</sub> (OH) <sub>2</sub>	18 800±70	18 070	17 360	(16 650)			720±5
× 2H <sub>2</sub> O							
Silicates:							
uranophane	19 400±80	18 670	17 960	(17 250)			(730)
Ca[UO <sub>2</sub> (SiO <sub>3</sub> )OH] <sub>2</sub> ·5H <sub>2</sub> O							
β-uranotil	19 570±10	18 840	18 110	(17 500)			750±10
Ca[UO <sub>2</sub> (SiO <sub>3</sub> )OH] <sub>2</sub> ·5H <sub>2</sub> O							
soddyite	(19 250±10)	18 150	17 410	16 680	(15 940)		740±10
(UO <sub>2</sub> ) <sub>2</sub> SiO <sub>4</sub> ·2H <sub>2</sub> O							
boltwoodite							
Na[UO <sub>2</sub> (SiO <sub>3</sub> )OH]·nH <sub>2</sub> O	I. 19 720±10	18 950	18 200	17 450			770±10
	II. 19 580±30	18 820	18 080				(750)
NH <sub>4</sub> [UO <sub>2</sub> (SiO <sub>3</sub> )OH]·nH <sub>2</sub> O	I. 19 800±20	18 990	18 180	(17 360)			810
	II. 19 510±30	18 800	18 060				(740)
(K, Na, Ca)[UO <sub>2</sub> (SiO <sub>3</sub> )OH]	(19 750)	(18 950)	18 000				
× nH <sub>2</sub> O where n = 1 - 4)							
Carbonates and sulfates:							
uranotallite and bayleyite	21 000	20 080	(19 230)		17 550		
Ca <sub>2</sub> UO <sub>2</sub> (CO <sub>3</sub> ) <sub>3</sub> ·8H <sub>2</sub> O	20 840±20	19 990	19 170	18 340	17 510	16 730	830±10
	20 680				17 410	16 600	
Mg <sub>2</sub> UO <sub>2</sub> (CO <sub>3</sub> ) <sub>3</sub> ·18H <sub>2</sub> O	20 610				17 390		
schroekingerite	(20 740)	19 980	19 170	18 410	17 480	(16 450)	835±5
NaCa <sub>3</sub> UO <sub>2</sub> (CO <sub>3</sub> ) <sub>3</sub> SO <sub>4</sub> F·10H <sub>2</sub> O	20 700±10	19 920	19 110	18 330	17 450		
	20 660	19 830	19 090	18 230	17 360		
	20 610	19 640	19 000	18 170	17 250		
	20 530	19 580	18 930				
	20 470			18 100			
	20 420			18 010			
meta-uranopilite	19 650 ( $k_{10}$ )						
(UO <sub>2</sub> ) <sub>2</sub> SO <sub>4</sub> (OH) <sub>10</sub> ·5H <sub>2</sub> O	19 130 ( $k_0$ )	18 330	17 530	16 730			800±5
	(19 000) ( $k_{11}$ )						
zippeite	18 550±100	17 800	17 050	(16 300)			750±20
(UO <sub>2</sub> ) <sub>2</sub> SO <sub>4</sub> (OH)(3-5)H <sub>2</sub> O							
Vanadates:							
carnotite	18 980	18 120					
K <sub>2</sub> (UO <sub>2</sub> ) <sub>2</sub> (VO <sub>4</sub> ) <sub>2</sub> ·3H <sub>2</sub> O	18 690±20	17 890	17 090				800±5
calcocarnotite	19 480±10	(19 000)	18 300				
Ca(UO <sub>2</sub> ) <sub>2</sub> (VO <sub>4</sub> ) <sub>2</sub> ·8H <sub>2</sub> O		18 820					
U Molybdates	18 980±30	18 270	(17 600)				710±10
U hydroxides	18 350—18 570	17 860—17 940	17 280—17 420				(640—700)

Note. 1. The frequencies of the I series of uranocircite and uranospinite (\*) are by about 100  $\text{cm}^{-1}$  smaller than the indicated frequencies. 2. The frequencies of the antisymmetric oscillations are indicated in brackets. 3. Smeared "lines", which were approximately determined, are indicated in parentheses. 4. The frequencies of the fully symmetric oscillations were singled out in groups consisting of several lines.

The minerals of the first group are characterized by a bright yellow-green luminescence at 298°K; the spectrum consists of a series (I) of equidistant lines (Fig. 1a). The spectra of all the minerals are almost identical, but in the case of natroautunite, the lines are slightly shifted towards higher frequencies ( $k_0 \approx 19,980 \text{ cm}^{-1}$ ), whereas the shift goes toward lower frequencies in the case of uranospinite and uranocircite ( $k_0 \approx 19,830 \text{ cm}^{-1}$ ) when compared with autunite ( $k_0 \approx 19,920 \text{ cm}^{-1}$ ). The shifts are an important indicator for the recognition of these minerals which are hard to analyze. Three types of spectra are observed at 77°K. In the spectrum of type I, which is characteristic of all synthetic samples (Fig. 1a), only the series I of equidistant lines is observed, which is also found at 298°K. In the spectrum of type II (majority of natural samples), two series (II and II) of equidistant lines are present (Fig. 1b). In the spectrum of type III (Fig. 1c), a single, new series (III) of equidistant bands is observed; series I usually fails to appear at low temperatures.

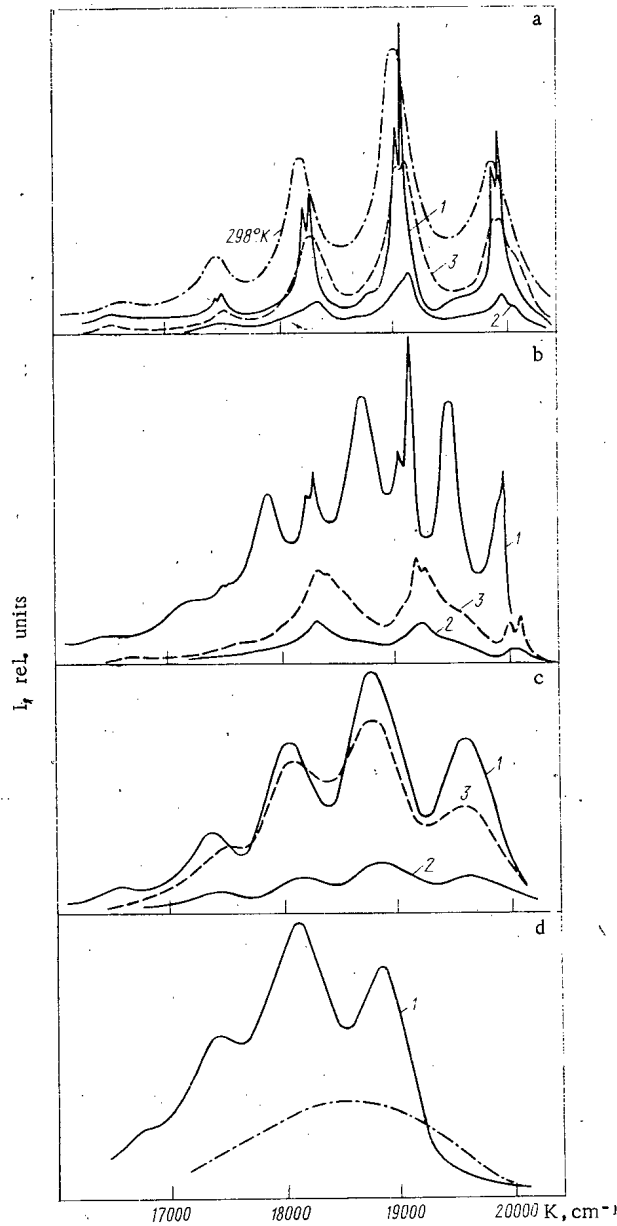


Fig. 1

Fig. 1. Luminescence spectra of uranyl phosphates and uranyl arsenates at 77°K (solid lines) and 298°K (dash-dot lines): a-c) meta-autunite group, spectra of types I, II, and III; 1) initial spectrum; 2) after 30 min heating at 150°C; 3) after storing the heated mineral for several days in air; ratio of the intensity scales:  $I_{77}^{\max} : I_{298}^{\max} \approx 3$ ;  $I_1 : I_2 : I_3 \approx 100 : 1 : 20$ ; d) phosphuranylite-renardite group,  $I_{77}^{\max} : I_{298}^{\max} \approx 100$ .

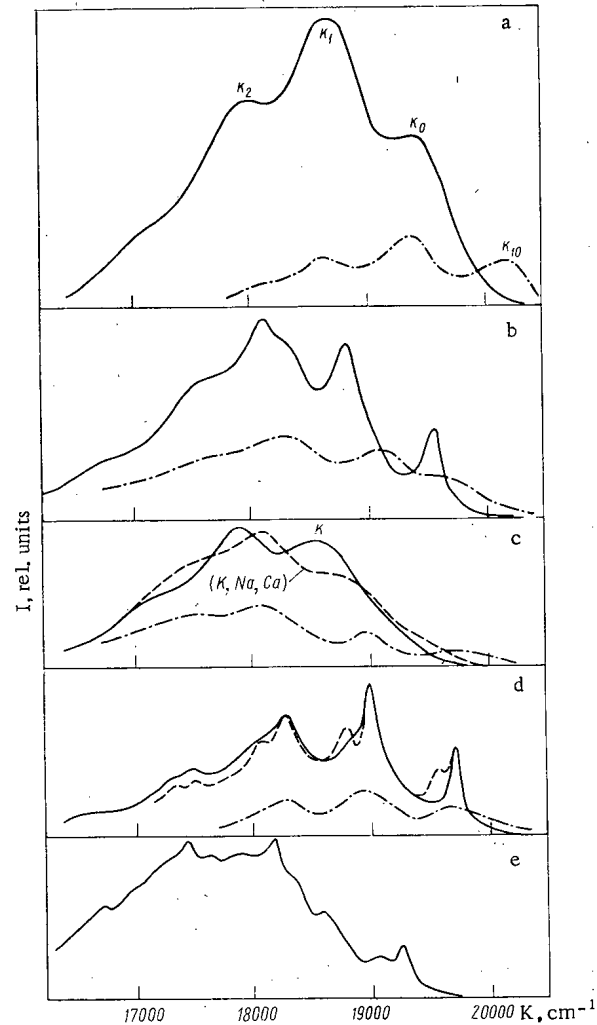


Fig. 2

Fig. 2. Luminescence spectra of uranyl silicates at 77°K (solid line) and 298°K (dash-dot line): a) uranophane; b)  $\beta$ -uranotil; c) K and (K, Na, Ca)-boltwoodites; d) Na-boltwoodites (the dashed curve refers to a mixture with an unknown phase); e) soddyite (Republic of Zaire);  $I_{77}^{\max} : I_{298}^{\max} \approx 10-100$  for the various samples.

The interpretation of the luminescence spectra of the minerals is based upon both experimental and theoretical data which were previously obtained for synthetic uranyl compounds [4]. The line with the highest frequency  $k_0$  corresponds to a pure radiative electron transition from the lowest excited uranyl state  $\sigma_u^2 \sigma_g^2 \pi_u^4 \pi_g^3 \phi_u^1$  into its ground state  $\sigma_u^2 \sigma_g^2 \pi_u^4 \pi_g^4$ . In accordance with the Franck-Condon principle, the relaxation of the nuclei begins after the transition. The oxygen nuclei tend to assume a new equilibrium position in the linear O-U-O molecule. Three types of oscillations of the oxygen nuclei relative to the uranium nucleus can be excited: fully symmetric oscillations, antisymmetric oscillations, and deformation oscillations

TABLE 2. Crystallochemical Formulas of the Meta-Autunites Examined (in the order of increasing structural imperfection); Results of Chemical Analyses

Formula	Type of the radiation center at 77°K	Remark
$\text{Ca}_{1.00}(\text{UO}_2)_{2.00}(\text{PO}_4)_{2.00} \cdot 9,1\text{H}_2\text{O}$	I	Synthetic, spectrum on Fig. 1a
$\text{Ca}_{0.97}(\text{UO}_2)_{2.03}(\text{PO}_4)_{1.96} \cdot 6,1\text{H}_2\text{O}$	I, II	Natural, spectrum on Fig. 1b
$\text{Ca}_{0.90}(\text{UO}_2)_{2.12}(\text{PO}_4)_{2.00} \cdot 7,4\text{H}_2\text{O}$	I, II	The same
$\text{Ca}_{0.90}(\text{UO}_2)_{2.13}(\text{PO}_4)_{2.00} \cdot 7,6\text{H}_2\text{O}$	I, II	
$\text{Ca}_{0.73}\text{Sr}_{0.19}(\text{UO}_2)_{2.19}(\text{PO}_4)_{2.00} \cdot 8,5\text{H}_2\text{O}$	III	Natural, spectrum on Fig. 1c

the radiation series I, II, and III, the minerals were dehydrated by heating them for 30 min in air at some temperature between 50 and 250°C. Heating at 50–100°C irreversibly destroyed almost all II centers (see Fig. 1b). The stability of the I and III centers is higher, and their radiation disappears completely only after heating to 250°C. The process is partially reversible: after keeping the samples for several days in air, the lines of the I and III series were restored to about 20% of the initial intensity (see Figs. 1a–c, dashed lines).

In order to determine the nature of the I, II, and III centers, we considered the structure of meta-autunite. It is generally accepted [7, 8] that meta-autunite consists of  $\{[\text{UO}_2]^{2+}[\text{PO}_4]^{3-}\}_n^{n-}$  layers the charge of which is compensated for by interlayer  $\text{Ca}^{2+}$ ,  $\text{Na}^+$ , and other cations.  $\text{Ca}^{2+}$  ions occupy half of the cation positions, which results in various degrees of order in the redistribution of  $\text{Ca}^{2+}$  and the coordinated water molecules.  $\text{Na}^+$  ions occupy all cation positions and, hence, the structure of natroautunite has increased order and stability. Four water molecules enter into the first coordination sphere of the cation (water I) and the other water molecules, usually two (water II), appear in the second coordination sphere. The excess over these six molecules can be present in the form of a weakly bound interlayer water or in the form of oxonium ( $\text{H}_3\text{O}^+$ ) which compensates for deficiencies in the  $\text{Ca}^{2+}$  and  $\text{Na}^+$  cations.

Substantial deviations from stoichiometry (Table 2), with which various degrees of order of the interlayer cations and, hence, of the water are correlated, are observed in natural autunites. I, II, and III centers are formed as a consequence of the nonuniform binding of the uranyl to the various forms of water. The form of the binding of the water in the autunites was studied on the same samples with the technique of weight-loss (DTG) curves. Three steps of the weight loss  $[2 + 4 + (0-2)]\text{H}_2\text{O}$  are characteristic of synthetic autunite, which is distinguished by complete stoichiometry and a completely ordered structure from natural autunite (see Table 2). Two molecules of II water, which is weakly bound to the cation, are lost at temperatures of about 50°C. The removal of this water does not influence the luminescence spectrum. The second step corresponds to the loss of I water ( $4\text{H}_2\text{O}$ ) in the range 50–250°C, whereupon autunite transforms into the form  $\text{Ca}(\text{UO}_2)_2(\text{PO}_4)_2(0-2)\text{H}_2\text{O}$  and no longer emits luminescence radiation (the subsequent step of losing  $(0-2)\text{H}_2\text{O}$  at 400–500°C is therefore not associated with a transformation of radiation centers). Thus,  $4\text{H}_2\text{O}$ , along with  $\text{UO}_2$ , are constituents of I centers, i. e., these centers are complexes with water. These centers are the main luminescence centers in phosphates and arsenates of the uranite-structure group.

The lowest thermal stability (up to 50–100°C), irreversible destruction of the centers, and luminescence at low temperatures only are characteristic of the II centers. II centers do not appear in synthetic autunites in which stoichiometry is rigorously observed. All these properties imply that, obviously, the  $\text{H}_3\text{O}^+$  oxonium of low thermal stability ( $2\text{H}_2\text{O} = \text{H}_3\text{O}^+ + \text{OH}^-$ ) and uranyl are constituents of the II centers. The attenuation of II centers at 298°K seems to be related to the simultaneous presence of oxonium and  $\text{OH}^-$ , which dissipates the energy of the optical excitation of uranyl [9].

[4]. Fully symmetric oscillations are most closely associated with electron transitions. The corresponding quantum is characteristic of the spectrum of type I (Fig. 1a) and is  $\Delta k_s = 825 \text{ cm}^{-1}$  in autunite; up to 6 of these quanta, which correspond to equidistant lines  $k_n = k_0 - n\Delta k_s$  (where  $n = 1, 2, \dots$ ) can be emitted (see Table 1). In the antisymmetric oscillations, the potential energy excess which appears after an electron transition does not decrease in a first approximation and, hence, these oscillations should not be excited at all. Nevertheless, the emission of one quantum of antisymmetric oscillations is observed in structures in which O–U–O is structurally unbalanced [4]. For example, in autunite in which the uranyl imbalance amounts to 0.2 Å, one observes at 77°K, in addition to the  $k_n$  lines of series I, narrow lines of an antisymmetric uranyl oscillation beginning with  $n = 1$ :  $k_n^{(a)} = k_{n-1} - \Delta k_a$ , where  $\Delta k_a \approx 900 \text{ cm}^{-1}$  (see Table 1 and Figs. 1a and b).

In order to study the contribution of water to the formation of I, II, and III centers which correspond to

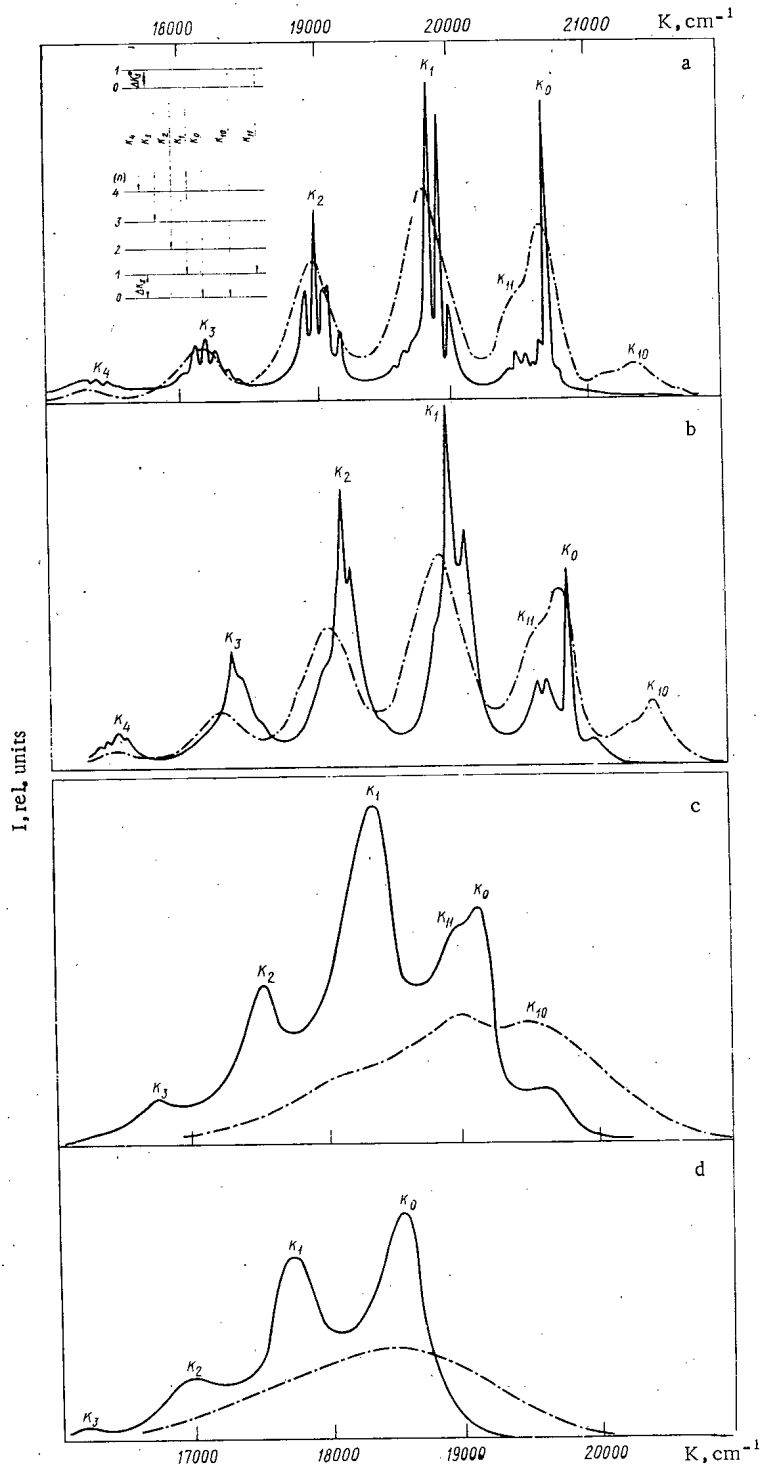


Fig. 3. Luminescence spectra of carbonates, sulfate-carbonates, and sulfates at 77°K (solid line) and 298°K (dash-dot line): a) schroekingerite (the electron-oscillation terms are indicated in the insert); b) uranotallite,  $I_{77}^{\max} : I_{298}^{\max} \approx 2$ ; c) meta-uranopilite,  $I_{77}^{\max} : I_{298}^{\max} \approx 3$ ; d) zippeite,  $I_{77}^{\max} : I_{298}^{\max} \approx 30$ .

In autunites, which are characterized by a III spectrum, the water is also lost in the temperature range 50-250°C, but, in distinction to the autunites with I and II spectra, the DTG curves are smooth, because the gradual loss of "unordered" water is superimposed upon the steps corresponding to the loss of the fixed I and II water ( $2 + 4\text{H}_2\text{O}$ ). The III centers are, in essence, groups of centers which can be formed by uranyl when order-destroying water molecules accumulate in the neighborhood of an uranyl molecule.

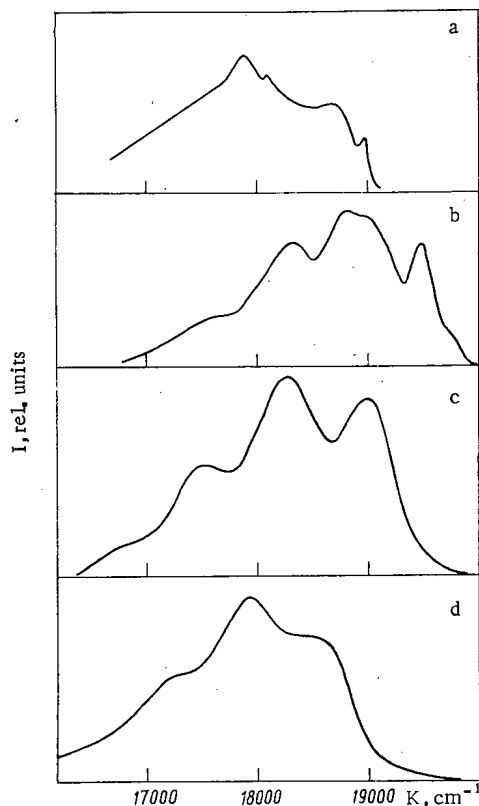


Fig. 4. Luminescence spectra at 77°K of: a, b) vanadates: carnotite and calciocarnotite; c) uranyl molybdates; d) uranium hydroxides.

the uranyl luminescence. Both the low intensity and the diffuse band structure at 298°K are related to the reduced number of water molecules in the coordination sphere of uranyl (e.g., reduced relative to the I centers in autunite), and to the presence of OH<sup>-</sup> ions. Similar reasons for the attenuation of the uranyl luminescence in aqueous solutions at 298°K were described in [9], where electrolytes stimulating the dissociation of H<sub>2</sub>O molecules into H<sup>+</sup> and OH<sup>-</sup> were introduced into the solutions. However, uranyl luminescence is observed at lower temperatures, because, due to the enhanced association of the water in the coordination sphere of the uranyl, the interaction between uranyl and the quenching OH<sup>-</sup> ions is reduced. The same arguments can be used for an (at least qualitative) explanation of the partial or full attenuation of the luminescence of silicates, some sulfates, uranium molybdates, and uranium hydroxides at 298°K.

### Silicates

We studied uranophane (9),  $\beta$ -uranotil (8), boltwoodite (5), soddyite (2), and some of their synthetic analogs. All these minerals (except for soddyite) are characterized by a weak green radiation at 298°K and a bright yellow radiation at 77°K. The luminescence spectra of these minerals are a reliable characteristic for their recognition at 77°K (Fig. 2). Uranophane and  $\beta$ -uranotil, which have identical composition but different structures, are particularly distinguished (see Figs. 2a, b). An important detail is observed in the spectra of several Na boltwoodites (Fig. 2d, dashed line) and of synthetic NH<sub>4</sub> boltwoodites (see Table 1) in which two series (I and II) of fully symmetric oscillations have been detected. Series I is homologous and the relative shift of the lines of series I is related to different influences of Na<sup>+</sup> and NH<sub>4</sub><sup>+</sup> cations upon uranyl. The II series coincide in Na and NH<sub>4</sub> boltwoodites. Series II can be explained by the presence of a finely dispersed admixture of a certain "cation-less" uranium phase, the low concentration of which in these minerals has so far prevented the identification of these minerals from x-ray diffraction patterns. The decrease in  $\Delta k_s$  to 740-770 cm<sup>-1</sup> indicates that the uranyl ion is extended by about 5% in the structure of the silicates.

It seems that small regions of I and II autunites are present in the III autunites, because the luminescence of the "ordered" I centers is observed at 298°K; the I centers so far appeared attenuated as "unordered" III centers. The III centers begin to emit luminescence radiation at low temperatures, when the narrow lines of the I centers usually cannot be recognized on the background of the smeared lines of the fully symmetric oscillations of the III centers (line width 500-600 cm<sup>-1</sup>).

The influence of Ca<sup>2+</sup>, Ba<sup>2+</sup>, and Mg<sup>2+</sup> cations upon the uranyl radiation is necessarily smaller than the influence of the various types of bound water. The luminescence spectra of autunite, uranocircite, and the other minerals are therefore hardly distinguishable. However, the influence of the Cu<sup>2+</sup> cation upon the uranyl is clearly visible in torbernite: torbernite does not emit luminescence radiation. It is well known that Cu<sup>2+</sup> is an active attenuator of the luminescence and, at the same time, a highly polarizing agent. The consequence is a substantial overlap of the wave functions of Cu<sup>2+</sup> and uranyl and the subsequent quenching of the (external) luminescence. But even when only a few percent of Ca (in mixed copper-calcium uranites) are present, luminescence is excited and spectra of types I, II, or III are observed in the various samples. This luminescence must be most likely related to layers of Ca-autunite in the bulk of torbernite, because an isomorphous Ca<sup>2+</sup>-Cu<sup>2+</sup> replacement is unlikely.

A weak, green radiation at 298°K and a bright yellow-green radiation at 77°K (Fig. 1d) are characteristic of the minerals of the isostructural group of phosphuranylite-reardonite. The cations (Ca, Sr, Pb) have no influence upon

Carbonates, Sulfate - Carbonates, and Sulfates

The most frequently found minerals of these classes were studied: uranotallite (2), bayleyite (1), schroekingerite (7), meta-uranopilite (2), and zippeite (4). No differences were observed in the luminescence spectra of isostructural carbonates, i. e., in the luminescence spectra of uranotallite and bayleyite (Fig. 3b). The spectrum of schroekingerite is distinguished from the two spectra at 77°K (Fig. 3a). The high brightness of the bluish-green radiation within a broad temperature interval can be explained by the high concentration of water of crystallization and by the absence of OH<sup>-</sup> in these minerals. The value  $\Delta k_S \approx 830-840 \text{ cm}^{-1}$ , which is the usual value for the known uranyl salts [4], is characteristic of  $\text{UO}_2^{2+}$ . The emission lines are narrow, which means that the structure has a high order and the minerals are homogeneous. Numerous lines of O-U-O deformation oscillations are observed, and other lines, which are apparently related to oscillations of lattice ions associated with uranyl, appear in the spectra. Antisymmetric uranyl oscillations were not established in carbonates and sulfates, because the O-U-O configuration is balanced. Anti-Stokes transitions ( $k_{10}$  and  $k_{11}$  on Fig. 3) are observed at 298°K. These transitions are photothermal transitions: the energy of the optical excitation of an electron in  $\text{UO}_2^{2+}$  appears added to the energy of the thermal lattice vibrations so that a stationary population of the sublevel  $n^* = 1$  of the excited  $\text{UO}_2$  state is formed during a lifetime of about  $10^{-4}$  sec. In this case, a fluorescence transition can take place from the two sublevels  $n^* = 0$  or  $n^* = 1$  of the excited state to the sublevels  $n = 0$  or  $n = 1$  of the ground state. In this case, the following emission frequencies are observed:  $k_{10} = k_0 + \Delta k_S^*$  and  $k_{11} = k_1 + \Delta k_S^*$  (the meaning of the notation can be inferred from the insert of Fig. 3a). The anti-Stokes lines make it possible to determine the wavelengths of the fully symmetric O-U-O oscillation in the excited state:  $\Delta k_S^* \approx 650 \pm 30 \text{ cm}^{-1}$  in the case of uranotallite and  $700 \pm 30 \text{ cm}^{-1}$  in the case of schroekingerite; it is well known [4] that  $\Delta k_S^*$  is always smaller than  $\Delta k_S$ , because the force constant of the bond in the O-U-O molecule is in the excited state smaller than in the ground state.

The sulfates uranopilite ( $5\text{H}_2\text{O}$ -meta-form) and zippeite are characterized by a moderate green luminescence. The corresponding spectra are shown in Figs. 3c and d. The radiation at 77°K is bright and yellow-green; broad bands of fully symmetric oscillations appear in the spectra.  $k_{10}$  and  $k_{11}$  anti-Stokes transitions are observed in uranopilite at 298°K as well as at 77°K. The  $\Delta k_S^*$  value is about  $600 \text{ cm}^{-1}$ , whereas  $\Delta k_S \approx 800 \text{ cm}^{-1}$ . The partial attenuation of the luminescence at 298°K proves that OH<sup>-</sup> ions are present in zippeite and uranopilite.

Vanadates, Molybdates, and Hydroxides

Common features of the minerals of these classes are the absence of radiation at 298°K, a bright yellow luminescence at 77°K, smeared "lines" in the spectra, and low  $\Delta k_S$  values. The vanadates were represented by carnotite (3), calciocarnotite (3), and francevillite (1). The luminescence spectra of carnotite and calciocarnotite are complicated. There appear at least two uranyl centers of different nature (Figs. 4a, b). So far it has been difficult to interpret these centers. The radiation spectrum of francevillite consists of a diffuse band with  $\lambda_{\text{max}} \approx 18,300 \text{ cm}^{-1}$ .

Almost identical are the luminescence spectra of the molybdates which were represented by umohoite (5)  $\text{UO}_2(\text{MoO}_4(\text{H}_2\text{O}_2)) \cdot 2\text{H}_2\text{O}$ ; (Ca, Na)-uranomolybdates (8)  $(\text{Ca}, \text{Na}) \cdot (\text{UO}_2)_3(\text{MoO}_4)_3(\text{OH})_3 \cdot 8\text{H}_2\text{O}$ ; and iriginite (1)  $\text{UO}_2(\text{Mo}_2\text{O}_7(\text{H}_2\text{O})_2) \cdot \text{H}_2\text{O}$  (Fig. 4c). Obviously, a uranyl center of a certain type causes the luminescence in these minerals. The structural similarity between (Ca, Na) uranomolybdates and iriginite is beyond any doubt. These molybdates are typical hydrated  $\text{U}^{6+}$  molybdates with a rather incomplete structure. The additional  $\text{Ca}^{2+}$  and  $\text{Na}^+$  cations are rather unimportant. Umohoite has a particular structure, but is related to both (Ca, Na) molybdates and iriginite by a layer structure, weak binding between the layers, and interlayer water. Umohoite is a mineral with variable  $\text{U}^{4+}/\text{U}^{6+}$  ratios; the color of the mineral becomes brighter when  $\text{U}^{6+}$  predominates. Luminescence can be observed in the bright varieties of umohoite, whereas no radiation is emitted from the dark varieties.

Uranium hydroxides form a group of minerals having the formula  $\text{Me}_x [\text{UO}_2]_y \text{O}_{2x} (\text{OH})_{2(y-x)} \cdot [z + x + y] \cdot \text{H}_2\text{O}$ , wherein Me stands for Ca, Ba, or Pb. The luminescence spectra of the hydroxides consist of three highly diffuse bands (Fig. 4d). The luminescence spectra of the hydroxides are distinguished from those of the molybdates by the absence of the band at  $19,000 \text{ cm}^{-1}$ . An influence of the  $\text{Me}^{2+}$  cation upon the radiation centers could not be observed in hydroxides. X-ray diffraction patterns have revealed that hydrogen-oxygen molecules of various forms are the principal connecting link in the cementing of the layer of U hydroxides. It seems that a polymerization of the uranyl-hydroxyl radicals  $[\text{UO}_2(\text{OH})_2]^{2+}$  takes place. It is generally accepted [10] that the polymerization leads to an attenuation of the luminescence at 298°K and causes a yellow-orange luminescence at 77°K.

Recognition of Uranyl Minerals

Considerable difficulties are encountered in the recognition of secondary uranium minerals, because these minerals are similar in their color, optical constants, type of aggregation, and paragenesis. Furthermore, the difficulties originate from the problem to isolate the minerals in pure form in amounts which suffice for chemical analysis. The possibilities of Debye diffraction patterns are limited because extensive work must be done to obtain these patterns, though their reproducibility is low. It is therefore most convenient to use the luminescence technique in the beginning for the recognition of the minerals, particularly since the minerals are not destroyed and need be present in amounts of only a few milligrams. In order to supplement the previously known [1-3] luminescence determinations at room temperature, we propose to make luminescence measurements at low temperatures, because a greater number of luminescent minerals can be studied at low temperatures and the accuracy of the measurements increases considerably. It is then usually possible to unambiguously recognize a particular mineral or to determine at least the crystallochemical group of related minerals with the same structure. The standard luminescence spectra of Figs. 1-4 or the characteristics listed in Table 1 can be used for the determination of the minerals.

The proper choice between two or three minerals of a single class is the greatest problem in routine mineralogical determinations. Typical errors are made in the pairs uranophane- $\beta$ -uranotil, uranopilite-zippeite, carnotite-calcio-carnotite. Low-temperature luminescence spectra are particularly useful in similar cases.

## LITERATURE CITED

1. V. G. Melkov and L. Ch. Pukhal'skii, Search for Uranium Deposits [in Russian], Gosgeoltekhizdat, Moscow (1957).
2. M. I. Chaplygin, in: Geochemical Exploration of Ore Deposits in the USSR [in Russian], V. I. Krasnikov (editor), Gosgeoltekhizdat, Moscow (1957), p. 377.
3. E. Z. Bur'yanova, Identification Manual of Uranium and Thorium Minerals [in Russian], Nedra, Moscow (1972).
4. E. Rabinovich and R. Belford, Spectroscopy and Photochemistry of Uranyl Compounds [Russian translation], Atomizdat, Moscow (1968).
5. W. Tufar, Neues Jahrb. Mineral. Abhandl., 106, No. 2, 191 (1967).
6. B. S. Gorobets, et al., in: Radioactive Elements in Rocks. Abstracts of the Reports of the 1st All-Union Radiochemical Conference [in Russian], Press of the Inst. of Geology and Geophysics of the Siberian Division of the Academy of Sciences of the USSR, Novosibirsk (1972), p. 150.
7. E. S. Makarov and V. I. Ivanov, Dokl. Akad. Nauk SSSR, 132, No. 1, 673 (1960).
8. M. Ross, et al., Amer. Mineralogist, 49, 1603 (1964).
9. T. S. Dobrolyubskaya, Zh. Prikl. Spekt., 15, No. 4, 642 (1971).
10. T. S. Dobrolyubskaya, Luminescence Techniques of Uranium Determinations [in Russian], Nauka, Moscow (1968).



## ION FIELD-EMISSION MICROSCOPY OF URANIUM.

## PRELIMINARY RESULTS

A. L. Suvorov, G. M. Kukavadze,  
T. L. Razinkova, B. V. Sharov,  
V. A. Fedorchenko, A. F. Bobkov,  
and B. Ya. Kuznetsov

UDC 535.82:546.791

The unique possibilities provided by ion field-emission microscopy (first of all, the resolution on the atomic scale on surfaces of objects examined) are nowadays by no means fully used. The reason is that it is difficult to obtain ion field-emission images of nonstandard materials (which are of greatest importance for practical applications). Furthermore, it is difficult to interpret the resulting images and to identify on these images atoms of a particular species, molecular complexes, defects of various types, etc.

Analyses by ion field-emission microscopy were not made on new materials (particularly fission materials), mainly because a complete theory of image formation in field-emission microscopes is missing and because the principles on which the evaporation by a field is based are not yet fully understood. The present state of the theory and the most important papers which resulted in progress in this field have been discussed in a review [1].

The goal of the first stage of our work was to determine the possibilities provided by field-emission microscopical investigations of uranium samples, to find the most efficient conditions for the analysis of these samples, and to develop several related methodological details. No doubt, research on the crystal structure, defects, and the dynamics of several processes occurring on both the surface and in the bulk of uranium (and other fission materials) can render new information, when field-emission microscopes are employed.

Except for work on the field-emission microscopy of uranium dioxide [2], there are practically no publications on the ion field-emission or electron field-emission microscopy of fission materials and, particularly, uranium. The work must concern primarily the ion field-emission microscopical investigation of alloys, since the results obtained in this area are of greatest importance.

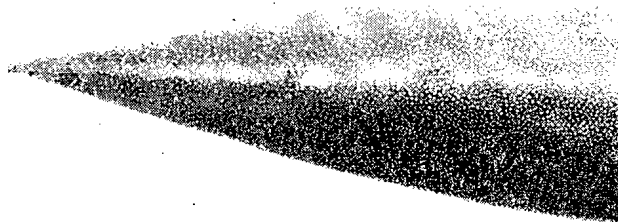


Fig. 1. Optical image of the profile of a typical symmetric uranium point ( $\times 600$ ).

Translated from *Atomnaya Energiya*, Vol. 36, No. 1, pp. 14-18, January, 1974. Original article submitted March 6, 1973.

© 1974 Consultants Bureau, a division of Plenum Publishing Corporation, 227 West 17th Street, New York, N. Y. 10011. No part of this publication may be reproduced, stored in a retrieval system, or transmitted, in any form or by any means, electronic, mechanical, photocopying, microfilming, recording or otherwise, without written permission of the publisher. A copy of this article is available from the publisher for \$15.00.

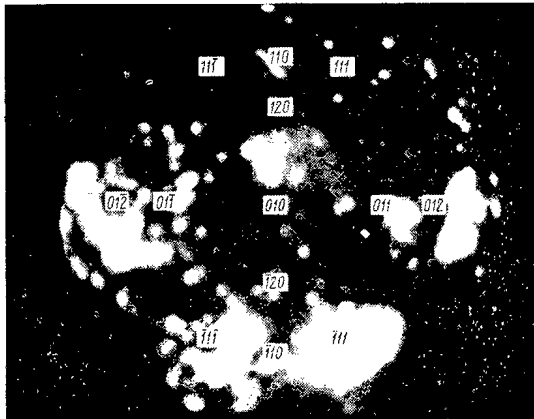


Fig. 2

Fig. 2. Ion field-emission image of the surface of a sample of  $\alpha$ -uranium; the image was obtained in a gas mixture of He + 0.5%  $H_2$  at  $T = 78^\circ K$ . The (010) pole protrudes into the center of the image.

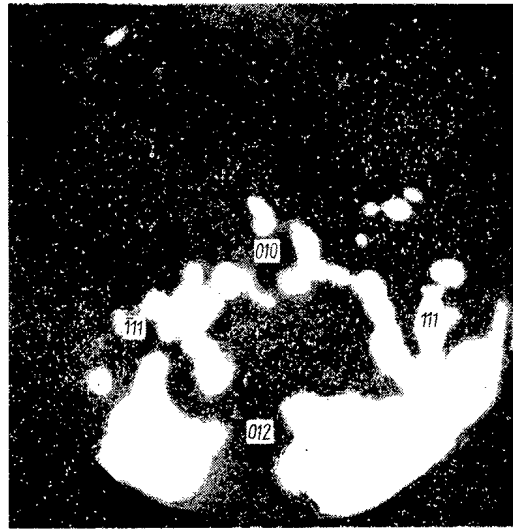


Fig. 3

Fig. 3. Electron field-emission image of a sample of  $\alpha$ -uranium which was smoothed by heating and additionally purified by field-induced evaporation in vacuum.

1. Samples. We used in our work as initial materials wire with a diameter of 0.3 mm (technical, natural uranium) for the samples which had the form of sharp points. We employed the well-known technique of automatic electrochemical etching [3]. The electrolyte consisted of 12% by weight chromium anhydride, 8% by weight orthophosphoric acid, and a small amount of water. The etching was effected in two stages at a constant voltage. In the first stage, the diameter of the wire was reduced to 0.1-0.05 mm ( $U = 12$  V,  $I_{\text{etch}} \approx 100$  mA); in the second stage, the voltage was reduced to 4 V in proportion to the decrease in the current ( $I \approx 30-5$   $\mu A$ ). Sharp points with a typical radius of curvature of less than 1000  $\text{\AA}$  at the tip were formed (Fig. 1). When the etching was effected with a variable voltage, the surfaces of the resulting points were rough and "pitted." After the etching, the finished points were washed in alcohol.

2. Experimental Setup. All experiments were made in the semimetallic sectional field-emission microscope of [4] at a sample temperature of  $78^\circ K$ . The vacuum system of the setup was modernized and made it possible to work with spectrally pure  $H_2$ , He, Ar, and Ne, and mixtures thereof as image-forming gases. The partial pressures of the gases were monitored with the aid of the omegatron of [5]. First, an oil-diffusion pump was used for the pumping and, afterwards, an electric discharge sorption pump. The entire system was heated. The initial minimum pressure amounted to about  $5 \cdot 10^{-8}$  mm Hg.

A three-chamber electro-optical UM-92 converter with magnetic focusing [6] was used to enhance the brightness of the field-emission image. The images were photographed with a "Zenith B" camera having a "Helios-40" lens. The photographs were made on fluorographic RF-3 film. The exposure time depended upon the gas used and amounted to 1-30 sec.

The electron field-emission images of uranium samples were obtained in a sealed electron field-emission microscope of glass. The highest vacuum was in this case  $\sim 1 \cdot 10^{-10}$  mm Hg.

3. Experimental Results and Their Discussion. Theoretical estimates of the evaporating field, which were given in [7] for uranium in vacuum at  $T = 0^\circ K$ , rendered the value  $F_{\text{evap}} = 424$  MV/cm. This means that the use of pure helium as the image-producing gas does not provide a stable ion field-emission image, because the field which is required for autoionization of helium is 450 MV/cm, i. e., the uranium sample evaporates while the reflection image of the sample is made. Neon ( $F_{\text{image}} = 370$  MV/cm) or argon ( $F_{\text{image}} = 230$  MV/cm) are more advantageous from the theoretical viewpoint. However, it is generally accepted that a satisfactory, stable ion field-emission image of a sample depends not only upon the relation between the image-producing and the evaporating fields. Of additional importance is the dynamics of the field-induced evaporation process which is introduced for the final polishing of the sample surface to be

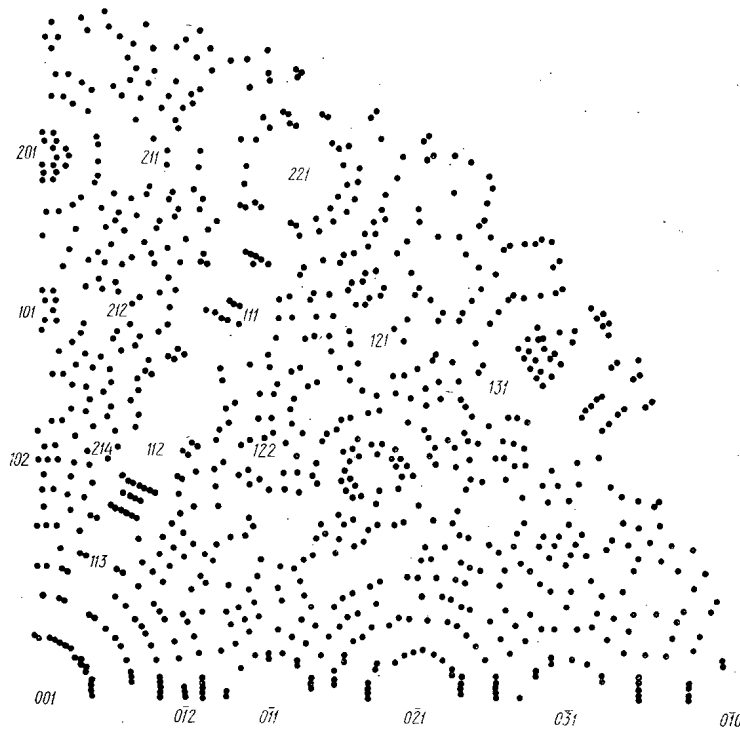


Fig. 4. Computer-calculated model of a sector of the ion field-emission image of a uranium sample oriented parallel to the [001] axis.

projected. The conditions of field-induced evaporation determine the final form of the sample surface. Since no complete theory is available at the present time, the corresponding conditions can be correctly chosen only on an empirical basis derived from numerous experimental data and general concepts. The highly efficient technique of interaction ("facilitating" or "promoting") between field-induced evaporation and autoionization is in a similar development stage [8, 9].

We used  $H_2$ , He, Ne, Ar, and gas mixtures of He + 0.5%  $H_2$ , He-Ne, and Ne-Ar as image-forming gases in research on uranium samples.

**Helium.** The first good result was that high mechanical strength of the needle-like uranium samples could be obtained. The samples sustained the tensile stresses generated by fields of the order of 500-550 MV/cm. A total of about 50 samples were analyzed four of which, i. e., 8%, were destroyed by the interaction with the field. This proves that the theoretical strength of materials [10] can be obtained in samples used for autoionization microscopical analysis. Thus, there exist unique possibilities of verifying the theory. The destruction of the samples can be explained by their symmetry [11] which results in a shearing stress component.

Moreover, our results make it appear doubtful that the above estimates of the evaporating field are reliable. The figures are apparently higher in the case of real samples. This conclusion was drawn in observations of stable helium autoionization images of uranium, which were obtained after field-induced evaporation at increased temperatures. However, information on the crystal structure of the samples cannot be deduced from the resulting images, though a certain symmetry can be recognized on some of the images and though some sets of bright spots can be tentatively identified with rings of plane nets (edges of crystallographic planes).

**Argon.** Argon was more efficient as the image-forming gas. The images obtained with argon exhibit to an increased extent the "tendency to the formation of a ring-shaped structure." However, we must recall that the argon autoionization images were unstable in all cases. This can be explained by the inadequate vacuum conditions which in the case of field-emission microscopy with argon played a deciding role. (The examples of autoionization images of aluminum samples are very significant in this context [12, 13]; changes in the vacuum resulted in a sharp improvement of both quality and resolution of the autoionization images obtained with argon.)

Neon. The autoionization images which were obtained of uranium samples in pure neon had a quality similar to those obtained in argon, but were characterized by increased stability. The brightness of the images obtained in neon is by about an order of magnitude lower than the brightness of the images obtained with argon or helium.

The results of the experiments which were made with pure gases in the above-indicated vacua lead to the general conclusion that the field-induced evaporation in these gases does not result in a final form of the tip of the point required for a detailed reflection pattern of the point's surface.

The best results were obtained when helium with added hydrogen was used as the working gas. The preliminary evaporation of the sample with the aid of a field was effected in this gas mixture and also the

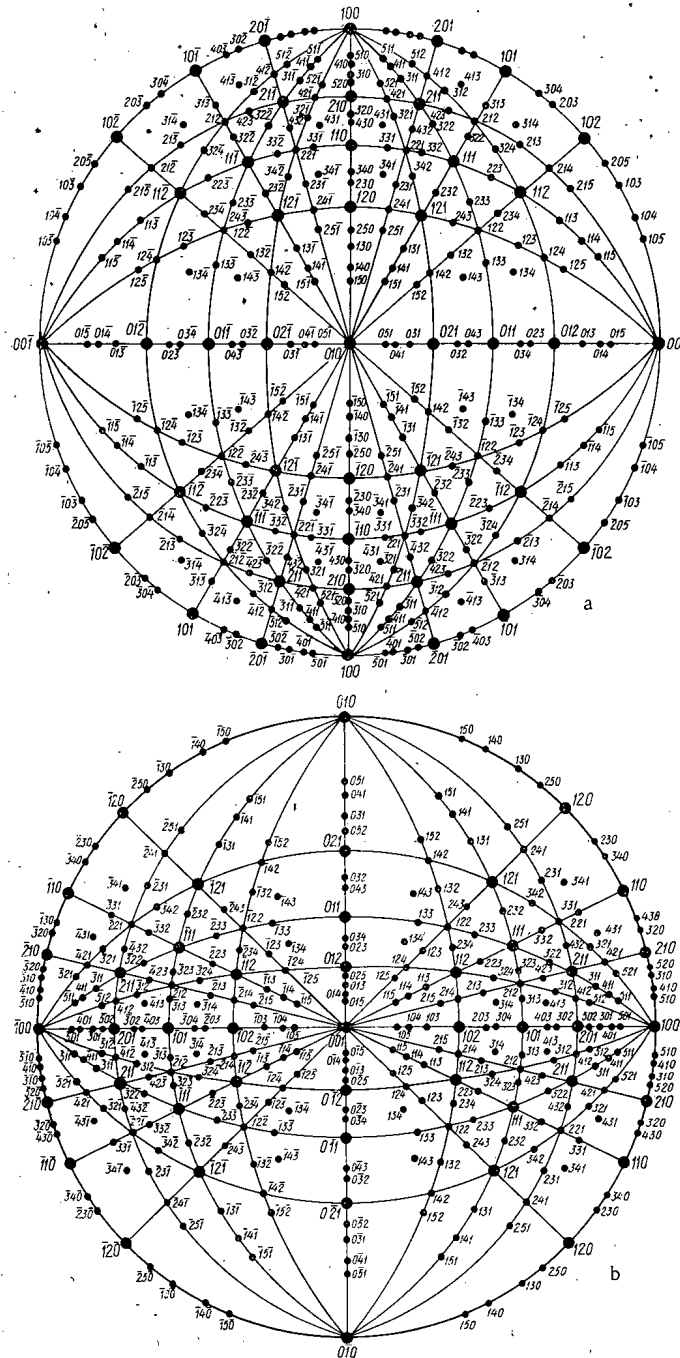


Fig. 5. Standard stereographic projections of  $\alpha$ -uranium upon a) the (010) plane; b) the (001) plane.

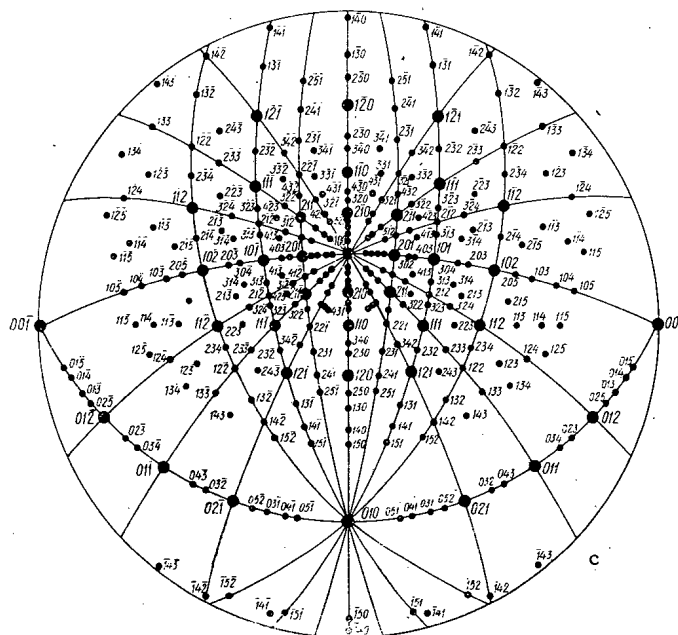


Fig. 5. (Continued, c) the (110) plane.

ion-emission image was obtained. A typical ion field-emission image is shown in Fig. 2. This image made it possible to determine the crystallographic orientation of the sample and to make the crystal faces appear. The images obtained were rather stable. It seems that a further improvement of the image quality will depend upon a careful selection of the amount of hydrogen added and, no doubt, upon improvement of the vacuum.

Attempts to obtain ion field-emission images in pure hydrogen and in He-Ne and Ne-Ar gas mixtures (concentration 50 : 50) were unsuccessful.

The possible plastic deformation and partial destruction of the uranium samples in the field-emission microscope imply that distorted rings of the edges of crystallographic planes, which are unresolved in their atomic details, appear on the image. Moreover, typical streaks of contrast, which were several times discussed [14], appear on all these images. Since asymmetry can be the reason for the deformation and the destruction of the tip in the ion field-emission microscope — with certain contrasts developing — checking the samples (preliminary checks under an optical microscope and subsequent checks after the analysis in the ion field-emission microscope by means of an electron microscope) is not only desirable but also necessary for the correct interpretation of the ion field-emission images.

Figure 3 is the electron field-emission image of an uranium tip which had been smoothed by heating and additionally cleaned by field-induced evaporation in vacuum. Though this image cannot be considered satisfactory, the image still provides some information. With the aid of the methods of electron field-emission microscopy, one can obtain even in the present stage some information on the emission characteristics of uranium.

**4. The Interpretation of the Images.** The interpretation of the images, particularly the determination of the crystal orientation of samples and the indexing of the crystal faces, were effected in two ways: modeling of ion field-emission images, and calculation of standard projections.

Figure 4 shows a computer-calculated model of an ion field-emission image of an  $\alpha$ -uranium sample which was oriented parallel to the [001] axis. The description of the program used for the calculations is included in [15]. A qualitative comparison of the calculated models and the real ion field-emission images makes it possible to determine the crystallographic orientation of the sample. Moreover, the modeling of ion field-emission images of uranium samples must evidently aid in the subsequent understanding of the field-induced evaporation process (obtention of the required final form of the tip). The interpretation of the ion field-emission images by means of the defect structure of uranium cannot be completed without modeling.

Three stereographic projections of  $\alpha$ -uranium (Fig. 5) on the (001), (010), and (110) planes were calculated for indexing the faces on the images of the uranium samples. Our interpretation of the ion

field-emission images has shown that a (010) pole protrudes into the center of the image. This effect is related to the technology of preparing the samples for the investigations. A wire with a diameter of 0.3 mm is usually obtained [16] by wire drawing at low temperatures (150-200°C), which renders a texture of the {010} type.

The calculations were made for the faces with the low indices (it is well known that the morphological importance of a crystal face is inversely proportional to the quantity  $S = \sqrt{h^2 + k^2 + l^2}$ , where h, k, and l denote the Miller indices). The calculations were extended to the {521} faces. The calculated stereographic projections made it possible to determine the crystallographic orientation of the uranium samples examined and to provide the main faces with indices (see Fig. 2).

The authors thank Yu. G. Abov for his interest in the present work.

#### LITERATURE CITED

1. A. L. Suvorov and V. V. Trebukhovskii, *Usp. Fiz. Nauk*, **107**, 657 (1972).
2. R. Morgan, *J. Mater. Sci.*, **5**, 445 (1970).
3. M. I. Elinson, V. A. Gor'kov, and G. F. Vasil'ev, *Radiotekhnika i Élektronika*, **11**, 204 (1957).
4. V. A. Kuznetsov, G. M. Kukavadze, and A. L. Suvorov, *Pribory i Tekh. Éksperim.*, No. 2, 152 (1969).
5. A. P. Averina, *Pribory i Tekh. Éksperim.*, No. 3, 123 (1962).
6. M. M. Butslov et al., *Pribory i Tekh. Éksperim.*, No. 6, 137 (1971).
7. E. V. Muller, *Usp. Fiz. Nauk*, **92**, 293 (1967).
8. E. Muller et al., *J. Appl. Phys.*, **36**, 2496 (1965).
9. E. V. Muller, in: *The Field-Emission Microscope* [Russian translation], Mir, Moscow (1971), p. 94.
10. R. I. Garber, Zh. I. Dranova, and I. M. Mikhailovskii, *Fizika Metallov i Metallovedenie*, **30**, 445 (1970).
11. E. V. Muller, *Usp. Fiz. Nauk*, **77**, 481 (1962).
12. R. Morgan, *J. Mater. Sci.*, **7**, 361 (1972).
13. P. Turner, B. Regan, and M. Southon, *Electron Microscopy and Analysis*, The Institute of Physics, London-Bristol (1971), p. 252.
14. S. Ranganatan, in: *The Field-Emission Microscope* [Russian translation], Mir, Moscow (1971), p. 127.
15. T. L. Razinkova, A. G. Sokolov, and A. L. Suvorov, *Automation of Scientific Investigations* [in Russian], Zinatne, Riga (1972), p. 208.
16. Yu. N. Sokurskii, Ya. M. Sterlin, and V. A. Fedorchenko, *Uranium and its Alloys* [in Russian], Atomizdat, Moscow (1971).

THE FLEXURAL STRENGTHS OF DISPERSE MATERIALS  
 BASED ON URANIUM AND MOLYBDENUM DIOXIDES  
 BETWEEN 293 AND 1870°K

L. E. Kakushadze and R. B. Kotel'nikov

UDC 621.039.542.33

The serviceability of disperse fuel elements depends largely on their mechanical strength. The strengths of ceramic materials are usually measured by means of flexural or compression tests.

We investigated cermets of uranium dioxide particles,  $-315 + 200 \mu$  diameter, covered with molybdenum, and mixtures of uranium dioxide granules with molybdenum powder. The preparation technology and some properties of these materials were described in a previous article [1]. By hot pressing we first prepared billets in the form of cylinders 10 mm in diameter and 20 mm long. With a diamond disc, without cooling liquid, from each billet we cut four rectangular specimens  $3 \times 3$  mm in cross section and 15 mm long. In the cross section of each such specimen there were about 150 uranium dioxide particles. In the course of his argument, Tret'yakov [2] remarks that in flexure tests on cermets of the VK (tungsten-cobalt) hard-alloy type, the admissible ratio between the intersupport spacing and the specimen thickness is 3-4. In our experiments this quantity was 3.43. The marks left by the diamond cutter were longitudinal in direction. Specimens with surface defects were smoothed along the axis with dry M-20 emery paper. In all cases at least one face was left untouched after diamond cutting. In the tests, the specimen was placed on the support so that the diamond-cut face was subjected to tension. Thus we can assume that all the specimens had identical mechanical treatment of the surface — diamond cutting with the marks along the principal axis. The specimens were not heat-treated after cutting. The density of the specimens was  $96 \pm 1.2\%$  of the theoretical value. The scheme of loading and heating is shown in Fig. 1. The distance between the tungsten support prisms was 10.3 mm. The specimen was loaded at  $4.08 \cdot 10^5 \text{ N/m}^2 \cdot \text{sec}$  (or  $2.5 \text{ kg/mm}^2 \cdot \text{min}$ ). The specimen was heated by radiation from a strip heater through which power-frequency current was passed. To reduce heat losses, the high-temperature zone was protected by a system of screens. The specimen surface temperature was measured by means of an OPPIR-09 optical pyrometer through holes in the screens and heater. The pyrometer was calibrated against a platinum-platinum-rhodium thermocouple attached to the specimen. The working medium for the tests was high-purity helium containing about 0.012 vol. % of impurities (according to its rating). Before admission to the apparatus, the helium was repurified by passing it through silica gel, copper shavings at 1000°K, and silica gel again. The fact that the lattice parameters of the phases of the cermets and the specimen surface color remained unaltered after the high-temperature experiments showed that the helium was pure enough for the work. During the experiments, the excess helium pressure in the furnace chamber was  $5 \cdot 10^2 \text{ N/m}^2$  (or 3.7 mm), and the volumetric flow rate through the chamber (which was about  $5 \cdot 10^{-3} \text{ m}^3$  in volume) was  $4.2 \cdot 10^{-6} \text{ m}^3/\text{sec}$ . At each temperature we tested at least three or four specimens from

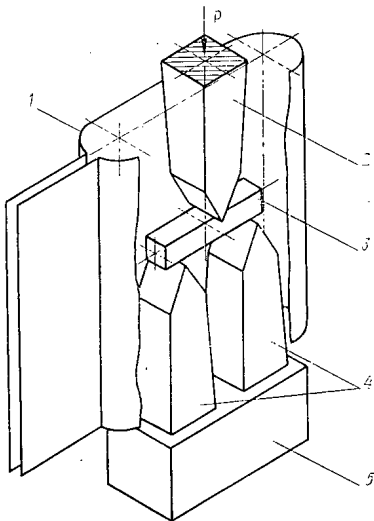


Fig. 1. Scheme of apparatus for flexural tests. 1) Tantalum sheet heater; 2) tungsten loading prism; 3) specimen; 4) tungsten support prisms; 5) molybdenum block.

Translated from *Atomnaya Energiya*, Vol. 36, No. 1, pp. 19-23, January, 1974. Original article submitted April 12, 1973.

© 1974 Consultants Bureau, a division of Plenum Publishing Corporation, 227 West 17th Street, New York, N. Y. 10011. No part of this publication may be reproduced, stored in a retrieval system, or transmitted, in any form or by any means, electronic, mechanical, photocopying, microfilming, recording or otherwise, without written permission of the publisher. A copy of this article is available from the publisher for \$15.00.

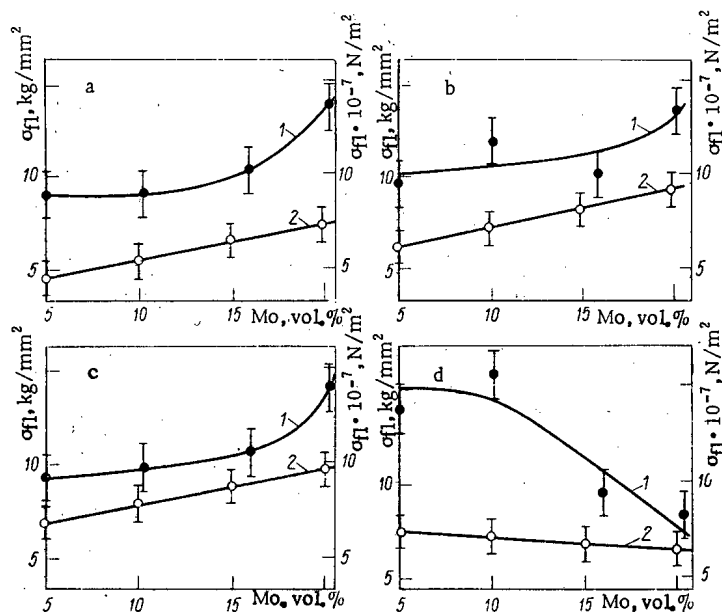


Fig. 2. Static flexural strength of cermets of uranium dioxide and molybdenum vs composition at various temperatures in °K: a) 293; b) 1240; c) 1570; d) 1870. 1) Cermet of molybdenum-coated particles; 2) mixed cermet.

a given batch. The flexural strength was calculated by means of the usual formula. On inspecting the broken specimens we found no appreciable bending even after tests at 1870°K. Fracture occurred in a plane perpendicular to the principal axis of the specimen. Regardless of the type of cermet, the composition, and the test temperature, fracture occurred across the particles of uranium dioxide. There was no preferential fracture in the molybdenum interlayers or "husking" of the uranium dioxide particles from the molybdenum matrix. The deviations from the mean value, plotted in Figs. 2 and 3, correspond to the root-mean-square deviations of the experimental points for the given type of cermet. From these results we can draw the following conclusions.

Over the whole range of compositions and temperatures examined, the coated-particle cermet is stronger than the mixed cermet.

At temperatures between 293 and 1500°K we observe that the strengths of both types of cermet tend to rise with increasing molybdenum concentration. The cause of this is apparently that molybdenum is stronger than uranium dioxide, as we see from Fig. 4. Here we must bear in mind that the experimentally measured flexural strength may be several times greater than the tensile strength, despite the fact that fracture is due to tensile stresses in both cases. For example, Rudeňko [3], who investigated a material based on silicon carbide at 290-1670°K, showed that the flexural strength is 2.5 times higher than the tensile strength. Consequently the tensile strength of uranium dioxide must be below the values given by curves 1-3 in Fig. 4.

When the temperature increases from 293 to 1500°K we observe a tendency for the strengths of both types of cermet to increase. On the basis of investigations of a number of substances, Savitskii [4] showed that the strengths of brittle materials increase on heating owing to the appearance of a certain amount of plasticity which reduces the stress concentrations and makes it possible for the material to exert its total strength. The temperature range of maximum strength of brittle materials is 0.5-0.8 times the absolute melting point for tension, and 0.5-0.7 times the absolute melting point for compression. So we can assert that the strengths of the cermets increase with temperature, mainly owing to increase in the strength of the uranium dioxide (see Fig. 4) and decrease of the microstresses in the cermet. The strength of molybdenum decreases with rise of temperature. But the strength of the cermets can nevertheless rise over a certain temperature range owing to the increasing strength of the uranium dioxide, because the molybdenum concentration is not very great. The thermal expansion coefficient of uranium dioxide is about twice that of molybdenum. Therefore stresses arise in microvolumes of the cermet during cooling of the specimens in the course of preparation. A similar problem of the stresses in a two-phase system was solved theoretically by Zaitsev [5], and the results were confirmed in investigations of the microstresses in the carbide



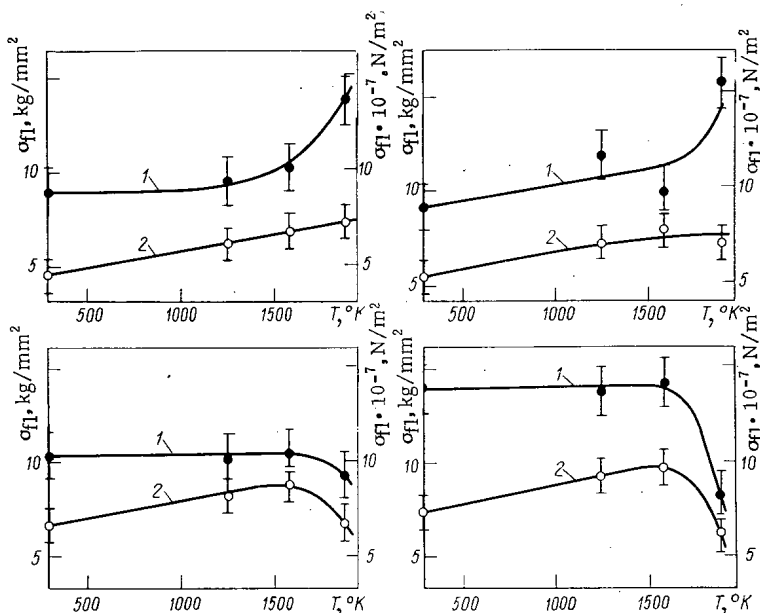
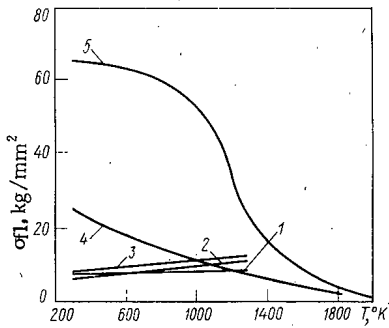


Fig. 3. Static flexural strength of cermets of uranium dioxide and molybdenum, of various compositions, vs temperature. 1) Cermet of molybdenum-coated particles; 2) mixed cermet. Molybdenum concentrations in cermets: a) 5.2 and 5; b) 10.3 and 10; c) 16.0 and 15; d) 20.3 and 20 vol. %.

phase of a VK alloy by the x-ray method [6]. The theoretical results for cermets of molybdenum-coated uranium dioxide particles are plotted in Fig. 5. In the calculation it was assumed that  $E_{Mo} = 2.94 \cdot 10^{11}$  N/m<sup>2</sup> [7],  $E_{UO_2} = 1.71 \cdot 10^{11}$  N/m<sup>2</sup> [8], and  $\mu_{Mo} = \mu_{UO_2} = 0.3$ . Information on the thermal expansion of the phases was taken from [9] and [10]. During cooling, in uranium dioxide undergoing "hydrostatic" pressure from the molybdenum, all three principal stresses are equal, but in the molybdenum the determining stresses are the shear stresses  $\tau$ , which reach a maximum at the interior surface of the coating lying against the uranium dioxide. At high temperatures, stress relaxation occurs. When the cermet is cooled below the recrystallization temperature of molybdenum (about 1270°K), the stress removal process ceases. The stresses should not exceed the yield point for molybdenum or the breaking strength for uranium dioxide. At 293°K the yield point of molybdenum is  $70 \cdot 10^7$  N/m<sup>2</sup> [7], which is below the calculated value  $\tau_{max} \approx 100 \cdot 10^7$  N/m<sup>2</sup> (see Fig. 5). Consequently, on cooling, either the molybdenum should undergo plastic deformation, or the dioxide should break, or fracture should occur at the boundary between the uranium dioxide and the molybdenum. From Figs. 4 and 5 we see that the stresses in the uranium dioxide particles, at any rate for molybdenum concentrations less than 10 vol. %, exceed even the flexural strength, which, as we have stated, is higher than the tensile strength. Despite the decrease of these stresses due to plastic deformation of the molybdenum, they remain high. It was on account of precisely these stresses that, in all the prepared cermets we observed particles of uranium dioxide broken by cracks, as we see, for example, on a photograph of the microstructure (see figure in [1]). During heating, the tensile stresses in the uranium dioxide particles decrease, and at a certain temperature compressive stresses, which of course are much better withstood by brittle materials, can arise in them. In this state the cermet can be likened to prestressed concrete. Under the compressive stresses, the cracks, which arose in the uranium dioxide particles during cooling, begin to grow. Therefore the strength of the cermets increases as the temperature rises to a certain limit.

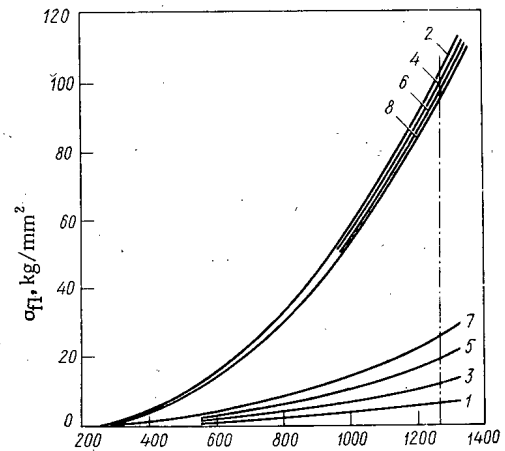
As the temperature increases from 1500 to 1870°K, for cermets with molybdenum concentrations of 5 and 10 vol. % we observe a tendency to increase of strength, whereas the strength of cermets with molybdenum concentrations of 15 and 20 vol. % falls. This phenomenon is apparently due to a decrease in the strength of pure molybdenum to a value below that of uranium dioxide. It must be borne in mind that the area of contact between the uranium dioxide particles and the molybdenum is four times as great as the diametral cross section of the former. Therefore fracture does not at all have to occur in the weakest phase, i. e., the molybdenum. In tests throughout the investigated temperature range, fracture occurs across the uranium dioxide particles, as we have already stated. A decrease in the strength of the molybdenum has little effect on the strength of specimens in which its concentration is low, but specimens in



Curve	Material	Method of preparation	Characteristics of material	Reference
1	UO <sub>2</sub>	Cold-pressed and sintered in argon at 2270°K for 30 min. Specimen dimensions: 38.1 × 6.4 × 3.2 mm	γ = 84.3% theor. Particle dimensions of original powder, 10 - 15μ	[11]
2	UO <sub>2</sub>		γ = 90% theor. Particle dimensions of original powder, 0 - 5μ	
3	UO <sub>2</sub>		γ = 82.8% theor. Particle dimensions of original powder, 0 - 5μ	
4		Pressed powder, sintered, hot-rolled recrystallized	Purity of original powder, 99.98%	[12]
5		Same material without recrystallization		

Fig. 4

Fig. 4. Temperature dependences of flexural strength of uranium dioxide and tensile strength of molybdenum.



Curve	1	2	3	4	5	6	7	8
Mo concentration vol. %		5	10		15		20	
Phase	UO <sub>2</sub>	Mo	UO <sub>2</sub>	Mo	UO <sub>2</sub>	Mo	UO <sub>2</sub>	Mo

Fig. 5

Fig. 5. Thermal stresses in phases of cermet at 293°K vs the temperatures at which they cease to relax during cooling.

which its concentration is high lose strength. Furthermore, molybdenum present in cermet, as suggested with some justification by us to explain the conductivity [1], must contain uranium and oxygen from the dioxide as impurities. The strength of such a solid solution at high temperatures may be higher than that of pure molybdenum. Since impurities penetrate the molybdenum layers only to a certain depth, if the molybdenum concentration is low the layers will consist wholly of solid solution, but if it is high they will consist largely of pure molybdenum. Therefore the influence of the impurities decreases as the molybdenum concentration increases, and the strength at high temperatures thus falls.

## LITERATURE CITED

1. L. E. Kakushadze and R. B. Kotel'nikov, *At. Énerg.*, 36, No. 1 (1974).
2. V. I. Tret'yakov, *Cermet Solid Solutions* [in Russian], Metallurgizdat, Moscow (1962).
3. V. I. Rudenko, *Poroshkovaya Met.*, No. 4, 86 (1961).
4. E. M. Savitskii, *The Influence of Temperature on the Mechanical Properties of Metals and Alloys* [in Russian], Izd-vo AN SSSR, Moscow (1957).
5. G. P. Zaitsev, *Fiz. Metallov i Metallovedenie*, 2, No. 3, 494 (1956).
6. A. E. Koval'skii et al., in: *Data on Metallurgy and the Technology of Preparation of Cermet Solid Solutions, Refractory Metals, and Materials Based on Them* [in Russian], V. F. Funke (editor), Izd. TsIItsvetmet, Pt. 2 (1963), p. 29.
7. A. K. Natanson (editor), *Molybdenum* [Russian translation], IL, Moscow (1959).
8. Yu. N. Sokurskii (editor), *Materials for Nuclear Reactors* [Russian translation], Gosatomizdat, Moscow (1963).

9. J. Belle (editor), Uranium Dioxide, USAEC, Washington (1961).
10. A. E. Coldstith, A Handbook of Thermophysical Properties of Solid Materials, Vols. I-III, Pergamon Press, Oxford-Paris (1961).
11. M. Burdick and H. Parker, J. Amer. Ceram. Soc., 39, No. 5, 180 (1956).
12. B. L. Mordai, Probl. Sovrem. Metallurgii, No. 4, 149 (1960).

## RADIATION-INDUCED SWELLING OF 0Kh16N15M3B STEEL

V. N. Bykov, A. G. Vakhtin,  
V. D. Dmitriev, L. G. Kostromin,  
A. Ya. Ladygin, and V. I. Shcherbak

UDC 621.039.54

A large number of published papers have been devoted to studying the radiation-induced porosity of the austenitic steels used as construction materials in the active zone of fast reactors. Nevertheless, there is still no reliable information as to the temperature and dose dependence of the radiation-induced swelling of 0Kh16N15M3B steel, which is widely employed as a material for the fuel-element cans of fast reactors.

In this paper we shall present certain results obtained by the electron-microscope analysis of radiation-induced porosity in 0Kh16N15M3B steel irradiated with neutrons in the BR-5 reactor.

## MATERIALS AND METHOD

The samples for electron-microscope study were discs 3.5 mm in diameter and 0.4 mm thick, cut from various parts of fuel-element cans irradiated in the BR-5 reactor with integrated fluxes of  $4.3 \cdot 10^{22}$  neutrons/cm<sup>2</sup> at 430-580°C. After preparation the fuel-element cans were annealed at 950°C for 10 min in vacuo.

The preparation of the objects for examination under the electron microscope and the method of analyzing the results were described earlier [1]. We should only mention that, in contrast to the present investigation, the film thickness there lay between 1200 and 2000 Å, the porosity being calculated by another method [2].

Swelling of 0Kh16N15M3B Steel

Electron-microscope examination of the irradiated samples revealed the presence of inclusions,

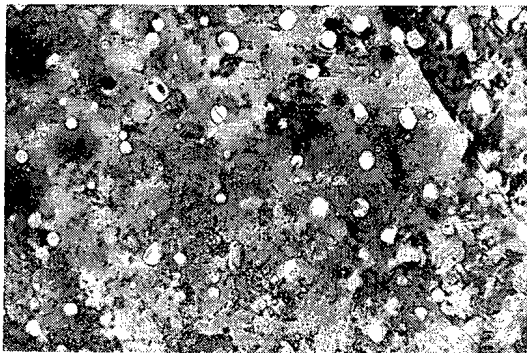


Fig. 1

Fig. 1. Microstructure of 0Kh16N15M3B irradiated with a dose of 36 displacements/atom at 520°C ( $\times 100,000$ ).

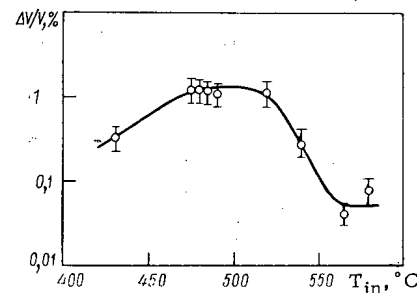


Fig. 2

Fig. 2. Swelling of 0Kh16N15M3B steel irradiated with a dose of 30 displacements/atom as a function of the irradiation temperature.

Translated from *Atomnaya Energiya*, Vol. 36, No. 1, pp. 24-26, January, 1974. Original article submitted May 28, 1973.

© 1974 Consultants Bureau, a division of Plenum Publishing Corporation, 227 West 17th Street, New York, N. Y. 10011. No part of this publication may be reproduced, stored in a retrieval system, or transmitted, in any form or by any means, electronic, mechanical, photocopying, microfilming, recording or otherwise, without written permission of the publisher. A copy of this article is available from the publisher for \$15.00.

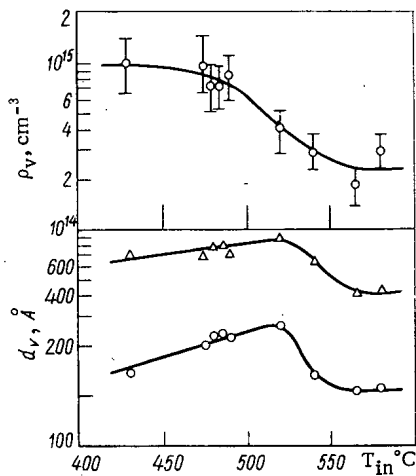


Fig. 3

Fig. 3. Concentration, mean diameter (O), and maximum diameter (Δ) of cavities in 0Kh16N15M3B steel irradiated with a dose of 30 displacements/atom, as functions of the irradiation temperature.

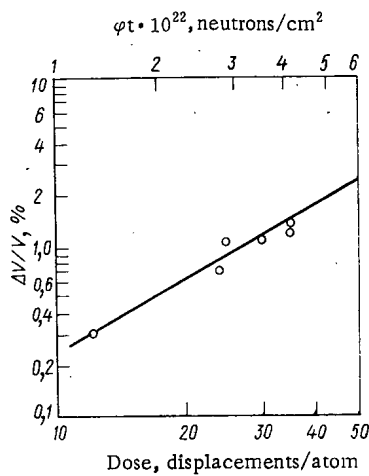


Fig. 4

Fig. 4. Dose dependence of the swelling of 0Kh16N15M3B steel at 525°C.

loops, and cavities, the dimensions and concentrations of these varying with the conditions of irradiation. Figure 1 shows the microstructure of 0Kh16N15M3B steel irradiated with an integrated flux of  $4.3 \cdot 10^{22}$  neutrons/cm<sup>2</sup> at 520°C. The concentrations  $\rho_v$ , mean diameter  $d_v$ , and total volume of the cavities  $\Delta V/V$  (the latter being taken as equal to the total swelling of the steel) calculated on the basis of the electron micrographs are illustrated in Figs. 2-5. The size distribution of the cavities is shown in relation to the dose of irradiation in Fig. 6.

Since the experimental results as to the radiation-induced swelling were obtained for samples irradiated in neutron fluxes having a variety of spectral characteristics, the experimental data were compared by reference to the number of displacements per atom (kt) (d/a) rather than by reference to the integrated flux. For this calculation we used a modified displacement model developed for the irradiation of materials by fast neutrons [3]. For comparison, Figs. 4 and 5 also show the integrated neutron fluxes for an energy spectrum corresponding to the center of the active zone in the BR-5 reactor.

Experimental examination shows that the radiation-induced swelling of steels depends on a large number of factors, primarily the irradiation dose and temperature. It is accordingly of particular interest to devote more detailed attention to the way in which the total volume of the cavities depends on these factors.

Temperature Dependence of the Swelling. The total volume of the cavities first increases with temperature (Fig. 2), reaching a value of 1.4% for 30 displacements/atom, and then falls, i. e., the temperature dependence of  $\Delta V/V$  has a bell-shaped form with a maximum in the region of 500°C. The increase in  $\Delta V/V$  on raising the temperature from 430 to 500°C (Fig. 3) is associated with an increase in the dimensions of the cavities, since the concentration of the cavities has a tendency to fall with rising temperature in this region. On further raising the irradiation temperature to 560°C the concentrations and mean diameter of the cavities both diminish. For an irradiation temperature of over 560°C the concentration and mean diameter of the cavities hardly depend on the temperature at all — if anything they increase slightly. The dependence of  $\rho_v$  on T may be explained as being due to a fall in the rate of formation of the cavity nuclei with increasing temperature, owing to a reduction in the degree of supersaturation of the matrix with point defects.

As regards the physical reasons for the change in the mean size of the cavities, the following should be noted. It follows from the expression for the rate of growth of a vacancy-type cavity of radius r [4]

$$\frac{dr}{dt} = \frac{1}{r} \left[ (C_v D_v - C_I D_I) - D_s \exp\left(\frac{2\gamma\Omega}{rkT}\right) \right],$$

where  $C_v D_v$  and  $C_I D_I$  are the diffusion flows of vacancies and interstitial atoms at the surface of the cavity,  $D_s$  is the self-diffusion coefficient,  $\gamma$  is the surface energy, and  $\Omega$  is the atomic volume, that the quantity

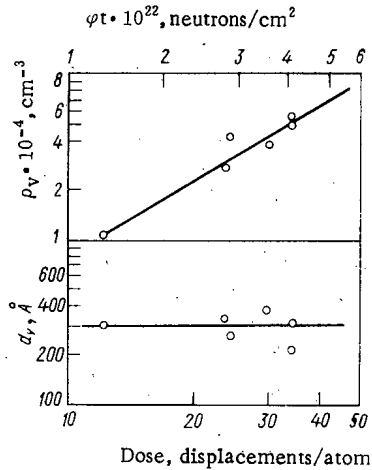


Fig. 5

Fig. 5. Dose dependence of the mean diameter and concentration of the cavities in 0Kh16N15M3B steel at 525°C.

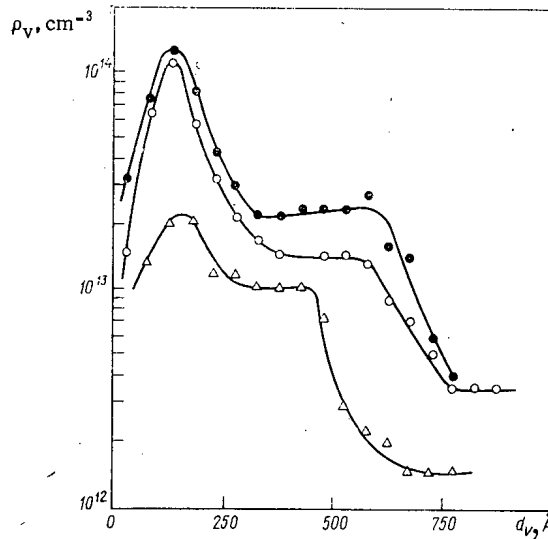


Fig. 6

Fig. 6. Size distribution of the cavities in 0Kh16N15M3B steel irradiated with doses of 36 (●), 30 (○), and 12 (Δ) displacements/atom at 525°C.

$dr/dt$  is determined by the ratio of two terms: the first describes the difference in the diffusive flows of point defects at the surface of the cavity, the second describes the thermal annealing of the cavity.

On increasing the irradiation temperature from 430 to 525°C, the radius of the cavity may also increase owing to the increase in the excess flow of vacancies to the surface of the pore as a result of the increase in the mobility of the vacancies, despite the reduction in the concentration of these as the temperature rises. At the same time, the second term in the equation for  $dr/dt$ , always negative for vacancy pores, also increases with rising irradiation temperature, owing to the increase in the self-diffusion coefficient.

The reduction in the supersaturation of the matrix with point defects and the intensification of the thermal dissociation of the cavities may be used to explain the reduction in the mean diameter of the cavities for 0Kh16N15M3B steel for irradiation temperatures above 525°C.

However, from 560°C the character of the temperature dependence of  $\rho_V$  and  $d_V$  changes once again: on further raising the temperature the concentration and mean diameter of the cavities hardly depend on temperature at all. This kind of change in the kinetic characteristics representing the generation and growth of the cavities may presumably be explained as being due to the stabilizing influence of the helium formed as a result of  $(n, \alpha)$ -reactions in the steel under consideration. Estimates based on the van der Waals equation, in fact, showed that the stabilization of these cavities at 560°C required  $2 \cdot 10^{-3}$  at. % of helium for a value of  $\gamma = 1500$  erg/cm<sup>2</sup> and a van der Waals constant of  $4 \cdot 10^{-23}$  cm<sup>3</sup>/atom He. We note that recent work on the experimental determination of the amount of helium in irradiated steels of the 304 [5] and 347 [6] types has shown that the helium content of these materials (for comparable dose of irradiation) greatly exceeds the calculated contents, being equal to  $3 \cdot 10^{-2}$  and  $(9-10) \cdot 10^{-2}$  at. %, i. e., an order of magnitude greater than is required for the stabilization of the cavities in our own case.

**Dose Dependence of the Swelling.** The volume increment due to the formation of cavities in both 0Kh16N15M3B steel and steel of the 316 type [7] varies with the irradiation dose in accordance with a power law (Fig. 4). The graphically-determined power index for an irradiation temperature of 525°C is slightly less for our present material than for steel 316 and equals 1.5. Extrapolation of the experimental data to a dose of 85 displacements/atom, corresponding to an integrated flux of  $10^{23}$  neutrons/cm<sup>2</sup>, shows that, on allowing for the foregoing power index, the maximum swelling of the steel for this dose may amount to 6-7%.

The increase in  $\Delta V/V$  with increasing  $kt$  is chiefly associated with the development of new cavities (Fig. 5), since the mean diameter of the cavities hardly depends on the dose at all.

We see from the size distributions of the cavities illustrated in Fig. 6 (for irradiation with a variety of doses at the same temperature) that the size dependence of  $\rho_V$  is of a complex nature. The reason for this may lie in the effects of a whole series of factors (stress, the presence of gas, and so on) on the generation and growth of the cavities.

Analysis of the changes taking place in the size-distribution curves of the cavities with increasing irradiation dose indicates that with increasing number of displacements per atom the character of the relationship between  $\rho_V$  and  $d$  remains almost constant; there is only a slight rise in these curves in the direction of greater concentrations and a slight displacement in the direction of greater sizes. Thus the experimental results indicate that, on irradiating 0Kh16N15M3B steel, the development of porosity takes place chiefly by virtue of the growth of new cavity nuclei.

## LITERATURE CITED

1. V. N. Bykov et al., *At. Énerg.*, 34, No. 4, 247 (1973).
2. E. Wolff, *Metallography*, 2, 89 (1969).
3. K. Ohmae and B. Hida, *J. Nucl. Mater.*, 42, 86 (1972).
4. D. Norris, *Radiation Effects*, 14, 1-37 (1972).
5. K. Robins, *J. Nucl. Mater.*, 33, 102 (1969).
6. A. Bauer and M. Kangilaski, *J. Nucl. Mater.*, 42, 91-95 (1972).
7. H. Brager and I. Straalsund, *Trans. Amer. Nucl. Soc.*, 15, 725 (1973).

## UTILIZATION OF PULSED SORPTION COLUMNS FOR THE DECONTAMINATION OF LIQUID RADIOACTIVE WASTES

F. V. Rauzen, E. I. Zakharov,  
B. E. Ryabchikov, V. D. Konorchenko,  
and E. G. Odintsova

UDC 621.039.325

An increase in the efficiency and economy of the decontamination of liquid radioactive wastes by an ion exchange process can be attained by improvement in its technology and instrumentation. Pulsed columns with special partition plates, developed in the USSR [1-2], which are prospective ion-exchange apparatus, are applied in a number of hydrometallurgical processes, including the decontamination of waste liquids [3, 4]. In industry, continuous ion-exchange installations operate with a performance of up to 300 m<sup>3</sup>/h, utilizing columns up to 3.4 m in diameter. The advantages of these apparatus are the small once-only charging of the sorbent into the installation (5-15 times smaller than into filters), high specific performance ( $W_p = 35-45 \text{ m}^3/\text{m}^2\text{h}$ ), small size, and simplicity of design and control [5].

The purpose of the present study was an examination of the possibility for applying these apparatus to the decontamination of liquid radioactive wastes.

### Design and Operation of Pulsed Columns

A pulsed counterflow column with multilayer column packing (MCP) is a vertical cylinder inside which downfall plates are mounted; settling zones for separating the sorbent and the solution are spaced from top to bottom (Fig. 1).

Connections for the pulse chamber and the air-lift, which pumps the resin to the connecting pipe for the inlet and outlet of the sorbent and the solution, are found in the zones. Downfall plates with a 40-60% transfer cross section in conjunction with the pulsations (reciprocating oscillation of the liquid in the column) provide a better distribution of the components over the cross section of large apparatus with little longitudinal mixing.

During operation of the column, the sorbent is fed into the upper zone, from which it enters the packed section, where it moves owing to the difference in the densities of the phases (as a pseudoliquid) in the flow of the solution.

The saturated sorbent is collected in the lower settling zone, from which it is pumped by the air-lift into the next device, as shown in the diagram. Draining from the upper zone, the solution proceeds to further treatment.

A continuous-action sorption facility usually consists of three columns: sorption, regeneration, and washing (Fig. 2). Separators are used to recover the solution conveying the sorbent in the air-lift. The sorbent moves from the separators into the next column, but the transporting solution returns to the apparatus.

During pulsation, the solution is intensively agitated by each plate; therefore the rate of diffusion of the ions in the solution does not restrict the process and the rate of exchange. Because of this, the requisite contact time of the sorbent with the solution and its charging time are reduced.

The velocity of the solution in the column must be somewhat lower than that, for which a small fraction of the sorbent can be removed. This velocity ( $V_s$ ) is  $0.8V_0$  during sorption, where  $V_0$  is a characteristic velocity of the sorbent, i. e., the rate of fall of an average fraction of it in a motionless solution.

---

Translated from *Atomnaya Energiya*, Vol. 36, No. 1, pp. 27-31, January, 1974. Original article submitted April 20, 1972; revision submitted March 6, 1973.

© 1974 Consultants Bureau, a division of Plenum Publishing Corporation, 227 West 17th Street, New York, N. Y. 10011. No part of this publication may be reproduced, stored in a retrieval system, or transmitted, in any form or by any means, electronic, mechanical, photocopying, microfilming, recording or otherwise, without written permission of the publisher. A copy of this article is available from the publisher for \$15.00.



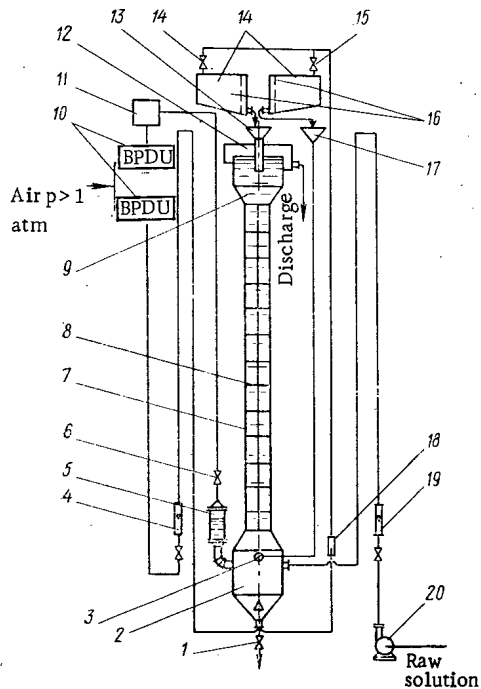


Fig. 1

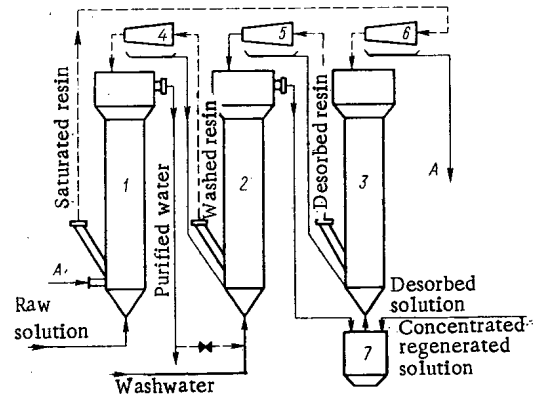


Fig. 2

Fig. 1. Diagram of the framework of a pulsed sorption column in a test facility: 1) connecting pipe for emptying the column; 2) lower settling zone; 3) connecting pipe for recovery of the solution; 4) air rotameter; 5) pulse chamber; 6) valve; 7) packing zone; 8) column packing; 9) upper settling zone; 10) pressure stabilizer; 11) pulser; 12) overflow box; 13) funnel; 14) sorbent and solution feeder-separators; 15) valve; 16) screen; 17) solution recovery line; 18) air-lift; 19) raw solution rotameter; 20) pump.

Fig. 2. Diagram of a continuous-action facility: 1) sorption; 2) washing; 3) regeneration columns; 4-6) separators for the recovery of the sorbent from solution; 7) container for preparation of regenerating solution.

Provided that retention of the sorbent  $\Omega$  (holdup) in the column for a flow rate ratio  $n = Q_{sb}/Q_l = 1:50-1:500$  is small and comprises 0.5-5% (the sorbent occupies a very small part of the volume and the cross section of the column), the actual velocity of the solution and the specific performance agree numerically. Therefore, the specific performance of these columns is significantly higher than other apparatus [6, 7] with a quasi-liquid layer of sorbent.

The rate of movement of the sorbent through the apparatus depends on the velocity of the solution:  $V_{sb} = (V_0 - W_p)\varphi$ , where  $\varphi$  is a coefficient which takes into account the retardation of the movement of the solution. The coefficient equals one during sorption, when the retardation is small, and 0.6-0.8 during regeneration and washing, when  $\Omega = 10-30\%$ . Under optimal conditions, the rate of fall of the sorbent is  $V_s = 20-30$  m/h, which corresponds to a residence time  $\tau_{sb} = 2-3$  min/m of column height.

Calculation of Columns. The calculation of pulsed sorption columns is known from the methods applicable to the calculation of extraction columns [8, 9], since the behavior of the sorbent particles in them is similar to the behavior of the dripping of the dispersed phase during extraction. Data on the kinetics and the statics of the processes, the hydrodynamics of the column, as well as a mathematical model of the apparatus are required for the calculation. Knowing these parameters, one can calculate the diameter and the height of the apparatus, and then design an industrial facility, using mathematical simulation techniques.

The kinetics and statics of a process have been studied in standard solutions which duplicate the composition of solutions from Moscow decontamination plants, in which the cations  $Na^+$  and  $Ca^{2+}$  and the anions  $Cl^-$  and  $SO_4^{2-}$  comprise the main bulk of the contaminants.

Knowing the kinetics of a process, one can calculate the height equivalent to a theoretical plate (HETP). From Fig. 3, it is seen that equilibrium is established in the system after  $\sim 20$  min. With a

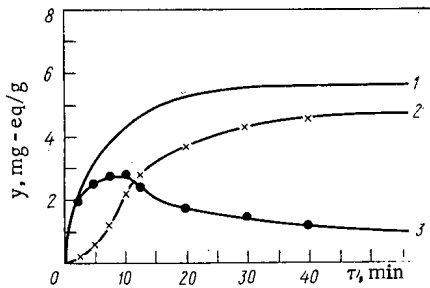


Fig. 3

Fig. 3. Kinetics of the sorption of cations on KU-2-8 resin ( $y$  is the concentration of ions in the resin): 1)  $\Sigma\text{Na}^+ + \text{Ca}^{++}$ ; 2)  $\text{Ca}^{++}$ ; 3)  $\text{Na}^+$ .

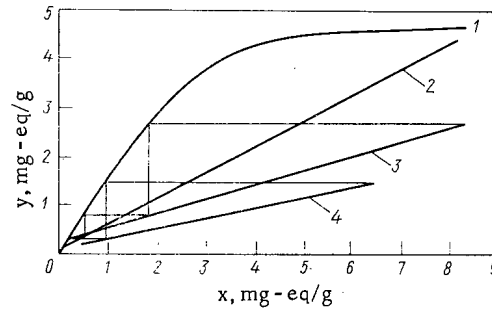


Fig. 4

Fig. 4. Determination of the number of theoretical plates ( $x$  is the concentration of ions in the solution): 1) sorption isotherm for the sum of  $\text{Na}^+$  and  $\text{Ca}^{2+}$  cations on Kationite KU-2-8 in  $\text{H}^+$ -form; 2) optimal operating curve; 3) operating curve for test 3; 4) operating curve for test 2.

3 min/m sorbent residence time for these kinetics, there corresponds a calculated HETP = 1.5-2.0 m. The distribution of cations between the sorbent and the solution is shown in Fig. 4.

The plotting of the operating curve of a process for optimal conditions showed that about 10 theoretical plates (NTP) are required with sufficient impregnation of the sorbent for the complete decontamination of the solution; the flow rate ratio in this case is  $n \approx 1:200$ .

Thus, a column of height  $H_{\text{opr}} = \text{NTP} \times \text{HETP} = 15\text{-}20$  m is required for complete decontamination of the solution. Similar dependences are also obtained for other operations involving KU-2 and AV-17 resins, for which the height of the column required for the decontamination of the solution was determined.

Description of Test Facility. The possibility of the application of pulsed columns for the decontamination of liquid radioactive wastes, operational designs, and the optimal operating regions of new apparatus were tested in a laboratory facility with a performance of 100-150 liters/h. The processes conducted in various apparatus (sorption and regeneration) in a continuously operative facility occurred at intervals and were studied successively in two apparatus, during which the column functioned continuously in each operation until the establishment of a stationary state.

The test facility consisted of two sorption columns, 76 mm in diameter and 4.8 m high each (since the housing for the apparatus was not tall enough) operating on KU-2 and AV-17 resins, sorbent feeder-separators, regeneration solution preparation tanks, raw and treated water storage tanks, pump, compressor, pulser, and rotameter rack. The framework for each column is shown in Fig. 1.

The columns were situated at different points in order to coordinate the self-flowing movement of the solution. The sorbent feeder-separators were placed in pairs above the columns. They functioned alternately as feeders and separators of the sorbent and the transporting solution.

In order to simplify the operation of the facility as a pulser, a valveless reciprocating pump with a performance of 150 liters/h was utilized. In addition the pulse strength  $J = 600$  mm/min in both columns. In order to stabilize the level of the solution in the pulse chambers of the column, the pulser was actuated by compressed air from a compressor through a pressure stabilization unit.

Pulsed Column Tests. After rolling and hydraulic tests with tap water, tests were conducted on the decontamination of liquids and radioactive wastes processable by the Moscow decontamination station. In these tests, the flow rates, concentrations, and radioactivity of the raw solution and the filters were measured after the cationite and anionite processes in the columns during sorption and regeneration. We determined the cubic content of the resins before and after sorption. The "sorption-desorption-washing of resins" cycle was repeated four times. Each test of the sorbent took about 10 h. Regeneration and washing occupied 1-2 h. The first two cycles were conducted under conditions of free fall for the sorbent. The operating conditions were altered in the next two cycles in order to increase the residence time of the sorbent in the column.

TABLE 1. Decontamination of Liquid Wastes with a Low Level of Activity by Pulsed Sorption Columns and Filters

Test No.	Performance, liter/h	Specific performance, $m^3/m^2 \cdot h$	Ratio of flow rates $n = V_{sb}/V_1$	Specific electrical conductivity, mho/cm	Oxidizability, mg O/liter	Concentration, mg-eq/liter				Resin capacity, mg-eq/g				β-activity decontamination coeffic.		NTP
						Na+	Ca <sup>2+</sup>	Cl-	SO <sub>4</sub> <sup>2-</sup>	KU-2		AV-17		per column	total	
										before test	after test	before test	after test			
Pulsed columns																
1	100	23,8	1:55	7,5·10 <sup>-4</sup> 1,1·10 <sup>-4</sup> 6,9·10 <sup>-4</sup>	29,4 6,0 45,6	3,98 0,38 3,98	2,64 0,45 2,48	0,62 0,1 2,35	2,0 0,4 1,84	—	0,89	0,3	0,62	7	25	1,5-2
2	120	28,6	1:65	2,0·10 <sup>-4</sup> 6,4·10 <sup>-4</sup> 4,4·10 <sup>-5</sup>	1,1 58,5 4,0	0,1 6,0 0,1	0,4 2,32 0,05	0,1 1,23 0,1	0,1 1,68 0,1	0,2	1,25	0,6	1,34	6	14	1,5-2
3	120	28,6	1:110	—	53,0 4,0	3,39 0,1	2,68 0,05	0,81 0,2	1,48 0,1	0,4	2,7	1,0	1,89	35	55	3-5
4	100	23,8	1:100	—	4,0	0,1	0,05	0,2	0,1	0,7	2,4	0,9	1,48	13	50	3-5
Filters																
5	25	6,5	1:173	7,6·10 <sup>-4</sup> 5,6·10 <sup>-5</sup> 6,9·10 <sup>-4</sup>	37,5 1,3 15,7	3,98 0,1 5,0	2,7 0,05 2,45	0,66 0,1 1,32	2,22 0,1 1,89	—	3,0	0	0,38	32,9	57,5	—
6	25	6,5	1:120	9,7·10 <sup>-5</sup> 5,7·10 <sup>-4</sup> 6,5·10 <sup>-5</sup>	7,8 31,8 1,6	0,4 4,97 0,1	0,05 2,66 0,05	0,1 0,74 0,1	0,1 1,44 0,1	0	2,23	0	0,54	9,3	36,1	—
7	25	6,5	1:145	6,5·10 <sup>-5</sup> 6,5·10 <sup>-4</sup> 5,1·10 <sup>-5</sup>	12,8 5,37 1,2	5,37 0,1 0,1	2,68 0,05 0,1	0,73 0,1 0,1	2,44 0,1 0,1	0	2,84	0	1,15	5,9	27	—
8	25	6,5	1:113	—	1,2	0,1	0,05	0,1	0,1	0	2,58	0	1,05	7,2	30,4	—

Note. 1. Volume of charged resin in tests 1 and 2  $V(KU-2) = 3,75$  liters,  $V(AV-17) = 7,5$  liters; in tests 3 and 4  $V(KU-2) = 4,0$  liters,  $V(AV-17) = 3,75$  liters. 2. The capacity was calculated at equilibrium. It was assumed that the sorbent is regenerated completely. 3. The first line gives the properties of the raw solution, the second gives the properties of the column effluent.

For comparison, tests were conducted simultaneously on the decontamination of the same solutions in sorption filters 69 mm in diameter, with ion-exchange layers 1 and 2 m in height.

Averaged results of tests on pulsed columns and filters are presented in Table 1. From a comparison of the data obtained, it is seen that the performance of the columns is 4-5 times greater than that of the filters. As one should have also expected, the decontamination coefficients in the first two tests of the columns were found to be smaller than those for the filters. In succeeding tests, it was not possible to bring the decontamination up to the same (or larger than for the filters) values. The capacity of the sorbent in the first two tests is much less, and in subsequent tests approaches the capacity of the filters.

Analysis of the data from hydraulic tests indicates that the performance of the facility is limited by the throughput of the anionite columns and that one can increase it up to 140-160 liters/h, employing coarser anion-exchange resin. The amount of sorbent found in the column during sorption is 0.5-1.0 liter in the first tests, and 3-5 liters in the rest, which is much lower than in a filter with the same performance.

The first tests showed that the NTP during sorption of cations is small, and is 1.5-2, which corresponds to an HETP = 2.1-2.7 m. This value is somewhat larger than the theoretical value, which can be explained by the low performance of the cationite column, i. e., the apparatus operated under nonoptimal conditions. In order to obtain the prescribed decontamination parameters, a column or a cascade of columns,  $H = 21-27$  m in height, is required. Under these conditions, a pulsed column facility has a smaller once-only charge of sorbent and higher specific performance than the filters, but its size is greater. In order to reduce its size, it is necessary to reduce the HETP, which can be achieved by the use of sorbents with better kinetic properties, for example, macroporous ones, or to increase the residence time of the sorbent in the apparatus, for which one should increase the retardation of the resin. The next two cycles were conducted under such conditions. For this purpose, a layer of quasi-liquid resin, 3-3.5 m in height, maintained either with the aid of an air-lift or a special "transport" pulser, was established in the column [2]. The layer of sorbent is subdivided by the plates, and the movement of its particles occurs during the transporting pulses.

The results showed (tests 3 and 4, Table 1) that, with the same performance as in the preceding tests, the decontamination coefficient and the sorbent capacity increased sharply. The discharge solutions surpassed in quality those obtained in a facility with filters. The value of the NTP increased to 4-5, and the HETP was correspondingly reduced to 0.8-1.0 m. Under these conditions, one can obtain the prescribed properties in a column up to 10 m in height.

The regeneration and washing in a system with transport pulsation also proved to be efficient. Thus, under these conditions, the columns possess advantages in all essentials.

At the present time, designs for columns with transport pulsation, which provide an even greater efficiency that allows one to reduce the size of the apparatus, to increase the capacity of the sorbent in comparison with that of filters, and, correspondingly, to increase the concentration coefficient, are under development.

Based on the results obtained, the raw data are provided for the design of a combined continuous action facility with a performance of 1 m<sup>3</sup>/h.

#### LITERATURE CITED

1. S. M. Karpacheva et al., Chemical and Petroleum Processing Machine Design [in Russian], Izd. Tsintikhimneftemash, Moscow (1971).
2. B. E. Ryabchikov et al., Problems in Atomic Science and Technology. Series: Machinery, Apparatus, Means of Mechanization and Automation of Industrial Processes. Pulsed Apparatus [in Russian], No. 1 (41), Izd. TsNIIatominform, Moscow (1972), p. 63.
3. E. I. Zakharov et al., Ibid., p. 77.
4. E. I. Zakharov et al., Ibid., p. 84.
5. S. M. Karpacheva et al., in: Extraction and Sorption in the Metallurgy of Molybdenum, Tungsten, and Rhenium [in Russian], Izd. Tsvetmetinformatsiya, Moscow (1971), p. 182.
6. A. A. Komarovskii and G. F. Mironov, in: Ion-Exchange Technology [in Russian], Nauka, Moscow (1965), p. 114.
7. Ya. M. Zagrai et al., Ion-Exchange Decontamination of Industrial Sewage by Cation-Exchange Resins in a Quasi-Liquid Layer [in Russian], Izd. UKRNITI, Kiev (1966).
8. S. M. Karpacheva et al., Pulsed Extractors [in Russian], Atomizdat, Moscow (1964).
9. R. Treibal, Liquid Extraction [in Russian], Khimiya, Moscow (1966).

CALCULATION AND PREDICTION OF RADIOACTIVE  
CONTAMINATION OF THE LOWER ATMOSPHERE  
BY ATOMIC POWER STATION STACK DISCHARGES

N. E. Artemova

UDC 551.510.72

In the selection of an area for any reactor installation, one primarily takes into consideration the level of possible radiation hazard both for the population in general and for individuals living near the unit since the radiation effects on the population must be as low as possible. This can be achieved mainly by high-quality planning, construction, and operation of an atomic power station. However, no minor role can be assigned to the location of an atomic power station, in the selection of which one must take into account all the features of meteorological dilution of the radioactive products discharged into the atmosphere during operation of the atomic power station that are characteristic of the proposed area of construction.

Experience with operating atomic power stations shows that the fundamental criteria and physical premises which are the basis for estimating atmospheric diffusion in the operating area of an atomic power station are valid. Dispersion of a contaminant discharged into the atmosphere occurs, as is well known, as a result of its entrainment in turbulent atmospheric vortices of various scales with the intensity of the turbulence being determined by the thermodynamic state of the surface layer of the atmosphere. The direction of contaminant transport depends on the predominant wind direction. All cases of contaminant dispersion can be classified for the several categories of thermodynamic stability responsible for contaminant transport to the ground and the formation of a surface concentration field. For each class of atmospheric stability, definite values of maximum surface-layer contaminant concentration and definite localization distances from the source are observed and can be calculated.

At the present time, there are a large number of papers devoted to the evaluation of the degree of atmospheric contamination by discharges from various types of sources. However, if one is speaking of rapid methods for calculating atmospheric contamination suitable for practical use and having the necessary nomograms and curves, two such groups of techniques should be mentioned.

1. Methods of Sutton and Pasquill. The latter was subsequently further developed by Mead, Beatty, and Bryant, and was incorporated by them into the procedures of the United Kingdom Atomic Energy Authority and was recommended to the World Meteorological Organization as a method for calculating the dispersion of discharges from atomic reactors.

2. Methods for calculating industrial contamination of the atmosphere developed in the USSR at the Main Geophysical Observatory (MGO), at the Leningrad Hydrometeorological Institute (LHI), and at the Institute of Experimental Meteorology (IEM) which have been checked by a large amount of experimental material and which were used successfully for planning and forecasting.

These two groups of techniques are based on two different approaches to the description of atmospheric diffusion: statistical and semiempirical using analogy with molecular diffusion (and in some cases a combination of both approaches). Each has certain advantages and deficiencies. The difference between them is mainly that the statistical theory is based on the study of fluctuations as a statistical ensemble and considers their influence on the nature of the entire field including the average flow while the semiempirical theory assumes the average flow to be a steady state and studies its features and its influence on other properties. The use of one or the other method for calculations of surface-layer contaminant concentration

---

Translated from *Atomnaya Energiya*, Vol. 36, No. 1, pp. 32-37, January, 1974. Original article submitted April 11, 1973.

© 1974 Consultants Bureau, a division of Plenum Publishing Corporation, 227 West 17th Street, New York, N. Y. 10011. No part of this publication may be reproduced, stored in a retrieval system, or transmitted, in any form or by any means, electronic, mechanical, photocopying, microfilming, recording or otherwise, without written permission of the publisher. A copy of this article is available from the publisher for \$15.00.

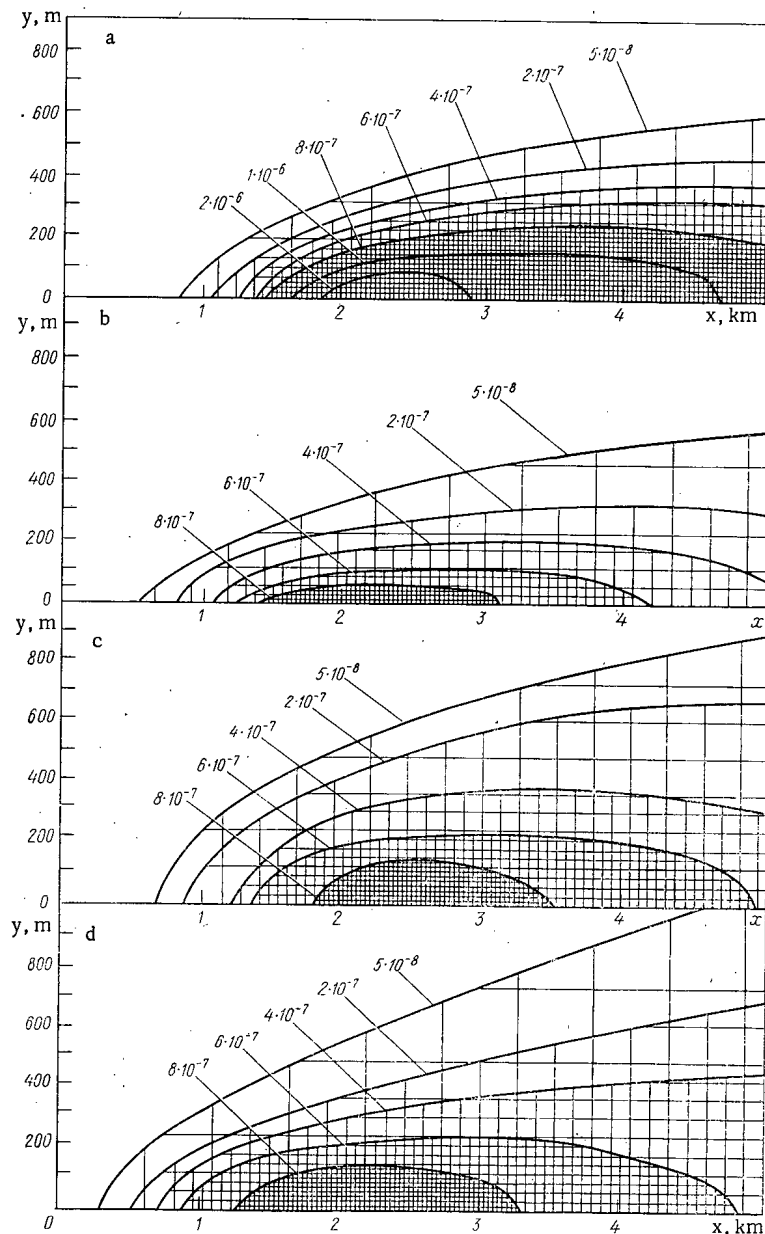


Fig. 1. Surface-layer concentration field for a weightless, long-lived contaminant calculated by the Sutton (a), LHI (b), IEM (c), and MGO (d) methods.

leads to identical results if one takes into account the averaging period for the set of meteorological parameters used and the accuracy of each method. The best agreement with experimental data, and consequently the best accuracy, is obtained with calculations of contaminant dispersion under averaged conditions, i. e., for those weather categories which are characterized by conditions of weakly developed convection and an equilibrium (neutral) thermodynamic state in the surface atmosphere.

As an illustration, Fig. 1 shows the surface-layer concentration field of a weightless long-lived contaminant calculated for a continuous discharge of unit intensity by the methods of Sutton [1], LHI [2], MGO [3], and Bosanke-Pearson-Denisov [4, 5] (the last is a variation of the IEM method for a nonsettling contaminant). The discharge height is 110 m, the thermodynamic stratification is slightly unstable and close to equilibrium, and the wind velocity at anemometer height, or the average velocity in the 0-110 m layer, is 5 m/sec. Table 1 gives brief characteristics of the methods for calculating contamination of the surface layer of the atmosphere by the different techniques. The error in concentration determination by the IEM and LHI methods is approximately 50%. The accuracy of the MGO method is 30%. The relative error was not determined for the Sutton method.

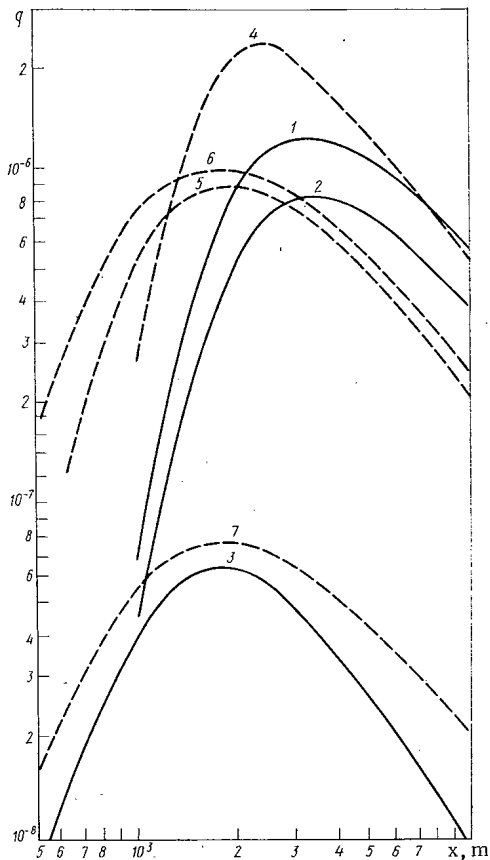


Fig. 2. Change in axial surface concentration of a weightless, long-lived contaminant.

concentration averaged over 2-3 min. In the main, this explains the difference in concentration values obtained from Sutton's method and from single-discharge averaging methods. In addition, the Sutton method can lead to significant errors in the calculation of surface concentration at large distances from the source because of the lack of justification for the assumed scheme for spatial variation of the turbulent diffusion coefficients.

The Pasquill-Mead method [6-8] offers an opportunity to determine comparatively simply contaminant concentration in the surface layer of the atmosphere for instantaneous, single discharge, and continuous discharge, for various categories of atmospheric stability, and at sufficiently large distance from the source by using the tables and curves of Pasquill for averaged values of the lateral and vertical expansion of a jet. Gifford's model of a fluctuating jet [9], which is extensively used in studies of the features of horizontal dispersion of a jet from a continuously operating source, makes it possible to identify the operating time of a source of finite duration (instantaneous, single discharge) with the time of sample collection or the time of averaging the concentration from a continuously operating source. Consequently, the Pasquill-Mead method can also be used for estimating instantaneous, single-discharge, and mean annual concentrations from a continuously operating source. The error in the determination of concentration by the Pasquill-Mead method is approximately 100%. Figure 2 shows the change in axial concentration for instantaneous (curve 1), single-discharge (curve 2), and mean annual (curve 3) averaging calculated by the Pasquill-Mead method for continuous discharge of unit amount per second of a weightless, long-lived contaminant at a height of 110 m and for equilibrium stratification of the atmosphere and an averaged wind speed of 5 m/sec. For comparison, the dashed curves show the change in axial concentration from a continuously operating source calculated by the Sutton method with instantaneous averaging (curve 4), the MGO and LHI methods with single-discharge averaging (curves 5 and 6), and for mean annual averaging in the case of a circular wind rose by the method of the Institute of Applied Geophysics (curve 7), which is described in [10]. The Pasquill-Mead equations are:

The following notation is used in Table 1:  $x$ ,  $y$ , and  $z$  are the axes of a Cartesian coordinate system. The wind direction is in the  $x$  direction. The source is located at the point  $(0, 0, H)$ ;  $H$  is the stack height, m;  $q$  is the contaminant concentration in the surface layer of the atmosphere,  $1/m^3$ ;  $C_y$  and  $C_z$  are the Sutton virtual coefficients for turbulent diffusion,  $m^{n/2}$ ;  $u$  is the wind velocity, m/sec;  $n$  is the Sutton stratification parameter;  $\bar{y}^2$  is the contaminant dispersion in the  $y$  direction,  $m^2$ ;  $b_y$  and  $b_z$  are empirical constants;  $q_M$  is the maximum surface concentration;  $x_M$  is the distance from the base of the source to the point of maximum surface concentration;  $m$ ;  $u_M$  is the critical wind velocity, m/sec;  $A$  is a climatological parameter;  $m$  and  $F$  are respectively parameters which characterize the emission rate from the stack of the gas-air mixture and its gravitational settling;  $V$  is the volume of discharged gas-air mixture per unit time,  $m^3/sec$ ;  $\Delta T$  is the temperature difference between the discharged gases and the ambient air, deg.

As is well known, the vertical temperature gradient in the lower layer of the atmosphere and the wind characteristics, which are responsible for the thermodynamic state of the atmosphere, and the intensity of vertical and horizontal transport of a contaminant are quite variable quantities and can change their values even over comparatively short periods of time. The LHI, IEM, and MGO methods take into account the variation in wind direction over periods of 20-30 min and therefore make it possible to estimate "single-discharge" values of the concentration, i. e., a concentration averaged over 20-30 min. The Sutton method assumes a constant wind direction and consequently makes it possible to calculate instantaneous values of contaminant concentration, i. e., con-

TABLE 1. Computational Formulas and Parameters Used in the Various Methods

Method	Basic equation for concentration	Parameter values	Averaging time
Sutton	$q(x, y, 0) = \frac{\frac{y^2}{2e^{C_y^2 x^{2-n}}} \frac{H^2}{e^{C_z^2 x^{2-n}}}}{\pi C_y C_z u x^{2-n}}$	$C_y = 0,21$ $C_z = 0,12$ $n = 0,25$	2-3 min (instantaneous)
LHI	$q(x, y, 0) = \frac{\frac{y^2}{54 e^{2y^2} e^{-14,5H^{1,18}}}}{u x^{1,9}}$	$\bar{y}^2 = (0,2x^{0,9})^2$	20-30 min (single discharge)
IEM	$q(x, y, 0) = \frac{\frac{H}{b_z x} e^{-\frac{y^2}{2b_y^2 x^2}}}{\sqrt{2\pi} b_y b_z u x^2}$	$b_y = 0,08$ $b_z = 0,024$	from 10 to 40 min
MGO	$q(x, y, 0) = q_M S_1(x/x_M) S_2(y/x) r(u/u_M)$ $q_M = \frac{AmF}{H^2 \sqrt[3]{V\Delta T}}$ $x_M = 20H; u_M = 0,65 \sqrt[3]{\frac{V\Delta T}{H}}$	$A = 0,12^*$ $m = 1$ $F = 1$ $V\Delta T = 280$ $r, S_1, S_2$ are taken from the appropriate curves in [3]	20-30 min (single discharge)

\*The value  $A=0,12$  is recommended in the MGO method for calculating the dispersion of a contaminant discharged into the atmosphere from an elevated source under conditions of developed turbulent exchange in the central zone of the European portion of the USSR. There are no instructions in [3] for neutral stratification conditions.

$$q_{inst} = \frac{168 e^{-2,303 \frac{H^2}{h^2}}}{\theta h x u} \quad (\text{instantaneous source})$$

$$q_{sing} = \frac{168 e^{-2,303 \frac{H^2}{h^2}}}{\theta_p h x u} \quad (\text{prolonged source; from 20-30 min to several hours})$$

$$q = \frac{e^{-2,303 \frac{H^2}{h^2}}}{1,16\pi h x u} \quad (\text{continuous source})$$

Here,  $H$  is stack height, m;  $h$  is the vertical expansion of the jet, m;  $\theta$  is the lateral expansion of the jet in the case of an instantaneous discharge, deg;  $x$  is distance from the source, m;  $\theta_p$  is the lateral expansion of the jet in the case of a prolonged discharge, deg;  $u$  is the wind velocity, m/sec.

The parameters  $\theta$ ,  $\theta_p$ , and  $h$  are taken for various distances from the source for weather categories D and C-D in accordance with the recommendations of Pasquill and Bryant [6, 8].

Analysis of Figs. 1 and 2 shows that within the limits of accuracy indicated for the various methods, the calculated results of surface-layer concentration of a contaminant discharged from the stack of a continuously operating installation agree rather well for identical averaging periods. Consequently, any of the methods can be used for estimating possible or existing atmospheric contamination from a source discharging radioactive products. One should remember, however, that in each specific calculation it is necessary to be guided by the necessary accuracy in the determination of the concentration and by typical dispersion conditions for the given region.

The coefficients of turbulent diffusion obtained by Sutton and used in calculations of contaminant concentration by his method are only valid for dispersion under neutral conditions and only for 2-3 min averaging. The Pasquill-Mead method is attractive because of its simplicity; however, determination of concentration by this method, as acknowledged by the authors, may give errors of several orders of magnitude under extreme stability conditions (strongly developed instability and moderate and strong stability). The MGO method is mainly used for calculation of contaminant dispersion under conditions of developed convective exchange and for the determination of single-discharge (20-30 min) concentrations. In general form, the LHI method (for various stability conditions) uses a number of parameters that are difficult to measure and cumbersome calculations which require a certain amount of preparation. The IEM method is mainly suited for the determination of the deposition density of contaminants that settle out.



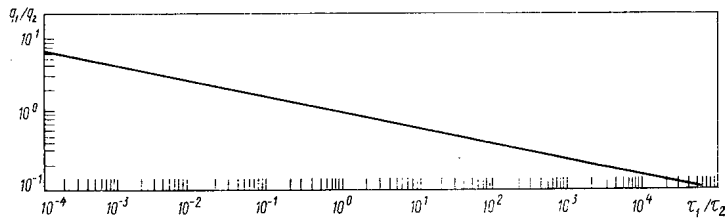


Fig. 3. Dependence of  $q_1(\tau_1)/q_2(\tau_2)$ , the ratio of concentrations averaged over different periods of time, on  $\tau_1/\tau_2$ , the ratio of the averaging periods.

There is much experimental data obtained in the Soviet Union and abroad [1, 5] which indicates that the magnitudes of surface-layer contaminant concentrations averaged over different periods of time are related to the length of the averaging period. This dependence is given by

$$\frac{q_1}{q_2} = k(\tau_2/\tau_1)^{0.2},$$

where  $q_1$  and  $q_2$  are the surface-layer concentrations of the contaminant;  $\tau_1$  and  $\tau_2$  are the corresponding averaging periods;  $k$  is a coefficient of proportionality which takes into account the stability of the basic parameters that determine diffusion of the contaminant, mainly the stability of wind direction;  $k = 1$  for short-period concentrations (averaging over a day or less).

The relation presented is rather universal and can be used, for example, for predictions of possible mean annual contamination of the surface atmosphere around an operating plant from measurements over a finite sample-collecting period. In this case, the magnitude of the coefficient  $k$  is determined by the elongation index  $n/n_0$  of the mean annual wind rose where  $n_0$  is the frequency of any direction of the eight-point wind rose for equal probability of all directions and is 0.125;  $n$  is the actual frequency of the predominant wind direction (in this case,  $k = (1/2)n/n_0$ ). Figure 3 shows the relation given in graphic form for  $k = 1$ .

The relation given makes it possible to use the simplest and most effective methods for calculating surface-layer concentrations of contaminants in order to predict the magnitude of atmospheric contamination for any period of source operation and for meteorological information collected over an arbitrary time.

Since radiation safety standards regulate the mean annual maximum permissible intake of radioactive isotopes into the body and the mean annual dose of external radiation, they are a basis for estimating the allowable atmospheric contamination produced during normal operation of an atomic power station in accordance with the mean annual meteorological characteristics of the given region. Having information covering a period of many years about the frequency of various types of atmospheric instability and the mean annual wind in a specific region, one can determine, as shown in [10] and by other methods as well, the probable mean annual atmospheric contamination and calculate the possible external irradiation of people and the intake of radioactive isotopes into the body through the lungs.

A comparison of calculated mean annual surface layer concentrations with the maximum permissible mean annual concentration is a basis for establishing norms for the amount of power station discharges or for establishing the parameters for the ventilation stacks. However, such calculations can be carried out only in those cases where the premises underlying the computational scheme are valid (primarily, a smooth and level topography in the area where the source of the discharge is located and homogeneity of the vertical thermodynamic structure of the surface layer of the atmosphere). Topographical features (mountains, river valleys), high frequency of unfavorable meteorological conditions observed during formation of elevated inversions at discharge height, or a combination of these and other conditions (which exists rather often) are extremely undesirable at the location of an atomic power station.

Thus, in considering plans for the location of an atomic power station, it is necessary to know the following from the viewpoint of ensuring radiation safety of the population in the surrounding territory during normal operation:

1. Data about the projected atomic power station — power and type of reactor, composition and amount of products discharged, height, rate, and velocity of discharge, temperature of the discharged gas — air mixture.

2. Climatological data — mean annual wind rose, chart of wind velocities with corresponding mean annual frequency, mean annual wind velocity (preferably for each compass point), mean annual frequency of elevated inversions (at discharge height), mean annual frequency of calms and fog, their average and maximum duration, mean annual daily and maximum air temperature during the warm season.

The frequency of elevated inversions at discharge height can be obtained from temperature and wind soundings taken at points no more than 100-150 km from the location of the atomic power station. The other data can be taken from observations made at weather stations in the standard network which are located as close as possible to the proposed location of the atomic power station and no farther than 40 km if the topography is smooth and level. If the locality is hilly and cut by river valleys, one should determine the most representative weather station in order to avoid using data from those stations which are located in areas with a specific microstructure of the wind regime (for example, those in river valleys). In this case, the distance to the reference weather station should be no more than 20 km.

In considering the problems associated with the estimate of possible atmospheric contamination by radioactive products during the operation of an atomic power station, one also needs a plot (sketch map) of the region around the location of the atomic power station out to a radius of not less than 200 stack heights (20-50 km) on which the topography of the region should be shown along with the location and absolute datum for the reference weather stations closest to populated points, residential areas around the power station, and industrial areas. It should be noted that when it is necessary to locate an atomic power station in areas with complex topography and wind and temperature regimes, a 4-5 year set of weather observations must be planned and carried out ahead of time at the proposed point of construction with obligatory temperature and wind soundings of the 200-300 meter layer of the atmosphere (height of the soundings is determined by the height of the ventilation stacks).

#### LITERATURE CITED

1. Meteorology and Atomic Energy, N. A. Byzova and K. P. Makhon'ko (editors), Gidrometeoizdat, Moscow (1972).
2. D. L. Laikhtman, F. A. Gisina, and S. N. Kaplan, Tr. Leningr. Gidrometeorolog. Inta., No. 15, Izd. LGU (1963), pp. 37-47.
3. Instructions on the Calculation of Atmospheric Dispersion of Harmful Materials Contained in Industrial Discharges (SN 369-67) [in Russian], Gidrometeoizdat, Leningrad (1967).
4. A. I. Denisov, Izv. Akad. Nauk SSSR, Ser. Geofiz., No. 6, 834-837 (1957).
5. N. L. Byzova, Tr. Inta. Éksperim. Meteorologii, No. 15, Gidrometeoizdat, Moscow (1970).
6. F. Pasquill, Meteorological Magazine, 90, No. 1063 (1961).
7. P. S. Mead, WMO-No. 97, TP41 (1960).
8. P. Bryant, Rep. AHSB(RP) R42, UKAEA (1964).
9. F. Gifford, in: Atmospheric Diffusion and Air Contamination, A. S. Monin (editor), Izd. Inostr. Lit., Moscow (1962), pp. 143-165.
10. N. E. Artemova and E. N. Teverovskii, At. Énerg., 31, No. 6, 573 (1971).

## REVIEWS

## MIXED-RADIATION DOSIMETRY

B. A. Briskman and R. B. Novgorodtsev

UDC 539.1.01/539.1.08

In titling the review in this manner, we have in mind the measurement of absorbed doses\* in materials irradiated in nuclear reactors. In addition, since such measurements involve an extremely extensive group of problems which have been discussed in a number of reviews mainly by foreign authors, we shall confine our considerations only to those problems associated with the determination of the contributions to absorbed dose from the separate components in reactor radiation fluxes. Obviously, these problems are most complicated and are of great interest for in-reactor measurements. Their solution is necessary for the following reasons. First, in studies of the interaction mechanism in radiation physics, chemistry, biology, and material studies, the question often arises as to whether the effect produced by the same absorbed dose from different types of radiation will be the same. Second, data on absorbed doses are needed for the very broad range of materials being irradiated in nuclear reactors. Direct measurement of them for each chemical element in an actual reactor is unrealistic. As a rule, a method is used in which data obtained for some standard material is converted to the dose in the desired material. To do this, it is necessary to know the dose composition in the standard material and the neutron and  $\gamma$ -ray spectra. Third, for correlation of irradiation results in different reactors, it is necessary to use certain irradiation parameters which can be the total absorbed dose or its neutron component.†

A large number of papers on in-reactor dosimetry has been published. The IAEA reports [1-3], the papers devoted to calorimetry alone [4-8], and the monograph on chemical dosimetry [9] should be considered as the most complete reviews in this field. The problem is discussed in an extensive chapter in the monograph [10]. However, with the possible exception of the very complete and interesting book [3], relatively little consideration is given to separation dosimetry in all the papers mentioned. Since the determination of the composition of absorbed dose does not depend in principle on what method is used (calorimetric, chemical, etc.) for this purpose, we shall also consider the problem of separation dosimetry in its most general form.

Just how is dose composition determined? Breaking up the entire reactor neutron spectrum into fast ( $E > 0.1$  MeV) and thermal neutrons (as a rule, the contribution from neutrons of intermediate energy can be neglected under the condition that it is taken into account in the fast-neutron contribution), we have

$$D_i = D_i^\gamma + D_i^f + D_i^{\text{th}}, \quad (1)$$

where  $D_i$  is the absorbed dose in the  $i$ -th material. We shall assume a charged-particle contribution to the absorbed dose accompanies radiative capture of thermal neutrons or the interaction of  $\gamma$  rays with matter.

The quantity  $D_i^{\text{th}}$  is determined from the known thermal-neutron flux including consideration of radioactive decay scheme, capture  $\gamma$  radiation,  $\nu$  radiation accompanying  $\beta$  decay,  $\beta$ -particle energy, etc. Capture  $\gamma$ -ray spectra are given in [11]. A scheme for the calculation of absorbed energy of capture  $\gamma$  radiation from surrounding materials is discussed rather thoroughly in [12]. Equations for the calculation of self-absorption in large, cylindrical samples are given in [13]. Examples of the calculation of  $D_i^{\text{th}}$  including

\*For specialists in reactor engineering, more familiarly energy deposition although these quantities are not equivalent, strictly speaking, and have different physical significance.

†For brevity, we shall call the collection of methods for solving the problem separation dosimetry for reactor radiations.

---

Translated from *Atomnaya Energiya*, Vol. 36, No. 1, pp. 39-49, January, 1974. Original article submitted October 31, 1972; revision submitted March 20, 1973.

© 1974 Consultants Bureau, a division of Plenum Publishing Corporation, 227 West 17th Street, New York, N. Y. 10011. No part of this publication may be reproduced, stored in a retrieval system, or transmitted, in any form or by any means, electronic, mechanical, photocopying, microfilming, recording or otherwise, without written permission of the publisher. A copy of this article is available from the publisher for \$15.00.

self-shielding are given in [3], in [14, 15] for aluminum without consideration of self-shielding, and in [16] for polyethylene. It is shown in [15] that the dose in Al for radiative capture of thermal neutrons results from the absorption of the primary  $\gamma$  ray ( $E = 7.7$  MeV), the secondary  $\gamma$  ray during  $\beta$  decay ( $E = 1.8$  MeV), and the  $\beta$ -particle energy ( $E = 1.23$  MeV) in the following ratio, 0.30:0.09:0.61. In this case,  $D_{Al}^{th} = 5.48 \cdot 10^{-13} \Phi^{th}$  Mrad/h. In a number of cases, the dose from the reaction  $H(n, \gamma)D$  with  $E_\gamma = 2.2$  MeV is important [17, 18].

The calculation of  $D_i^\gamma$  in an irradiated sample from the  $(n_{th}, \gamma)$  reaction in the jacket around the sample is similar to the calculation of  $D_i^{th}$  [5, 19]. The quantity  $D_i^{th}$  can be determined more easily if heavy charged particles result from the interaction of thermal neutrons in reactions such as  $^{10}B(n, \alpha)^7Li$ ,  $^6Li(n, \alpha)^3H$ , and  $^{14}N(n, p)^{14}C$ . It is logical to refer here to the dose from fission fragments, which is of great importance in chemonuclear processes. This dose is calculated on the basis of  $\Phi^{th}$ , the uranium fission cross section, fragment energy, self-absorption in uranium, and the range of fission fragments in the irradiated material [20-22]. Thus it is only necessary to know  $\Phi^{th}$  (thermal-neutron flux density) for a determination of  $D_i^{th}$  from input data.

It is considerably more complicated to determine the first two components of the dose since the fast-neutron spectrum is known inaccurately as a rule and there is thus far no experimental data on the spectrum of in-reactor radiation (with the exception of [23] and information on the performance of spectral measurements in [24]). Apparently beginning with [25] (although the first separation of effects from various kinds of  $\gamma + \alpha + \beta$  radiations by calorimetric methods was described in [26, 27]), greatest consideration was given to the measurement of absorbed dose rate or the dose itself in two materials in which the  $\gamma$  ray and fast-neutron interactions differed rather markedly (the quantity  $D^{th}$  was taken into account in advance). We write down the following relations (here, the additivity of dose is taken into consideration):

$$\begin{aligned} D_1 &= D_1^\gamma + D_1^n; \\ D_2 &= D_2^\gamma + D_2^n. \end{aligned} \quad (2)$$

We introduce the following notation:  $(D_1/D_2)^\gamma = K_\gamma$ ;  $(D_1/D_2)^n = K_n$ ;  $D_1/D_2 = K$ , where  $K_\gamma$  is the ratio of the  $\gamma$ -ray energy mass-absorption coefficients  $\mu_a/\rho$  (this statement is only valid for sufficiently thin samples where self-shielding can be neglected) and  $K_n$  is the ratio of the neutron mass-absorption coefficients  $\mu_n/\rho$  (or the neutron scattering integrals). Then the relative fraction for the neutron component in material 1 is calculated from

$$m_1 = \frac{K_n}{K_n - K_\gamma} (1 - K_\gamma/K), \quad (3)$$

and in material 2, from

$$m_2 = (K - K_\gamma)/(K_n - K_\gamma). \quad (4)$$

The most complete and reliable information on values of  $\mu_a/\rho$  for monoenergetic  $\gamma$  radiation is given in [28, 29]. There is selected data, for example, in [3, 30]. Values of  $\mu_a/\rho$  for  $\gamma$ -ray sources of complex spectral composition are given in [3, 31]. In Table 1, taken from [31] with some exceptions, average values of  $\mu_a/\rho$  ( $cm^2/g$ ) are given for various  $\gamma$ -ray spectra.

Values of  $K_n$  for elements with  $Z \leq 8$  and for chemical compounds such as  $CH_2$ ,  $H_2O$ , etc. can be calculated from data in [32] for sources of monoenergetic neutrons. For  $Z > 8$ , there is similar data [33] for a number of elements in a narrower energy range. Values of  $K_n$  relative to the dose in graphite are given in [5, 14, 34, 35] for various types of reactors and other sources of complex spectra with the contribution from inelastic neutron scattering to the absorbed dose taken into account in [35]. The scattering integral ratios  $D_i/DC$  for neutron spectra described in [36, 37] are given in Table 2 ( $DC$  is the dose in graphite).

Theoretical and experimental neutron dose data for BEPO and DIDO reactor spectra normalized to unit thermal neutron flux is given in [38] for an extensive set of elements.

Without analyzing the accuracy and correctness of the concept behind the published values for  $K_n$  and  $K_\gamma$ , we only point out that determination of absorbed dose composition using the method described above has been accomplished many times. Ionization, chemical, solid-state, and calorimetric detectors are extensively used for the purpose.

Ionization Methods. The application of these methods reduces to the use of homogeneous ionization chambers (IC) made of materials differing in hydrogen content [3, 10, 18].

TABLE 1.  $\gamma$ -Ray Energy Mass Absorption Coefficients for Various Radiation Sources

Element	Radiation source							
	HIFAR		BSR		IRT	RPT	fission	exp
	U	L	I	II				
	average energy, MeV							
	0,88	1,05	1,20	1,40	1,15	4,5	0,97	1,00
energy range, MeV								
0,1-4,0	0,1-4,0	0,19-8,2	0,42-10,0	0,13-10,0	0,4-10,0	0,3-7,6	0,1-10,0	
H	0,0486	0,0483	0,0468	0,0449	0,0471	0,0309	0,0504	0,0490
C	0,0246	0,0245	0,0238	0,0231	0,0240	0,0169	0,0255	0,0248
H <sub>2</sub> O	0,0274	0,0272	0,0264	0,0256	0,0266	0,0188	0,0283	0,0275
Al	0,0242	0,0239	0,0233	0,0229	0,0236	0,0182	0,0248	0,0243
Ar	0,0235	0,0229	0,0222	0,0218	0,0227	0,0181	0,0234	0,0232
Fe	0,0274	0,0255	0,0241	0,0235	0,0253	0,0207	0,0251	0,0257
Mo	0,0426	0,0339	0,0293	0,0270	0,0362	0,0271	0,0288	0,0342
Pb	0,0900	0,0633	0,0500	0,0379	0,0632	0,0290	0,0511	0,0664
U	0,120	0,0879	0,0743	0,0524	0,0761	0,0412	0,0725	0,0918

Note. HIFAR-enriched U-Al alloy, D<sub>2</sub>O moderator and coolant (U, L are the upper and lower limits of the intensity of the low-energy portion of the spectrum); BSR-I, BSR-II, IRT-highly enriched fuel, H<sub>2</sub>O moderator and coolant. In all these reactors, the data is given for the edge of the core; RPT measurements were in the graphite thermal column (there is a large contribution to the RPT spectrum from capture  $\gamma$ -radiation in graphite and steel); fission is the <sup>235</sup>U fission spectrum; exp is the empirical approximation  $(E) = \exp(-1.11E)$ .

Two ionization chambers were discussed in [10] for measurement of dose composition; a tissue-equivalent chamber and a C-CO<sub>2</sub> (or Teflon-CO<sub>2</sub>) chamber. In this case, a system of equations similar to Eqs. (2) was used:

$$\begin{aligned} T &= 1.04I' + N; \\ C &= 1.04I' + KN, \end{aligned} \quad (5)$$

where T is the ionization in the tissue-equivalent IC produced by  $\Gamma$  (rad) of  $\gamma$  radiation + N (rad) of neutron radiation in units of the ionization produced by 1 R of  $\gamma$  radiation; C is the ratio of the ionization in the C-CO<sub>2</sub> IC produced by the  $\gamma + n$  dose to the ionization produced by 1 R of  $\gamma$  radiation; K is the ratio of the ionization produced by 1 rad of neutrons in tissue to the ionization from 1 R of  $\gamma$  radiation. In [18], the following relation,

$$\frac{K}{K_0} \cdot \frac{1}{W_e} \cdot D_0^\gamma + \frac{E}{E_0} \cdot \frac{1}{W_r} \cdot D_0^n = 10^{-5}I, \quad (6)$$

was proposed for the determination of dose composition in a sample where K and K<sub>0</sub> are the  $\gamma$ -ray mass absorption coefficients in the chamber material and in the irradiated sample; E and E<sub>0</sub> are the kerma in the chamber material and in the samples when in identical neutron fluxes; W<sub>e</sub> and W<sub>r</sub> are the average ion-formation energy for secondary electrons from  $\gamma$  rays and for protons and recoil nuclei respectively, electron volts per ion pair; D<sub>0</sub> <sup>$\gamma$</sup>  and D<sub>0</sub><sup>n</sup> are the corresponding dose rates in the sample, rad/sec; I is the current in the chamber, A/g. Values of W in various gases (air, argon, CO<sub>2</sub>, C<sub>2</sub>H<sub>2</sub>, C<sub>2</sub>H<sub>4</sub>) for electrons,  $\gamma$  rays, and  $\alpha$  particles are given in [39]. Values of W are given in [2] for a considerably larger set of elements. As a rule, it is assumed that W for protons and recoil nuclei agrees with the W for  $\alpha$  particles although averaging (for example, over the fission spectrum) leads to a difference amounting to ~6%. The values of E/E<sub>0</sub> are ratios of neutron scattering integrals, which have been mentioned above. Some are given in Table 2. In [18], these quantities are given for muscle and bone (sample materials) and also for CH<sub>2</sub>, CH, C, and aerion (a conducting plastic used for the construction of IC in [40]) for three kinds of neutron spectrum. Such methods for the determination of dose composition were used in [41-43]. For the determination of fast-neutron kerma in biological samples irradiated in horizontal channels of the IRT reactor, the same authors used IC made of polyethylene and polystyrene [44].

In Eq. (6), the value of W for  $\gamma$  rays and recoil protons in a given material differs little (a few percent at most). At the same time, Boyd showed [3, p. 193] that oxygen and carbon ions formed during irradiation of a C-CO<sub>2</sub> IC have energies of 1-1000 keV and the value of W for these ions is twice the value of W for electrons (from measurements with the chamber mentioned and with a graphite calorimeter). The sensitivity of such an IC is 0.1  $\mu$ A/mW for  $\gamma$  radiation and 2.5  $\mu$ A per 10<sup>12</sup> n-cm<sup>-2</sup>-sec<sup>-1</sup> for neutrons with energies above the nickel threshold. This difference makes it possible to use an IC and a calorimeter made

TABLE 2.  $D_i/DC$  for the Neutron Component of Dose

Fast neutron spectrum	Material			
	H	D	O	Mg
1/E spectrum over				
0-1 MeV	87.9	16.4	0.75	0.42
0-2 MeV	81.1	19.4	0.84	0.38
0-3 MeV	77.0	20.9	0.75	0.38
Homogeneous moderator				
C	71.2	20.7	0.78	0.36
D <sub>2</sub> O	67.3	20.5	0.75	0.36
H <sub>2</sub> O	60.3	21.4	0.72	0.34
Graphite lattice	70.1	22.0	0.77	0.37
DIDO reactor; Mk III fuel elements	67.9	22.7	0.73	0.38
Fission spectrum	57.7	21.9	0.71	0.33

of the same material [45] instead of IC made of different materials. Since such a conclusion is not in accord with the premises of [41-43], the question of the variation of  $W$  in  $CO_2$  remains unsolved for mixed radiation; this is also noted in [18].

Liquid IC appear promising for separation dosimetry. They consist of two electrodes separated by a few millimeters and are filled with a dielectric fluid of high purity. Four dielectrics were used in [46-48] for this purpose: pentane, hexane, heptane, and isooctane (the last proved to be the best). An electrochemical dosimeter [49] can also be used for this purpose, employing an aqueous solution of  $H_2SO_4$  in which hydrogen peroxide and pure hydrogen are formed through the action of radiation.

The chambers mentioned can also be used for the determination of the thermal neutron contribution to the absorbed dose. Thus an IC with copper electrodes and filled with boron trifluoride was used in [50]. With the IC belong the Hurst proportional counters [51-53] in which the pulses from  $\gamma$ -ray secondary electrons have a considerably smaller amplitude than those from recoil protons, making it possible to separate the dose from fast neutrons by discrimination against pulses from  $\gamma$  radiation. Simultaneous recording of  $D_\gamma$  and  $D^n$  is achieved by the modification of the Hurst counter proposed in [54].

It should be noted that in most cases the use of IC in nuclear reactors has an upper limit on dose rate because of temperature effects.

Chemical Methods. These methods were reviewed in 1963 [9]. Papers published after 1963 are mainly discussed below.

The use of chemical methods in separation dosimetry is based on the fact that in a number of materials the change occurring because of the effects of ionizing radiation does not depend, or is slightly dependent, on LET. Such materials can be used for the determination of the total absorbed dose from mixed radiations over a broad spectrum. At the same time, a strong dependence of radiochemical effects on LET appears in many materials. A combination of materials in the first and second groups provides a solution for the problem formulated. In this case, the relation used for the determination of the radiochemical total yield is

$$G_{ef} = G_n D^n / D + G_\gamma D^\gamma / D, \quad (7)$$

where  $G_\gamma$  and  $G_n$  are the radiochemical yields for  $\gamma$  rays and fast neutrons respectively. The fundamental difference between Eq. (7) and Eqs. (2)-(4) is in the replacement of the coefficients  $K_\gamma$  and  $K_n$  by the ratio of the corresponding radiochemical yields.

In the first group of chemical dosimeters is a cerium sulfate solution, the  $G$  of which for  $\gamma$  rays and fast neutrons is 2.32 [55, 56]. Its basic deficiency is temperature dependence of the response (for temperatures above 35°C). The upper limit of the response is 100 Mrad. In the 0.1-3000 Mrad range, nitrous oxide,  $N_2O$ , has been used repeatedly [2, 57-59]. In its dissociation,  $N_2$  and  $O_2$  are formed, the amount of which is a measure of the absorbed dose ( $G_{N_2} = 10.0 \pm 0.2$ ,  $G_{O_2} = 4.0 \pm 0.4$ ). For the proper interpretation of the response of this dosimeter, one should take into account the contribution from the  $^{14}N(n, p)^{14}C$  reaction, which amounts to 50% of the total dose in a number of cases [60].

Cyclohexane can be used for doses up to 16 Mrad. Hydrogen is obtained from its radiolytic dissociation ( $G_H = 5.2$  [61]). For the determination of dose composition, deuterated cyclohexane,  $C_6D_{12}$ , is used

simultaneously with  $C_6H_{12}$  [3]. One can obtain only a crude estimate of the dose components with this method.

Aqueous solutions of glucose and maltose [62-64], for which  $G_\gamma/G_n = 1.15-1.10$ , are used for doses up to approximately 100 Mrad. At high dose rates (more than  $10^4$  rad/sec), however, it is recommended [65] that one use dry glucose and analyze the gaseous products of radiolysis by gas chromatography. Aqueous solutions of oxalic acid are also used for the same purpose [66, 67]. Determination of dose composition is performed by means of oxalic acid solutions in  $H_2O$  and  $D_2O$  [66]. In this case,  $G_n = 3.3$  was obtained for protons and  $G_n = 2.8$  for deuterons. These same solutions together with calorimeters were used for carrying out comparative dosimetric measurements at the ISIS reactor [68].

For fluorocarbons, which are used in reactors in the 3-50 Mrad dose range, the values of  $G_n$  and  $G_\gamma$  agree within 10-15% [69]. Dyed polymer films, the optical properties of which change under irradiation [70, 71], belong among the chemical systems having a yield slightly dependent on LET.

Above all, the ferrosulfate dosimeter (FSD), for which  $G_\gamma/G_n = 2.0$ , ought to be placed in the second group of chemical dosimeters. Although the FSD has not found application in reactors because of the low upper limit on measured dose ( $4 \cdot 10^4$  rad), various modifications of it (the introduction of copper ions [72], increasing the upper limit to 10 Mrad) make it possible to use this system in separation dosimetry. The limitation on the use of the FSD for determination of the  $\gamma$  and neutron components of the dose is also associated with a known uncertainty in the quantity  $G_n$ , particularly for recoil protons with  $E < 150$  keV. A theoretical calculation of  $G_n^{ef}$  for recoil protons was made in [73] on the basis of the concept of a local radiochemical yield determined at each point of the proton range. Values of  $G_n^{ef}$  equal to 6.4 and 6.9 respectively were obtained for two horizontal channels of the BR-5 reactor.

Chlorinated hydrocarbons used for this purpose (in particular, tetrachlormethane [74] for doses up to approximately 2 Mrad and tetrachlorethylene [75] up to 0.2 Mrad) are practically insensitive to neutrons. A combination of a deaerated FSD and a bichromate dosimeter was proposed [76] for doses up to  $\sim 5$  Mrad.

The use of plastic [77] and liquid [78] scintillators is based on principles similar to those given above. In the second paper, the reduction of radioluminescence in liquid activators (*n*-terphenyl and 2,5-diphenyloxazole) was used in an experiment designed for the determination of dose composition. The radioluminescence degradation effect was used with polycrystalline scintillator films [79].

In most solid detectors, dose composition is determined through a difference in hydrogen content. Thus the use of polymer films of polyethylene and cellulose diacetate [80] and also of polytrifluoroethylene [81] proved to be technically feasible. Such an approach also occurred in [82] where the gaseous system  $CO_2$ ,  $C_2H_4$  (or  $C_2H_2$ ), and  $N_2O$  was proposed. Free stable radicals formed by the irradiation of amine salts of organic acids were detected by means of EPR in [83]. They contain up to 14% of hydrogen making it possible to separate out the neutron component of the dose. Because a number of solid-state detectors have a response with a marked dependence on LET, such detectors are often combined with chemical detectors. Thus a combination of liquid chemical dosimeters (FSD and cerium solutions) and thermoluminescent dosimeters (aluminum phosphate glass, manganese activated) was used in [84], and in [85], a combination of chemical dosimeters (oxalic acid and glucose) and solid-state dosimeters (the same glass, but measurements in the megarad region were made through the change in optical density). At a lower dose range, SGD-8 glass can be used [86]. In some cases, the combination of a chemical dosimeter and a calorimeter is feasible [32].

As with IC, it is possible to pick out the thermal neutron contribution to the absorbed dose in a number of cases by means of appropriate additions to the chemical system. Thus, a glucose dosimeter with  $^{10}B$  introduced in the form of boric acid was used in [87].

Solid-State Methods. In most cases, such detectors are used in the low-dose region of the biological range. Nevertheless, present progress in the construction of microdetectors leads one to hope for considerable increase in the limit on the dose measured with them. Their use in reactor dosimetry is described most completely in [3, 88]. As a rule, these detectors are insensitive to fast neutrons and are used for measurement of the  $\gamma$  component of the dose or the thermal neutron contribution (for example, through the formation of tracks in mice which are fixed after irradiation by etching [89]). The manganese-activated phosphate glasses mentioned above [90] make it possible to measure  $D_\gamma$  up to 20-30 Mrad. In the thermoluminescence region, it is convenient to use LiF. A TLD-700 (almost pure  $^7Li$ ) and TLD-600 (highly enriched in  $^6Li$ ) pair provides a determination of  $D_\gamma$  and  $D_{th}$  [91]. The sensitivity of TLD to fast

neutrons when using a TLD in combination with a tissue-equivalent IC for separation dosimetry was investigated [92] and the variation in  $\gamma$  sensitivity of a TLD-700 during neutron irradiation has also been studied [93]. No change was detected up to 1600 rad. An increase in TLD sensitivity to fast neutrons is achieved by dispersion of the phosphor in hydrogenous materials. The semiconductor dosimeters are practically solid-state IC. Their sensitivity to fast and thermal neutrons is provided by the deposition of a thin layer of hydrogenous material on a silicon diode or by a coating of boron or uranium respectively [94]. In the first case, the conduction current arises because of recoil protons, and in the second case because of  $\alpha$  particles or fission fragments.

A scintillation spectrometer with a stilbene crystal has been used for separation dosimetry [95]. In this case, the well-known method of pulse-shape discrimination was used.

Calorimetric Methods. The most widely used method for separation dosimetry is the calorimetric method [5, 14, 15, 34, 38, 66, 96-114]. The construction of the calorimeters is most diverse: adiabatic, quasi-adiabatic, "kinetic," isothermal, "pedestal," with temperature differential in a gas gap, in a solid, etc. A review of such calorimeters and methods is given in [3-8]. Despite the diversity in technique, the principle of separation dosimetry remained the same: measurement of absorbed dose rate in different materials with subsequent application of Eq. (3). In this work, as a rule, the absorbers used in the calorimeters were hydrogenous materials ( $\text{CH}_2$ ,  $\text{CH}$ ,  $\text{H}_2\text{O}$ , etc.) in combination with heavy materials or with elements making up the chemical compound ( $\text{C}$ ,  $\text{CO}_2$ ,  $\text{D}_2\text{O}$ , Teflon, etc.) or an element and its hydride ( $\text{Zr}$  and  $\text{ZrH}_n$ ).

In all the methods described above for the determination of the components of absorbed dose, two detectors were most often used. To increase accuracy, a set of materials which made it possible to "overdetermine" an equation system such as Eqs. (2) was used in a number of cases (for example, in [34, 66, 99]). The use of least squares was recommended for its solution in [3], the proposed approach being a particular case of the more general method for solution of overdetermined systems of linear equations [115].

As far as we know, none of the authors evaluated the accuracy of the method used with the exception of [5]. This also explains why the published data is often quite contradictory, particularly the values for  $G_n$ .

One of the authors of this review showed [116] the mean-square error in the determination of the relative magnitude of the neutron component  $m$  of the dose is given by

$$\epsilon_m^2 = \left( \frac{K_n}{K_n - K_\gamma} \cdot \frac{m-1}{m} \right)^2 \epsilon_{K_\gamma}^2 + \left( \frac{K_\gamma}{K_n - K_\gamma} \right)^2 \epsilon_{K_n}^2 + \left[ \frac{K_n}{m(K_n - K_\gamma)} - 1 \right]^2 \epsilon_K^2. \quad (8)$$

We shall analyze the error  $\epsilon_m$  for two pairs of materials usually used in separation dosimetry of reactor radiations:  $\text{CH}_2\text{-C}$  and  $\text{ZrH}_n\text{-Zr}$  ( $n = 1.42$  [15]) in a light-water reactor. We discuss two versions: 1) the fraction of the neutron component in the absorbed dose for hydrogen is  $m_H = 0.82$  (usual for experimental channels located in the reactor core); 2)  $m_H = 0.5$  (for channels in a reflector). For these materials  $K_{n1} = 8.80$ ,  $K_{\gamma 1} = 1.14$  [34],  $K_{n2} = 22.8$  [15], and  $K_{\gamma 2} = 1.013$  ( $E = 0.6$  MeV). In both cases, the estimate of the errors  $\epsilon_{K_\gamma}$  and  $\epsilon_{K_n}$  are  $\pm 1\%$  and  $\pm 5\%$  respectively. The results are given in Table 3. The last two columns of the table give the error in measurement when using the "outstripping" effect about which more will be said later. The value of  $K$  is obtained from

$$K = D_{\text{BH}_n}/D_B = 1 + \rho_H \left[ \frac{1}{K'_\gamma - m_H(K'_\gamma - K'_n)} - 1 \right], \quad (9)$$

where  $\rho_H$  is the weight fraction of hydrogen in the hydride of the desired element B;  $K'_\gamma = (D_B/D_M)^\gamma$ ;  $K'_n = (D_B/D_H)^n$ ;  $\epsilon_{m_1}^2$ ,  $\epsilon_{m_2}^2$ , and  $\epsilon_{m_3}^2$  are respectively the first, second, and third terms on the right side of Eq. (8);  $m = D_{\text{BH}}^B/D_{\text{BH}}$ . Values of  $\epsilon_{m_2}^2$  and  $\epsilon_m$  were calculated for two values of the error  $\epsilon_D$  in the measurement of absorbed dose rate equal to 3% (in the numerator of the fraction) and 5% (in the denominator of the fraction). As is clear from Table 3, a completely acceptable value of 5-8% for  $\epsilon_m$  is obtained for irradiation in the reactor core only for the  $\text{CH}_2\text{-C}$  pair. For the same pair in the reflector the error reaches 25-40%, and for the  $\text{ZrH}_n\text{-Zr}$  pair the error is 35-56% in the core and 180-300% in the reflector. The values of  $\epsilon_m$  rise sharply for  $m_H < 0.5$ . It should be pointed out that the estimates of  $\epsilon_D$  amounting to 3 and 5% are rather optimistic if only because they are related to measurements of energy deposition and not of absorbed dose. The violation of electron equilibrium in the calorimeters used makes a realistic evaluation of the error in the measurement of absorbed dose rate extremely difficult.



TABLE 3. Error in Measurement of Neutron Dose Component

Material	$m_H$	$\frac{K_n}{K_n - K_\gamma}$	$K$	$m$	$\epsilon_{m_1}^2 \times 10^4$	$\epsilon_{m_2}^2 \times 10^4$	$\epsilon_{m_3}^2 \times 10^4$	$\epsilon_m \times 10^2$	$\epsilon_{m_3}^2 \times 10^4$	$\epsilon_m \times 10^2$
CH <sub>2</sub> -C ( $\rho_H = 0,143$ )	0,82	1,45	2,18	0,548	0,9	0,55	$\frac{22,4}{60,0}$	$\frac{4,9}{7,8}$	1,25	1,65
ZrH <sub>n</sub> -Zr ( $\rho_H = 0,0154$ )		1,05	1,443	0,419	60	0,60	$\frac{1130}{3060}$	$\frac{34,5}{56,0}$	62	11,0
CH <sub>2</sub> -C	0,50	1,15	1,34	0,170	31,5	0,55	$\frac{616}{1670}$	$\frac{25,5}{41,2}$	34,2	8,1
ZrH <sub>n</sub> -Zr		1,05	1,04	0,027	4430	0,06	$\frac{30\ 200}{86\ 500}$	$\frac{178}{296}$	1730	56,0

Analysis of the structure of the error in the determination of the quantity  $m$  shows that the error  $\epsilon_{K_n}$  can be neglected when using a pair of materials which are markedly different in their interactions with neutrons and  $\gamma$  rays ( $K_n \gg K_\gamma$ ). The main contribution to  $\epsilon_m$  is made by the error  $\epsilon_K$ , i. e., the error in determination of the dose rates in the two materials. The quantity  $\epsilon_{K_\gamma}$  is rather small but not always. In fact, the CH<sub>2</sub>-C pair received widespread acceptance particularly because the ratio of the mass absorption coefficients  $\mu_a/\rho$  remains practically constant over a broad range of  $\gamma$ -ray energies, and consequently the error  $\epsilon_{K_\gamma}$  can be neglected because of the absence of data for the  $\gamma$ -ray spectrum. Sometimes a pair consisting of polyethylene and a heavy metal (Bi [105], Pb [106]) is used. The use of such pairs, which at first glance seem very suitable, leads to quite large values for  $\epsilon_{K_\gamma}$ . Since  $K_n \gg K_\gamma$  in these cases, Eq. (8) takes the form

$$\epsilon_m \approx \frac{1-m}{m} (\epsilon_{K_\gamma}^2 + \epsilon_K^2)^{1/2}. \quad (10)$$

Since the  $\gamma$ -ray spectrum is poorly known, the quantity  $\epsilon_{K_\gamma}$  may be  $\sim 100\%$ . In fact, in the range  $0.3 < E_\gamma < 2$  MeV, we have  $0.93 < (\mu_a/\rho)_{Pb}/(\mu_a/\rho)_{CH_2} < 7.74$  and  $0.94 < (\mu_a/\rho)_{Bi}/(\mu_a/\rho)_{CH_2} < 8.01$ ; one can note for comparison that in the same  $\gamma$ -ray energy range  $1.139 < (\mu_a/\rho)_{CH_2}/(\mu_a/\rho)_C < 1.141$ . Then, for example, we obtain  $\epsilon_m = 300\%$  with  $m_{CH_2} = 0.25$  when using the pairs CH<sub>2</sub>-Pb or CH<sub>2</sub>-Bi.

A similar situation holds in the determination of the absorbed dose rate  $D_H$  in hydrogen proposed by some investigators [117] for correlation of the results of neutron irradiation of metals. In fact,  $\epsilon_{D_H}$  is determined from

$$\epsilon_{D_H}^2 = \frac{K^2 + (1 - \rho_H)^2}{(K - 1 + \rho_H)^2} \cdot \epsilon_{D_B}^2 + \left( \frac{K - 1}{K - 1 + \rho_H} \right)^2 \epsilon_{\rho_H}^2, \quad (11)$$

and the quantity  $D_H$  itself is determined from consideration of additivity with respect to the data for dose rate in the element B and in its hydride BH:

$$D_H = D_B \frac{K - 1 + \rho_H}{\rho_H}. \quad (12)$$

Here, as before,  $K = D_{BH}/D_B$ . It is assumed  $\epsilon_{D_B} = \epsilon_{D_{BH}}$ . Analysis of Eq. (11) shows how important the correct choice of material pairs is for the determination of  $D_H$ . Numerical calculations for the two pairs CH<sub>2</sub>-C (1) and ZrH<sub>1.88</sub>-Zr (2) for the two values 0.82 and 0.5 for  $m_H$  yield

$$\begin{aligned} (\epsilon_{D_H})_2/(\epsilon_{D_H})_1 &= 4.20 \cdot \epsilon_{D_{Zr}}/\epsilon_{D_C}, \quad m_H = 0.82; \\ (\epsilon_{D_H})_2/(\epsilon_{D_H})_1 &= 6.32 \cdot \epsilon_{D_{Zr}}/\epsilon_{D_C}, \quad m_H = 0.50 \end{aligned}$$

(it is assumed  $\epsilon_{\rho_H} = 0$ ; the conversion from  $m_H$  to  $K$  is in accordance with Eq. (9); the subscripts 1 and 2 correspond to the element pairs), i. e., for  $\epsilon_{D_{Zr}} = \epsilon_{D_C}$  the measurement error  $\epsilon_{D_H}$  when using the second pair of materials is four to six times greater than for the first pair. When  $\epsilon_{\rho_H}$  is taken into consideration, this difference becomes even greater.

The values given above are related not only to calorimetry but also to any dosimetric method or system which is used for solution of the problem being discussed with the sole difference that other methods

give poorer results in comparison with calorimetry. The consequences of such errors in application to radiation processes using mixed radiations can be quite serious [116].

One can therefore reach the following conclusions: 1) the error in determination of absorbed dose composition is quite large; 2) the magnitude of these errors is mainly determined by errors in measurement of dose rate or of the dose itself; 3) the existence of such errors is a chronic defect of the separation method for determination of dose composition; 4) since the error in the measurement of dose rate by chemical methods is considerably greater than for calorimetric methods as a rule, we consider the use of chemical methods for separation dosimetry of reactor radiations to be inadvisable. In technical reactor dosimetry, their area of application may be the measurement of total doses (when  $G_n \approx G_\gamma$ ) and in measurements of exposure doses in a number of cases (when  $G_n \ll G_\gamma$ ). Liquid or gas chemical dosimetric systems are irreplaceable in performing loop experiments [118].

Where should one look for an escape from the situation that has developed? If one considers the complexity of in-reactor measurements and the effects of some factors which often cannot be taken into account, one must not count on a significant increase in the accuracy of absorbed dose measurements. We consider most realistic a fundamental rejection of direct measurement of dose rate preceding the determination of composition. We have developed two methods for simultaneous determination of absorbed dose rate and composition for reactor radiations in which (and this is the point) the determination of the relative contribution of the radiation components to the dose is not associated with a previous measurement of total dose rate in different materials.

Relaxometer Method [119-121]. To determine dose composition one can use not only the difference in energy mass absorption coefficients for a given form of radiation in two materials but also the difference in the linear absorption coefficients for two forms of radiation in a single material. This idea is also the basis for the relaxometer method. During irradiation of a detector of given geometry, the temperature field in it depends on the distribution of internal heat sources, i. e., on the nature of the radiation flux attenuation which, in turn, is a function of the absorbed dose composition. Thus the problem reduces to the establishment of this last dependence and a temperature measurement at given points in the detector. The error of the relaxometer method is considerably below the error of existing methods for  $m_{CH_2} < 0.5$ , i. e., for reactor channels in a reflector, and is 8-10% over practically the entire range of  $m_{CH_2}$  values.

"Outstripping" Method [121, 122]. Unfortunately, the relaxometer method can be used only in symmetric radiation fields and the time required to make the measurement is quite prolonged (approximately 3-4 h). This gave us the incentive to return to the use of the difference between  $\mu_a/\rho$  in two materials but at a qualitatively new level. An attempt was made to measure in in-reactor experiments not the dose rates but their ratio  $K$  (to replace absolute measurements by relative ones). Furthermore, one can immediately determine  $m$  and then obtain from an independently measured value of the dose rate the absolute value of  $D_n$ . The experimentally determined dependence of the time to intersection of the temperature curves of two calorimeter elements on the ratio of the energy deposition in them was used. The method was realized in the design of an adiabatic isothermal calorimeter [123]. In the course of a single experiment, the ratio  $K$  and the total absorbed dose rate are measured. The systematic error in the measurement of  $K$  does not exceed 0.6-0.9% and the convergence is no worse than 1%. Use of the "outstripping" effect made it possible to reduce  $\epsilon_m$  by factors of 3.3-5.3 in comparison with existing methods (see Table 3) and to reduce measurement time markedly.

Obviously, the use of the outstripping method significantly facilitates the determination of absorbed dose composition.

In conclusion, we turn to the choice of material for the determination of composition and dose rate. As follows from the examples given above, the use of a pair of materials — a chemical element plus its hydride with maximum possible hydrogen content — is best. Taking this into consideration, the polyethylene-graphite pair is preferable. The Zr-ZrH<sub>n</sub> pair, of course, is without competition for investigations at high temperatures but is markedly inferior to the CH<sub>2</sub>-C pair with regard to accuracy. At times the supplementary use of polystyrene in combination with C or CH<sub>2</sub> has been proposed [34, 104]. Polyethylene is inferior to polystyrene with respect to radiation stability. In those cases where an investigator is interested only in the total absorbed dose in a given material, its direct measurement by any calorimetric method is undoubtedly the most precise. However, since knowledge of the dose in an extensive set of materials is required in point of fact and the replacement of absorbers in irradiated calorimeters is extremely difficult (particularly because of their activation) (even in heat deflectors [124]), measurement of the dose  $D_s$  in some standard material is most convenient. Conversion from  $D_s$  to  $D_i$  in a given material is accomplished by means of the expression

$$D_i = D_s^\gamma K_\gamma + D_s^n K_n. \quad (13)$$

In most cases, polyethylene can be such a standard material. This conclusion is based on the following considerations.

1. As shown in a number of papers [5, 35], the quantity  $K_n = (D_i/D_{CH_2})^n$  in the range  $6 < Z < 82$  and over a broad set of neutron spectra (from a  $1/E$  spectrum to a fast-reactor spectrum) is independent of the type of spectrum within 6-10% and with  $\epsilon_{K_n}$  affecting  $\epsilon_m$  very slightly.
2. The quantity  $K_\gamma = (D_i/D_{CH_2})^\gamma$  for  $Z_{ef} < 20$  depends little on the effective energy of a reactor  $\gamma$ -ray spectrum (see examples for  $CH_2$  and C). For  $Z = 20$ ,  $K_\gamma$  varies by  $\pm 2\%$  over the range  $0.4 < E_{av} < 2.0$  MeV.
3. As shown above, the maximum accuracy in the determination of dose composition is obtained when using the  $CH_2$ -C pair.
4. Limitation of the accuracy in  $K_\gamma$  to the value  $Z = 20$  does not play an important part in many cases since the magnitude of the total absorbed dose is mainly required in radiochemical studies where the radiation yields for  $\gamma$  rays and neutrons are approximately the same in most cases. In radiochemistry problems, low- $Z$  elements are mainly considered. In radiation physics problems where elements with medium and high  $Z$  are used only the neutron component of the dose is required, obviously, since  $\gamma$  irradiation in a background of neutron radiation does not yield significant radiation transformation. In this case, the quantity  $K_\gamma$  is not needed.
5. Graphite is a radiation-resistant material for use as a standard material in the measurement of  $\gamma$ -ray absorbed dose [125]. The change in its thermophysical properties under neutron irradiation is quite small, which is important for calorimetry, and it has been thoroughly studied [126]. Polyethylene is considerably less radiation resistant; however, its mechanical strength increases under moderate irradiation, the working temperature increases to  $\sim 200^\circ C$ , and the change in thermophysical characteristics as a function of absorbed dose has been studied rather thoroughly [127, 128]. We have shown previously that the energy stored in polyethylene during irradiation does not exceed 0.7% [129]. Unfortunately, the low thermal conductivity of polyethylene increase the calorimeter time constant.

From our estimates, the error in the determination of total absorbed dose in elements with  $Z < 20$  by conversion of data for absorbed dose rate and composition in polyethylene obtained by the outstripping method is 5-15% in the range  $0.85 > m_H > 0.40$  and  $3 < \epsilon_D < 5\%$ . Under the same conditions,  $\epsilon_{D_n}$  is 7-11%, which satisfies present requirements.

At the present time, work is being done on standardization of  $\gamma$ -ray absorbed dose measurements [86] and neutron flux measurements in reactors [130]. The time has come for standardization of reactor-radiation dosimetry also. We hope that this review will prove to be useful in the performance of such work.

The authors thank V. I. Ivanov, Yu. I. Bregadze, and V. V. Generalova for discussions and valuable advice.

#### LITERATURE CITED

1. In-Pile Dosimetry, Techn. Rep. Ser., No. 46, IAEA, Vienna (1965).
2. Neutron Fluence Measurements, Tech. Rep. Ser., No. 107, IAEA, Vienna (1970).
3. Determination of Absorbed Doses in Reactors, Techn. Rep. Ser., No. 127, IAEA, Vienna (1971).
4. S. Gunn, Nucl. Instrum. and Methods, 29, 1 (1964).
5. J. K. Linacre and R. Thomas, AERE-R 4805 (1965).
6. J. Kott, Jaderna Energie, 12, 289 (1966).
7. S. Gunn, UCRL-50173 (1967).
8. S. Gunn, Nucl. Instrum. and Methods, 85, 285 (1970).
9. A. M. Kabakchi, Ya. I. Lavrentovich, and V. V. Pen'kovskii, Chemical Dosimetry of Ionizing Radiation [in Russian], Izd. AN Ukrainian SSR, Kiev (1963).
10. Radiation Dosimetry, F. Attix et al. (editors), 2nd edition, Vol. 3, Academic Press, New York (1969).
11. B. R. Bergel'son and G. A. Zorikoev, Handbook on Protection against Radiation from Extended Sources [in Russian], Atomizdat, Moscow (1965).
12. A. Boyd et al., Nucl. Sci. and Engng., 22, 487 (1965).

13. W. Dixon, Nucl. Instrum. and Methods, 103, 415 (1972).
14. A. Anderson and R. Waite, AERE-c/R 2713 (1961).
15. S. Stolte, Atomkernenergie, 14, 417 (1969).
16. D. Kline and A. Jacobs, J. Appl. Phys., 20, 1741 (1959).
17. N. G. Gusev et al., Protection against Ionizing Radiation [in Russian], Atomizdat, Moscow (1969).
18. B. M. Isaev and Yu. I. Bregadze, Neutrons in Radiobiological Experiments [in Russian], Nauka, Moscow (1967).
19. W. Primak, J. Appl. Phys., 27, 54 (1956).
20. E. Lewis and R. Pfeffer, Nucl. Sci. and Engng., 27, 581 (1967).
21. S. Kahn et al., Nucl. Sci. and Engng., 23, 8 (1965).
22. A. Boyd and O. Miller, Canad. J. Chem., 46, 3773 (1968).
23. V. S. Karasev and V. M. Kolyada, At. Énerg., 19, 532 (1965).
24. J. Kott, Techn. Dig. (Prague) Scoda Works, 10, 3 (1968).
25. D. Richardson, ORNL-129 (1948).
26. C. Ellis and W. Wooster, Phil. Mag., 50, 521 (1925).
27. J. Zlotowski, J. Phys. Rad., 6, 241 (1935).
28. E. Storm and H. Israel, Gamm-Ray Interaction Cross Sections [Russian translation], Atomizdat, Moscow (1973); Nuclear Data Tables, 7, No. 6, 565 (1970).
29. J. Hubbel, NSRDS-NBS-29 (1969).
30. D. I. Leipunskii, B. V. Novozhilov, and V. N. Sakharov, Propagation of  $\gamma$  Rays in Matter [in Russian], Fizmatgiz, Moscow (1960).
31. W. Unruh and M. Tomlinson, Nucl. Appl., 3, 548 (1967).
32. R. Bach and R. Caswell, Radiat. Res., 35, 1 (1968).
33. F. A. Makhlis and I. M. Kolpakov, At. Énerg., 18, 51 (1965).
34. E. Proksch and H. Bildstein, Atomkernenergie, No. 11/12, 431 (1964).
35. B. A. Briskman and V. P. Savina, Proceedings I All-Union Conference on Metrology of Neutron Radiation [in Russian], Standarty, Moscow (1972).
36. J. Rowlands, J. Nucl. Energy, 13, 14 (1960).
37. J. Hayder and R. Kenward, AERE-R 2886 (1959).
38. A. Anderson and J. Linacre, Selected Topics in Radiation Dosimetry, IAEA, Vienna (1961).
39. G. Whyte, Rad. Res., 18, 265 (1963).
40. K. Zimmer, Z. Phys., 42, 360 (1941).
41. Yu. I. Bregadze, B. M. Isaev, and V. A. Kvasov, At. Énerg., 9, 126 (1960).
42. Yu. I. Bregadze et al., Neutron Dosimetry, IAEA, Vienna (1963).
43. B. R. Kirichinskii et al., in: Biological Effects of Neutron Radiation [in Russian], Naukova Dumka, Kiev (1965).
44. B. M. Isaev and Yu. I. Bregadze, Radiobiologiya, 6, 140 (1966).
45. J. DeGoer, C. Fiche, and J. P. Noel, CEA-N-1219 (1969).
46. M. Ladu and M. Pelliccioni, Nucl. Instrum. and Methods, 39, 339 (1966).
47. M. Ladu and M. Pelliccioni, Nucl. Instrum. and Methods, 53, 35 (1967).
48. M. Ladu and M. Pelliccioni, Nucl. Instrum. and Methods, 53, 71 (1967).
49. G. Z. Gochaliev and S. I. Borisova, At. Énerg., 31, 138 (1971).
50. G. Neary et al., Chronic Radiation Hazards — An Experimental Study with Fast Neutrons, Pergamon Press, Oxford (1957), pp. 28-89.
51. G. S. Hurst, R. H. Ritchey, and V. A. Mills, in: Dosimetry of Ionizing Radiation [Russian translation], Gostekhizdat, Moscow (1956).
52. G. S. Hurst et al., Rev. Scient. Instrum., 27, 153 (1956).
53. G. S. Hurst and K. Wagner, in: Collected Papers from Symposium on Selected Problems in Dosimetry [Russian translation], Gosatomizdat, Moscow (1962).
54. V. I. Ivanov, Neutron Dosimetry, IAEA, Vienna (1963).
55. J. Pucheault, J. Chim. Phys., 53, 750 (1956).
56. S. Kondo, Isotop. Radiation, 2, 120 (1959).
57. D. Flory, Nucleonics, 21, No. 12, 50 (1963).
58. P. Harteck and S. Dondès, Nucleonics, 14, No. 3, 66 (1956).
59. E. Jeltsch, Atomkernenergie, 14, 369 (1969).
60. A. Boyd, Nucleonics, 22, No. 7, 6 (1964).
61. F. Moseley and A. Truswell, AERE-R-3078 (1960).
62. S. V. Starodubtsev, Sh. A. Aslaev, and V. V. Generalova, At. Énerg., 8, 264 (1960).

63. S. V. Starodubtsev, V. V. Generalova, and G. V. Polyak, in: Radiation Physics [in Russian], Izd. AN Latvian SSR, Riga (1964), No. 11, p. 27.
64. V. V. Generalova, in: High-Dose Dosimetry [in Russian], FAN, Tashkent (1966), p. 29.
65. E. P. Kovaleva, E. P. Petryaev, and E. P. Kalyazin, in: Dosimetry and Radiation Processes in Dosimetric Systems [in Russian], FAN, Tashkent (1972), p. 167.
66. I. Draganic et al., Internat. J. Appl. Rad. and Isotopes, 16, No. 3 (1965).
67. V. Marcovic and I. Draganic, Rad. Res., 36, 588 (1968).
68. M. Labrousse et al., Note CEA-N-1168 (1969).
69. E. Proksch, Atompraxis, 13, No. 4, 5190 (1967).
70. H. Angstrom and L. Ehrenberg, in: Collected Papers from Symposium on Selected Problems in Dosimetry [Russian translation], Gosatomizdat, Moscow (1962).
71. Ya. I. Lavrentovich et al., At. Énerg., 19, 273 (1965).
72. G. Ahnstrom et al., RT/BJO (64) 26 (1964).
73. Yu. S. Ryabukhin, in: Dosimetry and Radiation Processes in Dosimetric Systems [in Russian], FAN, Tashkent (1972), p. 485.
74. Z. Spurny, Jaderna Energie, 9, 329 (1963).
75. S. Sigloff, Nucleonics, 14, No. 10, 54 (1956).
76. E. P. Petryaev, E. P. Kalyakhin, and E. P. Kovaleva, in: Dosimetry and Radiation Processes in Dosimetric Systems [in Russian], FAN, Tashkent (1972), p. 170.
77. E. E. Baroni et al., Pribory i Tekh. Éksperim., No. 5 (1968).
78. M. N. Gurskii and A. N. Tsoi, in: Radiation Dosimetry and Spectrometry of Ionizing Radiation [in Russian], FAN, Tashkent (1970), p. 174.
79. V. V. Generalova et al., Abstracts of Papers at IV All-Union Conference on Dosimetry of Intense Fluxes of Ionizing Radiation [in Russian], Izd. VNIIFTRI, Moscow (1971).
80. Ya. I. Lavrentovich et al., At. Énerg., 27, 296 (1969).
81. Ya. I. Lavrentovich et al., in: Dosimetry and Radiation Processes in Dosimetric Systems [in Russian], FAN, Tashkent (1972), p. 178.
82. J. Jasumasa et al., J. Nucl. Sci. and Technol., 8, 394 (1971).
83. J. Peters, US Patent 3673107 (1972).
84. V. V. Tkachenko, in: Radiation Dosimetry and Spectrometry of Ionizing Radiation [in Russian], FAN, Tashkent (1970), p. 169.
85. G. S. Bologova et al., in: Dosimetry and Radiation Processes in Dosimetric Systems [in Russian], FAN, Tashkent (1972), p. 162.
86. Yu. I. Bregadze and V. V. Generalova, idem, p. 3.
87. G. S. Bologova et al., in: Radiation Dosimetry and Spectrometry of Ionizing Radiation [in Russian], FAN, Tashkent (1970), p. 165.
88. A. H. Muggleton, J. Sci. Instrum., 5, 390 (1972).
89. G. M. Obaturov and Yu. K. Chumbarov, in: Collected Papers on Problems in Dosimetry and Radiometry of Ionizing Radiation [in Russian], Atomizdat, Moscow (1972).
90. V. V. Tkachenko et al., At. Énerg., 35, 210 (1973).
91. A. Seedy et al., Rad. Res., 40, 552 (1969).
92. P. McGinley, Health Phys., 23, 105 (1972).
93. P. Block and R. Weber, idem, p. 123.
94. G. Dearnaley et al., Trans. Nucl. Sci., 9, 174 (1962).
95. V. P. Kovalev, S. P. Kapchigashev, and L. P. Pavlov, At. Énerg., 34, 7 (1973).
96. D. Richardson et al., I Geneva Conference (1955), US Paper 8/P/154.
97. P. Dyne and W. Thurston, CRC-696 (1957).
98. A. Anderson and R. Waite, AERE-C/R 2253 (1960).
99. B. Radak et al., Bull. Boris Kidric Institute, 12, No. 253 (1961).
100. D. Bopp and R. Towns, Nucl. Sci. and Engng., 13, 245 (1962).
101. W. Lewis, Nucl. Sci. and Engng., 18, 1 (1964).
102. J. De Goer, CEA-R-2443 (1964).
103. H. Leyers, Nukleonik, 7, 300 (1965).
104. B. A. Briskman et al., in: High-Dose Dosimetry [in Russian], FAN, Tashkent (1966), p. 185.
105. K. Ohno and S. J. Hayakawa, Nucl. Sci. and Technol., 4, 555 (1967).
106. G. Cummings, Nucl. Appl., 3, 641 (1967).
107. V. A. Terekhin and L. V. Poret'skii, At. Énerg., 25, 156 (1968).
108. B. A. Briskman, Yu. V. Matveev, and A. G. Vasil'ev, At. Énerg., 27, 342 (1969).

109. L. Bod and B. Radak, Bull. Boris Kidric Institute, 20, Chemistry, No. 2 (1969).
110. Sakata et al., Nucl. Sci. and Technol., 8, 563 (1971).
111. C. Nycz et al., JNR-1347 (1971).
112. K. Mehta, Trans. Amer. Nucl. Soc., 14, 911 (1971).
113. Karsten Haack, Riso Rept. No. 256 (1972), p. 29.
114. Hayashi Takao et al., J. Nucl. Sci. and Technol., 9, No. 2 (1972).
115. N. S. Berezin and N. P. Zhidkov, Computational Methods [in Russian], Fizmatgiz, Moscow (1962), Ch. 1.
116. B. A. Briskman, Khimiya Vysokikh Énergii, 6, No. 1, 38 (1972).
117. E. A. Kramer-Ageev et al., Abstracts of Papers at All-Union Symposium on Radiation Defects in Semiconductors [in Russian], Izd. BGU, Minsk (1972).
118. I. Kh. Abdukadyrova et al., in: High-Dose Dosimetry [in Russian], FAN, Tashkent (1966), p. 168.
119. B. A. Briskman et al., Heat and Mass Transport, Vol. 7 [in Russian], Nauka i Tekhnika, Minsk (1968), p. 229.
120. B. A. Briskman et al., At. Énerg., 27, 50 (1969).
121. B. A. Briskman et al., in: Radiation Dosimetry and Spectrometry of Ionizing Radiation [in Russian], FAN, Tashkent (1970), p. 148.
122. B. A. Briskman and V. D. Bondarev, in: Dosimetry and Radiation Processes in Dosimetric Systems [in Russian], FAN, Tashkent (1972), p. 157.
123. B. A. Briskman, Inzh. Fiz. Zhurn., No. 4, 681 (1973).
124. S. S. Ogorodnik, Dissertation, Moscow (1969).
125. Report MKRE No. 14 (1969).
126. V. S. Chirkin, Thermophysical Properties of New Technical Materials [in Russian], Atomizdat, Moscow (1968).
127. B. A. Briskman and V. D. Bondarev, Heat and Mass Transport, Vol. 7 [in Russian], Nauka i Tekhnika, Minsk (1968), p. 464.
128. V. P. Savina, B. A. Briskman, and V. D. Bondarev, Vysokomolekulyarnya Soedineniya, A14, No. 5, 1180 (1972).
129. B. A. Briskman, Khimiya Vysokikh Énergii, 8, No. 1, 80 (1974).
130. R. D. Vasil'ev, Metrology of Neutron Radiation in Reactors and Accelerators. Abstracts [in Russian], VNIIFTRI, Moscow (1971), p. 16.

## ABSTRACTS

APPLICATION OF THE BUBNOV - GALERKIN METHOD  
TO A MULTIGROUP CALCULATION OF A  
TWO-DIMENSIONAL REACTOR

I. P. Kukharenek

UDC 621.039.51.12

Using an example of a solution of an integrodifferential equation with three variables:

$$M(u, r, z) \varphi(u, r, z) + \omega N(u, r, z) \varphi(u, r, z) = 0$$

we give a new method for obtaining calculation formulas of variational methods, on the basis of which certain concepts of tensor analysis are assumed. It is possible that this method has an analogy with the Dirac method [1] and reduces to the following: at first, in simple spaces, to find reference operators; then, using tensor transformations, to construct an operator that represents the reactor in the complex space of interest to us. Evidently, the principal advantages of such a method are the uniformity of the procedures and the quick operation with a given number of trial functions.

The method is realized in a program for calculating a cylindrical reactor [2]. The spatial-energy distribution of neutrons is sought in the form of a triple series:

$$\varphi(u, r, z) = t_{j\lambda} h_j^i(u) f_\lambda^i(r) f_z^i(z),$$

where the  $h_j(u)$  are local functions (this is equivalent to using a group method for describing the energy dependence). The functions  $f_\xi(x) = f_\lambda(r), f_l(z)$  can be as follows: a) given in the form of tables, i. e., practically arbitrary; b) polynomials of the form  $f_\xi(x) = b_{\xi i} g_i^i(x)$ , where the functions  $g_i(x)$  are given in the form of standard tables, and the coefficients  $b_{\xi i}$  can be arbitrary; c) the coefficients  $b_{\xi i}$  are eigenvectors of the matrix that represents a multiregion one-dimensional one-group reactor-model in the space  $g_i(x)$ ; the diffusion coefficients, the absorption cross section of the thickness of the band of the model can be arbitrary.

The principal constraints on the program are the following: no more than 26 groups, up to 25 trial functions in the given group, and up to 40 bands. Presently the program is included in the complex of [3], according to which macro- and micro-cross sections are calculated taking account of the blocking of resonances, the number of processes, and the breeding ratios; we derive the reactor criticality by variation of concentrations. This complex is in the code of a BESM-4 and is formulated just as the standard program of an IS-2 system. The volume of the complex is 8500 words.

The calculation time of the program [2] for 26 groups,  $5 \times 3$  trial functions, 10 zones is  $\sim 6$  min. Examples are given (the  $f_\lambda$  are Bessel functions, and the  $f_l$  are cosinusoidal functions) showing that for such a number of trial functions, a calculation accuracy of the neutron fields of multizone profiled fast reactors that is sufficient for practice is attained.

## LITERATURE CITED

1. Ya. A. Skhouten, Tensor Analysis for Physicists [in Russian], Nauka, Moscow (1965), pp. 333-372.
2. I. P. Kukharenek, Preprint of NIIAR, P-103 (1971).
3. I. P. Kukharenek, Preprint of NIIAR, P-164 (1972).

---

Translated from Atomnaya Énergiya, Vol. 36, No. 1, pp. 51-52, January, 1974. Original article submitted January 15, 1973.

© 1974 Consultants Bureau, a division of Plenum Publishing Corporation, 227 West 17th Street, New York, N. Y. 10011. No part of this publication may be reproduced, stored in a retrieval system, or transmitted, in any form or by any means, electronic, mechanical, photocopying, microfilming, recording or otherwise, without written permission of the publisher. A copy of this article is available from the publisher for \$15.00.

MEASUREMENT OF THE ABSOLUTE INTENSITY OF  
THE 278 keV LINE OF  $\text{Np}^{239}$ 

L. N. Yurova, A. V. Bushuev,  
V. I. Petrov, A. G. Inikhov,  
V. N. Ozerkov, and V. V. Chachin

UDC 539.122.164

Using a Ge(Li) spectrometer, we have measured the absolute intensity of the 278 keV line of  $\text{Np}^{239}$ . The line was observed in the spectrum of a uranium sample irradiated in the thermal column of the F-1 reactor at the I. V. Kurchatov Institute of Atomic Energy.

In order to determine the absolute intensity, we used the expression

$$\gamma_{239\text{Np}}^{278} = \frac{A_0}{N_8 \sigma_{\text{ctn}}^8 n g n v_0 (1 - e^{-\lambda_{\text{Np}^{239}} t_0}) e^{-\lambda_{\text{Np}^{239}} t_0} K} \left( 1 - \frac{1}{R_{\text{Cd}}} \right),$$

where  $A_0$  is the total number of pulses in the peak;  $N_8$  is the number of  $\text{U}^{238}$  nuclei in the sample;  $\sigma_{\text{ctn}}^8$  is the cross section for radiative capture of thermal neutrons in  $\text{U}^{238}$  ( $\sigma_{\text{ctn}}^8 = 2.69 \pm 0.03$ );  $\epsilon$  is the efficiency of the Ge(Li) spectrometer for  $E_\gamma = 278$  keV, which was determined by using a  $\text{Hg}^{203}$  source (No. 049 in the IAEA collection);  $R_{\text{Cd}}$  is the cadmium ratio for the foils used, which was found experimentally to be  $70 \pm 3$ ;  $n v_0$  is the neutron flux at the sample during the period of irradiation, estimated using gold foils  $20 \mu$  thick which were loaded together with the uranium samples.

The coefficient  $K$  takes into account the self-absorption of the 278 keV gamma radiation within the uranium sample; the value of  $K$  was determined experimentally from measurements with a collection of samples of various thicknesses. The activities of the gold foils were measured with a calibrated scintillation spectrometer.

An ÉVM M-220 computer was used to analyze the spectra obtained. We list below the values of the absolute intensities (for comparison, the results of [1, 2] are listed as well):

	Absolute Intensity
Results of [1]	$0.141 \pm 0.007$
Results of [2]	$0.145 \pm 0.004$
Present results	$0.141 \pm 0.004$

It is clear that the results are identical within the limits of error.

## LITERATURE CITED

1. G. Ewan et al., Phys. Rev., 108, 1308 (1957).
2. G. Ewan and M. Wahlgram, Nucl. Instr. and Meth., 99, 337 (1972).

---

Original article submitted March 20, 1973.



PARAMETERS OF THE RADIATION FIELD NEAR AN  
APPARATUS USED FOR AGRICULTURAL IRRADIATION

V. P. Bulatov and E. I. Tsygankov

UDC 621.039.83

The "Gamma-field" radiation engineering apparatus is used for agricultural irradiation under natural conditions in a vegetation process in order to obtain source material for selection, and also to solve a number of problems connected with plant-growing. The apparatus was placed in a field. An earth embankment was built at a radius  $R_2 = 30$  m from the apparatus, and a protective zone terminated at a radius  $R_1 = 200$  m. A 1660 Ci  $\text{Co}^{60}$  source was placed in a container at a height of 3.5 m from ground level. The radius of the irradiation zone  $R_3 \sim 25$  m. We studied the regularities of the formation of the radiation field in the irradiation zone as well as outside its boundaries, and developed the engineering technique for calculating the optimal parameters for such types of apparatus. It should be noted that few studies of the radiation field of such a geometry have been published.

The present experimental studies are used to obtain semiempirical relations which enable one to calculate the spatial distribution of the dosage rate within the irradiation zone and beyond its boundaries. The dosage rate at the surface of the ground in the irradiation zone can be calculated with the formula

$$P(r) = \frac{Q_0 h E_\gamma}{4\pi (h^2 + r^2)^{3/2}} \bar{\gamma}_a \cdot 1.6 \cdot 10^{-8} \left( 1 + \frac{2r^4}{(r^2 + h^2)^2} \right) \text{ R/sec} \quad (1)$$

where  $Q_0$  is the activity of the source in photons/sec,  $\bar{\gamma}_a$  is the mass absorption coefficient in  $\text{cm}^2/\text{g}$  of photons with energy  $E_\gamma$  in air,  $r$  is the distance in cm between the detector and the projection on the earth's surface of the point at the location of the source, and  $h$  is the height in cm at which the source is located. The variation of the dosage rate beyond the boundaries of the earthen embankment is given by the following expression:

$$P(r) = 8.9 \cdot 10^{-4} Q (9.0e^{-2.73 \cdot 10^{-4} r} + 2.0e^{-1.2 \cdot 10^{-4} r}), \quad (2)$$

where  $r$  is expressed in cm,  $P$  in  $\mu\text{R}/\text{sec}$ , and  $Q$  in Ci. The first term in Eq. (2) is dominant in the region  $r \leq (1-2)\lambda$ , where  $\lambda$  is the gamma photon mean free path in air, and the index of the exponent of this term is close to the coefficient of linear attenuation in air of gamma photons whose energy is  $\sim 180$  keV. The second term in Eq. (2) results from the radiation reflected from the ground in the zone of irradiation and passing (glancing) over the embankment in the direction of the detector, while the index of the exponent has an absolute value approximately equal to the linear attenuation coefficient in air of gamma rays with energy  $\sim 700$  keV.

The error in the radiation level estimated with the semiempirical formulas (1) and (2) is at most  $\pm 10\%$ . In order to determine the optimal dimensions of the shielding embankment for the given dimensions of the shielding zone (400 m in diameter), the Monte Carlo method was used to make theoretical calculations on the ÉVM M-22 computer, with an error of  $\pm(15-20)\%$ .

The calculations showed that for  $R_3 = 30$  m and  $R_1 = 200$  m, the optimum height of the embankment  $H = 6$  m. The formula which is given in the present article can be used to calculate the height of the protective embankment when the dimensions of the zone of irradiation lie in the interval  $10 \text{ m} < R_2 < 30 \text{ m}$ . For  $R_2 > 50$  m, the height of the embankment is almost independent of the radius of the zone of irradiation and is equal to the height at which the source is located plus two or three meters.

## LETTERS TO THE EDITOR

CALCULATION OF INTEGRATED CROSS SECTIONS OF  
COMPTON INTERACTION, SCATTERING, AND  
ABSORPTION OF  $\gamma$  QUANTA FOR STATISTICAL  
MODELING OF TRANSPORT PROCESSES

O. S. Marenkov and V. N. Mitov

UDC 539.121.72/75

The energy dependences of the integrated cross sections of Compton interaction and actual scattering of  $\gamma$  quanta with accuracy up to a constant multiplier are determined by the following expressions:

$$\sigma(\beta) = \left( \frac{2}{\beta} - \frac{8}{\beta^2} - \frac{16}{\beta^3} \right) \ln(1+\beta) + \frac{16}{\beta^2} + (1+\beta)^{-1} + (1+\beta)^{-2}; \quad (1)$$

$$\sigma_s(\beta) = \frac{8}{\beta^3} \ln(1+\beta) - \frac{8}{\beta^2} (1+\beta)^{-1} + \frac{2\beta^2 - 4}{\beta} (1+\beta)^{-2} + \frac{2\beta^2}{3} (1+\beta)^{-3}, \quad (2)$$

where  $\beta$  is twice the energy of  $\gamma$  quanta in units of electron potential-energy. The integrated cross section of actual Compton absorption  $\sigma_a(\beta) = \sigma(\beta) - \sigma_s(\beta)$ .

For statistical modeling of  $\gamma$  transport in a substance by the Monte Carlo method, the linear attenuation factors for Compton interaction, scattering, and absorption are calculated based on (1) and (2). In the energy region  $\beta < 1$ , degradation of the energy of the quanta during "slowing" occurs comparatively slowly, and repeated application of Eqs. (1) and (2) from the point of view of expenditure of computer time becomes less economical owing to the presence of a logarithmic function, which can be calculated using a standard subprogram.

It is known that in the  $\gamma$ -quanta energy region  $\beta < 1$  for the functions  $\sigma(\beta)$ ,  $\sigma_s(\beta)$ ,  $\sigma_a(\beta)$  we can obtain expressions in the form of series in powers of  $\beta$ . Like powers of the expansion can be a source of approximation formulas of polynomial type for calculation of the cross sections. We obtain power expansions in general form. To do this we use the well-known expansions in powers of series of logarithmic and binomial functions:

$$\ln(1+\beta) = \sum_{h=1}^{\infty} (-1)^{h+1} \frac{\beta^h}{h}; \quad (3)$$

$$(1+\beta)^m = 1 + \sum_{h=1}^{\infty} \binom{m}{h} \beta^h. \quad (4)$$

Series (3) converges in the interval  $-1 < \beta \leq 1$ , and series (4) converges for  $|\beta| < 1$ . In our problems  $\beta > 0$  always; therefore, we will not consider the values  $\beta < 0$  in what follows. Substituting (3) and (4) for the cases  $m = -1, -2, -3$  into Eqs. (1) and (2), after simple transformations we obtain

$$\sigma(\beta) = \sum_{h=0}^{\infty} (-\beta)^h \left( \frac{2}{k+1} + \frac{8}{k+2} - \frac{16}{k+3} + k+2 \right); \quad (5)$$

$$\sigma_s(\beta) = \sum_{h=0}^{\infty} (-\beta)^h \left( \frac{8}{k+3} + \frac{5}{3} k + \frac{k^2}{3} \right); \quad (6)$$

$$\sigma_a(\beta) = \sum_{h=0}^{\infty} (-\beta)^h \left( \frac{2}{k+1} + \frac{8}{k+2} - \frac{24}{k+3} - \frac{2}{3} k - \frac{k^2}{3} + 2 \right). \quad (7)$$

Translated from *Atomnaya Energiya*, Vol. 36, No. 1, pp. 53-54, January, 1974. Original article submitted May 18, 1972.

© 1974 Consultants Bureau, a division of Plenum Publishing Corporation, 227 West 17th Street, New York, N. Y. 10011. No part of this publication may be reproduced, stored in a retrieval system, or transmitted, in any form or by any means, electronic, mechanical, photocopying, microfilming, recording or otherwise, without written permission of the publisher. A copy of this article is available from the publisher for \$15.00.

TABLE 1. Energy Dependence of Accuracy of Approximation Formula (12)

$\beta$	Energy, keV	$\delta$ , %
0,2	51,1	0,0005
0,4	102,2	0,006
0,6	153,3	0,02
0,8	204,4	0,04
1	255,5	0,05

The series (5), (6), and (7) converge comparatively slowly for  $\beta < 1$ , which is due to the slow convergence of the series (3) and (4). Thus, use of the first five terms of the expansions (5) and (6) gives for the case  $\beta = 0.4$  an error in the calculation of  $\sigma$  and  $\sigma_s$  of 2.3 and 7%, respectively.

It makes sense to use polynomial-type approximations based on (5), (6), and (7) for calculational purposes only for the case  $\beta \ll 1$ , which is of little interest in the practical relation of the energy regions. For the case

$\beta \leq 1$  we develop expansions that are of interest also in the calculated relation. For this purpose we apply the Euler transformation one time to the slowly converging series (3):

$$\ln(1+\beta) = -\frac{1}{1+\beta} \left[ \sum_{k=1}^{\infty} \frac{(-\beta)^k}{k} + \sum_{k=1}^{\infty} (-1)^k \frac{\beta^{k+1}}{k} \right] = \frac{1}{1+\beta} \left[ \beta + \sum_{k=2}^{\infty} \frac{(-\beta)^k}{k(k-1)} \right]. \quad (8)$$

Series (8) converges for  $\beta \leq 1$ . It is not difficult to verify the expansions (8) in comparison with (3) using refined calculations. Substituting (8) into (1) and (2), after transformations, we obtain

$$\sigma(\beta) = \frac{1}{1+\beta} \left[ \frac{\beta^2}{1+\beta} + \frac{8}{3} + 6 \sum_{k=2}^{\infty} (-\beta)^k \frac{k^2 - 3k - 2}{k(k+1)(k+2)(k+3)} \right]; \quad (9)$$

$$\sigma_s(\beta) = \frac{1}{1+\beta} \left[ \frac{2\beta(\beta^2 - 2)}{3(1+\beta)^2} + \frac{8}{3} - 8 \sum_{k=2}^{\infty} \frac{(-\beta)^k}{(k+2)(k+3)} \right]; \quad (10)$$

$$\sigma_a(\beta) = \frac{1}{1+\beta} \left[ \frac{\beta(\beta^2 + 3\beta + 4)}{3(1+\beta)^2} + 2 \sum_{k=2}^{\infty} (-\beta)^k \frac{7k^2 - 5k - 6}{k(k+1)(k+2)(k+3)} \right]. \quad (11)$$

The series in Eqs. (9), (10), and (11) converge for  $\beta \leq 1$ .

The calculational advantages of the expansions (9), (10), and (11) in comparison with (5), (6), and (7) are illustrated in example (9). Restricting ourselves to two terms of the series in (9), we obtain the approximation formula

$$\sigma(\beta) \approx \frac{1}{1+\beta} \left( \frac{\beta^2}{1+\beta} + \frac{8}{3} - \frac{1}{5} \beta^2 + \frac{1}{30} \beta^3 \right). \quad (12)$$

The errors  $\delta$  of the calculation  $\sigma(\beta)$  based on the formula (12) are presented in Table 1.

As follows from Table 1, the errors in the calculation of  $\sigma$  in the region  $\beta \leq 1$  are small and decrease with decreasing energy. There is practical sense in the successive use of expressions (1) and (12) for statistical modeling of the "slowing" of  $\gamma$  quanta, which economizes the computer time.

Note that expression (12) can be used in a wider energy range. For  $\beta > 1$  the series in (9) is diverging; however, the partial sums of the series can serve as a good approximation for calculating the corresponding function in a definite range of variation of  $\beta$ : thus, the error in calculation of  $\sigma$  using (12) for  $\beta = 2$  is 0.6%; we can recommend the use of expression (12) in the energy region  $\beta \leq 2$ .

CALORIMETRIC DOSIMETRY AND A PROCEDURE FOR  
IRRADIATING SAMPLES, IN ELECTRON ACCELERATOR  
INVESTIGATIONS OF THE RADIATION STABILITY  
OF PETROLEUM OILS

A. D. Stukin and G. I. Shor

UDC 539.12.08:621.384.658

We carried out our investigations on an electron accelerator mounted on the stand of a RUP-400-5 (RUP-3) x-ray set [1] with a BPV-400 x-ray tube. The anode reflector of the tube was replaced by a flange with an aluminum foil diaphragm (diameter 40 mm, thickness  $\sim 2 \mu$ ), so that the beam of accelerated electrons could exit to impinge on the specimen. The accelerating voltage was regulated over a range from 20 to 400 kV, the maximum current of the extracted electron beam was about 500  $\mu$ A (the foil was perforated at higher currents).

The range of low-energy electrons (0.3 to 0.4 MeV) traversing organic materials was roughly 1 mm, and the thickness of the layer of oil to be irradiated, in amounts sufficient for the subsequent analyses, was much greater. Moreover, the electron intensity in the beam transverse cross section decreased from the center edgeward [2], while the distribution pattern was not known precisely. The entire volume of the specimen was therefore agitated, in order to secure uniform irradiation of the oil.

Favorable conditions for heat transfer from the surface layer of oil to the bulk of the specimen exist in the process of intensive and uniform agitation. This then favors reliance on the method of adiabatic calorimetry [3], using the irradiated oils themselves as sensors [4], in the dosimetry of the electron beam.

The dosimetry and the irradiation were carried out in cells of two distinct types, depending on the nature of the specimen under investigation and the irradiation conditions specified.

The cell (Fig. 1) was a glass vessel about 50 cm<sup>3</sup> in volume, into which was poured the oil to be irradiated. A four-blade agitator paddle mounted in this vessel was actuated by a rotating magnet (MM-2 device), through the aid of a tiny steel beam soldered to the glass for that purpose. Recesses on the side surface of the vessel provided wells for four thermocouples. The top and bottom wells were located in mutually perpendicular vertical planes. The cell was lined with a layer of asbestos as lagging to cut down heat losses.

When oil or grease samples of high viscosity were irradiated, we used another cell (Fig. 2) with a mechanically driven agitator. This cell was a stainless steel vessel 65 mm in diameter and 50 mm high; the vessel was screwed down to the flange of the accelerator output window. A shaft protruding through the bottom of the vessel had a multibladed agitator at one end and was connected via an ebonite hard rubber coupling to the shaft of a PD-09 miniaturized electric motor at the other end ( $\sim 3$  rev/sec). Two thermocouples were inserted into the vessel through leaktight seals, so that they were insulated electrically from the walls of the vessel. Two pipe connections on the side surface of the vessel made it possible to establish the required gas medium, to evacuate air, or to sample off gases released in radiolysis. A tin plate jacket connected to the thermostat was fitted onto the body of the vessel in order to maintain the temperature of the specimen at the preset level throughout the irradiation process.

The oil to be irradiated heats up when acted upon by the electron beam. The temperature  $T$  of the specimen will rise linearly, for a certain time  $0 < t \leq \tau$  ( $t = 0$  is the time of onset of irradiation), no matter

---

Translated from *Atomnaya Energiya*, Vol. 36, No. 1, pp. 54-55, January, 1974. Original article submitted January 30, 1973.

© 1974 Consultants Bureau, a division of Plenum Publishing Corporation, 227 West 17th Street, New York, N. Y. 10011. No part of this publication may be reproduced, stored in a retrieval system, or transmitted, in any form or by any means, electronic, mechanical, photocopying, microfilming, recording or otherwise, without written permission of the publisher. A copy of this article is available from the publisher for \$15.00.

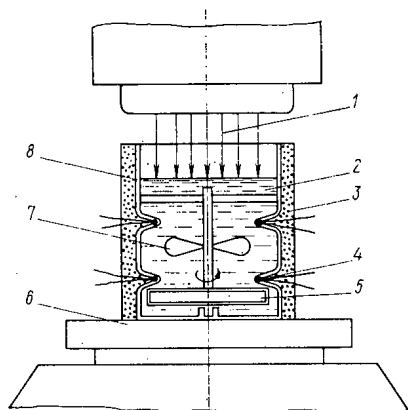


Fig. 1

Fig. 1. Cell with magnetically actuated agitator paddle: 1) stream of electrons; 2) sample to be irradiated; 3) asbestos lagging; 4) thermocouples; 5) steel beam soldered to glass; 6) magnetic agitator; 7) agitator paddle; 8) glass vessel.

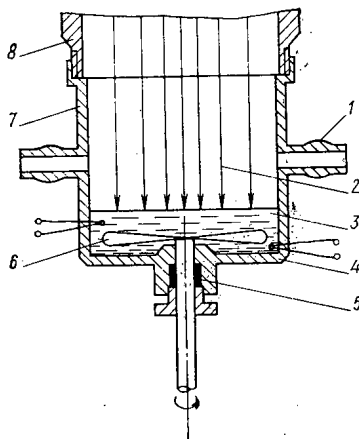


Fig. 2

Fig. 2. Cell with mechanically driven agitator paddle: 1) pipe connections; 2) electron stream; 3) sample to be irradiated; 4) thermocouples; 5) packing gland; 6) agitator paddle; 7) stainless steel vessel; 8) flange of accelerator output window.

what the ambient temperature. Since the heating rate  $dT/dt$  is determined solely by the dose rate  $P$  and the specific heat  $C$  of the material irradiated over the linear portion, we have

$$P = C (dT/dt). \quad (1)$$

The rate at which the temperature of the specimen rises is recorded with the aid of a M95 microammeter and thermocouples included in a compensation circuit. The dose rate is calculated from the formula

$$P = C \left( \frac{dT}{dI} \cdot \frac{dI}{dt} \right)_0. \quad (2)$$

The constant  $dT/dI = K$  is determined with the aid of a laboratory thermostat [4]. Its value depends on the type of thermocouples employed, the manner in which they are included in the circuit, and their number.

The formula used in calculating the absorbed dose power is:

$$P = 1.5 \cdot 10^3 KC (dI/dt)_0 \text{ Mrad/h}, \quad (3)$$

where the constant  $K$  is expressed in  $\text{deg}/\mu\text{A}$ ,  $C$  in  $\text{cal}/(\text{g} \cdot \text{deg})$ , and  $dI/dt$  in  $\mu\text{A}/\text{sec}$ .

#### LITERATURE CITED

1. D. M. Margolin and L. A. Vasil'ev in: *Advances in Physical Chemistry*, No. 3 [in Russian], Goskhimizdat, Moscow (1963), p. 134.
2. L. A. Vasil'ev and L. A. Dmitriev, in: *Advances in Physical Chemistry*, No. 3 [in Russian], Goskhimizdat, Moscow (1963), p. 140.
3. M. B. Fiveiskii, Yu. S. Lazurkin, and M. A. Mokul'skii, *At. Énerg.*, 9, 321 (1960).
4. Yu. S. Zaslavskii, A. D. Stukin, and G. I. Shor', *Khim. i Tekhnol. Toplív i Masel*, No. 10, 44 (1964).

STAGES OF FORMATION OF URANIUM AND RARE  
EARTH METAL MINERALIZATION IN  
SEDIMENTARY ROCKS

V. I. Danchev

UDC 553.495:553.068

Insufficient attention has been paid to the formation of higher concentrations of uranium and a number of other elements (germanium, beryllium, molybdenum, vanadium, selenium, rare earths, etc.) under exogenetic conditions, although such research could shed much light on the laws of spatial location of minerals of great practical importance.

The different migratabilities of uranium and its accompanying elements are due to the diversity of their concentration forms (sorption forms, organometallic complexes, mineral segregations), which appear in the early stages of formation and alteration of the adjoining rocks. This enables one to designate a number of mineral-geochemical indicators of the lithogenesis stages characterizing the paragenetic associations of elements for each stage.

The manifestation and the role of the various different stages of origin of ores (early — sedimentation-diagenetic and late — epigenetic) differ from one type of ore-adjoining rock to another. In carbonate shales, coals, and phosphate rocks the early stages are usually most distinct. In detrital rocks of high filtration capacity, the late (imposed) epigenetic concentrations are more marked. These exhibit a specific zonation and sequence of ore deposition. Carbonate rocks are characterized by the occurrence of both the early and latest processes of migration and concentration of the ore substance, as shown by the diverse textural and structural characteristics. Of course, to assess the occurrence of the early and late stages of ore genesis in each specific deposit we can also make use of a number of specific features: the presence of signs of erosion and redeposition of rocks of the ore-bearing horizon, the involvement of ore-bearing deposits in zones of submarine slumping, the appearance of late-diagenetic clastic dikes intersecting ore beds in uranium-coal deposits, etc. The sequence of secondary processes of ore genesis is established from the ratio of the ore-bearing intercalations with dislocations of different ages, and from the character of the epigenetic fissuration of the ore-adjoining rocks.

Experience in the investigation of exogenetic deposits and a number of rare metal deposits indicates that higher concentrations, including ore concentrations, are formed in different stages of lithogenesis of the adjoining rocks. In accordance with this, four exogenetic uranium concentrations are distinguished with different conditions of formation: sedimentation-diagenetic (essentially sedimentary); polygenetic, bearing traces of different stages of the exogenetic ore process; essentially epigenetic, imposed or hydrogenetic [1]; metamorphogenetic with clear traces of the sedimentary process and later migration of uranium in abyssal zones of the Earth's crust (Table 1).

Ideas regarding the stages of exogenetic ore formation have suggested the use of special methods for investigating ore and the adjoining rocks, revealing their characteristics in the early and later stages of ore genesis. These methods include:

- a) compilation of a series of facies-paleogeographical, lithological-geochemical profiles and maps for deposits of the pre-ore, ore, and post-ore stages of formation of the adjoining rocks, which enables one to reveal the basic principles of early (sedimentation-diagenetic) ore genesis;
- b) construction of geochemical and epigenetic profiles and maps, enabling one to reveal in greater detail the epigenetic zonation, to which the accompanying imposed ore concentrations may be related.

---

Translated from *Atomnaya Energiya*, Vol. 36, No. 1, pp. 55-57, January, 1974. Original article submitted February 19, 1973.

© 1974 Consultants Bureau, a division of Plenum Publishing Corporation, 227 West 17th Street, New York, N. Y. 10011. No part of this publication may be reproduced, stored in a retrieval system, or transmitted, in any form or by any means, electronic, mechanical, photocopying, microfilming, recording or otherwise, without written permission of the publisher. A copy of this article is available from the publisher for \$15.00.

TABLE 1. Formation of Exogenetic Uranium Deposits

STAGES OF FORMATION AND ALTERATION OF ADJOINING ROCKS							
Sedimentogenesis			Diagenesis			Epigenesis (Catagenesis)	
I	II	III	early	IV	late	V	
Disintegration of parent rocks	Transport of disintegration products	Accumulation of components of sediment	Diagenetic conversion of sediment to sedimentary rock			regressive	hypergenetic processes
						progressive	metamorphic processes
PROCESSES OF MIGRATION AND CONCENTRATION OF URANIUM							
Mechanical disintegration and chemical decomposition of rocks, a prominent part being played by living matter	Active migration of uranium in an oxidizing environment as uranyl carbonate, uranoorganic, uranyl molybdate and other complexes, and also as hydroxyl-uranyl, uranyl sulfate, etc.	Reaction of the sediment components with one another and with the ambient medium Biochemical decomposition of organic matter with formation of organic acids and their salts, with evolution of CO <sub>2</sub> , H <sub>2</sub> S, NH <sub>3</sub> , CH <sub>4</sub> , H <sub>2</sub> , etc.				1. Formation of reducing geochemical barriers with corresponding associations of elements in aquifers of sedimentary strata containing organic matter and sulfides  [U + Cu, Pb, Zn (Se) etc.] and [U + Se, etc.]	
	Sorption of uranium and accompanying elements (V, Cu, Mo, Pb, Zn, Se, Tr, Ge, Be, Ni, Co, etc.) by organic and mineral colloids, phosphates, clay minerals, hydroxides of Fe, Al, Mn, etc.)	1. Predominantly in Marine and Lacustrine Deposits Exchange reaction between bottom water and mud solutions Compaction of sediment, redistribution of substance, partial dehydration of sediment Removal of readily soluble salts $\text{Bottom water} = \text{Mud solution} = \text{Solid phases of sediment}$ $U \leq 11 \cdot 10^{-5} \text{ g/l} \quad   \quad U \leq 11 \cdot 10^{-5} \text{ g/l} \quad   \quad U = 11 \cdot 10^{-4} - 11 \cdot 10^{-2} \%$	Redox reactions with formation of nodules and concretions, replacement by iron sulfides and sooty uraninite of organic residues 2. Predominantly in Alluvial and other Stream Deposits and Peat Bogs In addition to processes characteristic of basin sediments, superimposition of interaction with uranium-bearing subsurface waters A characteristic feature is formation of reducing barriers on which uranium is concentrated ("exodiagenesis" concentration)				2. Rupture of sorption bonds of uranium (and a number of other elements) with organic matter, and their deposition as dispersed oxides (and other compounds); partial migration of these to the most deformed and fissured sectors of the bed  Metasomatic replacement of various components of the rock sooty uraninite and pitchblende
EXOGENETIC URANIUM DEPOSITS							
Oxidation zones of endogenic and exogenetic deposits	Clastogene deposits	Sheetlike-lenticular ore bodies with stratified and coagulation structures; nodules, concretions, uniformly dispersed mineralization forms				Epigenetically altered sedimentary uranium deposits, frequently with imposed fissured-streaky texture of ores	
Residual and infiltration uranium concentrators	Marine and alluvial uranium-thorium placers	1. Predominantly in marine and lacustrine deposits in carbonaceous-argillaceous, phosphate, and carbonate rocks, marls, etc.				1. Essentially hydrogenic epigenetic deposits with ore bodies of characteristic roll shape	
Adsorption accumulation of uranium in arid regions (deserts)	Sorption-biogenic and sorption-chemogenic uranium concentrations in the sediment	2. Predominantly in alluvial and other stream deposits in sandstones and siltstones, clays with residues of carbonized vegetable matter, in brown coals, lignites, peat bogs, etc. ("exodiagenesis" deposits)				2. Metamorphogenetic deposits with stratified ore banks including dispersed and vein forms of mineralization	
Weathered deposits	Sedimentation-diagenetic (essentially sedimentary) deposits					Epigenetic minerals	
	Polygenetic (multistage) deposits						

Within epigeosynclinal and epiplatform orogenic depressions of activated ancient mountain regions there is the possibility of entry of uranium and a number of other elements together with effusive material, and there may also be fumarole and hydrothermal activity, both during sedimentation and diagenesis and in the later stage of alteration of the ore-adjointing rocks. This is accompanied by convergence and interaction of exogenetic and endogenic processes of ore formation [2]. Table 1 also shows the possible role of endogenic sources, of uranium and other elements.

#### LITERATURE CITED

1. A. E. Fersman, Geochemistry, Vol. 2 [in Russian], ONTI, Leningrad (1934).
2. V. I. Smirnov, Geology of Useful Minerals [in Russian], Nedra, Moscow (1965).



GEOCHEMICAL ISOTOPIC ANOMALIES AND THE  
HYPOTHESIS OF NATURAL NUCLEAR REACTORS

R. S. Prasolov

UDC 539.183.2+621.039.5

Some experimental data have by now been accumulated concerning variations in the abundance of isotopes of a number of elements found in natural substances. For example, deviations of 3-20% from the Clarke isotope ratios have been observed in the case of  $^2\text{H}$ ,  $^{13}\text{C}$ ,  $^{18}\text{O}$ , and other isotopes. These differences may be attributable to isotopic fractionation in gravitational and temperature fields, to diffusive and biogeochemical separation, and also to phenomena involved in evaporation and radioactive recoil following alpha disintegration [1-4].

However, in addition to the minor differences mentioned above, observations reveal some very substantial isotopic anomalies which are difficult or impossible to explain on the basis of the above-mentioned mechanisms. For example, isotopic variations of the order of  $10^3$ - $10^{10}\%$  [1, 3-9] have been observed in the case of isotopes of helium, neon, xenon, samarium, plutonium, and other elements. One of the most probable reasons for such large deviations may be the occurrence of various nuclear reactions, including reactions of the  $(n, \gamma)$  type, in natural neutron fields, as the result of cosmic radiation, spontaneous fission of heavy nuclei, and other neutron-generating processes, which have been discussed in [3, 5]. It must be noted that some studies for determining the value of the natural neutron background (in particular, on the basis of the accumulation of fission-produced xenon in minerals) have shown a discrepancy between the calculated and measured values of the background, with the calculated neutron flux sometimes greater by several orders of magnitude than the measured value.

In the light of these facts, an explanation of the observed anomalies should be sought on the basis of the hypothesis of natural nuclear reactors (NNR) [3, 5, 8, 10, 11]; the anomalies conform to the laws deduced from this hypothesis. In particular, if other conditions are equal, there should exist a correlation between the effective neutron cross section and the value of the isotopic deviation for each particular isotope. We give below the results of a study bringing out such a correlation in the form of a single-parameter function  $\varphi = f(\sigma)$ ; this is only a crude first approximation and does not take into account the length of time the neutron field has been acting, the probable migration of isotopes under geophysicochemical influences, and other factors.

The most probable kinds of NNR are those which involve thermal neutrons produced by the fission of  $^{235}\text{U}$ ; for this reason, the effective neutron cross section,  $\sigma$ , for  $(n, \gamma)$  reactions, or the partial cross section of the  $(n, f)$  reaction for fragment products, was taken on the basis of known data used in reactor design for thermal reactors [12, 13], although in theory a number of anomalies may be caused by fluxes of intermediate and fast neutrons, resonance-absorption phenomena, etc.

The numerical value of the isotopic deviation  $\varphi$  was found from the ratio  $\varphi = (x_{\text{max}} - x_{\text{min}})/x_{\text{min}}$ , where  $x_{\text{max}}$  and  $x_{\text{min}}$  are the maximum and minimum experimental values of the percentage of the isotope under consideration in the natural mixture of isotopes of a particular specimen, as given in a number of studies [1-9], or else the extremum values of ratios of the type  $^{234}\text{U}/^{238}\text{U}$ .

Since the generation of a particular isotope from different original isotopes may have different values of  $\sigma$ , we first found the value of the Clarke factor of the element — the abundance of the isotope — the cross section of the nuclear reaction, on the basis of which we can make a rough choice of the cross-section value  $\sigma$  corresponding to a particular value of the parameter  $\varphi$ . We assumed an  $(n, \gamma)$  reaction for all of the

---

Translated from *Atomnaya Energiya*, Vol. 36, No. 1, pp. 57-59, January, 1974. Original article submitted February 19, 1973.

© 1974 Consultants Bureau, a division of Plenum Publishing Corporation, 227 West 17th Street, New York, N. Y. 10011. No part of this publication may be reproduced, stored in a retrieval system, or transmitted, in any form or by any means, electronic, mechanical, photocopying, microfilming, recording or otherwise, without written permission of the publisher. A copy of this article is available from the publisher for \$15.00.

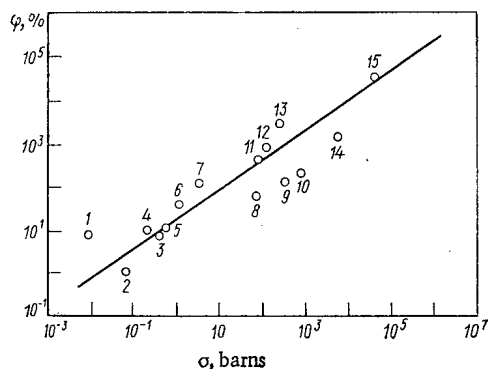


Fig. 1. Relative isotopic deviations as a function of effective neutron cross sections of the  $(n, \gamma)$  reaction: 1)  $^{13}\text{C}$ ; 2)  $^{15}\text{N}$ ; 3)  $^{18}\text{O}$ ; 4)  $^{34}\text{S}$ ; 5)  $^{24}\text{Mg}/^{26}\text{Mg}$ ; 6)  $^{87}\text{Sr}/^{86}\text{Sr}$ ; 7)  $^{148}\text{Nd}/^{150}\text{Nd}$ ; 8)  $^{144}\text{Nd}/^{145}\text{Nd}$ ; 9)  $^{235}\text{U}$ ; 10)  $^6\text{Li}/^7\text{Li}$ ; 11)  $^{140}\text{Ce}/^{142}\text{Ce}$ ; 12)  $^{234}\text{U}/^{238}\text{U}$ ; 13)  $^{143}\text{Nd}/^{142}\text{Nd}$ ; 14)  $^{151}\text{Eu}/^{153}\text{Eu}$ ; 15)  $^{149}\text{Sm}/^{147}\text{Sm}$ .

isotopes analyzed; an exception was made in the case of  $^{140}\text{Ce}$ , for which the NNR [8] was found to be more probable with an  $(n, f)$  reaction, whose partial cross section (taking into account the yield of fission fragments) is about 30-60 b. Despite the relative abundance of experimental data for inert gases, we did not analyze these data in the present study, since the values of  $\phi$  are very poorly defined, owing to the difficulty of preserving these gases [5].

In Fig. 1 we show the results obtained by processing experimental data for elements whose chances of being preserved in the crystal lattice of a mineral from the NNR zone are much higher than those of inert gases. In keeping with the concept of NNR, we find the expected correlation: as the effective neutron cross section increases, the isotopic deviation increases approximately as  $\phi \sim \sigma^{0.7}$ . It seems that if the results of geochronological measurements of the age of the anomalous specimens or the integral neutron fluxes were available, the dispersion of the points along the correlation line  $\phi = f(\sigma)$  would be smaller.

We shall consider below the results of findings on the plutonium content of specimens of natural substances, since plutonium can also serve as an indicator of NNR sites; the same is true of isotopic deviations of samarium, neodymium, and other elements [8].

Originally, the searches for natural plutonium were undertaken in order to determine whether the artificial production of plutonium was worth the considerable effort it required. It was found that in uranium minerals, under the influence of spontaneous-fission neutrons and other components of the natural neutron background, the maximum plutonium content was no higher than  $^{239}\text{Pu}/\text{U} \approx 10^{-11}$ , i. e., that the concentration of plutonium was too low for practical purposes [3, 14]. Later, however, higher concentrations of plutonium were discovered.

In [6, 7] plutonium-content ratios of  $^{239}\text{Pu}/\text{U} \approx 10^{-6}$  were reported. The excess of  $^{235}\text{U}$  may also be due to the formation of plutonium in the  $^{238}\text{U}(n, 2\beta)^{239}\text{Pu}$  reaction and the subsequent disintegration  $^{239}\text{Pu} \rightarrow ^{235}\text{U} + ^4\text{He}$ . A  $^{235}\text{U}$  excess of the order of 0.3-0.02% was found in [8, 15]; when recomputed in relation to the original  $^{239}\text{Pu}/\text{U}$  ratio in the NNR, this yields a value of  $10^{-3}$ - $10^{-4}$ , which may be of interest for practical purposes.

Hoffman et al. [9] describe the results of searches for  $^{244}\text{Pu}$ , which was found to occur in quantities  $10^6$ - $10^8$  times as large as the estimates based on the concept of  $^{244}\text{Pu}$  arriving on earth from outer space. The first substances in which  $^{244}\text{Pu}$  was observed were products of thermonuclear explosions accompanied by neutron fluxes of high density. If we consider the possibility of pulsed operation of NNR not only in the earlier but also in the later geological epochs, including the present [11], it becomes possible to explain on the basis of the NNR hypothesis the observed differences in both  $^{239}\text{Pu}$  content and  $^{244}\text{Pu}$  content [11, 16]: both isotopes are produced in NNR from uranium subjected to high NNR neutron fluxes.

The last assumption is partly confirmed by a comparison of the values of integral neutron fluxes found on the basis of direct neutron-flux measurements [3] and calculated from the values of isotopic deviations in NNR [8]. For measured fluxes of up to  $10^4$  neutrons/cm<sup>2</sup>·day and geological time values of the order of  $10^9$  yr, which is characteristic for uranium minerals, the integral background reaches values of  $\Phi_0 \approx 10^{15}$  neutrons/cm<sup>2</sup>. For isotopes from an NNR site the integral neutron flux is  $\Phi \approx 10^{21}$  neutrons/cm<sup>2</sup>, yielding a ratio of  $\Phi/\Phi_0 \approx 10^6$ .

Just as the  $^{239}\text{Pu}/\text{U}$  ratio was found to vary by factors of  $10$ - $10^8$ , so the  $^{244}\text{Pu}$  content and the integral neutron fluxes are found to vary by factors of  $10^6$ - $10^8$ .

On the basis of the above results obtained from comparisons of isotopic and neutron characteristics of geological specimens, there is reason to hope that the NNR hypothesis will prove useful for various practical and theoretical lines of study in a number of research programs.

## LITERATURE CITED

1. A. P. Vinogradov, Introduction to the Geochemistry of the Ocean [in Russian], Nauka, Moscow (1967).
2. Vulcanism and the Depths of the Earth [in Russian], Nauka, Moscow (1970).
3. G. V. Gorshkov et al., Natural Neutron Background of the Atmosphere and the Crust of the Earth [in Russian], Atomizdat, Moscow (1966).
4. P. I. Chalov, *At. Énerg.*, 27, No. 1, 26 (1969); *Izd. AN Kirg. SSR*, No. 5, 13 (1970).
5. Yu. A. Shukolyukov, Fission of Uranium Nuclei in Nature [in Russian], Atomizdat, Moscow (1970).
6. V. V. Cherdyntsev et al., *Geokhimiya*, No. 4, 3 (1968); No. 4, 7 (1969).
7. V. V. Cherdyntsev, N. B. Kadyrov, and N. V. Novichkova, *Geokhimiya*, No. 3, 16 (1970).
8. M. Neuilly et al., *Compt. Rend. de l'Acad. Sci., Paris*, 275, D-1847 (1972); R. Bodu et al., *ibid.*, D-1731 (see translations into Russian in: *Atomic Technology Outside the USSR*, No. 6, 6-9 (1973)).
9. D. Hoffman et al., *Nature*, 243, 19 (1971).
10. P. Kuroda, *J. Chem. Phys.*, 25, 781 (1956).
11. R. S. Prasolov, in: *Heat and Mass Transfer* [in Russian], Nauka, Minsk (1972); Vol. 2, Part 2, p. 540.
12. *Physics of Nuclear Reactors* [in Russian], Atomizdat, Moscow (1964).
13. I. V. Gordeev, D. A. Kardashov, and A. V. Malyshev, *Nuclear-Physics Constants* [in Russian], Atomizdat, Moscow (1963).
14. G. Seaborg, in: *Outline of Modern Geochemistry and Analytical Chemistry* [Russian translation], Nauka, Moscow (1972), p. 560.
15. V. V. Cherdyntsev, *Geokhimiya*, No. 4, 373 (1960).
16. E. Hyde, I. Perlman, and G. Seaborg, *The Transuranium Elements* [Russian translation], Atomizdat, Moscow (1967).

## THE THERMAL CONDUCTIVITY OF URANIUM DIOXIDE

V. I. Kolyadin, É. P. Il'in,  
A. G. Kharlamov, and V. V. Yakovlev

UDC 536.21:546.791

The thermal conductivity of uranium dioxide is a structure-sensitive property depending on a number of factors such as temperature, density, stoichiometric composition, preparation technology, burn-up, etc. This is the cause of the discrepancies between the results of measurements made by different authors (especially above 2000°K). Therefore to obtain reliable information on the thermal conductivity of uranium dioxide prepared by any particular technology, we need further experimental investigation.

According to the theory, heat transfer in uranium dioxide can be effected by phonon, electron (including ambipolar diffusion of electrons and holes), and radiative components. The total thermal conductivity [1] takes the form

$$\chi = \chi_{ph} + \chi_e + \chi_{rad} \quad (1)$$

The contributions of the components depend on the temperature. The thermal conductivity of uranium dioxide due to the phonon component is given by

$$\chi_{ph} = \frac{1}{A + BT}, \quad (2)$$

where the coefficients A and B are found empirically from the experimental results.

Above 1500°K, uranium dioxide acquires semiconducting properties, and complex structural transitions can occur in it (grain growth, formation of columnar structure). At high temperatures, an important role in the process of heat transfer can be played by internal radiation and diffusion of the charge carriers. The radiative component is given by

$$\chi_{rad} = \frac{16kn^2T^3}{3\alpha}, \quad (3)$$

while the contribution made to the thermal conductivity of uranium dioxide by the semiconductive mechanism of charge carrier diffusion is given by a modification of the Wiedemann-Franz law

$$\chi_e = 2T \frac{k^2}{e^2} \sigma \left[ 1 + \frac{2\sigma_1\sigma_2}{\sigma^2} \left( 2 + \frac{E_a}{2kT} \right)^2 \right], \quad (4)$$

where e is the elementary charge,  $\sigma$  is the total electrical conductivity,  $\sigma_1$  and  $\sigma_2$  are the electron and hole conductivities,  $E_a$  is the activation energy,  $\alpha$  is the absorption coefficient, n is the refractive index, k is the Stefan-Boltzmann constant, and T is the temperature in degrees Kelvin.

We chose for consideration the results of experimental work in which the authors investigated specimens of sintered polycrystalline uranium dioxide of the stoichiometric composition (O : U = 2.00). The data on the thermal conductivity of uranium dioxide [2-14] were first corrected to 95% of the theoretical density. In averaging the values, by analogy with Eq. (1) we supposed that  $\chi_e \sim T$ , and that the absorption coefficient  $\alpha$  is an exponential function of temperature. This led to a unified analytical relation (curve 1, Fig. 1):

$$\chi(T) = (3.77 + 0.0258T)^{-1} + 1.1 \cdot 10^{-6}T + 1.01 \cdot 10^{-13}T^3 \exp 7.2 \cdot 10^{-4}T. \quad (5)$$

Translated from *Atomnaya Energiya*, Vol. 36, No. 1, pp. 59-60, January, 1974. Original article submitted March 7, 1973.

© 1974 Consultants Bureau, a division of Plenum Publishing Corporation, 227 West 17th Street, New York, N. Y. 10011. No part of this publication may be reproduced, stored in a retrieval system, or transmitted, in any form or by any means, electronic, mechanical, photocopying, microfilming, recording or otherwise, without written permission of the publisher. A copy of this article is available from the publisher for \$15.00.

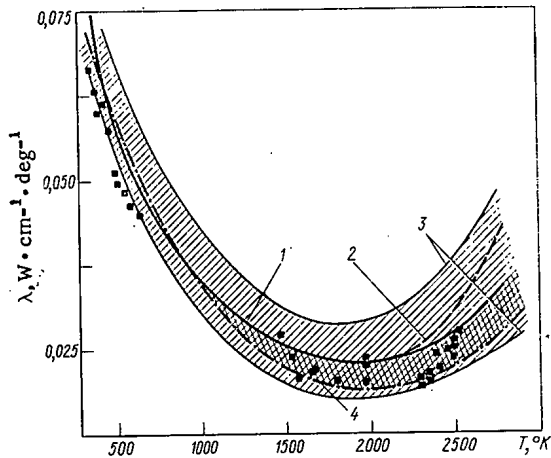


Fig. 1

Fig. 1. Temperature dependence of thermal conductivity of polycrystalline uranium dioxide. 1) Recommended values according to Eq. (5); 2) possible graphs from [8, 12]; 3) region of scatter of experimental data; 4) values averaged by "Round-Robin" program [15]:  $\lambda = 0.115 - 1.14 \cdot 10^{-4}T + 4.4 \cdot 10^{-8}T^2 - 5 \cdot 10^{-12}T^3$ . ■) Present authors' results.



Fig. 2

Fig. 2. Microstructure of specimen (etched,  $\times 40$ ). a) Before tests ( $\times 340$ ); b-d) after tests (on outer surface, in central region, and in axial hole, respectively,  $\times 340$ ).

Muller [15] recently published the results of an investigation of the thermal conductivity of uranium dioxide based on the "Round-Robin" program. In this project, nine laboratories made measurements on specimens prepared by the same technology, but using different methods. The averaged results, in the form of a cubic polynomial, are plotted by curve 4 in Fig. 1.

With the aim of checking the data, we also carried out experimental investigations of the thermal conductivity of polycrystalline sintered uranium dioxide of the stoichiometric composition. The measurements were made by two different methods at 350-2500°K [16]. Up to 700°K we used the method of quasi-stationary linear heating. The experiments were performed in vacuum. We measured the temperature dependence of the thermal diffusivity, and calculated the thermal conductivity values with the aid of data from [9] on the thermal capacity.

The experiments at high temperatures were performed on specimens of cylindrical shape by the stationary method of radial heat flow in purified argon. This method is based on Fourier's well-known solution of the equation of thermal conductivity. By means of an optical micropyrometer we measured the temperature in radial boreholes in the specimen, imitating the black-body model. The ratio of the total height of the assembled specimens to the external diameter was over nine. To avoid breakage of the specimens by thermal stresses we used two heaters, one of which gave the overall temperature level, while the other gave a radial temperature drop within about 30-100°C. The heat flux (needed to calculate the thermal conductivity) was determined by means of the current and voltage in the working part of the internal heater. The test specimens were tablets with an external diameter of 18 mm and a length of 6 mm, with a density equal to 95.5-97.7% of the theoretical value. In the experiments with linear heating, the relative maximum error of a single measurement of the thermal conductivity was 8%; in the experiments with the stationary method of radial heat flow, it was 15-25%.

The results of the thermal conductivity measurements are shown in comparison with similar data of other authors in Fig. 1. We can expect that the thermal conductivity values for uranium dioxide included between curves 1 and 4 will represent the region of most reliable data. The results of our own measurements lie in this interval to within  $\pm 10\%$ .

By microstructural examination of the specimens after the heat tests, we found a marked growth in grain size, reaching about 200  $\mu$ , as against the original values of about 6  $\mu$  (Fig. 2).

The results of our experiments above 2000°K confirm the increase in the thermal conductivity of uranium dioxide which has been observed by various authors. This phenomenon is usually attributed to an increase in the transparency of the coarse-grained ceramic or to intensification of the processes of charge-carrier diffusion.

#### LITERATURE CITED

1. Thermal Conductivity of Uranium Dioxide, Report 59, Vienna, IAEA (1966).
2. R. Reiswig, J. Amer. Ceram. Soc., 44, 48 (1961).
3. J. Daniel et al., Report HW-69, 945 (1962).
4. A. Feith, Report TM-63-9-5 (1963).
5. J. Vogt et al., Report RMB-527 (1964).
6. T. Godfrey et al., Report ORNL-3556 (1964).
7. T. Stora et al., Report CEA-R-2586 (1964).
8. A. Nishijima et al., J. Amer. Ceram. Soc., 48, 31 (1965).
9. M. Wheeler, Brit. J. Appl. Phys., 16, 365 (1965).
10. J. Ainscough and M. Wheeler, Brit. J. Appl. Phys., 7, 859 (1968).
11. R. Asamoto et al., J. Nucl. Materials, 29, 67 (1969).
12. Van Graeynets et al., Report CEA-R-3764 (1969).
13. H. Schmidt, High Temperatures-High Pressures, 1, 309 (1969).
14. A. Walter et al., Rev. Internat. Hautes Temperatures et Refract., 7, 271 (1970).
15. E. Muller, Atomwirtsch.-Atomtechn., 17, 37 (1972).
16. V. I. Kolyadin et al., Preprint IAE-2227, Moscow (1972).



storm develops. From July 28 to 31 and August 1 to 9 the geomagnetic field was quiescent; during this time the natural radioactivity of the atmosphere over the Abramov glacier remained at a low level. The disturbance of the level of radioactivity before the beginning of the magnetic storm of July 26-27 is possibly a consequence of the magnetic storm of July 21-22 [3].

The daily variation of the natural radioactivity of the layer of air near the ground is determined by the emanations which are emitted from the earth and remain close to the surface [4]. The normal daily variation in the absence of atmospheric fallout, fogs, strong winds, and other perturbing phenomena, depends mainly on the daily variation of the turbulent volume of the atmospheric layer near the earth's surface [5]; this volume increases as the surface temperature of the earth rises. The high-altitude measurements show that the daily minimum occurs at 6 p. m. and the maximum at 8 a. m. Tashkent time. No measurements were performed before 8 a. m. A correlation is observed between the variation in the radioactivity of the air and the daily variation of the air temperature which is maximum at 5 p. m. and minimum at 8 a. m. No nocturnal or predawn temperature measurements were made.

It is interesting to compare the concentration of natural radioactive aerosols over the rocky slope of the glacier and over its center. Since rocks and soil form an exhaling surface and since radioactivity decay products can enter the air layer above the ice only through moving air masses, it is obvious that this kind of investigation can be useful in studying the circulation of the air in the vicinity of the glacier. Aerosol samples were taken simultaneously in the center of the glacier and on the slope at heights of 1.5 and 0.25 m above the surface. As might be expected the concentration of radioactive nuclei turned out to be higher above the rocks than over the surface of the ice. At heights of 1.5 and 0.25 m the air above the rocks contained respectively  $1.6 \pm 0.2$  and  $2.5 \pm 0.5$  times more short-lived radioactive decay products than the air above the ice surface. It is known that the concentration of natural radioactive nuclei above an exhaling surface decreases with height [4]. Therefore the increase in the ratio of the concentrations over ice with a decrease in the heights at which the samples were taken can be accounted for in two ways. In order to obtain a unique answer to this question we calculated the ratio of the concentration of radioactive nuclei at 1.5 m to that at 0.25 m. For the rocky slope of the glacier it was  $0.8 \pm 0.2$ , and for the ice surface  $1.3 \pm 0.1$ . Consequently the level of natural radioactivity of air layers decreases as the ice surface is approached.

In conclusion we note that the relatively low natural radioactivity of the air recorded at high altitudes is perhaps a consequence of the proximity of the extensive nonexhaling ice surface.

#### LITERATURE CITED

1. A. É. Shem'i-zade, *Atomnaya Énergiya*, 23, No. 1, 80 (1967).
2. A. E. Shem'i-zade, Paper at the Third Scientific Conference of Young Specialists IZMIRAN [in Russian], IZMIRAN, Moscow (1971), p. 248.
3. *Cosmic Data*, No. 7 and 8 [in Russian], Nauka (1971).
4. B. I. Styro, *Problems of Nuclear Meteorology* [in Russian], Mintis, Vilnius (1959).
5. V. B. Milin et al., *Radioactive Isotopes in the Atmosphere and their Utilization in Meteorology* [in Russian], Atomizdat, Moscow (1965), p. 47.



## CONDENSATION TYPE CRYOSTAT CHANNEL FOR LOW-TEMPERATURE EXPOSURES

V. D. Parkhomenko, B. N. Goshchitskii,  
S. F. Dubinin, P. M. Korotovskikh,  
S. K. Sidorov, V. G. Chudinov,  
and Yu. G. Chukalkin

UDC 621.039.555.34

The following can be used for cooling purposes in facilities designed for in-pile irradiation at temperatures close to the boiling point of liquid nitrogen: 1) gaseous coolant (usually nitrogen or helium) [1-3]; 2) technical grade liquid nitrogen (oxygen content to 10 wt. %) [4, 5]; 3) pure liquid nitrogen (oxygen content 0.1 to 0.001 wt. %) [6-10].

Some fairly complicated technical problems remain to be solved in the operation of facilities of the first type mentioned when fast flux and accompanying  $\gamma$ -emission are of high intensity: evacuation, purification and storage of large amounts of gaseous coolant, use of special high-capacity oil-free compressors, etc. [1-3]. Simpler systems are available [2], but their use calls for large amounts of tonnage nitrogen.

The use of tonnage nitrogen as coolant in facilities of the second type mentioned involves a serious explosion hazard [1, 11, 12] the nature of which has been described in sufficient detail in the literature [12]. Special precautionary measures are called for [11] in the design of this type of system, and these entail a penalty in terms of larger amounts of coolant.

Apparently, facilities of the third type (condensation type with natural coolant circulation), operating on the thermosiphon principle [7-10], are the most convenient in service. These systems eliminate reliance on special-purpose compressors to transfer coolant, are explosion proof, and make it possible to attain reasonably high thermal capacities. Since the coolant flows through a closed loop, no additional purification steps are required to keep the system going.

The condensation type channel-cryostat that has been developed and fabricated was placed in the reactor reflector beyond a beryllium layer with thickness of the order of 64 mm. The working volume zone of the channel-cryostat is characterized by the following average radiation levels:  $\gamma$ -radiation dose rate  $6 \cdot 10^8$  R/h; thermal flux  $8 \cdot 10^{13}$  neutrons/cm<sup>2</sup>·sec; fast flux ( $E \geq 0.8$  MeV)  $5 \cdot 10^{12}$  neutrons/cm<sup>2</sup>·sec. As a result of special measurements taken [13], it was established that radiative heat release at the location of the channel-cryostat amounts to roughly 0.6 W/g in all of the materials used in the design of the system.

Figure 1 shows the basic layout of the facility, consisting of the following principal components: channel head with shield plug, heat exchanger, channel-cryostat, and vacuum jacket. Tonnage nitrogen is supplied from a TRZhK-4M vessel, under 2 to 2.5 bar pressure, to the heat exchanger through vacuum-insulated piping. When the operating level is attained, further supply of nitrogen is handled automatically with the aid of a level sensor ( $D_1$ ) installed in the heat exchanger. The signal from the level sensor is fed to an ÉPV-2 potentiometer controlling the magnetically actuated valve MK, which controls the flow of technical liquid nitrogen to the heat exchanger. An electrically heated copper-constantan thermocouple was used as the sensor. The operating principles of the sensor are based on the difference in the heat transfer coefficients in gaseous nitrogen and liquid nitrogen.

After the heat exchanger is filled, pure nitrogen gas is fed into the channel-cryostat under pressure on the order of 2 bar, and the gas condenses on the inner surface of the heat exchanger and trickles to the bottom of the channel-cryostat. The two thermocouple level sensors  $D_2$ , spaced 4 cm apart are designed to

---

Translated from *Atomnaya Énergiya*, Vol. 36, No. 1, pp. 62-64, January, 1974. Original article submitted April 4, 1973.

© 1974 Consultants Bureau, a division of Plenum Publishing Corporation, 227 West 17th Street, New York, N. Y. 10011. No part of this publication may be reproduced, stored in a retrieval system, or transmitted, in any form or by any means, electronic, mechanical, photocopying, microfilming, recording or otherwise, without written permission of the publisher. A copy of this article is available from the publisher for \$15.00.

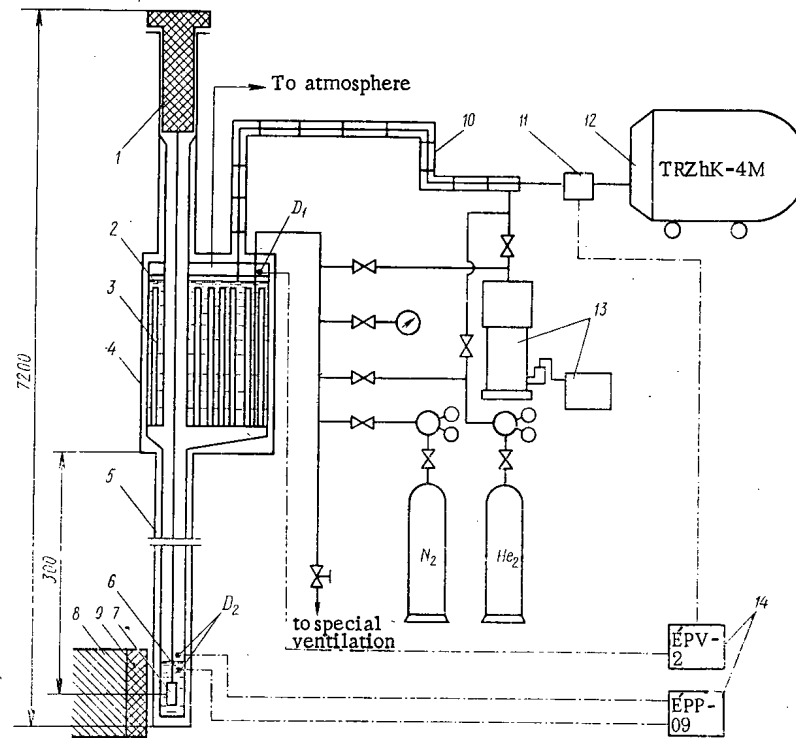


Fig. 1. Basic layout of system: 1) shield plug; 2) technical grade liquid nitrogen; 3) heat exchanger; 4) vacuum jacket; 5) channel-cryostat; 6) pure liquid nitrogen; 7) specimen; 8) core; 9) reflector; 10) feed line for technical grade nitrogen; 11) magnetically actuated valve; 12) technical grade liquid nitrogen tank; 13) roughing pump and diffusion pump; 14) electronic potentiometers;  $D_1$ ,  $D_2$  liquid nitrogen level sensors.

maintain the level of liquid nitrogen in the channel-cryostat. The lower sensor is immersed in the liquid nitrogen, the upper sensor in the nitrogen gas. The thermocouples of the sensors are calked in 5 mm diameter stainless steel spheres. The thermocouples are heated by radiative energy release in the spheres, so that the final setting of the level is carried out as the reactor is brought up to full power. Pure liquid nitrogen evaporates while the system is in operation, thereby removing heat from the object irradiated and from structural parts of the channel-cryostat and moving over to the heat exchanger, where the nitrogen recondenses, and so on. A certain equilibrium pressure (on the order of 1.3 bar) is established in the channel-cryostat when the system is in operation, and this equilibrium pressure is arrived at on the basis of the amount of heat released in the channel-cryostat, in the specimen, coolant, and the heat exchange surface.

The thermal conductivity of the heat exchanger material exerts some slight effect on the total thermal resistivity. For example, replacing the stainless steel with copper reduces the thermal resistivity by roughly 3-5%. That made it possible to fabricate the system entirely of 1Kh18N10T stainless steel. The channel-cryostat was made of a tube  $40 \times 0.5$  mm extending 2850 mm in length, which was threaded into the heat exchanger with an indium seal. The heat exchanger itself is a cylindrical vessel (diameter 169 mm, length 950 mm, wall thickness 2 mm) presenting a total heat exchange surface (90 thin-walled 10 mm diameter tubes) of the order of  $2 \text{ m}^2$ . The outer shell of the vacuum jacket is made of 3 mm thick stainless steel, and imparts sufficient strength to the design so that the channel-cryostat is capable of coping with leaks.

Flexible stainless steel leakproof sleeves are employed to feed the liquid nitrogen to the heat exchanger. The outer sleeve is 32 mm in diameter, the inner one 10 mm. The spacing between the sleeves is utilized in order to pump out the vacuum jacket. Spacer rings in the intervening space keep the two sleeves apart. Gaseous technical grade nitrogen from the heat exchanger passes through the flexible 32 mm diameter sleeve without vacuum insulation.

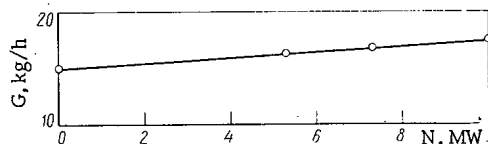


Fig. 2. Flowrate G of tonnage nitrogen as a function of reactor output power.

After the specimens have been loaded in, the channel is hermetically sealed with a plug, and the channel-cryostat and the internal cavity of the heat exchanger are both evacuated, with the reactor on power, to a pressure of  $10^{-2}$  torr. The vacuum jacket is then filled with helium gas under 2.5 bar pressure, so that the radiative warmup temperature of the design elements can be lowered to 300-350°C. If it is felt that the specimens should not be warmed up, then they can be raised up to the plug in their initial state and lowered into the exposure zone, with the reactor shut down and without depressurizing the channel, with the aid of a special device. The vacuum jacket is pumped out and the heat exchanger is filled with the reactor off power, since the temperature of the design components rises to 700-800°C as a result of radiative heating, when the reactor is at the rated power level of 10 MW and the pressure in the jacket is  $5 \cdot 10^3$  torr. The channel-cryostat is then filled with pure nitrogen, the specimens are transferred to the exposure zone, and there they are cooled by pure liquid nitrogen.

The flowrate of technical grade nitrogen with the reactor on power at an output level of 10 MW, and with the total weight of materials to be irradiated at 300 g (specimens 80 g, liquid nitrogen 80 g, channel-cryostat 140 g) is 17-18 kg/h, of which 11.2 kg/h is accounted for by losses in the piping, 2.8 kg/h by losses in the heat exchanger and in the channel-cryostat, and 3.6 kg/h by the flowrate of material for cooling the specimen and cooling the design components. The large losses in the piping seem to be due to the considerable extent of the piping (which is on the order of 20 meters). Figure 2 shows how the flowrate of tonnage nitrogen varies with the reactor output power, given the above quantity of materials to be irradiated.

The boiling point of the nitrogen in the channel-cryostat is determined by the boiling point of the nitrogen in the heat exchanger and by the thermal resistivity of the heat exchanger. Consequently, stabilization of the temperature of the specimens requires maintaining the nitrogen vapor pressure in the heat exchanger at a constant level both during the time the tonnage liquid nitrogen is being pumped and during the period of stationary performance. When the 32 mm diameter effluent piping is employed to remove vapor from the heat exchanger, pressure fluctuations in the channel-cryostat are found to be roughly  $\pm 0.1$  bar, which matches temperature fluctuations  $\pm 1^\circ$ . The temperature of the specimens immersed in the pure liquid nitrogen was 78-80°K.

Several exposures each lasting 50 to 100 h were carried out in the channel-cryostat facility. The channel-cryostat became depressurized within one hour after operation started, as the first irradiation was being carried out. An investigation of the channel in a hot cave revealed that the piping bulged out at the site where it was welded to the bottom, and came loose from the bottom at several points. Apparently, an explosion was the cause of the depressurization, since mass spectrometric data show the "pure" nitrogen we were using to contain 0.5% oxygen. In subsequent experiments, the pure nitrogen obtained from the liquifying machine was subjected to supplementary dry-out in a zeolite-packed column, and was run through copper shavings at a temperature of 550°C with the object of reducing oxygen content still further. After that purifying step, the oxygen content in the gas was brought down to a level of 0.002% or lower, and the channel-cryostat functioned unimpaired in all further work.

In conclusion, the authors express their gratitude to V. F. Onishchenko, M. T. Telichko, V. G. Volgin, and G. I. Vachkova for their kind assistance in fabricating the facility and performing the tests.

#### LITERATURE CITED

1. R. Coltman et al., *Rev. Sci. I.*, **28**, 375 (1957).
2. S. R. Novikov et al., *At. Énerg.*, **20**, 275 (1966).
3. L. A. Vachkadoriya et al., *At. Énerg.*, **26**, 288 (1969).
4. M. Thompson and D. J. Jefferson-Loveday, *J. Sci. Instrum.*, **35**, 397 (1958).
5. G. Bortels, *J. Sci. Instrum.*, **36**, 11 (1959).
6. C. Sartain and H. Yocket, *Rev. Sci. I.*, **29**, 118 (1958).
7. L. Bewilogia and R. Kononer, *Cryogenics*, **2**, 46 (1961).
8. L. Weil, *Cryogenics*, **1**, 129 (1961).

9. H. Hofgen, Kernenergie, 11, 216 (1968).
10. C. Chen et al., J. Sci. Instrum., 2, Series 2, 146 (1969).
11. L. Heyne, Cryogenics, 2, 332 (1962).
12. C. Chen and R. Struss, Cryogenics, 9, 131 (1969).
13. V. P. Gerasimenko et al., At. Energ., 31, 7 (1971).

DISPERSITY OF AEROSOLS FORMED DURING COMBUSTION  
OF THE COOLANT AND MATERIALS OF THE CORE OF  
A FAST REACTOR

B. N. Rakhmanov, S. V. Malyutin,  
O. M. Zараev, and I. E. Konstantinov

UDC 621.039'58

In [1] mechanisms for the formation of radioactive aerosols during breakdowns in fast reactors are considered. We note that there are two types of possible breakdowns. First, breakdowns in which there is a leak in the first reactor loop and a loss of part of the coolant without destruction of the core. In this case radioactive sodium at 500-600°C [2] ignites when it comes in contact with the air, forming a large number of aerosol particles in the form of a mist. Second, breakdowns in which, besides the combustion of sodium, there is a partial melting of the reactor core [3]. For such a breakdown the air medium of industrial areas is contaminated by radioactive aerosols owing to the combustion of sodium, which leads to vaporization of the nuclear fuel, and separation of the fission products and structural materials.

We investigate, under laboratory conditions, the dispersity of aerosols formed during combustion of sodium. The apparatus for the combustion consists of an electric heater and a six-stage impactor located in a Sh-I fume hood having volume 0.55 m<sup>3</sup>. The electric heater, which is designed to operate at up to 1000°C, is supplied from a low-voltage VSA-6M rectifier. The characteristics of the six-stage impactor are described in [4].

Sodium samples of weight 0.1-20 g are first heated up to 540°C, and then burned until an aerosol mass concentration of  $2 \cdot 10^{-2}$ -15 g/m<sup>3</sup> is obtained. The amount of metal deposited on the stages of the impactor is determined by the standard method of neutron-activation analysis [5, 6].

Experimental results show that the spectrum of the dimensions of sodium aerosol particles is described well by a logarithmic normal law, where with increasing mass concentration there is an increase in the aerosol median diameter. By processing the results of a series of experiments by the least-squares method, we determine an empirical power dependence between the median mass aerodynamic diameter  $d_a$  ( $\mu$ ) and the aerosol mass concentration  $G$  (g/m<sup>3</sup>):

$$d_a = 1.1G^{0.3}$$

Experimental results are shown in Fig. 1, which gives, for comparison, the curve obtained in [7].

In addition to the noted dependence we determine the magnitude of the coefficients that characterize the rate of combustion of sodium  $p$  and its transition during the combustion into the aerosol state  $\varphi$ . Mean values are determined for the following coefficients:  $p = 2.1 \text{ kg/m}^2 \cdot \text{h} \cdot \text{vol.} \% \text{ O}_2$ ;  $\varphi = 0.23$ . These values agree with the values recommended in [8].

To study properties of aerosols formed during condensation of vapors of various materials we constructed apparatus for obtaining aerosols in a constant-current arc [6]. It consists of an arc furnace and a six-stage impactor. The arc furnace contains two electrodes positioned at an angle of 135° to each other. The lower electrode is the copper bottom, in which the sample vaporizes; the upper electrode is made of tungsten and is fastened using sylphon bellows. Both electrodes are water-cooled. The arc electrode is fed with a 30 V constant voltage from a PSO-300 welding transformer, which supplies an arc current of up to 250 A. The sample being consumed is fastened to the furnace bottom using a threaded coupling. The

---

Translated from *Atomnaya Energiya*, Vol. 36, No. 1, pp. 64-65, January, 1974. Original article submitted April 11, 1973.

© 1974 Consultants Bureau, a division of Plenum Publishing Corporation, 227 West 17th Street, New York, N. Y. 10011. No part of this publication may be reproduced, stored in a retrieval system, or transmitted, in any form or by any means, electronic, mechanical, photocopying, microfilming, recording or otherwise, without written permission of the publisher. A copy of this article is available from the publisher for \$15.00.

TABLE 1. Data on Dispersity of Materials Being Investigated

Ignited material	Median mass aerodynamic diameter, $\mu$	Standard deviation
Tungsten	0,9 - 1,3	3,2 - 3,5
Aluminum + sodium	0,4 - 0,5	2,7 - 3,8
Steel + sodium	0,5 - 0,7	2,4 - 3,6

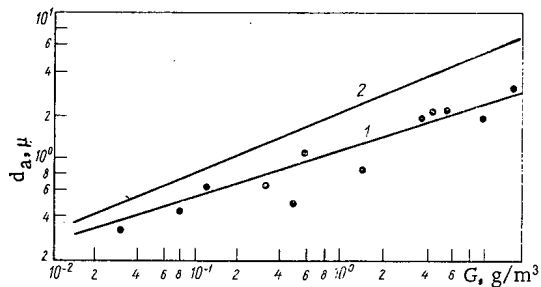


Fig. 1. Dependence of median mass aerodynamic diameter on initial aerosol mass concentration: 1) our results; 2) data of [7].

sample can have the form of a cylinder up to 15 mm high and up to 20 mm in diameter. The arc is ignited when the sample touches the upper electrode and burns between it and the electrode. The samples should be metallic; however, if nonmetallic samples must be used, this can be accomplished by placing them in metallic containers.

The entire experimental apparatus is placed in a type 3K-NZh hermetic glove box, which enables us to carry out experiments on the ignition of radioactive materials.

Using this apparatus we carried out experiments on the ignition of tungsten, stainless steel in a mixture with sodium, and also aluminum together with sodium. In all cases the ignition conditions were identical (current of 250 A). The aerosols were sampled from the six-stage impactor. The method of analyzing the samples is the same as that described above. Results obtained for an investigation of the dispersity are given in Table 1.

Experimental results on the combustion of various metals show that the distribution of aerosol particles with respect to aerodynamic diameters with good accuracy is described by a logarithmic normal law, where the median mass aerodynamic diameter 0.4-1.3  $\mu$ , and the standard deviation is within the limits 2.4-3.8. The coefficient of trapping of aerosols calculated in various regions of the respiratory system using the recommendations MKRZ-1966 [9], equals 0.15-0.34 for the pulmonary region, 0.08 for the tracheo-bronchial region, and 0.12-0.30 for the nasopharynx.

The apparatus that we have developed and tested allows us to investigate the characteristics of aerosols formed during combustion of various materials, i. e., we can estimate both the trapping of aerosols in the respiratory organs and the rate of decontamination of air in various areas.

## LITERATURE CITED

1. O. M. Zараev and B. N. Rakhmanov, in: Scientific Works of Institutes on the Protection of Workers of VTsSPS, No. 73 [in Russian], Profizdat, Moscow (1971), p. 25.
2. A. S. Zaimovskii et al., Atomic-Reactor Fuel Elements [in Russian], Atomizdat, Moscow (1966), p. 406.
3. W. Hafele et al., Annual Rev. Nucl. Sci., 20, 393 (1970).
4. B. N. Rakhmanov et al., in: Scientific Works of Institutes on the Protection of Workers of VTsSPS, No. 70 [in Russian], Profizdat, Moscow (1971), p. 27.
5. H. J. Bowen and D. Gibbons, Radioactivation Analysis, Oxford Univ. Press (1963).
6. O. M. Zараev et al., in: Scientific Works of Institutes on the Protection of Workers of VTsSPS, No. 79 [in Russian], Profizdat, Moscow (1972), p. 23.
7. R. Koontz et al., Treatment of Airborne Radioactive Wastes, IAEA, Vienna (1968), p. 51.
8. R. Koontz, Trans. Amer. Nucl. Soc., 20, 689 (1967).
9. Health Phys., 12, 137 (1966).

DETERMINATION OF THE YIELDS OF CERTAIN  
FRAGMENTS IN THE FISSION OF  $^{238}\text{U}$  BY REACTOR  
SPECTRUM NEUTRONS

L. N. Yurova, A. V. Bushuev  
and A. F. Kozhin

UDC 539.173.8

Information on the probability of the formation of various products of the fission of  $^{238}\text{U}$  by neutrons of the reactor spectrum is of interest not only for fission physics, but also essential for evaluating the intensity of the reaction  $^{238}\text{U} (n, f)$  in nuclear reactors and the burnout of nuclear fuel. However, in certain cases the accuracy of the available data is insufficient. The difference in the values of the yields cited by different authors for certain fission products reaches 30% (Table 1).

Information on the yields of fission products can be obtained from the results of measurements of the  $\gamma$  radiation spectra of fissioning materials irradiated in a reactor. With the aid of a Ge(Li) spectrometer, it is possible to isolate in the summary spectrum the lines belonging to definite fission products, and evaluate their intensity.

In this work a comparison was made of the intensities of the lines in the  $\gamma$  radiation spectra of the fission products of  $^{238}\text{U}$  and  $^{235}\text{U}$ . Using the available data on the yields of the products of fission of  $^{235}\text{U}$  by thermal neutrons [6], we determined their yields in the fission of  $^{238}\text{U}$ . The number of fissions of  $^{238}\text{U}$  and  $^{235}\text{U}$  was found according to the intensity of the  $\gamma$  radiation of  $^{140}\text{La}$ .

Since the yields of certain fission products depend substantially on the energy of the neutrons causing the fission of  $^{235}\text{U}$ , the values taken from [6] can be used in those cases when the irradiation of samples of  $^{235}\text{U}$  is conducted in a sufficiently thermalized neutron spectrum.

In this work foils enriched up to 90% with respect to  $^{235}\text{U}$  were irradiated in the vertical channels of an IRT-2000 reactor at a distance of 25 cm from the boundary of the active zone, where the cadmium ratio for the reaction  $^{235}\text{U} (n, f)$  reached 45. Foils with a  $^{235}\text{U}$  content reduced 200-fold, surrounded by a cadmium screen, were irradiated in the active zone of the same reactor. Special measurements showed that the ratio of the fission cross sections  $^{238}\sigma_f / ^{235}\sigma_f$  was  $5.6 \cdot 10^{-4}$ , and the contribution from the fission of  $^{235}\text{U}$  to the total intensity of the fission of the  $^{235}\text{U}$ -poor foil did not exceed 0.5%.

TABLE 1. Yields of Products of the Fission of  $^{238}\text{U}$  by Reactor Neutrons

Fission product	Results of this work				Values of other studies					Values used [6]	
	$Y_i^s$ , %	$E_1$ , %	$E_2$ , %	$E_3$ , %	[1]	[2]	[3]	[4]	[5]	$Y_i^s$ , %	$E_i$ , %
$^{95}\text{Nb}$	5,46	3,0	—	—	$6,1 \pm 0,5$	5,8	$5,47 \pm 0,19$	$7,24 \pm 1,31$	5,52	6,52	—
$^{97}\text{Nb}$	6,06	2,4	—	—	$5,9 \pm 0,6$	4,9	$5,91 \pm 0,18$	$6,00 \pm 0,37$	5,42	6,05	—
$^{103}\text{Ru}$	$5,94 \pm 0,33$	1,2	5,4	5,5	$6,6 \pm 1,0$	5,8	$6,26 \pm 0,19$	—	6,39	2,85	5
$^{131}\text{I}$	$2,91 \pm 0,15$	4,5	2,6	5,2	—	3,2	$3,62 \pm 0,11$	—	3,33	2,79	1,8
$^{132}\text{I}$	4,75	1,2	—	—	$4,7 \pm 0,3$	4,4	$5,27 \pm 0,32$	$4,23 \pm 0,34$	4,89	4,16	—
$^{133}\text{I}$	$6,92 \pm 0,23$	2,1	2,5	3,3	—	—	—	—	5,72	6,75	1,6
$^{141}\text{Ce}$	4,90	1,4	—	—	—	—	—	—	5,62	5,84	—
$^{143}\text{Ce}$	$4,84 \pm 0,14$	1,2	2,6	2,9	—	—	—	—	4,89	5,93	1,8
$^{144}\text{Ce}$	4,34	1,6	—	—	$4,8 \pm 0,3$	—	—	—	4,42	5,41	—
$^{147}\text{Nd}$	$3,14 \pm 0,13$	3,3	2,5	4,2	$2,83 \pm 0,25$	—	—	—	2,81	2,23	1,6

Note. Here  $E_1$  is the experimental error;  $E_2$  is the indeterminacy of the nuclear data;  $E_3$  is the total error.

Translated from *Atomnaya Energiya*, Vol. 36, No. 1, pp. 66-69, January, 1974. Original article submitted April 25, 1973.

© 1974 Consultants Bureau, a division of Plenum Publishing Corporation, 227 West 17th Street, New York, N. Y. 10011. No part of this publication may be reproduced, stored in a retrieval system, or transmitted, in any form or by any means, electronic, mechanical, photocopying, microfilming, recording or otherwise, without written permission of the publisher. A copy of this article is available from the publisher for \$15.00.

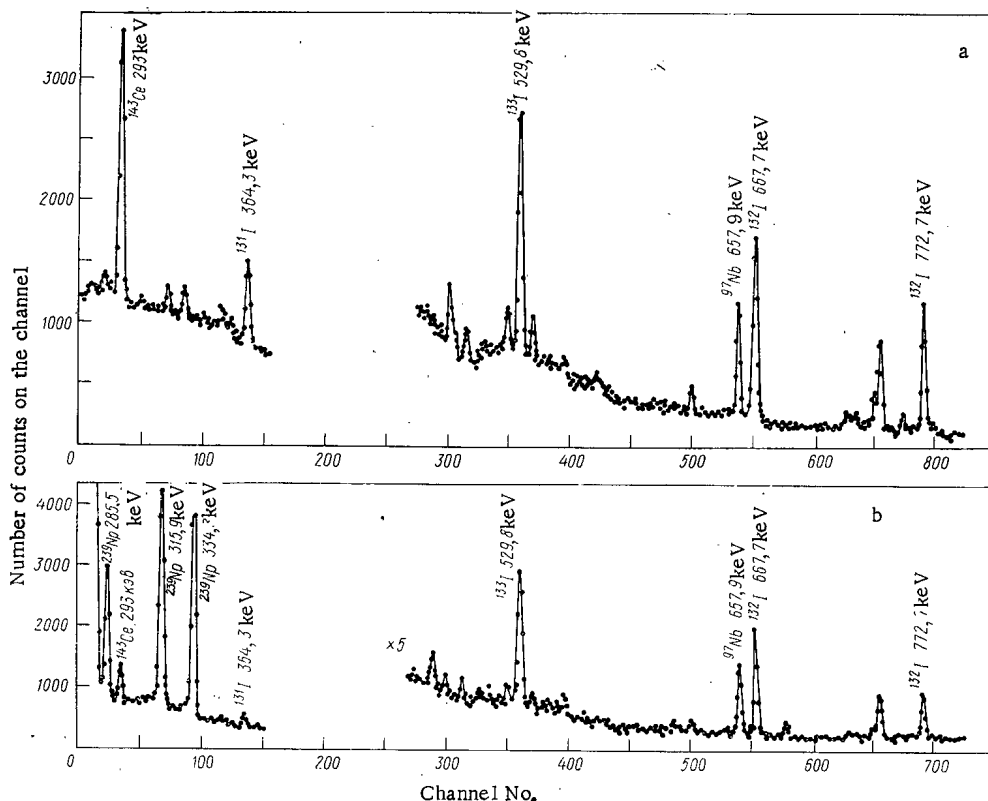


Fig. 1.  $\gamma$  Radiation spectra of products of the fission of  $^{235}\text{U}$  (a) and  $^{238}\text{U}$  (b) by reactor spectrum neutrons, with a time of exposure of three days.

TABLE 2. Relative Yield of Fission Products

Fission product	$\gamma_1^{\beta}/\gamma_2^{\beta}$	$E_1, \%$	$E_2, \%$	$E_3, \%$
$^{95}\text{Nb}$	$0,838 \pm 0,29$	3,0	1,9	3,5
$^{97}\text{Nb}$	$1,002 \pm 0,31$	2,4	1,9	3,1
$^{103}\text{Ru}$	$2,085 \pm 0,048$	1,2	1,9	2,3
$^{131}\text{I}$	$1,042 \pm 0,051$	4,5	1,9	4,9
$^{132}\text{I}$	$1,142 \pm 0,026$	1,2	1,9	2,3
$^{133}\text{I}$	$1,025 \pm 0,029$	2,1	1,9	2,8
$^{141}\text{Ce}$	$0,839 \pm 0,020$	1,4	1,9	2,4
$^{143}\text{Ce}$	$0,816 \pm 0,019$	1,2	1,9	2,3
$^{144}\text{Ce}$	$0,802 \pm 0,020$	1,6	1,9	2,5
$^{147}\text{Nd}$	$1,406 \pm 0,053$	3,3	1,9	3,8

As a result of the reaction  $^{238}\text{U} (n, \gamma)$ ,  $^{239}\text{Np}$  was accumulated in the impoverished foil; its  $\gamma$  radiation created a background in measurements with certain fission products. To reduce this background, the foil of impoverished uranium was covered with a shield of natural uranium during irradiation, which greatly attenuated the flux of neutrons with the resonance energies of  $^{238}\text{U}$ .

In measurements of the yield of fission products with half-lives less than one month, the duration of irradiation was 10 h, while in the case of measurements of more long-lived fission products it was 80 h. Foils of impoverished and enriched uranium were irradiated in the reactor simultaneously.

The relative intensity of the fission reactions in the foils was determined according to the recording of the  $\gamma$  radiation of  $^{140}\text{La}$  ( $E_{\gamma} = 1596$  keV) with a spectrometer with a crystal of  $\text{NaI}(\text{Tl})$ , possessing high efficiency of the recording of hard  $\gamma$  radiation. Measurements of  $^{140}\text{La}$  were begun 12 days after irradiation, when the radiation of other fission products close to the peak 1596 keV of  $^{140}\text{La}$  dropped to a negligible level. The spectra of the irradiated foils were measured on a planar  $\text{Ge}(\text{Li})$  detector with a volume of  $2 \text{ cm}^3$  and a 512-channel pulse-amplitude analyzer. The energy resolution of the spectrometer was 2.0 keV for  $E_{\gamma} = 122$  keV ( $^{57}\text{Co}$ ) and 2.9 keV for  $E_{\gamma} = 662$  keV ( $^{137}\text{Cs}$ ). The areas of the photopeaks were calculated on a NAIRI-2 electronic computer.

In a consideration of the  $\gamma$  radiation spectra of the fission products 2-10 days after irradiation (Fig. 1), it was discovered that the lines belonging to  $^{143}\text{Ce}$  (293 keV),  $^{131}\text{I}$  (364 keV),  $^{133}\text{I}$  (530 keV),  $^{97}\text{Nb}$  (658 keV), and  $^{132}\text{I}$  (668 and 773 keV) are always most clearly distinguished in them.

The lines of  $^{147}\text{Nd}$  (91 keV),  $^{144}\text{Ce}$  (134 keV),  $^{141}\text{Ce}$  (145.4 keV),  $^{103}\text{Ru}$  (497 keV),  $^{95}\text{Zr}$  (723 and 756 keV), and  $^{95}\text{Nb}$  (764 keV) were distinguished in the  $\gamma$  spectra of the fission products 30-90 days after irradiation (Fig. 2). The  $\gamma$  lines were identified according to the data of [7, 8].



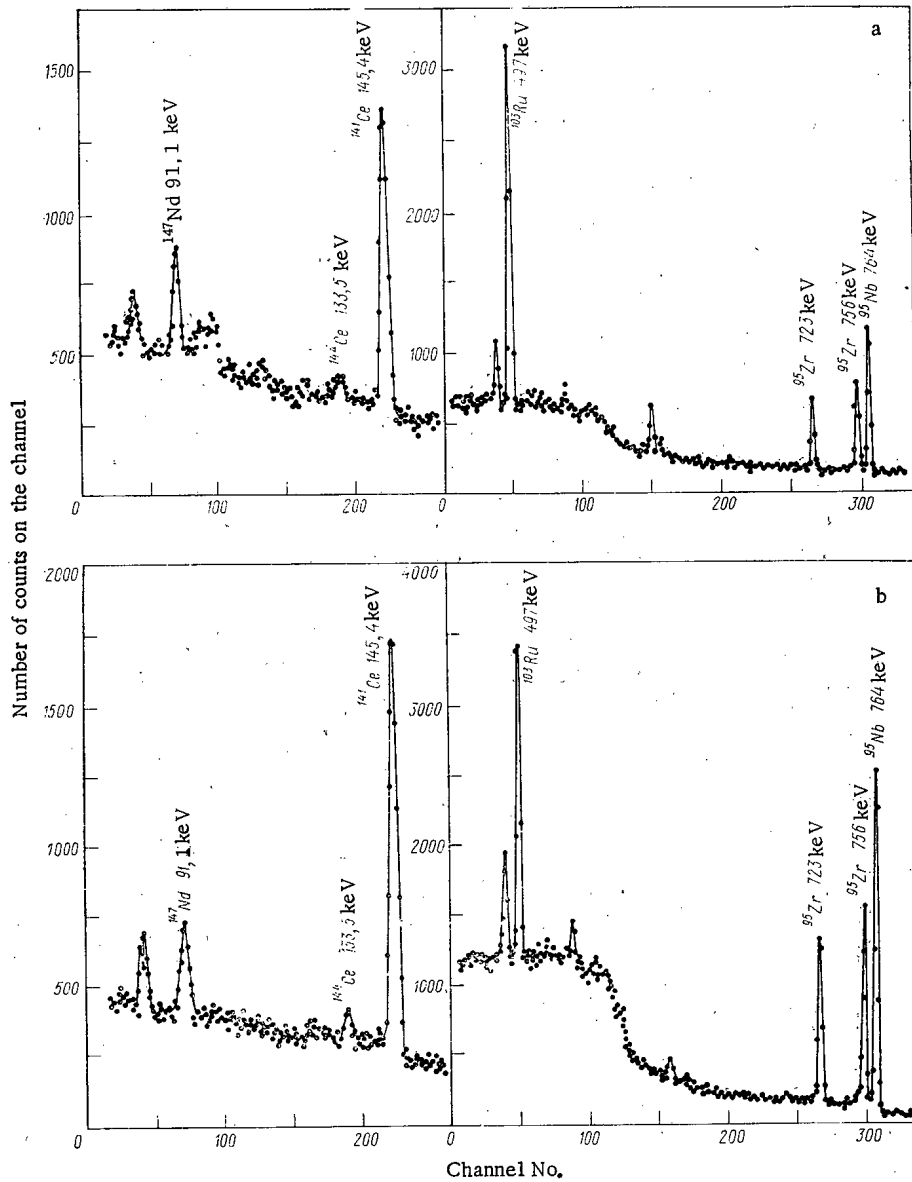


Fig. 2.  $\gamma$  Radiation spectra of products of the fission of  $^{235}\text{U}$  (a) and  $^{238}\text{U}$  (b) by reactor-spectrum neutrons, in the case of a time of exposure of 30 days.

The most accurate results were obtained in measurements of the yields of  $^{132}\text{I}$ ,  $^{103}\text{Ru}$ , and  $^{141}\text{Ce}$  — their peaks were most intense and the measurements performed under conditions of a high effect-background ratio. For photopeaks with low statistics ( $^{95}\text{Nb}$ ) or low effect-background ratio ( $<0.5$ ) of such isotopes as  $^{147}\text{Nd}$  and  $^{131}\text{I}$ , the accuracy of the results is reduced. A high accuracy of the yield for the fission of  $^{143}\text{Ce}$  was obtained on account of the large number of measurements performed with the given fission product.

For  $\gamma$  lines with energies up to 400-keV we measured the coefficients of self-absorption in impoverished and enriched foils. The difference in self-absorption was taken into consideration in the final results. Table 2 presents the averaged data on three independent experiments; in each experiment five measurements were performed for short-lived fission products, and 10 for long-lived products.

The yield of the  $i$ -th fission product of  $^{238}\text{U}$  was determined according to the working formula

$$Y_i^8 = Y_i^5 \frac{Y_{La}^8}{Y_{La}^5} \cdot \frac{A_i^8}{A_i^5} \cdot \frac{A_{La}^5}{A_{La}^8},$$

where  $A_i^8$  and  $A_i^5$  are the areas of the photopeaks belonging to the  $i$ -th fission products in the spectra of

impoverished and enriched foils;  $A_{La}^8$  and  $A_{La}^5$  are the activities of  $^{140}La$  accumulated in the impoverished and enriched foils;  $Y_i^5$  is the yield of the  $i$ -th product of the fission of  $^{235}U$  by thermal neutrons;  $Y_{La}^8$  and  $Y_{La}^5$  are the yields of  $^{140}La$  in the fission of  $^{238}U$  and  $^{235}U$ .

The probability of the formation of  $^{140}La$  in the fission of  $^{238}U$  has been studied in a number of investigations, in which the following values of  $Y_{La}^8$  (percent) are cited: 6.15 [1]; 6.0 [2]; 5.96 [3]; 6.03 [4]; 6.01 [9]; 5.70 [10]; 6.34 [11]. The first two values of  $Y_{La}^8$  are the recommended values, obtained by the authors as a result of the analysis of previously determined values; the remaining five values are the results of the latest experimental studies. If the same statistical weight is assigned to all the values, we obtain  $Y_{La}^8 = (6.03 \pm 0.07)\%$ . The yield of  $^{140}La$  in the fission of  $^{235}U$  by thermal neutrons has been investigated by many authors. According to the data of [1, 2, 6, 12], it is  $(6.34 \pm 0.10)\%$ . Using the indicated values of the yields, we find:  $Y_{La}^5/Y_{La}^8 = 1.05 \pm 0.02$ . Substituting this value into the working formula and using the experimental values of  $A_{La}^8$  and  $A_{La}^5/A_{La}^8$ , we obtain the ratios  $Y_i^8/Y_i^5$  cited in Table 2.

Table 1 presents the values of the yields of the fission products of  $^{238}U$  discussed in this work; these values were calculated on the basis of the data on  $Y_i^5$ , taken from [6]. Table 1 also contains the results of [1-5]. From the table it is evident that the results obtained agree on the whole with the data of previous studies and supplement them. The probable cause of certain observed differences lies in systematic errors inherent in the experimental methods. In the indicated studies, together with radiation chemistry, we also used mass spectroscopy and  $\gamma$  spectroscopy; the number of fissions in the samples was determined with double fission chambers, trap indicators, or according to a specially selected fragment indicator ( $^{99}Mo$ ,  $^{95}Zr$ ,  $^{140}La$ ).

#### LITERATURE CITED

1. I. Croall, AERE-R 5086 (1967).
2. M. Meek and B. Rider, USAEC, Report APED-5398-A (Revised) (1968).
3. R. Larson, Trans. Amer. Nucl. Soc., 15, No. 1 (1972).
4. I. Cuninghame et al., AERE-R 6862 (Revised) (1972).
5. W. Krappel et al., Nucl. Technol., 12, 226 (1971).
6. W. Walker, IAEA-CN-26/3 (1970).
7. Nuclear Data Tables, Vol. 8, No. 5-6, Academic Press, New York-London (1971), pp. 445-666.
8. C. Lederer et al., Tables of Isotopes 6th Ed., New York-London-Sydney (1967).
9. L. Cinffolotti, Energia Nucl., 15, 272 (1968).
10. R. Dierckx et al., J. Nucl. Energy, 25, 85 (1971).
11. R. Björnerstedt, Arkiv. Fys., 16, No. 28, 4 (1959).
12. F. Lisman et al., Nucl. Sci. and Engng., 42, 191 (1970).

URANIUM AND PLUTONIUM LOSSES WITH STEEL IN  
THERMAL DECLADDING OF FUEL ELEMENTS

G. P. Novoselov, Yu. D. Dogaev,  
and S. A. Perevozchikov

UDC 621.039.59

The separation of high-level fuel assemblies for fast reactors, decladding of those fuel elements, and separation of the steel from the fuel, are the most complicated topics in the study of the fuel recovery process. Minimizing losses of nuclear fuel with the declad steel is of the utmost importance, since that sets the prerequisites for long-term storage of the steel without further reprocessing.

It has been demonstrated both theoretically and experimentally that fused steels at temperatures of 1500°C in vacuum or in an inert protective atmosphere engage in practically no interaction with uranium dioxide or plutonium dioxide, and that the content of either of these elements in the slug is not greater than  $5 \cdot 10^{-2}$  wt.%. Studies of the distribution of uranium and plutonium in the declad slug have established the fact that over 99% of those elements is to be found on the surface of the slug, in the form of the dioxides, whereas only about 1% is found uniformly distributed throughout the bulk of the slug [1]. Another relevant finding [1] is that the fission products formed exert only an insignificant effect on interactions between the dioxides ( $UO_2$  and  $PuO_2$ ) and the chromium-nickel cladding steels [2].

Quite possibly, some of the fuel becomes destroyed in the irradiated assemblies. Even though the powders can sinter together during the thermal decladding process, at a rate proportional to the temperature, the time, and the degree of dispersion, the probability that large unsintered particles are present, as well as a slight quantity of powder formed as a result of mechanical damage to sinter pellets at the point of phase separation, is not to be discounted. Fuel losses through capture of individual fuel particles by the steel is therefore not ruled out. The wetting angles of the uranium dioxide and plutonium oxide attacked by molten Kh16N16M2B steel are respectively  $136 \pm 5^\circ$  and  $101 \pm 2^\circ$ . Surface tension retains uranium dioxide and plutonium dioxide pellets extending to 11 mm and 5 mm respectively [3], so that it is not too likely these will end up in the steel in powder form, but the possibility that the steel may entrap coarser particles is not excluded.

It is interesting to consider the behavior of solid particles within the volume of molten steel. Several papers have addressed themselves to this problem [4-7], showing that the rate at which the particles float to the surface is satisfactorily described by Stokes' law.

To calculate the rate at which uranium dioxide particles sized 100  $\mu$  or smaller undergo sedimentation in the molten chromium-nickel steel, we can resort to Stokes' equation:

$$v = \frac{2}{9} g \frac{D - D'}{\eta} r^2, \quad (1)$$

and for particles ranging from 100  $\mu$  to 2000  $\mu$  in diameter we can resort to Allen's equation [8]:

$$v = 51.53r^3 \sqrt{\left(\frac{D - D'}{D'}\right)^2 \frac{D'}{\eta}}, \quad (2)$$

where  $r$  is the particle radius, in cm;  $\eta$  is the viscosity of the stream, in poises ( $g \cdot cm^{-1} \cdot sec^{-1}$ );  $D$ ,  $D'$  are the densities of the materials forming the particle and the liquid, in  $g/cm^{-3}$ ;  $g$  is the force of gravitational acceleration, in  $cm \cdot sec^{-2}$ .

Translated from *Atomnaya Energiya*, Vol. 36, No. 1, pp. 69-70, January, 1974. Original article submitted April 26, 1973.

© 1974 Consultants Bureau, a division of Plenum Publishing Corporation, 227 West 17th Street, New York, N. Y. 10011. No part of this publication may be reproduced, stored in a retrieval system, or transmitted, in any form or by any means, electronic, mechanical, photocopying, microfilming, recording or otherwise, without written permission of the publisher. A copy of this article is available from the publisher for \$15.00.

TABLE 2. Sedimentation Rate and Sedimentation Time of Uranium Dioxide Particles in Molten Steel

Particle diameter, $\mu$	Sedimentation rate, mm/sec	Particle sedimentation time, in steel droplet of diameter*			
		3mm	5mm	7mm	10mm
10	$5,1 \cdot 10^{-2}$	58,8	98,0	139,3	196,0
60	1,8	1,7	2,8	4,0	5,6
100	5,1	0,6	1,0	1,4	2,0
1000	95,0	$\ll 1$	$\ll 1$	$< 1$	0,1
2000	190,0	$\ll 1$	$\ll 1$	$< 1$	$< 1$

\*Sedimentation time of particles given in seconds.

the surface of the droplet within a fraction of a second. Sedimentation time stretches to longer than a minute only in the case of particles of diameter less than  $10 \mu$ . If we take into consideration the marked effect of sintering of particles sized smaller than  $100 \mu$  diameter and the high surface tension presented by the molten steel, we see that the probability of fine particles ending up in the slug is very slight indeed. Moreover, fuel losses and hence steel activity losses are determined by entrapment of coarse fuel particles. Nevertheless, the difference in the densities of the fuel and of the medium are responsible for the emergence of the coarser particles from the steel, and also for the high degree of separation of steel and fuel.

These calculations confirm our earlier conclusions [14] to the effect that the separation process can be successfully realized within the steel droplet per se, since a continuous noncrucible process for thermal decladding of fuel elements can be achieved within the time it takes the steel droplet to form.

#### LITERATURE CITED

1. G. P. Novoselov and A. T. Ageenkov, in: 36th International Congress on Industrial Chemistry (Brussels, 1966), paper No. 11/755 (USSR).
2. U. D. Veryatin et al., *At. Énerg.*, 31, 375 (1971).
3. G. P. Novoselov and A. T. Ageenkov, *At. Énerg.*, 26, 232 (1969).
4. N. N. Dobrokhotov and K. K. Prokhorenko, *Stal'*, No. 11, 997 (1961).
5. L. S. Gorokhov et al., *Stal'*, No. 7, 604-5 (1964).
6. Yu. G. Gurevich, *Izv. Vuzov, Chernaya Metallurgiya*, No. 6, 27 (1969).
7. V. V. Khlynov and V. I. Ishimov, *Izv. Vuzov, Chernaya Metallurgiya*, No. 6, 27 (1970).
8. N. A. Figurovskii, *Sedimentometric Analysis [in Russian]*, Izd-vo AN SSSR, Moscow-Leningrad (1948), pp. 45-51.
9. V. B. Shevchenko and B. N. Sudarikov, *Uranium Technology [in Russian]*, Gosatomizdat, Moscow (1961), p. 35.
10. E. Goudremont, *Special Steels*, in: *Metallurgy [Russian translation]*, Moscow (1966), p. 105.
11. D. F. Elliott et al., *Thermochemistry of Steelmaking Processes*, in *Metallurgy [Russian translation]*, Moscow (1969), p. 225.
12. B. V. Tsarevskii, S. I. Popel', and B. F. Domozhirev, *Effect of Molybdenum and Chromium on Surface Properties and Density of Iron [in Russian]*, Kabardino-Balkarskoe Knizhnoe Izd-vo, Nal'-chik (1969), p. 319.
13. E. G. Shvidkovskii, *Some Aspects of the Viscosity of Molten Metals [in Russian]*, Gostekhteorizdat, Moscow (1955).
14. G. P. Novoselov, 2nd COMECON symposium on "Investigations in the field of spent fuel reprocessing" (Marianske Lazne, CSSR, 1971) [in Russian, Czech], izd. SEV, Prague (1972), Vol. 1, p. 304.

Upon computing the sedimentation rate of the particles on the basis of Eqs. (1) and (2), we can then determine the time it takes those particles to reach the surface of a drop of molten steel. Assigned values in these calculations are: density of uranium dioxide  $10.95 \text{ g/cm}^3$  [9], density of steel at  $1500^\circ\text{C}$   $7.10 \text{ g/cm}^3$  [10-12]; viscosity of stream  $4.1 \cdot 10^{-2} \text{ P}$  as determined from the equation  $\eta = \nu D$ , where  $\nu$  is the kinematic viscosity of EYaZS grade steel [13], which is  $4.1 \cdot 10^{-2} \text{ P}$ .

Table 1 lists computed values of the sedimentation rate and sedimentation time of uranium dioxide particles of different size in droplets of molten steel. It is evident from the tabular data that particles  $100 \mu$  in diameter emerge to the surface of the steel droplet within 1-2 sec, while particles larger than  $1000 \mu$  emerge at

THERMAL DECLADDING OF OXIDE FUEL ELEMENTS  
WITH STEEL SEPARATED FROM NUCLEAR FUEL  
BY FILTRATION

G. P. Novoselov, A. T. Ageenkov,  
V. F. Savel'ev, and S. E. Bibikov

UDC 621.039.5

The degree to which nuclear fuel meat can be separated from steel when thermal cladding of fuel elements is resorted to [1, 2] depends on the physicochemical properties of the molten steel, of the nuclear fuel, and on the design of the equipment employed. This article deals with an attempt to establish some of the regularities evident in the process which affect how efficiently the steel is separated from the fuel.

Experiments were conducted in a resistance furnace with a graphite heater (see Fig. 1). A crucible with holes in the bottom, and a movable ingot mold with a magnesium oxide screen support were placed inside the heater. A mechanism consisting of a supporting screw, rod, and bellows, to keep the furnace pressure-tight during filtration, is provided to facilitate vertical motion of the mold. The bottom of the mold covers the filtering holes of the crucible when the mold is in top position. The mold is lowered during filtration, so that the molten steel can escape from the crucible into the mold.

The fuel elements figuring in our experiments were in the form of Kh16N16M2B steel tubing 300 mm in length and 6 mm in diameter, filled with pellets of sintered uranium dioxide; each assembly consisted of 12 to 15 fuel elements. The assemblies were loaded into the crucible, the furnace was evacuated ( $p = 10^{-2}$  to  $5 \cdot 10^{-2}$  mm Hg), and heated at a heating rate of 10 to 20 deg/min to temperatures of 1450-1550°C, as measured with an OPPIR-09 optical pyrometer.

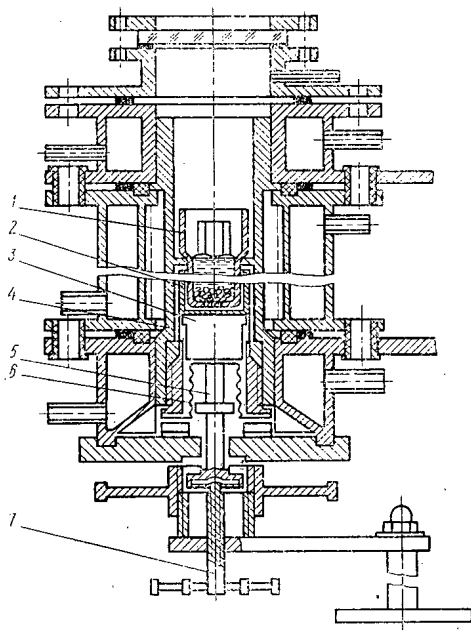


Fig. 1. High-temperature resistance furnace: 1) crucible; 2) movable mold; 3) support screen; 4) graphite heater; 5) rod; 6) bellows; 7) support screw.

In the first experiments, the mold was left in the bottom position, so that the steel could flow freely into it, when molten, through the channels between the pellets and through the holes in the crucible bottom. It is clear from the tabular data that some of the steel (see experiments Nos. 1, 2) remained on the pellets in the form of separate droplets. The weight of those inclusions ranged from 0.5 g to 10 g, and the coarsest such inclusions were detected in the top layers of the fuel. The probable reason is that the molten steel forms menisci (Fig. 2) as in melts in the channels. Surface tension hinders the flow of molten steel. The pressure exerted by the column of molten steel  $h$  is brought to equilibrium. The pressure exerted by the meniscus of molten steel is found from the formula [3]:

$$h = \frac{2\sigma \cos \theta}{rg\rho}, \quad (1)$$

where  $h$  is the pressure (mm) exerted by the column of molten steel;  $r$  is the radius of the channel between the pellets, in cm;  $\sigma$  is the surface tension of the molten steel (1340 to 1750

Translated from *Atomnaya Énergiya*, Vol. 36, No. 1, pp. 70-72, January, 1974. Original article submitted May 3, 1973.

© 1974 Consultants Bureau, a division of Plenum Publishing Corporation, 227 West 17th Street, New York, N. Y. 10011. No part of this publication may be reproduced, stored in a retrieval system, or transmitted, in any form or by any means, electronic, mechanical, photocopying, microfilming, recording or otherwise, without written permission of the publisher. A copy of this article is available from the publisher for \$15.00.

TABLE 1. Performance in Separation of Fuel Meat and Steel

Experiment number	Load		Steel/fuel ratio	Unload		Steel content in fuel, %
	fuel, g	steel, g		fuel-steel mixture, g	steel slug, g	
1	528,3	452,2	0,86	590,8	389,7	10,6
2	660,0	523,0	0,79	707,0	476,0	6,6
3	574,0	487,0	0,85	602,5	458,5	4,7
4	621,0	507,0	0,82	648,1	479,9	4,2
5	660,5	751,2	1,14	684,6	727,1	3,5
6	480,8	590,9	1,23	494,3	577,4	2,7
7	517,8	655,7	1,27	536,2	637,3	3,4
8	401,2	596,1	1,48	407,8	589,5	1,6
9	270,0	395,0	1,46	271,2	393,8	0,5
10	300,0	800,0	2,67	301,5	789,5	0,5

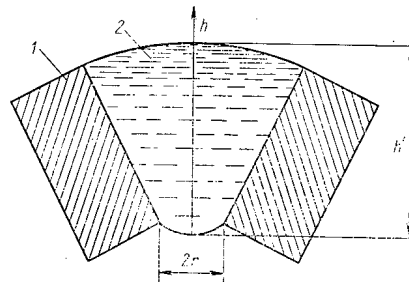


Fig. 2. Diagram illustrating cell with hanging droplet: 1) uranium dioxide pellets; 2) steel droplet.

dynes/cm [1]);  $\rho$  is the density of the steel (at temperature 1500°C, we have  $\rho = 7.1 \text{ g/cm}^3$  [4, 5]);  $\theta$  is the wetting angle for steel wetting uranium dioxide (130–145° [1]).

Figure 3 shows how the pressure of the molten steel meniscus  $h$  varies with the hole diameter  $2r$ , as calculated on the basis of Eq. (1). It is clear from the graph that the meniscus pressure at the 1 mm filtration hole offsets the pressure exerted by a column of molten steel standing 55–60 mm high. That constitutes evidence that the molten steel droplets retained in the pellets are capable of attaining large dimensions. The more droplets are left suspended in the pellets, the less efficiently will the molten steel be separated from the fuel. Accordingly, a single liquid-metal bath should be set up and the molten steel should then be filtered out. In that case we should find it easier to overcome any phenomena hindering filtration of the steel, first because the liquid-metal bath minimizes the number of menisci interfering with filtration, and second because it increases the hydrostatic pressure of the molten steel; third, because it causes fine droplets forming on account of other reasons to merge [6].

We melted down fuel element jackets with filter holes covered over (with mold in topmost position) with the object of verifying these conclusions. Steel accumulated in the crucible, forming a liquid-metal bath, in this instance. After the cladding had been melted down, the mold was lowered to the bottom position at a speed of 2 to 5 cm/min, and the steel was filtered out. It is clear from the tabular data that the formation of the liquid-metal bath brought the content of the steel in the fuel down from 10.6% to 4.4% (see Table 1, for experiments Nos. 3 and 4).

The completeness with which the steel is separated increases as the steel-fuel ratio is increased (see Table 1, for experiments 4–10). As the ratio increases, the pellets become more deeply immersed

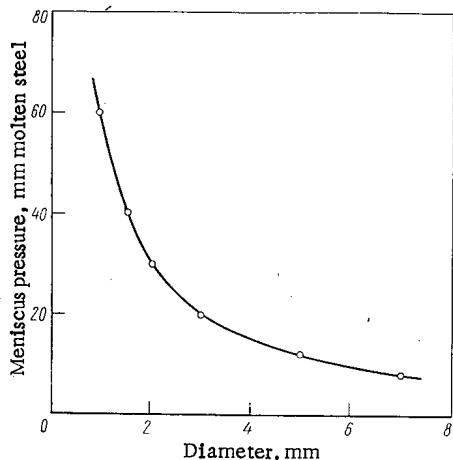
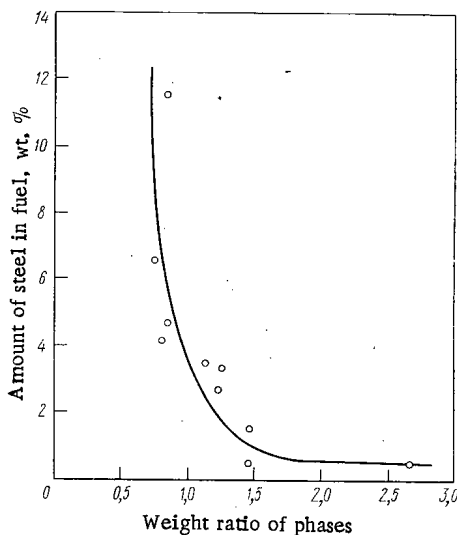
Fig. 3. Dependence of  $h$  on  $2r$ .

Fig. 4. Illustration of how efficiently fuel is separated from cladding steel, as steel:fuel ratio is varied.

in the molten steel, and that lessens the likelihood of discrete steel droplets taking shape in the fuel. When an additional amount of steel is introduced and the pellets are completely immersed into the melt, separation of fuel from steel becomes maximized. Figure 4 shows how the separation of steel from fuel varies with the steel-fuel ratio. It is obvious that the steel content in the pellets dropped from 10.6% to 0.5% as the steel-fuel ratio is stepped up from 0.9 to 2.7.

The results obtained show that the formation of the liquid-metal bath and filtration of the molten steel are responsible for the virtually complete separation of fuel from steel. If the steel-fuel ratio exceeds 1.0-1.5, the curve in Fig. 4 changes in slope, tending to some limit. That seems to be evidence that the pressure of the molten steel meniscus is not the only factor hindering more complete separation of the steel; further studies will be required to prove that point.

#### LITERATURE CITED

1. G. P. Novoselov and A. T. Ageenkov, *At. Énerg.*, 26, 230 (1969).
2. A. T. Ageenkov et al., *At. Energ.*, 32, 490 (1972).
3. B. Linczewski, *Experimental Techniques in Metallurgical Research* [in Russian], Metallurgiya, Moscow (1967), p. 202.
4. E. Guderman, *Special Steels* [Russian translation], Metallurgiya, Moscow (1966).
5. D. F. Elliott et al., *Thermochemistry of Steelmaking Processes* [Russian translation], Metallurgiya, Moscow (1969).
6. V. L. Aleksandrov, *Engineering Hydromechanics* [in Russian], Fizmatgiz, Moscow (1946).

## TEMPERATURE MEASUREMENT IN HIGH-FLUX REACTORS USING THERMOCOUPLES

N. V. Markina and V. A. Tsykanov

UDC 621.039.533+537.324

Reliable measurement of temperature is an obvious requirement in many investigations. The ability to measure temperature accurately and reliably is of especial importance within nuclear reactors. The present communication discusses the problems of temperature measurement in high-flux reactors.

Experiments to determine the differences in the readings of microthermocouples of ordinary industrial calibrations when operated in a reactor radiation field were carried out in the SM-2 water-moderated water-cooled intermediate reactor. It is known [1, 2] that effects of two kinds arise in thermocouples under the action of nuclear radiation: instantaneous effects (caused by ionizing radiation and disappearing when irradiation ceases), and integral effects (accumulating with integral dose and remaining when irradiation ceases).

The most important result of the SM-2 investigations is the experimental detection of the instantaneous effects. This is important for two reasons. Firstly, with previously employed methods (thermocouple studied after an integral dose in ordinary irradiation devices) instantaneous effects cannot be detected and a special procedure [3] is needed to investigate them; secondly, the widely-held opinion that instantaneous effects are small is incorrect for high-flux reactors [4, 5].

In the tests the thermocouples were calibrated absolutely in terms of reference points directly in the reactor channel [3]. We denote by  $E_0(t)$  the reading of the thermocouple at the reference temperature at zero reactor power or outside the reactor, and by  $E_N(t)$  the reading of the same thermocouple at the same temperature but at a reactor power  $N$ . The instantaneous effect is then characterized by

$$\Delta E = E_N(t) - E_0(t).$$

Figure 1 shows a plot of  $\Delta E$  versus thermal-neutron and gamma flux intensity for Chromel-Alumel and VR5/20 tungsten-rhenium thermocouples calibrated in the reactor.

In the experiments the thermocouples are constantly subjected to the action of reactor radiation and integral effects accumulate. After a sufficiently large integral dose has been accumulated, the measured reading of the thermocouple will contain both an instantaneous and an integral component, i. e., one is measuring the total effect of the radiation (Fig. 2). The two effects can nevertheless be separated from each other. To this end one must compare the readings

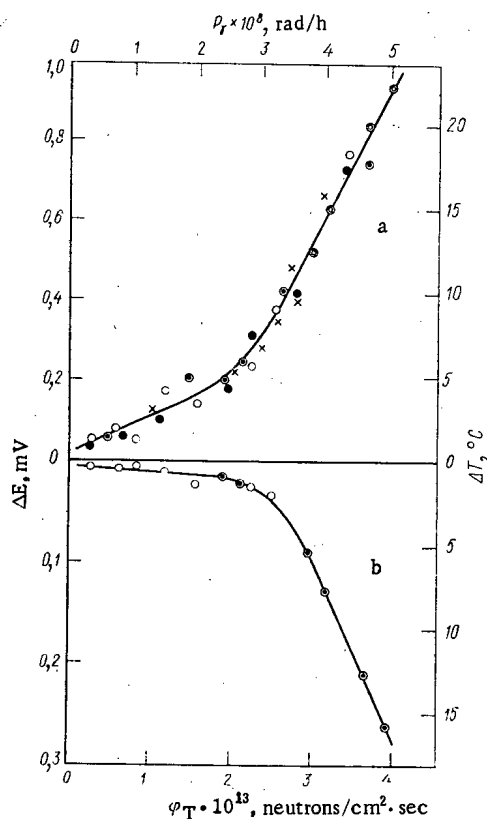


Fig. 1. Dependence of  $\Delta E$  (instantaneous effects) of Chromel-Alumel (a) and VR5/20 tungsten-rhenium (b) thermocouples on thermal neutron flux intensity  $\Phi_T$  and  $\gamma$  intensity  $P_\gamma$  at 660°C (differently indicated points correspond to independent experiments).

Translated from *Atomnaya Énergiya*, Vol. 36, No. 1, pp. 72-74, January, 1974. Original article submitted May 24, 1973.

© 1974 Consultants Bureau, a division of Plenum Publishing Corporation, 227 West 17th Street, New York, N. Y. 10011. No part of this publication may be reproduced, stored in a retrieval system, or transmitted, in any form or by any means, electronic, mechanical, photocopying, microfilming, recording or otherwise, without written permission of the publisher. A copy of this article is available from the publisher for \$15.00.



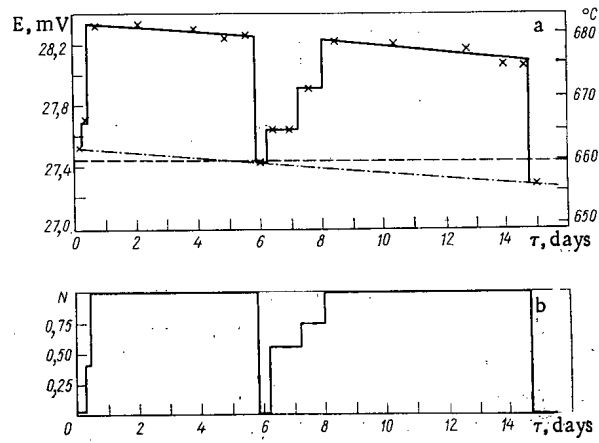


Fig. 2. Variation of Chromel-Alumel thermocouple readings  $E$  during experiment at hardening temperature of aluminum (a) and relative variation of reactor power  $N$  (radiation intensity) at corresponding moments of time (b).

of the thermocouple in the reactor at some value of the power not with readings before the thermocouple is installed in the reactor, but with readings at zero power measured almost immediately, i. e., at the same integral dose. Investigations showed that this sort of separation is sufficiently correct and that the instantaneous effects remain constant up to integral doses  $\sim 10^{20}$  neutrons/cm<sup>2</sup>.

The instantaneous effects were found to depend on the radiation spectrum and on the temperature at which the measurements were made. To elucidate the influence of temperature a special experiment was carried out exploiting the different signs of the instantaneous effects on Chromel-Alumel and tungsten-rhenium thermocouples [5]. The thermocouples were mounted in a copper block the temperature of which could be varied. According to calculation the temperature drop across the block could not exceed 3.6 $^{\circ}\text{C}$ . However, in experiments at intensities  $P_{\gamma} = 9 \cdot 10^5$  rad/sec,  $\Phi_T = 4 \cdot 10^{14}$  neutrons/cm<sup>2</sup>·sec,  $\Phi_0 = 4 \cdot 10^{14}$  neutrons/cm<sup>2</sup>·sec, the difference in the readings of the Chromel-Alumel and tungsten-rhenium thermocouples amounted to  $\sim 80^{\circ}\text{C}$ , which corresponded to the sum of their instantaneous effects. Further, the difference was observed to depend on reactor power (radiation intensity) and on temperature up to  $\sim 500^{\circ}\text{C}$  (Fig. 3).

An analysis of the experimental results obtained in these tests and in the reference measurements shows that instantaneous effects are independent of temperature in the temperature range 500-1100 $^{\circ}\text{C}$ . This made it possible to compare measurements in different channels at the hardening temperatures of zinc, aluminum, silver, and copper, equal respectively to 419.5, 660, 960, and 1083 $^{\circ}\text{C}$ . The comparison showed that the results in the various channels differ, which in our opinion is due to the influence on the thermocouple readings of the spectrum of the reactor radiations.

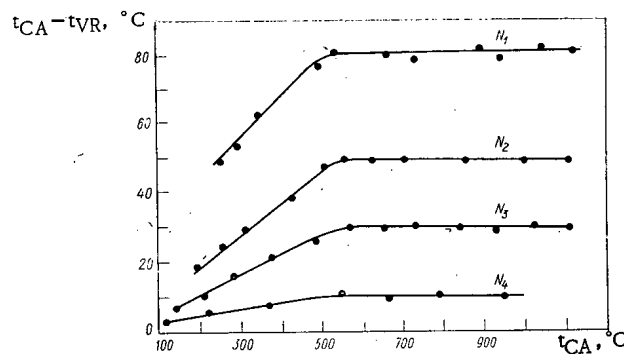


Fig. 3. Difference of readings of Chromel-Alumel (CA) and VR5/20 thermocouples due to instantaneous effects versus temperature for various reactor powers.

Our experiments thus lend strong support to the picture of instantaneous effects in thermocouples induced by the action of fluxes of mixed reactor radiations. In high-flux reactors (the SM-2, for example) the instantaneous effects may be sufficiently large that they must be taken into account in precision temperature measurements. The instantaneous effects remain constant up to an integral dose  $\sim 10^{20}$  neutrons/cm<sup>2</sup>. The instantaneous effects in Chromel-Alumel and VR5/20 tungsten-rhenium thermocouples are temperature independent in the temperature interval 500-1100°C.

## LITERATURE CITED

1. W. Browning, Prog. Nucl. Energy, 5, Ser. 4, 1-54 (1963).
2. N. V. Markina and B. V. Samsonov, "Temperature measurement under conditions of irradiation of materials [in Russian], NIIAR Preprint P-152, Melekess (1972).
3. N. V. Markina, B. V. Samsonov, and V. A. Tsykanov, "Methods of investigating the influence of reactor radiations on the accuracy of thermocouple readings" [in Russian], NIIAR Preprint P-130, Melekess (1970).
4. N. V. Markina, B. V. Samsonov, and V. A. Tsykanov, Fiz. Metal. Metalloved., 32, No. 4, 747 (1971).
5. N. V. Markina et al., Fiz. Metal. Metalloved., 32, No. 6, 1316 (1971).

THE CALCULATION OF THE SPACE-ENERGY  
DISTRIBUTION OF SECONDARY  
ANNIHILATION RADIATION

Sh. S. Nikolaishvili and G. N. Dzhashiashvili

UDC 539.122.13

In the usual calculations of the transmission of  $\gamma$  radiation through matter, the process of formation of electron-positron pairs is considered as pure absorption, and the secondary annihilation radiation is neglected. The first estimate of the contribution of secondary  $\gamma$ -rays to the dosage buildup factor was given by G. Gol'dshtein [1, 2]. The problem of the secondary annihilation radiation was considered most thoroughly in [3], which contained the results of numerical calculations for a number of standard sources. A new approach for solving the problem is presented in the present article. The apparatus of conjugate transfer equations is used in the form developed by G. I. Marchuk and V. V. Orlov [4]. The correction to the dosage buildup factor due to the annihilation radiation is calculated for a plane perpendicular source of unit strength emitting monoenergetic  $\gamma$ -rays in an infinite homogeneous medium.

If we denote this correction at a distance  $x$  from the source by  $\delta b(x)$ , we obtain

$$\delta b(x) = 2\pi \int_{-\infty}^{\infty} \psi_0^*(|x-t|) dt \int_{\lambda_0}^{0.5} \sigma_{\text{pair}}(\lambda) \varphi_0(t, \lambda) d\lambda, \quad (1)$$

where  $\psi_0^*(x)$  is the solution of the conjugate equation for  $\lambda = 1$  with a free term corresponding to the dosage buildup factor (the wavelength of the  $\gamma$ -rays is measured in Compton units),  $\varphi_0(x, \lambda)$  is a function describing the spectral distribution of the  $\gamma$  radiation at a distance  $x$  from the source, and  $\sigma_{\text{pair}}(\lambda)$  is the cross section for absorption of  $\gamma$ -rays with wavelength  $\lambda$ , resulting in pair formation.

At this point, we introduce into the discussion the spatial moments of the functions  $\psi_0^*(x)$  and  $\varphi_0(x, \lambda)$ , which are defined by the formulas

$$\mu_n^* = \frac{\sigma_1}{(2n)!} \int_{-\infty}^{\infty} \psi_0^*(x) (\sigma_1 x)^{2n} dx \quad (2)$$

and

$$\mu_n(\lambda) = \frac{\sigma_0}{(2n)!} \int_{-\infty}^{\infty} \varphi_0(x, \lambda) (\sigma_0 x)^{2n} dx, \quad (3)$$

where  $\sigma_0$  and  $\sigma_1$  are the values of  $\sigma(\lambda)$  for  $\lambda = \lambda_0$  and  $\lambda = 1$  respectively (here  $\lambda_0$  is the wavelength of the primary  $\gamma$ -ray emitted by the source). Using the notation

$$M_n = \int_{\lambda_0}^{0.5} \mu_n(\lambda) \sigma_{\text{pair}}(\lambda) d\lambda \quad (4)$$

and

$$h_n = \frac{\sigma_0}{(2n)!} \int_{-\infty}^{\infty} \delta b(x) (\sigma_0 x)^{2n} dx, \quad (5)$$

we obtain after simple transformations the result that

$$h_n = \frac{1}{2\pi} \sum_{k=1}^n \left( \frac{\sigma_0}{\sigma_1} \right)^{2k} M_{n-k} \mu_k^*. \quad (6)$$

Translated from *Atomnaya Energiya*, Vol. 36, No. 1, pp. 74-75, January, 1974. Original article submitted June 13, 1973.

© 1974 Consultants Bureau, a division of Plenum Publishing Corporation, 227 West 17th Street, New York, N. Y. 10011. No part of this publication may be reproduced, stored in a retrieval system, or transmitted, in any form or by any means, electronic, mechanical, photocopying, microfilming, recording or otherwise, without written permission of the publisher. A copy of this article is available from the publisher for \$15.00.

TABLE 1. The Relative Contribution of Annihilation Radiation to the Dosage Buildup Factor for a Plane Perpendicular Source, %

$E_0, \text{MeV}$	$\sigma_0 x$					
	1	2	4	7	10	15
Lead						
10	5,89	5,79	5,60	5,30	4,86	4,48
8	5,77	5,67	5,35	4,79	4,26	3,70
6	5,69	5,51	5,16	4,54	3,93	3,22
Iron						
10	7,42	7,44	7,05	6,45	6,10	5,65
8	7,18	7,05	6,49	5,97	5,58	5,19
6	6,65	6,40	5,74	5,20	4,85	4,49

TABLE 2. The Relative Contribution of Annihilation Radiation to the Dosage Buildup Factor for a Point Isotropic Source, %

$E_0, \text{MeV}$	$\sigma_0 x$					
	1	2	4	7	10	15
Lead						
10	6,85	6,54	5,66	5,09	4,54	3,76
8	6,69	6,26	5,36	4,65	3,96	2,98
6	6,60	6,02	5,09	4,29	3,64	2,70
Iron						
10	9,41	9,44	7,76	6,81	6,30	5,68
8	8,86	8,67	6,91	6,02	5,50	4,95
6	8,31	7,95	6,18	5,22	4,75	4,28

In this way, knowing the moments of the solutions of the original and conjugate equations, we calculate the moments of the function  $\delta b(x)$  from Eq. (5). By using well-known methods [1, 5, 6], the dependence of  $\delta b$  on  $x$  can be found from these moments. The problem of the spectral distribution of the annihilation radiation is solved in a similar manner.

The authors have used the method described here to calculate the function  $\delta b(x)$  for plane isotropic, point isotropic, and plane perpendicular sources in lead and iron. A number of results of the calculations for sources with initial energies of 10, 8, and 6 MeV are shown in Table 1 and 2.

The results given in Table 1 agree with those of [1, 3]. The displacement of the positron between the points of origin and annihilation was neglected in our calculations. It was shown in [3] that the error in the results of the calculations introduced by such a simplification is inconsequential. The Compton scattering cross section was calculated exactly by using the Klein-Nishina-Tamm formula. The cross section for pair formation and photoelectric absorption were calculated from tables [5], using the linear interpolation formula. For energies  $E = 0.5108/\lambda$ , which is less than the threshold for pair formation, the tabulated values of the photoelectric absorption function were first of all multiplied by  $E^{3.5}$  to be consistent with the known behavior in the low energy region of the function being calculated [1].

The authors are very grateful to S. G. Tsypin, V. G. Zolotukhiv, and A. A. Abagyan for discussion of the results and valuable comments.

## LITERATURE CITED

1. U. Fano, L. Spencer, and M. Berger, Gamma-Radiation Transfer [Russian translation], Gosatomizdat, Moscow (1963).
2. G. Gol'dshtein, Fundamentals of Reactor Shielding [in Russian], Gosatomizdat, Moscow (1961).
3. M. Berger et al., "Contribution of annihilation radiation to the gamma-ray flux in lead," Phys. Rev., 113, 857 (1959).
4. G. I. Marchuk and V. V. Orlov, The Theory of Conjugate Functions [in Russian], in: Neutron Physics, Gosatomizdat, Moscow (1961).
5. D. L. Broder et al. (editors), Handbook of Radiation Shielding for Engineers, Vol. 1 [Russian translation], Atomizdat, Moscow (1972).
6. Sh. S. Nikolishvili et al., At. Énerg., 32, 504 (1972).

TEST FACILITY FOR STUDYING KINETICS OF  
RELEASE OF GASEOUS RADIOACTIVE FISSION  
PRODUCTS FROM IRRADIATED MATERIALS

D. M. Skorov, A. I. Dashkovskii,  
A. G. Zaluzhnyi, and O. M. Storozhuk

UDC 621.039.548.343

Closer attention has been given to the study of the diffusion mobility of inert gases from reactor materials in the recent period, since gaseous fission products form in reactor materials in response to neutron bombardment, and these fission products are associated with undesirable effects such as radiation-induced swelling and embrittlement.

The diffusion mobility of gases in a reactor material can be calculated from the kinetics of gas release during the heating process. Several test facilities employed in determining the kinetics of release of radioactive isotopes of inert gases from test specimens during isothermal annealing processes have been described in the literature [1-4]. The operating principles of these facilities are based on the fact that the inert gas released from the test specimen during the annealing process becomes entrapped by the stream of helium sweeping over the specimen, and is then collected in a trap cooled by liquid nitrogen. The amount of gas collected in the trap is determined from the activity of the gas. The facilities described to date suffer from certain shortcomings. First, many other readily volatile radioactive fission products (cesium, iodine, etc.) having an emission energy close to the emission energy of the gas under analysis (say,  $^{133}\text{Xe}$  or  $^{131}\text{I}$ ) are contained in the irradiated fuel specimens to begin with, in addition to the inert gases. These radioactive fission products entrained in the helium stream can also end up in the nitrogen-cooled trap intended for the collection of the gas under analysis, and are responsible for a large error incurred in the determination of the quantity of gas released. And secondly, a rigorously high purity is required of the helium, since the test specimens can become oxidized during heating and the kinetics of gas release from the test specimens may be altered as a result.

The test facility we propose here (see Fig. 1) makes it possible to eliminate those shortcomings by heating the test specimen in a high vacuum with continuous oilless evacuation of the effective volume by high-vacuum pumps, and by keeping nongaseous fission products out of the trap intended to collect the inert gases.

Figure 2 displays a diagram of the vacuum system used. This system is made up of the high-vacuum chamber (see position 6 in Fig. 1, and position 1 in Fig. 2) fabricated from stainless steel with cermet leads. The chamber accommodates the test specimen in the form of foil and suspended from the current insulators. The test specimen is heated by bombarding electrons emitted from a tungsten cathode. The accelerating voltage is generated by a UIP-1 general-purpose power supplies pack. The cathode warmup is controlled with the aid of a RNO-250-10 transformer included in the circuit and operating through a S-0.5 voltage stabilizer. The temperature of the specimen is measured with the aid of a thermocouple. The temperature range in the investigation was limited in practice solely by the vacuum needed in the study of any particular material (at  $1500^\circ\text{C}$ , the required vacuum was  $10^{-6}$  to  $10^{-7}$  mm Hg). The chamber is flange-connected to the manometric tubes LT-2 and LM-2 and communicates via high-vacuum globe valves DU-25 to the zeolite-packed nitrogen trap, and to the ERA-100-2 electric discharge set generating the high vacuum in the system.

The vacuum system is evacuated, via the globe valves, by the electric discharge set, and in continuous evacuation the vacuum parts of the facility are heated to  $\sim 450^\circ\text{C}$  by an external heater. The specimen

Translated from *Atomnaya Énergiya*, Vol. 36, No. 1, pp. 76-77, January, 1974. Original article submitted June 14, 1973.

© 1974 Consultants Bureau, a division of Plenum Publishing Corporation, 227 West 17th Street, New York, N. Y. 10011. No part of this publication may be reproduced, stored in a retrieval system, or transmitted, in any form or by any means, electronic, mechanical, photocopying, microfilming, recording or otherwise, without written permission of the publisher. A copy of this article is available from the publisher for \$15.00.

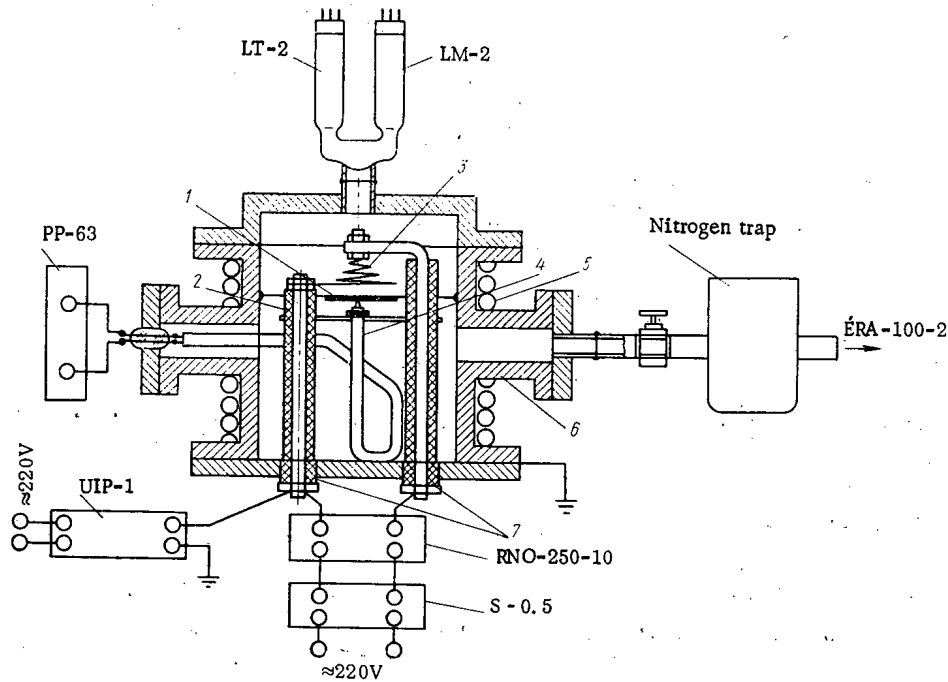


Fig. 1. Diagram of facility for determining kinetics of release of radioactive gaseous fission products: 1) test specimen; 2) current conductor insulators; 3) tungsten cathode; 4) thermocouple; 5) external heater; 6) annealing chamber; 7) current leads.

is then warmed up to the prespecified temperature in the outgassed chamber by electron bombardment, with one valve closed. The inert gases released by the specimen during the annealing process pass, in unison with the stream of chemically active gases generated by the partial pressure difference in the chamber and in the electric discharge pump, through the zeolite-packed liquid-nitrogen-cooled cold trap. Here the inert gases to be analyzed (krypton, xenon) are frozen out, since their critical liquefaction temperature is higher than the temperature of the liquid nitrogen. The vapors of volatile elements (cesium, iodine) released from the specimen with the gases during the high-temperature anneal do not end up in the nitrogen trap, since they condense on the walls of the vacuum piping (intensively cooled with water) connecting the trap and chamber. The relative amounts of gas collected in the trap within the specified diffusion anneal time are determined on the basis of the activity of the gas. Different recording techniques can be resorted to [1-4] to match the type of radiation to be analyzed. The total quantity of gas (in relative units) can be found by melting the specimen down.

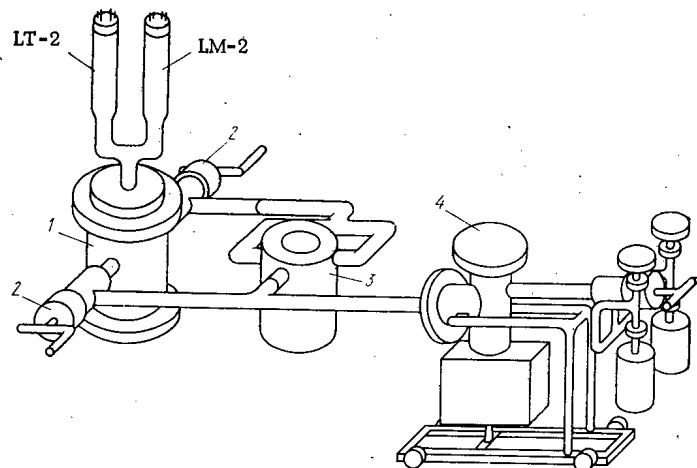


Fig. 2. Arrangement of vacuum system: 1) anneal chamber; 2) high-vacuum globe valves; 3) nitrogen trap; 4) electric discharge pump.

Consequently, we see that, by measuring the fraction of gas released from the specimen during the specified diffusion anneal time, we are able to calculate the diffusion coefficient of the inert gas in the material.

LITERATURE CITED

1. M. Gorun et al., *Rev. Roum. Phys.*, 11, No. 2, 191-200 (1966).
2. K. Iwamoto and J. Oishi, *N. Nucl. Sci. and Technol.*, 4, No. 5, 223-230 (1967).
3. D. Hilton, *J. Nucl. Mater.*, 36, No. 1, 61-76 (1970).
4. T. Elleman et al., *J. Nucl. Mater.*, 30, 89-106 (1969).

INTERACTION OF THERMAL NEUTRONS WITH  
 $^{152m}\text{Eu}$  NUCLEI

I. A. Kondurov, A. M. Berestovoi,  
 A. I. Egorov, E. M. Korotkikh,  
 and Yu. V. Petrov

UDC 539.171.017:539.184.5

In the interaction of neutrons with excited nuclei inelastic scattering of the second kind can occur with the transfer of the excitation energy of the nucleus to the scattered neutron [1]. Miyano and Morinaga [2] attempted to detect this effect indirectly from an analysis of the cross sections for the formation of  $^{148}\text{Pm}$  and  $^{149}\text{Pm}$  by the irradiation of  $^{147}\text{Pm}$  with thermal neutrons. We have measured the effect directly by searching for fast neutrons produced by the irradiation of isomeric  $^{152m}\text{Eu}$  nuclei with thermal neutrons.

The isomer was obtained by irradiating samples containing  $^{151}\text{Eu}$  in a reactor. The samples were made of natural or separated europium oxide brazed onto both sides of aluminum backing  $12\ \mu$  thick. Disc-shaped samples 34 mm in diameter with a  $^{151}\text{Eu}$  content of about 100 mg were pressed between two aluminum foils  $20\ \mu$  thick. The samples were irradiated in a vertical channel of the VVR-M reactor where the unperturbed thermal neutron flux was  $1.4 \cdot 10^{14}$  neutrons/cm<sup>2</sup>·sec<sup>-1</sup>. The perturbation introduced by a sample, and the self-shielding were taken account of by irradiating a test specimen and measuring its activity. The accuracy of determining the number of isomeric nuclei this way was 8%.

Samples containing about 1 mg of  $^{152m}\text{Eu}$  were placed in a horizontal channel of the reactor where the thermal neutron flux was  $(5.8 \pm 0.3) \cdot 10^8$  neutrons/cm<sup>2</sup>·sec. In view of the small size of the expected effect the beam of thermal neutrons was modulated by a disc of cadmium and aluminum rotating with a period of 1 sec. This does not modulate the background of fast neutrons. The accuracy of the period to the order of  $10^{-5}$  sec was ensured by a quartz oscillator.

The fast neutron detector was a  $^{235}\text{U}$  fission fragment spark counter surrounded by a Plexiglas moderator and a shield of cadmium and boron. The thermal neutrons resulting from the slowing down of fast neutrons in passing through the boron-cadmium shield were counted. The spark counter with particle discrimination by ionization density completely removes the effect of the intense  $\gamma$  radiation (up to 10 R/sec) from the sample. The counting efficiency of the fast neutron detector, measured with a calibrated Sb-Be source furnishing 24 keV neutrons, varied from 2.5 to  $3.5 \cdot 10^{-4}$ . The accuracy of determining this quantity ( $\pm 15\%$ ) depends mainly on the accuracy of the calibration of the neutron source.

The detector pulses were recorded in two counting channels which were gated in step with the modulation of the thermal beam. The variable component of the fast neutron counting rate was determined; it falls off with the half-life of  $^{152m}\text{Eu}$ , equal to 9.2 h [3]. The main limitation in this experiment was the background of fast neutrons from the reactor channel. The background count was  $1400\ \text{sec}^{-1}$ , of which 75% were counts of fast neutrons scattered directly by the sample. The accuracy of measuring the effect was approximately 0.003 of the background.

An analysis of the measurements gave an average value of the cross section for the "acceleration" of neutrons by the  $^{152m}\text{Eu}$  isomer

$$\sigma = (0.15 \pm 1.46)\ \text{b.}$$

This means that there is a 95% probability that the reaction cross section does not exceed 3 b.

---

Translated from Atomnaya Energiya, Vol. 36, No. 1, pp. 77-78, January, 1974. Original article submitted July 9, 1973.

© 1974 Consultants Bureau, a division of Plenum Publishing Corporation, 227 West 17th Street, New York, N.Y. 10011. No part of this publication may be reproduced, stored in a retrieval system, or transmitted, in any form or by any means, electronic, mechanical, photocopying, microfilming, recording or otherwise, without written permission of the publisher. A copy of this article is available from the publisher for \$15.00.



LITERATURE CITED

1. Yu. V. Petrov, Zh. Éksp. Teor. Fiz., 37, 1170 (1959).
2. K. Miyano and H. Morinaga, J. Phys. Soc. Japan, 26, 576 (1969).
3. B. S. Dzhelepov, L. K. Peker, and V. O. Sergeev, Decay Schemes of Radioactive Nuclei [in Russian], AN SSSR, Moscow-Leningrad (1963).

LIMITATIONS OF EFFECTIVE ACCELERATING  
FIELDS IN RING ACCELERATORS

V. G. Makhan'kov and M. G. Meshcheryakov

UDC 621.384.63

The efficiency of ion (proton) acceleration with the aid of relativistic electron rings is a subject that is being increasingly discussed. The interest in this matter stems from the paper of Mohl et al. [1] and the ensuing discussion at the 1972 Dubna Symposium on collective methods of acceleration. A further two theoretical papers subsequently appeared in which an attempt was made to consolidate the main results of [1]. The linear theory of ring stability was used in [1] to derive limitations on the maximum attainable accelerating fields and thereby on the ion energy increment per unit length.

The main results of [1] reduce to the following. In the simplest accelerator construction the energy increment per unit length  $e\epsilon_{\text{eff}}$  cannot exceed 10 MeV/m, but with a more sophisticated construction (introduction of an internal screening cylinder)  $e\epsilon_{\text{eff}}$  can reach  $\sim 40$  MeV/m. At the present time accelerating fields of this magnitude have already been obtained in ordinary ring accelerators. The authors of [1] make the conclusion that only heavy ions can be efficiently accelerated with the aid of relativistic electron rings. We emphasize that the conclusions and results of [1] were obtained on the basis of the linear theory of ring stability.

Electron-ion rings are known (theoretically and to some extent experimentally) to suffer from two main types of instability. The first instability is connected with electromagnetic radiation and azimuthal bunching of electrons (in the theory of ordinary accelerators it is known as the "negative" mass instability). The second instability, the so-called firehose instability, is inherent only to plasma electron-ion formations. The most stringent limitation on  $e\epsilon_{\text{eff}}$  is imposed by the first kind of instability. This instability is of a threshold character, however, as it appears only when the number of electrons in the ring  $N_e$  becomes greater than a certain critical value  $N_{\text{cr}}$  dependent on the energy spread.

The reason for this is that this instability is connected with particle bunching, while energy spread naturally opposes this bunching. Accordingly, the greater the spread the greater the value of  $N_{\text{cr}}$ , which can be roughly found by comparing the growth rate of the instability  $\gamma_n$  with the magnitude of the spread, i. e., from the condition

$$\gamma_n \leq n\alpha W. \quad (1)$$

Here  $n$  denotes the number of the perturbation harmonic;  $W = 2\pi m_e c R_0 \Delta\gamma_0$ ;  $\alpha = -(2\pi R_0^2 m_e \gamma_0)^{-1}$ , where  $R_0$  is the major radius of the ring;  $m_e$  is the electron rest mass;  $\gamma_0$  is the relativistic factor; and  $\Delta\gamma_0/\gamma_0 = \Delta E_0/E_0$  is the relative energy spread. Inserting the known expression for  $\gamma_n$  into (1) leads to the order-of-magnitude formula (3.1) of paper [1]:

$$N_e \leq \frac{1}{2} k H_0 \frac{R_0^2}{r_c} \frac{(\Delta E_0/E_0)^2}{|Z_n/nZ_0|} \frac{\pi}{2} \approx N_{\text{cr}}, \quad (2)$$

where  $r_c = (e^2/m_e c^2)$  is the classical radius of the electron;  $c$  is the free-space velocity of light;  $k = (e/m_e c^2)$ ;  $H_0$  is magnetic field;  $Z_n$  is the electron ring coupling impedance, the magnitude of which is essentially dependent on the accelerator construction; and  $Z_0(4\pi/c)$  is the free-space impedance.

Utilizing relationship (2) and the formula for the accelerating field in a ring accelerator

$$e\epsilon_{\text{eff}} \approx \frac{e^2 N_e}{\pi R_0 (a+b) \eta}, \quad (3)$$

Translated from *Atomnaya Énergiya*, Vol. 36, No. 1, pp. 78-79, January, 1974. Original article submitted July 9, 1973.

© 1974 Consultants Bureau, a division of Plenum Publishing Corporation, 227 West 17th Street, New York, N. Y. 10011. No part of this publication may be reproduced, stored in a retrieval system, or transmitted, in any form or by any means, electronic, mechanical, photocopying, microfilming, recording or otherwise, without written permission of the publisher. A copy of this article is available from the publisher for \$15.00.

where  $a$  and  $b$  are the semi-axes of the elliptical cross section of the ring, we find

$$e\epsilon_{\text{eff}} \leq 0.6m_e c^2 \frac{kH_0}{\pi\eta} \cdot \frac{\Delta E_0/E_0}{|Z_n/nZ_0|} \frac{\pi}{2}. \quad (4)$$

The previously cited values of  $e\epsilon_{\text{eff}}$  were obtained from this formula on setting  $H_0 = 22$  kG,  $(\Delta E_0/E_0) = 10\%$  and making certain assumptions concerning  $|Z_n/nZ_0|$ .

We note that in the subcritical regime, when  $N_e < N_{\text{CR}}$ , the parameters  $N_e$  and  $\Delta E_0/E_0$  are independent and determined by the initial conditions, i. e., to a large extent by the conditions of the experiment, so that the choice of value of  $\Delta E_0/E_0$  determines the entire range of values of  $N_e < N_{\text{CR}}$ .

In the above-critical regime  $N_e > N_{\text{CR}}$  the situation radically changes. In any case, for not too large values of  $N_e/N_{\text{CR}}$  a coupling between  $N_e$  and  $\Delta E_0/E_0$  clearly manifests itself. The problem consists, indeed, in finding this coupling. It turns out that the results are essentially dependent on the investigated mathematical models. The nonlinear theory advanced in [2] (the so-called single-mode approximation)\* at first glance confirms a coupling of the form of (2), i. e., a linear coupling, although, as the authors of this paper note, the results obtained by them are in poor accord with experiment.

On the other hand, an attempt has recently been made to follow through the behavior of the electron ring in the unstable regime when the number of electrons is 2-3 times in excess of the critical value  $N_{\text{CR}}$  [4]. This paper considers the excitation and interaction of ten coherent harmonics. The calculation shows that even at quite an early stage in the growth of the instability (times of order of 16-18 tenth-harmonic inverse growth rates and 4-5 first-harmonic inverse growth rates) mixing of the harmonics proves to be very important, which leads to phase separation of all the ten harmonics considered almost simultaneously and to a uniform distribution of energy over the harmonics. This confirms the essentially nonlinear and crosswise character of the interactions, as a result of which a certain self-consistent quasistationary regime is established. In this case the amplitudes of the perturbation fields are about 5-10 times smaller (for different values of  $N_e$ ) than the values given by the single-mode theory.

Further, a more detailed analysis of the final state obtained in [4] has led us to the conclusion that for a ring in free space the energy spread  $\Delta E_{\text{CR}}^{\text{non}}$  resulting from the saturation of the instability is less than the corresponding linear value  $\Delta E_{\text{CR}}^{\text{lin}}$  relating to the first harmonic by a factor of one-and-a-half to two. This means that (for a given  $\Delta E_0$ )  $N_e$  is increased in comparison with  $N_{\text{CR}}$  by a factor of four-six, so that the value of  $e\epsilon_{\text{eff}}$  is five-seven times greater than the value cited in [1].

This result can be interpreted as the nonlinear suppression of the instability of the low-frequency modes of oscillation by high-frequency modes which go over into a stable regime. If this is so, then increasing the number of considered harmonics and including in the analysis stable (damped) high-frequency harmonics must result in an even greater change in the coefficient  $\alpha$ :

$$\alpha = \frac{\Delta E_{\text{CR}}^{\text{non}}}{\Delta E_{\text{CR}}^{\text{lin}}}$$

Further, simple physical considerations indicate that the presence in an electron ring of ions (protons) uniformly distributed in azimuth must, in view of their large mass, have an effect on the growth of the investigated instability. A quantitative result can only be obtained, however, via experimental and numerical investigations of appropriate models.

The conclusion that suggests itself is that the contemporary state of the theory does not permit a final conclusion to be drawn concerning the attainable accelerating fields in accelerators of collective type. Accordingly, the pessimism that has arisen in connection with this matter is, like over-optimism, somewhat premature.

The complexity of the theory of the processes occurring in accelerators of collective type (nonlinearity, multi-mode behavior, and so on) means that one must resort to studying various models whose parameters would be essentially dependent on a suitable formulated set experiment. It seems to us that numerical simulation would shed some light on this problem.

#### LITERATURE CITED

1. D. Mohl et al., "On the performance characteristics of electron ring accelerators," Dubna Symp., Preprint LBL-1062 (1972).

\*See also the previously published paper [5].

2. C. Pellegrini and A. Sessler, "Theory of the nonlinear negative mass instability," Preprint LBL, ERAN-203 (1973).
3. A. Sessler, "Further contribution to the theory of the nonlinear negative mass instability," Preprint LBL, ERAN-207 (1973).
4. V. G. Makhanov and B. G. Shchinov, "Computer investigation of nonlinear dynamical problems of plasma theory," *Comp. Phys. Comm.*, 4, 327 (1972); B. G. Shchinov et al., *Plasma Phys.*, 15, 211 (1973); Joint Institute for Nuclear Research Preprint P9-5622 [in Russian], Dubna (1971).
5. A. G. Bonch-Osmolovskii et al., Joint Institute for Nuclear Research Preprint E9-1751, Dubna (1969).

## COMECON NEWS

Vth INTERNATIONAL CONFERENCE ON MÖSSBAUER  
SPECTROSCOPY (BRATISLAVA, SEPTEMBER, 1973)

A. G. Beda and E. P. Stepanov

The regularly scheduled international conference of COMECON member-nations on Mössbauer spectroscopy was held September 3-7, 1973, in Bratislava (Czechoslovakia). Both in the number of reports submitted (158) and in the number of participants (231), this Bratislava conference can be acknowledged the largest to date. In addition to specialists from the socialist countries, there were 80 specialists from capitalist nations participating in the deliberations of the conference. This conference, like its immediate precursor (Dresden 1971), emphasized the applied aspect of the topic, and was devoted to applications of the Mössbauer effect in various branches of science and industry.

The conference program included eight plenary sessions and six panel sessions held in parallel. A total of 147 reports were read, 13 of these being tutorial review papers. The following basic research trends were discussed at the panel sessions: 1) spinels and garnets; 2) physical metallurgy; 3) mineralogy and geology; 4) chemistry; 5) time dependences; 6) advances in techniques and methodology.

Theoretical aspects of the Mössbauer effect were discussed in a report by S. V. Koryagin (USSR) which covered the effect of anisotropy of atomic movements (vibrations and diffusion) on the shape of the Mössbauer spectra, and a report by D. Barba (Rumania) discussing polarized Mössbauer transitions in mixed hyperfine interactions.

Most of the review papers were also of an applied nature. For example, a report by K. Raclavsky (Czechoslovakia) dealt with geological applications of the Mössbauer effect. It was pointed out that this effect can be exploited in conducting structural and phase analyses of minerals, in prospecting for minerals, and that the Mössbauer effect can also be put to good use in the mining and ore processing industry. Advantages and disadvantages of Mössbauer spectroscopy as compared to other methods used for the same and similar purposes were discussed. A report by P. Flynn (USA) discussed possible applications of the Mössbauer effect in monitoring metallurgical processes, in analyzing corrosion products and metallurgical slags, in analyzing phase transitions, and in investigating the mechanism underlying tempering of steel. It was pointed out that the Mössbauer effect is useful, in measurements within the framework of scattering geometry, in nondestructive analysis of test specimens (e. g., in determining carbon content in steel and iron).

The audience responded with interest to a report by G. Frauenfelder (USA) on applications of the Mössbauer effect in biology where, it was pointed out, enormous possibilities are being opened up, so that information inaccessible and refractory to any other research techniques will become available.

A report by V. I. Gol'danskii (USSR) on the feasibility of a nuclear gamma-ray laser ("gaser") stimulated great interest. First, the physical fundamentals of the gaser were looked into, and its realization was shown to be feasible only through recourse to the Mössbauer effect. This was followed by formulation of stringent conditions imposed on the gaser design. Fulfillment of such conditions is entirely problematical at the present time.

G. Kalvius (West Germany) reported on the status of Mössbauer research in the field of the actinide elements (Th, Pa, U, Np, Am), and on opportunities for Mössbauer spectroscopy in the study of the electronic structure and magnetic properties of the actinide elements.

R. N. Kuz'min (USSR) presented a survey of work done on Mössbauer diffraction structural research. He took note of the major contribution rendered by Soviet scientists in the development of research in this

---

Translated from *Atomnaya Énergiya*, Vol. 36, No. 1, pp. 80-81, January, 1974.

© 1974 Consultants Bureau, a division of Plenum Publishing Corporation, 227 West 17th Street, New York, N. Y. 10011. No part of this publication may be reproduced, stored in a retrieval system, or transmitted, in any form or by any means, electronic, mechanical, photocopying, microfilming, recording or otherwise, without written permission of the publisher. A copy of this article is available from the publisher for \$15.00.

area, and pointed out trends in further research. The same topic was broached by E. P. Stepanov (USSR), in a report which cited recent experimental findings on diffraction studies of the interaction between resonance  $\gamma$ -emission at 14.4 keV energy and single crystals at the I. V. Kurchatov Institute of Atomic Energy [IAE].

Numerous reports on solid state physics centered primarily on the magnetic properties of various compounds and alloys (about 25 in all), as well as phase transitions, dynamical properties of crystal lattices, diffusion in solids and liquids, thin films and particles, and so on.

Noteworthy among papers submitted on relaxation processes is a paper by S. Morup (Denmark) reporting on an investigation into the effects of externally applied magnetic fields on relaxation times in ferric nitrate. A paper submitted by B. Balco and G. Howe (USA) dealing with investigations of electronic relaxation of the iron atoms in hematite near the Morin transition relied on the hitherto much neglected method of binary Mössbauer analysis with selective excitation of sublevels in the hyperfine structure of the test specimen; this approach yielded rather interesting results.

Close attention was paid to the reports presented by Yu. V. Baldokhin (Institute of Chemical Physics of the USSR Academy of Sciences) and I. A. Dubovtsev (Institute of Physics of Metals, Sverdlovsk) on the influence exerted by radio-frequency fields on the shape of Mössbauer spectra. The conference participants held a protracted discussion after the panel had been concluded; prominent contributors to the floor discussion included D. Walter (USA) and D. Albanese (Italy), who discussed various possible mechanisms that might underly mechanisms responsible for the interaction between atoms and an RF-field (magnetostriction, movement of domain walls, eddy current), and drew the inference that additional experiments are called for in order to shed further light on the roles played by each of them.

Research efforts centered mainly on complexes in organometallic compounds in the chemical papers reported on at the conference.

Some brief communications dealt with applications of the Mössbauer effect in investigations of the dynamics of ordering of alloys. The concentration dependence of quadrupole splitting and of the hyperfine  $H_{\text{eff}}$  was studied in these papers, and a relationship was established between these characteristics and the local atomic configurations.

Several original reports discussed a new and promising area of research; Mössbauer studies of radiation damage in solids. A paper by D. Walker (USA) dealt with investigations of temperature peaks. Other reports described a procedure for studying radiation damage involving implantation of Mössbauer emitter nuclei such as  $^{57}\text{Fe}$  (J. Sawicki, Poland),  $^{125\text{m}}\text{Te}$  and  $^{129\text{m}}\text{Te}$  (J. Langouche, Belgium) in different substrates, with subsequent determination of the dose dependence of the resulting hyperfine fields and quadrupole splitting.

G. Bortmann (West Germany) and A. G. Beda (USSR) reported on Mössbauer research in narrow lines. The former report cited research findings on the shift of the  $^{181}\text{Ta}$  line in response to temperature and pressure changes; the latter report presented new observational findings on the Mössbauer effect on the long-lived isomeric state of  $^{107}\text{Ag}$ , and pointed out factors that act to hinder observation of the Mössbauer effect.

Applications of the Mössbauer effect to the study of diffusion processes were discussed by Z. Bonchev (Bulgaria). The  $\beta$ -ray spectrometer was used in measurements of the energy and intensity of conversion electrons emitted by nuclei situated at different distances from the surface, after recoilless absorption of  $\gamma$ -photons.

Interesting reports on applications of the Mössbauer effect in hitherto nontraditional areas (such as archeology) were submitted by L. Keszthely (Hungary) and A. Semopoulos (Greece); in these studies, the Mössbauer techniques were applied in studies of iron compounds in pottery, ostraca, and earthenware to determine what methods were used in the fabrication of the wares in different historical periods.

In conclusion, we must point out that, despite the absence of fundamentally new and basic findings of a theoretical and experimental nature in the work reported on at this conference, the gathering yielded great scientific and practical information on a wide range of topics.

Members of the Soviet delegation visited the Mössbauer laboratory at the Slovak Polytechnic University. The experience acquired by Czechoslovak scientists who organized the laboratory for research projects involving technical applications of the Mössbauer effect, in response to requests by production organizations, is quite interesting and noteworthy.

The next regular scheduled conference of socialist countries on Mössbauer spectroscopy is to be held in Krakow (Poland), in September of 1975.

## COLLABORATION DAYBOOK

A conference of specialists of COMECON member-nations, and also the fourth session of the Coordination Scientific-Technical Council (KNTS) on nuclear power station spent fuels reprocessing, were held conjointly September 11-15, 1973, in Bialobrzeg (Poland). Participating were delegations from Bulgaria, the German Democratic Republic, Poland, the USSR, Czechoslovakia, and a staffmember of the COMECON Secretariat.

The status of research covered by points in the program of collaboration on reprocessing of nuclear power station fuels, and relating to the study of the physicochemical characteristics of solvent extraction processes, development of extractors of various types, and development of auxiliary equipment for solving extraction technology, was discussed at this conference. The timeliness of research on extraction kinetics of the actinoid and fission-fragment elements was emphasized, particularly in relation to the development and use of centrifugal extractors. The need to work out engineering procedures in the design of extraction process equipment was underlined. The feasibility and desirability of preparing engineering specifications in the development of extractors and auxiliary process equipment was acknowledged with the object of greater concretization in further research in this area.

The KNTS voiced its approval of an engineering specifications project for spent assemblies of fuel elements of nuclear electric power generating stations utilizing VVÉR-440 reactors as a standard document needed in working out and finalizing contracts for the delivery of spent fuel, and also as illustrative contents of general instructions on the proper procedures to be followed in shipping spent nuclear fuel from nuclear power stations of COMECON member-nations to reprocessing sites, and the sequence of operations to be followed in this line of work. Engineering specifications to be observed in working out methods and devices to be used in ascertaining the content and isotope composition of fissionable elements in spent fuel were discussed. Technological monitoring of extraction processes were discussed, and a setup for monitoring extraction reprocessing of spent fuel elements from VVÉR nuclear reactors was discussed and agreed upon, as well as engineering specifications for remote analytical monitoring devices applied to the composition of solutions and slurries, engineering specifications to be observed in the development of equipment for taking and transporting samples, listings of standards needed to check the methods, and calibration of monitoring instrumentation.

The council discussed the progress achieved to date in preparations for the III Symposium of COMECON member-nations on the topic: "Research on spent fuel reprocessing," to be held April 22-26, 1974, at Mariánské Lázně (Czechoslovakia). Basic trends in scientific and engineering research in the field of reprocessing of spent nuclear fuel from nuclear power stations, over the 1976-1980 period, were pinpointed, and proper sequencing of preparations of a program of collaborative efforts covering that period was mapped out.

In line with a PKIAÉ SÉV [Permanent COMECON commission on peaceful uses of atomic energy] resolution on development of the whole range of problems associated with radiochemical reprocessing of spent fast reactor fuel, and proposals entertained by delegations of the participating nations, the Council introduced appropriate refinements into the 1971-1975 collaboration program. The work plan drawn up for the KNTS covering the 1974-1975 period was discussed.

---

Translated from *Atomnaya Énergiya*, Vol. 36, No. 1, p. 81, January, 1974.

© 1974 Consultants Bureau, a division of Plenum Publishing Corporation, 227 West 17th Street, New York, N. Y. 10011. No part of this publication may be reproduced, stored in a retrieval system, or transmitted, in any form or by any means, electronic, mechanical, photocopying, microfilming, recording or otherwise, without written permission of the publisher. A copy of this article is available from the publisher for \$15.00.



## INFORMATION

THE INTERNATIONAL SYMPOSIUM ON MATHEMATICAL  
MODELS OF POWER-INDUSTRY ECONOMICS

Yu. I. Koryakin

The International Symposium on Mathematical Models of Power-Industry Economics, organized by the United Nations Economic Commission for Europe (ECE) in cooperation with the Ministries of Power of the USSR and the Kazakh SSR, was held from September 17-21, 1973 at Alma-Ata. The Symposium was attended by about 250 delegates, representing more than 20 European countries, as well as the United States and a number of international organizations: the European Economic Community (Brussels), the International Institute of Systems Analysis (Vienna), and others.

This was the first time a symposium on such a subject was being held under ECE auspices. It was made necessary by the increasing complexity of the study and management of the power industry and its various branches.

The participants heard 54 reports, grouped into the following four sections: survey of studies on the mathematical modelling of the economics of the power industry; description of models of the fuel-power industry as a whole and its various fuel sectors; description of models of electric-power systems and their development; and methodological questions concerning the construction of models of the fuel-power industry and forecasts of its development.

Each section included some general reports of a survey nature and some brief comments by individual authors on the reports presented.

The reports on the mathematical models of the power industry and the place of such models in the hierarchy of power-industry models were included in the fourth section.

The general report on the first section was presented by A. S. Nekrasov (USSR). He noted that there is today a very clear tendency toward the development of models covering the entire fuel-energy complex of a country and that this complex was being considered as a single entity because of the interchangeability of energy sources. The construction of such models, which in the Socialist countries are of a global optimization nature, is a logical development of the power-industry planning methods designed to ensure maximum effectiveness of the energy resources and the various forms of energy in the national economy of each country. The construction of complex power-industry models in countries with a market economy and those with a mixed economy often results from the State authorities' need to work out steps for stabilizing the country's energy supplies at a time when energy supply and demand are regulated by the price system.

In the second section the general report was presented by M. A. Rubin (USSR). He considered models constructed for various levels: overall national energy production at the country-wide level; specialized company-wide energy economies of individual sectors; regional overall energy production; and energy economies of individual energy-consuming enterprises and industrial combinations. Models at the country-wide level are formulated for the purpose of studying processes as functions of time. Depending on the problem, the development of systems may be examined for periods ranging up to 30 years. However, most of the problems are solved by using country-wide overall energy models covering periods of 10-15 years, since the longer the period under consideration, the less reliable and more indeterminate will be the initial information, in addition to the fact that for longer periods the solutions are less detailed. Therefore the

---

Translated from *Atomnaya Energiya*, Vol. 36, No. 1, pp. 82-84, January, 1974.

© 1974 Consultants Bureau, a division of Plenum Publishing Corporation, 227 West 17th Street, New York, N. Y. 10011. No part of this publication may be reproduced, stored in a retrieval system, or transmitted, in any form or by any means, electronic, mechanical, photocopying, microfilming, recording or otherwise, without written permission of the publisher. A copy of this article is available from the publisher for \$15.00.

models use variable time-scales, with calculation intervals of 1-2 years at the beginning of the period and 5 years at the end of the period.

The quantity taken as the fundamental criterion for optimal solutions is the minimum of the total expenditure for all stages of the process or the maximum profit on the assumption that the demand is satisfied. The view was expressed that additional criteria should also be taken into account: minimum energy consumption, labor resources, investments. The necessary combination of "vertical" and "horizontal" links in the process of optimal planning of the development of the power industry requires the construction of interrelated economic and mathematical models for optimization of a country's energy economy at various levels of the hierarchy of models. Algorithms for such interconnections were discussed in a number of reports.

The general report in the third section (A. I. Zeiliger and G. N. Lyalik, USSR) stated that problems involved in the planning and operation of electrical-energy systems (EES) that are being solved sequentially by means of models are approximately the same in all countries: investigators determine the optimal structure of power values to be generated and the distribution of these power values, they determined the requirements for new forms of energy installations, they select the optimal parameters for electric power stations and the times required for their construction, and they plan the annual, weekly, and daily operating regimes of the EES. The reports presented reflected the experience of a relatively small number of countries among those working on the construction and application of models for EES: the USSR, France, Great Britain, and Turkey.

The optimization of EES structure is a very complicated problem owing to its dynamic character, the discrete development of elements of the system, the large number of variable parameters, and the nonlinear relations between them. Since an exact solution of this problem is impossible at present, models are being developed for approximate solutions. Work is being done along two lines. The first is the approximation of the actual characteristics of EES in the components of the model, in the form of continuous functions which can be used in known mathematical methods of optimization (for example, linear and convex programming, etc.). This approach makes possible the construction of optimization models in which the variants of the desired solution are formulated, sorted out, and evaluated automatically, and the final result is one or more of the variants close to the optimum.

In the second approach the problem is simplified by specifying for the designers the variants of the desired solution. In this case models are used for an economic evaluation of the specified variants and for optimizing their secondary parameters (for example, optimizing the fuel costs by appropriately distributing the load among various power stations).

The authors of the reports considered in this section expressed a preference for a combination of the two types of models: first, optimization models are used for determining the region of optimal structures, and then the investigators make a comparison of the solution variants by selecting different types of equipment, different types and arrangements of power generation units, etc.

The general report in the fourth section (by A. A. Makarov and L. A. Melent'ev, USSR) emphasized the system approach that characterizes the methodology of the mathematical modeling of a country's fuel-energy economy. This approach is due to a very important feature of the power industry in the second half of the twentieth century: the fact that it is highly complex, as a result of the interchangeability of energy sources (electrical energy, gas, petroleum products, coal, atomic energy).

At all hierarchical levels, there are strong vertical (intra-industry) and horizontal (inter-industry) links between power systems. The hierarchical arrangement of large power systems should evidently be considered a fundamental methodological concept of present-day mathematical modeling in power-industry economics. Econometric models in the power industry should be constructed in the form of an interacting set of submodels approximating as closely the hierarchy of the actual power systems as possible.

In nuclear power generation, in addition to the complex optimization of the parameters of an atomic power station, with the aid of mathematical models, it is rational to study the nuclear power generation system as a single entity. By such a system we mean the entire cycle of extraction, enrichment, and processing of nuclear fuel for the production of electrical energy. It is useful today to study this process as a single unit because it has been shown that the effectiveness of the development of nuclear power depends on the choice of methods for utilizing the nuclear fuel to best advantage and also on the combination of rates of development of nuclear power-generating installations with the choice of optimum relations between the contributions of thermal-reactor and fast-reactor power-generating plants.

The special position of a nuclear power system as an element of the total system of power production is manifested primarily in the fact that the kinds of energy resources and the types of organic-fuel power stations replaced by nuclear plants will be different for different rates of development of the nuclear power industry. Therefore, in every calendar period there exists some optimal level of development of the sum total of the power contributed by atomic plants. It is determined from the fact that atomic power stations will first replace the most expensive forms of organic fuel (for example, pit-mined coal and, consequently, the basic stations fueled by such coal, next the less expensive fuel, and finally, for a given period of time, the development of atomic stations will reach a level at which the effect of adding further nuclear power would no longer be advantageous, or would in fact have a negative effect.

Thus, each particular rate of development of atomic power stations will, by replacing more expensive or less expensive organic fuel, affect not only the amount of "closed expenditure" ("shadow prices") of fuel but also the comparative economic efficiency of atomic power stations themselves. These important direct and inverse relations can be found by optimizing the rate of development of nuclear power generation of the model of the overall energy system. Thus, the optimal rate of development of atomic power stations can be determined only within the framework of the optimization of the overall energy system and the more precise optimization of the electrical-energy systems of a given country or group of countries whose energy systems are interconnected. In an evaluation of the role of atomic power stations in the energy-economy system it is also important to show the effectiveness of utilization of nuclear fuel for supplying heat, desalting water, and replacing technological heat and fuel in the energy-consuming branches of industry.

A report prepared by Soviet authors and read by S. Ya. Chernavskii described a system of dynamic mathematical models developed both for investigating the system of nuclear power generation in a country's overall power system and for making long-term forecasts concerning the nuclear-power system and optimizing its structure so as to minimize the total discounted design expenditures and minimize the system's natural-uranium requirements.

The model of the overall power system enables investigators to study the relative economic efficiency of atomic power stations and organic-fuel power stations and also to study (in a first approximation) the economic efficiency of the placement of atomic power stations in a country's territory as part of the electrical energy systems and their regimes of utilization for the years (intervals) of the design period, which usually do not exceed 20 years.

A number of variants were worked out for models to be used for long-term forecasting (25-30 years) of the development of nuclear power, with the variants differing in the degree of detail, in the various methods used for introducing the desired variables and the description of the relations between the elements of the system.

A similar theme was discussed in a report by W. Frankowski (Poland). The report discussed problems involved in the forecasting of the future use of nuclear power in Poland; such problems can be solved by means of 11 computer programs that have been worked out for the mathematical modeling of two-component nuclear-power systems which are closed with respect to plutonium balance. The solutions make use of (essentially) linear programming and nonlinear programming. They take account of factors such as delay time, discounting the growth of atomic power-station generating capacity, and changes in the isotope composition of the plutonium. Models have been developed for the startup of uranium fast reactors, with the uranium gradually being replaced by plutonium as operating time increases. Poland has no operating atomic power stations at present, and this fact makes it possible and makes it necessary to study with great care the initial stage of development of nuclear power generation in the country. A number of studies on mathematical modeling were devoted to the optimization of this stage.

S. Iliffe (Great Britain) also described a systems approach to the analysis of the long-term development of nuclear power generation. The model he described and the results of the calculations made with it involved the balance between the production of plutonium and the demand for it in a nuclear-power system (with a different power-stations structure) and the economic links between this system and the country's overall power system. The calculations dealt not only with the economics of a plutonium-balanced system but also with the economics of an unbalanced system. In the latter case the plutonium imbalance determines the reaction of the system in monetary terms.

The results of computer calculation of the model by the DISCOUNT-G program are obtained in the form of a printed complete picture of the principal indicators of the system for the years of the period

covered by the calculation. These indicators include the total number of stations put into operation, the types of stations, the load factors, the fraction of the base load used, the plutonium reserves and the minimum reserve levels, the maximum admissible losses ( /kW), total income, the market price of plutonium, the excess of plutonium left over, the import and export of plutonium, the removal of stations from operation, etc.

Because the results of calculations using the model can be shown easily in a visually recognizable form, the model has already been used for a number of years by the British Atomic Energy Authority for determining the possible economic effects of various lines of development of power reactors.

Thus, the reports and discussions indicated that the following are among the most important problems of mathematical modeling in the economics of the power industry:

1. Study of the effects that the development of the power industry produces on the environment. To solve this complex problem, which lies at the junction of technology, biology, and economics, will require enormous efforts. It is apparently necessary to develop special complex mathematical models. At the present time it is difficult to make any estimate of how complex and effective these models will be.

2. The establishment of a complete and reliable system of informative data. Today the initial information leaves a great deal to be desired, and therefore there is a great need, in particular, for the development of mathematical methods that will make it possible to take the optimal solutions while taking account of the indeterminacy of the initial information.

3. The problems of making mathematical models correspond to the research tasks for which they are to be used. It is by no means always true that the more accurate a model is, the better it will be. In the opinion of the general rapporteur, A. A. Makarov, there seems to be no sense in requiring a model to be so detailed that it can yield a formal solution accuracy greater than the probable error resulting from the incompleteness and poor quality of the initial information. Therefore we can justifiably use linear models for describing systems which we know to be nonlinear.

The Symposium demonstrated the rapid progress and increasing effectiveness of mathematical modeling in the power industry in general and in nuclear power generation in particular as the most advanced modern instrument for the investigation and control of these complex economic systems.

THE TENTH INTERNATIONAL MINERAL  
PROCESSING CONGRESS

M. L. Skrinichenko

The Tenth International Mineral Processing Congress was held in London from April 2 to April 6, 1973. The USSR delegation was headed by I. A. Strygin, Deputy Minister of Nonferrous Metallurgy, and included 73 specialists representing ministries and enterprises concerned with nonferrous and ferrous metallurgy and the chemical and coal industries, the Ministry of Geology, the Ministry of Higher Education, the USSR State Commission on Atomic Energy, and other organizations.

The Congress was opened by C. Chataway. He was followed by Professor Fleming, who delivered a lecture on "Man and Minerals."

The meetings were divided into the following technical sessions\*: comminution (7), screening and classification (3), gravity concentration (3), electrodynamic and magnetic concentration and sorting (4), flotation (12), process appraisal (3), plant design and practice (3), fine-particle processing (3), computer control (2), sorting (2), and chemical processing (6).

At the comminution session, G. Agar (Canada) and P. Somasundaran (United States) pointed out that by changing the number of revolutions of crushing mills according to the hardness and granulometric composition of the material being crushed, a considerable increase in output and a considerable saving of energy can be achieved. A report by W. Cowan and D. Rogers (United States) presented the results of investigations on ore comminution by the Snyder process. They indicated that the process was universally applicable: it is equally suitable for comminuting wood, paper, ore, and other materials. They remarked on the favorable granulometric characteristics of materials comminuted this process. In a report by D. Herbst, G. Grandi, and D. Fuerstenau (United States), it was shown that mathematical modeling of the comminution process makes it possible to answer many practical questions in the operation and design of comminuting equipment. In general, the reports and the discussion emphasized the need for expanding research on comminution and improving methods for investigating the degree of comminution of ores.

Reports presented at the gravity concentration session gave evidence of the growing use of methods of concentration in heavy suspensions in cylindrical separators and hydrocyclones. In a report entitled "Suspension hydrocycloning of diamond-bearing ores," presented by an Anglo-American corporation in South Africa, N. Chaston presented detailed data on the use of suspension hydrocycloning and described the characteristics of the hydrocycloning installations put into operation between 1955 and 1972.

The capacity of the installations with respect to input is as high as 560 tons/h. The total capacity of the installations described in the report is 2300 tons/h, and the particle size of the input ranges from  $-6 + 1$  to  $-6 + 0.5$  mm. The report specified the composition of the suspensoid (the ratios of magnetite to ferrosilicon used in the process) and the yield of suspensoid per ton of ore (330-700 g/ton). The diamond extraction amounts to 97-99%. R. Ignatovic (Yugoslavia) discussed methods of using heavy liquids for the separation of minerals. He showed that the use of surface-active substances for preliminary treatment of the initial ore improves the sharpness of the separation and reduces the consumption of tetrabromomethane.

At the electrodynamic and magnetic concentration and sorting session, a report by M. Carta et al. (Italy) showed that it was possible to determine in advance what form of energy effect was most acceptable

\*The numbers in parentheses indicate the number of reports in each session.

---

Translated from *Atomnaya Energiya*, Vol. 36, No. 1, pp. 84-86, January, 1974.

© 1974 Consultants Bureau, a division of Plenum Publishing Corporation, 227 West 17th Street, New York, N. Y. 10011. No part of this publication may be reproduced, stored in a retrieval system, or transmitted, in any form or by any means, electronic, mechanical, photocopying, microfilming, recording or otherwise, without written permission of the publisher. A copy of this article is available from the publisher for \$15.00.

for achieving a given separation result. He gave examples illustrating the preparation of a surface in which the energy structure was varied, making it possible to obtain better results in separation and flotation. The energy level of the surface was changed by irradiating it with x-rays,  $\gamma$ -rays, and  $\alpha$ -rays, by heat treatment, by controlling the conditions during the crushing process, and by triboelectric charging of the mineral particles before flotation.

At the process appraisal session, a report by M. Jones and L. Shaw (England) described a micro-analyzer that considerably expands the possibilities of mineralogical investigation. This device has a high efficiency and makes it possible to determine the size of mineral inclusions, as well as their relative content, and to obtain new additional information on the structure of ore minerals. The participants heard a description of how a microanalyzer could be transformed into a measuring device controlled by an electronic computer. P. Luckey and L. Osteen (United States) discussed the functions of an existing classifier and proposed a modeling methodology and statistical methods for obtaining the characteristics of classifiers that make it possible to construct an exact mathematical model of them.

The reports presented at the plant design and practice session included flow diagrams and data on the technological equipment of the plants, their indicators, and their operating costs. In particular, G. Hughes (Canada) described a pilot plant put into operation in 1970 for the concentration of copper-zinc ores, with a capacity of 3000 tons/day. It served as an auxiliary installation and a training center for the personnel of the Ruttan Lake processing plant, which has a capacity of 10,000 tons/day. These plants are characterized by central control systems, hydraulic drives for the pumps and conveyors, double hydrocycloning, the use of single-chamber flotation machines in the crushing cycle, cyclone feed secondary pumps, and automatic recording of particle-sizes. The process is monitored by means of a system of flow analysis on the Courier 300 installation.

The reports presented at the computer control session, as well as a number of reports presented at the other session, show that the use of electronic computers has become much more widespread in recent years. Today computers are used for monitoring the operation of enrichment plants and determining the mineral composition of the ore, in the automatic sorting of ores, in laboratory investigations, and for controlling the enrichment process at enrichment plants. In particular, as was pointed out in a report by J. Paekinen, S. Kreul, and S. Heikilla (Finland), the use of electronic computers over a four-year period for controlling the process of selective flotation at copper-zinc plants yielded substantial economic advantage.

Two reports presented at the sorting session indicate that the areas of application of some specific methods of sorting are becoming more extensive. D. Collier et al. (Australia) cited the results of investigations on the use of a thermoemission method for the sorting of asbestos ores and also reported on the development of a new variant of a luminescent separator for the concentration of scheelite ores, as well as on the results of the tests conducted with it. The electronic equipment used was a serial computer. A report by D. Jenningson et al. (England) contained information on the sorting of coal by an x-ray absorption method on a 14-stream belt separator.

The reports presented at the Congress, as well as the comments on them, indicate in general that new and progressive methods have been widely introduced into the practical operation of processing plants. Electronic computers are being used on larger scale, there has been more extensive use of nuclear-physics methods for mass analyses of the end product of the treatment process, and methods for the automatic sorting of ores are successfully being developed. Various ways have been proposed for finding engineering solutions to the problem of improving the separation process (settling and flotation) by a directed energy effect aimed at the surface of the minerals being separated (x-rays,  $\gamma$ -rays, and  $\alpha$ -rays, heat treatment, and triboelectric charging of particles). There has been a considerable increase in the monitoring and measuring equipment installed at new processing plants, and hydraulic drives for pumps, conveyors, and other equipment have come into use.

There is a tendency everywhere to set up and use large-scale equipment with large unit capacity.

At the last meeting of the Congress, I. A. Strygin spoke on behalf of the Soviet delegation, commenting on the large number of representatives attending the Congress and the very valuable work the participants had done. He said that plants in the Soviet Union were processing hundreds of millions of tons of ore every year and that all of the useful proposals made at the Congress could be very helpful in our country. He noted the importance and necessity of concentrating efforts on the protection of the environment and on the comprehensive and economical utilization of minerals.

The participants in the Congress visited several processing plants in Cornwall and the Midlands, including in particular a quarry and production plant for the manufacture of cement, crushed stone, and lime, as well as the West Plant Cavendish Mill, which processes lead-barite-fluorite ore. The flow diagram of the processing plant includes washing, crushing to 50 mm, screening and deslurrying, separation in heavy suspension, and flotation. Separation into three products in heavy suspension of class -50 + 9 mm is carried out in a single Wemco cylindrical separator. The separation takes place at a specific weight of 2.8 g/cm<sup>3</sup> in the first chamber of the separator and 3.15 g/cm<sup>3</sup> in the second. In the first stage, quartz, carbonates, and other minerals with a specific weight of less than 2.8 g/cm<sup>3</sup> are separated in the light fraction; these are put to commercial use as building material. In the second stage, a fluorite concentrate of the metallurgical type is separated in the light fraction. The heavy fraction of the separator and the deslurried class -9 mm are transported after comminution to the flotation stage. An ore containing 35% fluorite, 12% barite, 20-25% carbonates, 20% silicon dioxide, and 1-1.5% lead yields a lead concentrate with 70-75% lead, a fluorite concentrate with 97% fluorite, and a barite concentrate with 94-96% barite. The plant produces 140,000 tons of fluorite concentrate, 15,000 tons of barite concentrate, and 6000 tons of lead concentrate every year.

At the Cronwel Bishop Works, a British gypsum company, the participants in the Congress observed a plant producing high-purity gypsum. The flow charge of the plant includes crushing, screening, photometric sorting of classes from -40 to 6 mm on the Sortex 711 and Sortex 621 separators, and electrostatic separation of the -14 + 52 mesh class. An interesting feature of the plant is that the photometric processing made it possible to obtain extremely pure and highly valuable concentrates of gypsum. The use of other processes does not yield products of such high quality.

The participants also visited the Fauld Works, where gypsum is concentrated in heavy suspension. The flow charge of the plant includes separation of the -150 + 6 mm class, followed by washing and separation into three products in heavy suspension in a single Wemco cylindrical separator. Gypsum goes into the light fraction of the first chamber of the separator, and the part of the first chamber's heavy fraction that goes into the light fraction of the second chamber is barren rock, used as a building material. Anhydrite goes into the heavy fraction of the second chamber. Regeneration of the suspension is achieved by means of a magnetic separator. The carefully planned flow chart and the compactness of this plant make it stand out from the other plants visited. The plant is serviced by three workers per shift when operating at an input rate of 4600 tons of initial ore per day. The daily output of finished product is 2000 tons of high-quality gypsum. One interesting feature is that light structures — covered tents — are used for the semibunker storage and for the transport lines. Instead of windows, the tents use a transparent material similar in external appearance to ordinary corrugated tile.

A special exhibition on 68 stands was organized for the participants in the Congress at the Institution of Mining and Metallurgy. A relatively small number of items was exhibited. Most of them were flow sheets, photographs, and advertising prospectuses of various firms; A number of installations for the extractive recovery of copper and the gravity concentration of heavy minerals from thin slurries was shown in mockup form. Examples of protective meshes manufactured from rubber by Swedish and Norwegian firms were demonstrated.

The next International Mineral Processing Congress will be the eleventh; it is expected to take place at Cagliari, Italy, in April, 1975, and the twelfth Congress in May, 1977, in Canada.

ALL-UNION SYMPOSIUM ON RADIOBIOLOGY AND  
RADIOECOLOGY, SYKTYVKAR, SEPTEMBER, 1973

R. M. Aleksakhin

The second All-Union symposium devoted to the study of the biological effects of small doses of ionizing radiation, as a paramount aspect of the problem of protecting the biosphere and conservation of nature, was held at Syktyvkar September 4-6, 1973. The symposium, organized under the auspices and initiative of the "Radiobiology" Scientific Council of the USSR Academy of Sciences and the Komi branch of the USSR Academy of Sciences, drew participation from over 180 specialists.

Evaluation of the consequences of exposure to small doses is of interest from the standpoint of radiation safety in space flight, or from the standpoint of medicine and public health when radioisotopes and irradiation are used for diagnostic and therapeutic purposes (this applies above all to x-ray diagnostics).

Attention at the symposium was focused on the radioecological aspects of the problem of low radiation loads on plants, animals, and communities of plants and animals. Acquaintance with the radioecological regularities of migration of radionuclides and radiation effects on biogeocenoses lay the prerequisites for the solution of many practical problems.

A report by A. M. Kuzin cited reference data on current exposure doses experienced by humans in the vicinity of a variety of sources (natural background, global fallout levels resulting from nuclear weapons testing, medical procedures, worldwide use of atomic energy for peaceful purposes, etc.), and also presented forecasts of the degree of irradiation humans will be exposed to in the years 1990-2000. Even though the principal contribution to the exposure dose is that now made, and to be made in the immediate future, by the natural radiation background, radioecological concentration processes are still responsible for the formation of "hot spots" in some individual portions of the environment, and exposure doses will run well over the average at those spots. R. M. Aleksakhin presented the basic problems in radioecology in the light of nuclear power development and increasing amounts of radioactive wastes (these include migration of the more important components of wastes along biological and nutritional chains, radioadaptation processes, radiation-genetic effects when populations of living organisms are exposed to radiation).

Some of the reports reviewed results of many years of stationary research in regions with heightened contents of naturally occurring radionuclides in the Komi ASSR (V. I. Maslov, N. A. Titaeva, O. N. Popova, K. I. Maslova). Information was made available on the intensity of migration of uranium, thorium, and radium in the system soil-plants-animals; buildup factors were calculated, and the effect of the combined action by the external irradiation and incorporated radionuclides on plants and animals was ascertained. The results of experiments designed to estimate the long-term effects of heightened radiation background on plants and animals are of the greatest practical significance. A report by F. I. Pavlotska was devoted to the biogeochemistry of the most important fission products:  $^{90}\text{Sr}$  and  $^{137}\text{Cs}$ .

Various natural communities of fauna and flora are characterized by different levels of sensitivity to effects of ionizing radiations. One of the most sensitive biogeocenoses is the forest. F. A. Tikhomirov analyzed radiation injury processes affecting the forest, and described radionuclide circulation processes in forests.

One neglected area in radioecology, estimates of radiation effects on soil-dwelling animals and their role in the migration of radioactive materials, was the subject of an address by D. A. Krivolutskii.

---

Translated from *Atomnaya Energiya*, Vol. 36, No. 1, pp. 86-87, January, 1974.

© 1974 Consultants Bureau, a division of Plenum Publishing Corporation, 227 West 17th Street, New York, N. Y. 10011. No part of this publication may be reproduced, stored in a retrieval system, or transmitted, in any form or by any means, electronic, mechanical, photocopying, microfilming, recording or otherwise, without written permission of the publisher. A copy of this article is available from the publisher for \$15.00.



Public health regulations to be imposed on low radiation loads from a physiological standpoint, and relationships between radiation public health interests and radioecology, were discussed in papers presented by P. V. Ramzaeva and Yu. K. Kudritskii. The problem of small doses in outer-space radiobiology was broached by Yu. G. Grigor'ev. Attention was focused on the study of the combined effects of radiation and other factors in space flights. A. N. Sirotkin reported on research results in agricultural radioecology, throwing light on features of transport of the principal radioactive fission products and nuclides with induced activity where the participation of agricultural animals is involved, and also on the passage of radioactive animals into products of animal husbandry. It was pointed out that the agricultural link in the migration chain can be the predominant one in the formation of the radiation load on the human population.

Regularities of biological effects of ionizing radiations on living organisms are among those least well studied in radiobiology or in radioecology. Information on the effects of chronic exposure on organisms living under natural conditions, or on the biological significance of the natural radiation factor, is particularly inadequate. The symposium set down landmarks for the principal trends in further research, and contributed to better coordination of that research.

MEETING OF THE INTERNATIONAL COMMISSION  
ON RADIOLOGICAL PROTECTION

Yu. I. Moskalev

The International Commission on Radiological Protection (ICRP)\* met in April, 1973, at Brighton, England.

The Commission heard a report by Dr. D. J. Beninson on irradiation dose limits and decided that the report should be discussed in all the committees of ICRP in order that all the comments might be taken into account when ICRP Publication 9 was issued.

At the meetings of the Main Commission the participants heard reports on the work of its four Committees, as well as information from the International Commission on Radiation Units and Measurements (ICRU) on the concepts and principles of radiation protection and measurements.

Chairman H. B. Newcombe of Committee 1 informed the Main Commission of the results of the work done by the working groups on the biological effects of inhaled particles, the balance between genetic effects in the first and subsequent generations, epidemiological surveys of human populations exposed to radiation, and the radiosensitivity of embryos and fetuses. Reports on these questions were expected to be ready in 1974; they would be extremely important in working out practical measures for radiological protection.

The Main Commission concluded that in order to work out basic standards for radiological protection, it was necessary to establish some new working groups which would analyze the available radiobiological information on how radiation effects were influenced by such factors as the prolongation of radiation effects as a function of time and the value of the linear energy transfer in the development of genetic and somatic reactions. A further problem posed was that of finding a quantitative estimate of the detriment, i. e., the damage, that could be expected when radiation acted on human populations. In such an analysis it is desirable to compare the frequency of lesions and illnesses of various kinds among persons exposed to radiation with the frequencies among persons whose work did not involve radiation. An estimate of the radiation damage should take into account the severity of the effects and the natural death rate from cancer, equipment failures, and accidents.

In solving problems of radiological protection, special attention is given to the crystalline lens of the eye and to the skin. The maximum permissible doses for tissues situated at the surface are higher than the whole-body doses. ICRP recommends the use of average doses. However, in the determination of the crystalline-lens dose it is customary to evaluate it at the frontal surface of the lens, which is most radiosensitive and may develop cataracts as a result of radiation. It had been assumed that the frontal surface of the crystalline lens lies at a depth of 3 mm. However, standard morphological tables show that it is actually at a depth of 3.5 mm, and the center is at a depth of 4.1 mm. Therefore, when  $\beta$ -rays and soft x-rays act on the crystalline lens, the average dose will be considerably less than the dose for a depth of 3 mm.

On the basis of available data, Committee 1 concluded that the most radiosensitive part of the skin is the basal layer. It is assumed that in most of the skin the depth of this layer is 50-100  $\mu$  (5-10 mg/cm<sup>2</sup>). The Committee sees no immediate reason for changing the allowable radiation doses for the extremities.

\*Some results of the work of ICRP from 1969 to 1973 are mentioned in the report published in: Atomic Technology Outside the USSR (1973), No. 9, p. 36.

---

Translated from Atomnaya Énergiya, Vol. 36, No. 1, pp. 87-88, January, 1974.

© 1974 Consultants Bureau, a division of Plenum Publishing Corporation, 227 West 17th Street, New York, N. Y. 10011. No part of this publication may be reproduced, stored in a retrieval system, or transmitted, in any form or by any means, electronic, mechanical, photocopying, microfilming, recording or otherwise, without written permission of the publisher. A copy of this article is available from the publisher for \$15.00.

An analysis is being conducted on precise data concerning the genetic effects of radiation therapy on young people at the reproductive age, as well as the relative significance of radiation carcinogenesis and mutagenesis as factors limiting the radiation dose limits.

Committee 2 reported to the Main Commission on the preparation of a guide for the dosimetry of incorporated radioisotopes. The report explained the principles on which the calculations were based and gave specific examples of maximum permissible annual occupational levels of radioactive-isotope absorption and concentrations of radioactive isotopes in the air of working premises. The first volume of the guide will give the values for the 20 elements that are most important in practice ( $^3\text{H}$ ,  $^{32}\text{P}$ ,  $^{24}\text{C}$ ,  $^{35}\text{S}$ ,  $^{57}\text{Co}$ ,  $^{60}\text{Co}$ ,  $^{89}\text{Sr}$ ,  $^{90}\text{Sr}$ ,  $^{132}\text{Te}$ ,  $^{125}\text{I}$ ,  $^{131}\text{I}$ ,  $^{132}\text{I}$ ,  $^{134}\text{Cs}$ ,  $^{137}\text{Cs}$ ,  $^{224}\text{Ra}$ ,  $^{226}\text{Ra}$ , Th (nat.), U (nat.),  $^{238}\text{Pu}$ ,  $^{239}\text{Pu}$ ,  $^{241}\text{Pu}$ ,  $^{241}\text{Am}$ ,  $^{242}\text{Cm}$ ,  $^{252}\text{Cf}$ ,  $^{85}\text{Kr}$ ,  $^{133}\text{Xe}$ ,  $^{99}\text{Mo}$ , and  $^{99}\text{Te}$ ).

Preliminary estimates indicate that the new values will not differ substantially from those recommended earlier. It is expected that the work on the first volume will be completed by the end of 1973. The later volumes will contain information for other elements. The Committee also plans to prepare a special book giving data on decay schemes and effective radiation energies of various radioactive isotopes. This information will serve as a fundamental guide for the protection of professional workers from the effects of radioactive isotopes. They will be based on the latest data on the parameters of the "standard" human being, radiation energies and decay schemes of isotopes, and other data.

A book on the parameters of the "standard" human being is now ready for publication. It will be published by Pergamon Press in a blue cover\* during the second half of 1973.

The working groups of the Committee are continuing their work on the preparation of reports on radon, thoron, and their daughter products and on the mechanisms of the absorption and separation of radioactive isotopes from the respiratory tract.

Committee 3 of ICRP worked on protection against external radiation sources. It established a special group on the protection of patients being treated with ionizing radiation. It is considering problems involved in the processing and placement of radioactive materials in hospitals and scientific establishments. It is expected that the first version of the report will be ready some time in 1974.

The Committee believes that the recommendations of ICRP on protection against ionizing radiation from external sources (Publication 15) and protection of the patient in x-ray diagnosis (Publication 16) are as yet not widely used in practice, and for that reason attention must be drawn to them again and again. Accordingly, it was decided to prepare a brief report for the participants in the forthcoming International Radiological Congress and to publish it in radiological journals. The Committee asked for the Commission's advice on the possibility of selecting more suitable quantities than the genetically significant dose for evaluating the relative importance of various types of partial irradiation in comparison with whole-body irradiation. The Commission considered the question but did not come to any definite conclusion.

Committee 4 informed the Commission of the results of its work in 1972-1973. It is completing the preparation of recommendations on what action should be taken in cases of irradiation resulting from equipment failure or other accidents. It is expected that the report on this subject will be presented to ICRP in 1974. Also in 1974, the Committee will complete its work on radiological protection in uranium mines. The information published in this work may prove very useful in ensuring safe working conditions in other (nonuranium) mines as well, and it was therefore proposed that the work should be retitled "Radiological protection in uranium mines and some other types of mines." The Committee has completed preparing the information on the practical application of the recommendations contained in Section 52 of ICRP Publication 9, which deals with the need to reduce the irradiation doses as much as possible.

Earlier (in 1968 and 1971), the Committee prepared and published Reports 10 and 10A, which gave some information on the accumulation levels and tissue doses absorbed in the organs and tissues of the human body after single, periodic, and prolonged exposure to the most important radioisotopes. It was found desirable to combine these two reports into a single book published separately, and this work is expected to be finished during 1974. The Committee has prepared a proposal on dose equivalents, which is to replace part 11B of ICRU Report 19. The dose equivalent is of great practical importance, since the biological effectiveness of a given absorbed dose depends on the quality of the radiation and on the irradiation

\*As is known, ICRP issues its publications in either brown or blue covers. Works issued in a brown cover contain ICRP recommendations on radiological protection, while those in a blue cover usually contain handbook material and surveys of radiation medicine.

conditions. It is recommended that the dose equivalent  $H$  be determined by the formula  $H = QND$ , where  $D$  is the absorbed dose,  $Q$  is the quality factor, and  $N$  is a quantity which takes account of the influence of other factors. The unit of dose equivalent is the rem.

The members of the Main Commission of ICRP for 1973-1977 were elected at the meeting; in addition, the members of Committees 1, 2, 3, and 4 of the Main Commission were reelected. C. G. Stewart remains Chairman of the Main Commission; the USSR members elected were Yu. I. Moskalev (Main Commission), P. V. Ramzaev (Committee 2), E. E. Kovalev (Committee 3), and A. A. Moiseev (Committee 4).

According to present plans, the next meeting of ICRP will be held in March, 1974, at Geneva.

# breaking the language barrier

WITH COVER-TO-COVER  
ENGLISH TRANSLATIONS  
OF SOVIET JOURNALS

# in physics

SEND FOR YOUR  
FREE EXAMINATION COPIES

**PLENUM PUBLISHING CORPORATION**  
227 WEST 17th STREET  
NEW YORK, N. Y. 10011

Plenum Press • Consultants Bureau  
• IFI/Plenum Data Corporation

In United Kingdom: 4a Lower John Street,  
London W1R 3PD, England

Title	# of Issues	Subscription Price
Astrophysics <i>Astrofizika</i>	4	\$120.00
Fluid Dynamics <i>Izvestiya Akademii Nauk SSSR mekhanika zhidkosti i gaza</i>	6	\$180.00
High-Energy Chemistry <i>Khimiya vysokikh énergii</i>	6	\$155.00
High Temperature <i>Teplofizika vysokikh temperatur</i>	6	\$150.00
Journal of Applied Mechanics and Technical Physics <i>Zhurnal prikladnoi mekhaniki i tehnicheskoi fiziki</i>	6	\$175.00
Journal of Engineering Physics <i>Inzhenerno-fizicheskii zhurnal</i>	12 (2 vols./yr. 6 issues ea.)	\$175.00 (\$87.50/vol.)
Magnetohydrodynamics <i>Magnitnaya gidrodinamika</i>	4	\$125.00
Mathematical Notes <i>Matematicheskie zametki</i>	12 (2 vols./yr. 6 issues ea.)	\$185.00
Polymer Mechanics <i>Mekhanika polimerov</i>	6	\$140.00
Radiophysics and Quantum Electronics (Formerly Soviet Radiophysics) <i>Izvestiya VUZ, radiofizika</i>	12	\$180.00
Solar System Research <i>Astronomicheskii vestnik</i>	4	\$ 95.00
Soviet Applied Mechanics <i>Prikladnaya mekhanika</i>	12	\$175.00
Soviet Atomic Energy <i>Atomnaya énergiya</i>	12 (2 vols./yr. 6 issues ea.)	\$175.00 (\$87.50/vol.)
Soviet Physics Journal <i>Izvestiya VUZ, fizika</i>	12	\$180.00
Soviet Radiochemistry <i>Radiokhimiya</i>	6	\$165.00
Theoretical and Mathematical Physics <i>Teoreticheskaya i matematicheskaya fizika</i>	12 (4 vols./yr. 3 issues ea.)	\$160.00

Back volumes are available. For further information, please contact the Publishers.